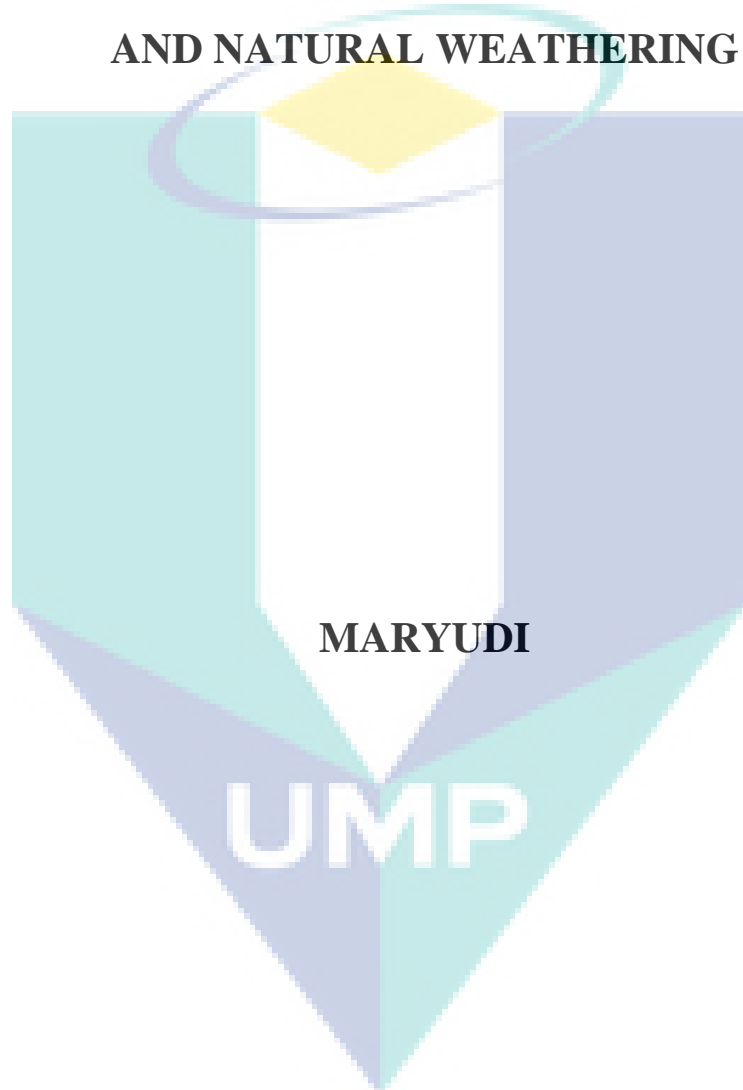
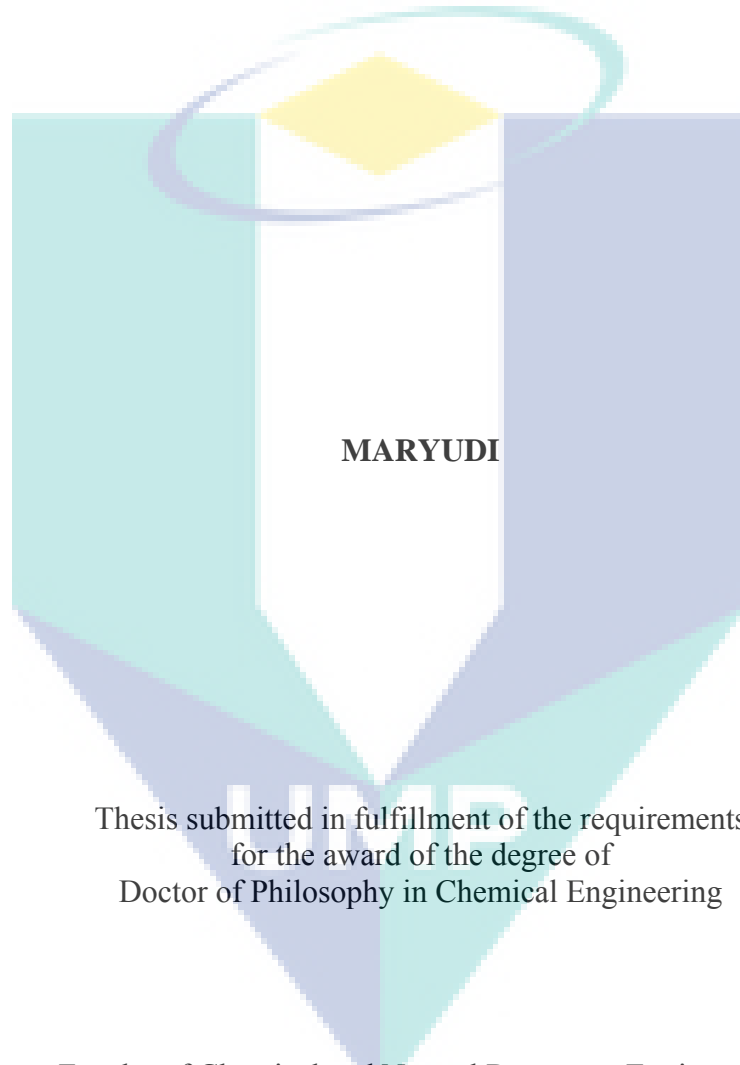


**DEGRADATION OF HIGH DENSITY POLYETHYLENE
CONTAINING MANGANESE CARBOXYLATES AS
PRO-DEGRADANT ADDITIVES UNDER ARTIFICIAL
AND NATURAL WEATHERING**



**DOCTOR OF PHILOSOPHY
UNIVERSITI MALAYSIA PAHANG**

**DEGRADATION OF HIGH DENSITY POLYETHYLENE CONTAINING
MANGANESE CARBOXYLATES AS PRO-DEGRADANT ADDITIVES UNDER
ARTIFICIAL AND NATURAL WEATHERING**




Thesis submitted in fulfillment of the requirements
for the award of the degree of
Doctor of Philosophy in Chemical Engineering

Faculty of Chemical and Natural Resources Engineering
UNIVERSITI MALAYSIA PAHANG

MAY 2012

SUPERVISOR'S DECLARATION

I hereby declare that I have checked this thesis and in my opinion this thesis is adequate in terms of scope and quality for the award of the degree of Doctor of Philosophy in Chemical Engineering.

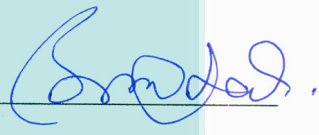


Prof. Dato Dr. Rosli Mohd Yunus

Supervisor

Date: 25/5/2012

PROFESSOR DATO' DR ROSLI BIN MOHD YUNUS
DEPUTY VICE-CHANCELLOR
(RESEARCH & INNOVATION)
UNIVERSITI MALAYSIA PAHANG
LEBUHRAYA TUN RAZAK
26300 GAMBANG, KUANTAN
PAHANG DARUL MAKMUR
TEL: 09-549 2004 FAKS: 09-549 2424



Assoc. Prof. Dr. Mohammad Dalour Hossen Beg

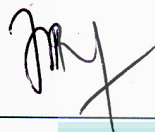
Co-supervisor

Date: 28/5/12



STUDENT'S DECLARATION

I hereby declared that the work in this thesis is my own except for quotations and summaries which have been duly acknowledged. The thesis has not been accepted for any degree and is not concurrently submitted for award of other degree.



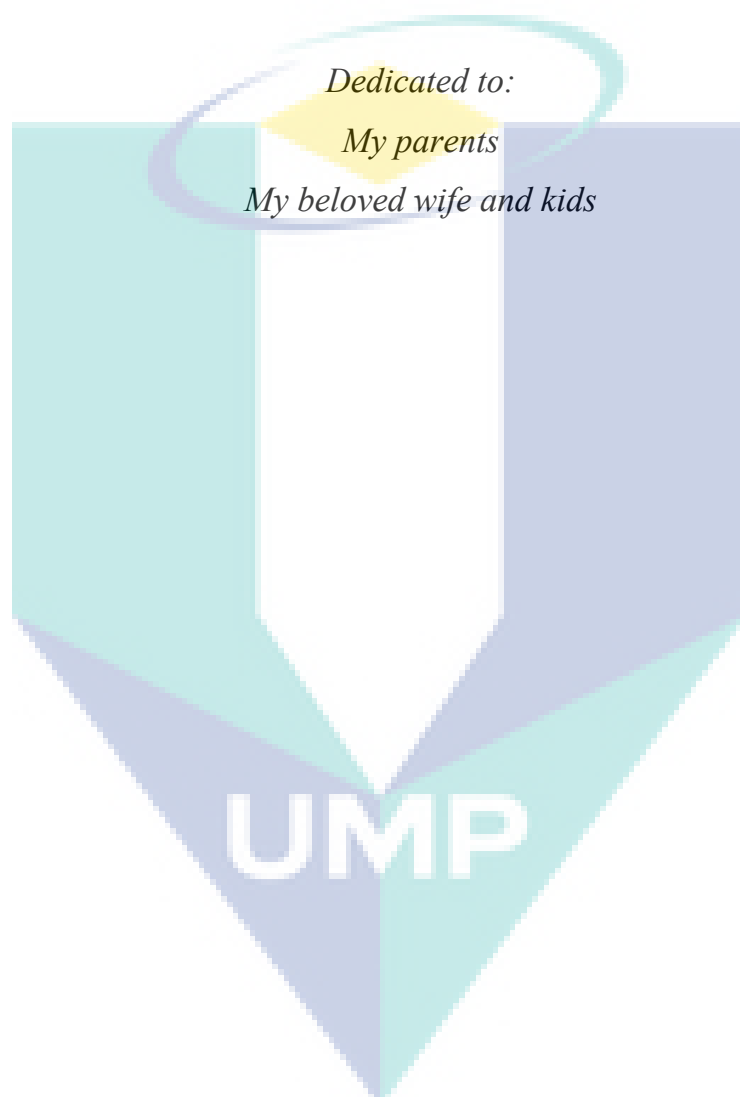
Maryudi

ID: PKC07007

Date: 23/05/2012



UMP



ACKNOWLEDGEMENT

I would like to take this precious moment to express my sincere and wholehearted appreciation to my supervisor, Prof. Dato' Dr. Rosli Mohd Yunus for kindness and support.

Grateful thank also addressed to my co-supervisor Assoc. Prof. Dr. Mohammad Dalour Hossen Beg for ideas, assistance and encouragement in writing thesis. Thank you to Assoc. Prof. Dr. Abdurahman Hamid Nour for his advice and encouragement. I would like also to thank to Assoc. Prof. Dr. Mohd Hanafiah Abidin, who has given permission for using facilities in UiTM Shah Alam, although I couldn't eventually access the facilities due to laboratory renovation.

I would like to express my gratitude to my lab-mates in polymer field for assistance in sample preparation and testing, discussion, and support. Special thanks to Anwaruddin Hisyam and Juwari for invaluable help and spending time together. Thanks to all my friends for their encouragement to complete the study, especially for friends in C11-3-10.

Finally, very special thanks for my beloved wife and kids, the inspiring persons, for kindness, sacrifice, great patience and constant support. Thank you for my parents, brothers and sisters for constant support to complete my study. My study was impossible unless they supported.

ABSTRACT

The tremendous utilization of synthetic plastics over last decades has led to environmental problems due to lack of degradability of plastics. The degradability issue has resulted in development of degradable plastics which degrade faster. This study deals with utilization of manganese carboxylates (i.e. manganese laurate, manganese palmitate and manganese stearate) on enhancing degradation of high density polyethylene (HDPE). Initially, manganese carboxylates were synthesized through two-steps reactions: (i) sodium carboxylates synthesis by reacting sodium hydroxide and carboxylic acids, (ii) manganese carboxylates synthesis by reacting manganese chloride and sodium carboxylates. Characterization of manganese carboxylates was then carried out. Incorporation of manganese carboxylates up to 1% (w/w) into HDPE resin was carried out using twin screw extruder followed by injection molding to produce specimens. Thermal treatment was performed at 70°C for maximum duration of 1000 hours to examine the degradation of pure HDPE and HDPE containing manganese carboxylates. Accelerated weathering was conducted up to 1000 hours combining thermal and UV exposure. Natural weathering was carried out for 24 weeks under weather conditions of Gambang, Malaysia. Analyses of tensile strength, elongation at break, FTIR spectra, average molecular weight, melt flow index (MFI), thermogravimetry (TG), differential scanning calorimetry (DSC), X-ray diffraction (XRD), and scanning electron microscopy (SEM) were carried out to assess the changes during treatments. Results have revealed that all manganese carboxylates have demonstrated adequate thermal stability. Their melting temperatures are in range of 108-117 °C. Manganese stearate has shown the highest thermal stability and melting point among manganese carboxylates synthesized. Thermal treatment has led to thermo-oxidative degradation of HDPE. Manganese carboxylates have significantly played a role in enhancing degradation of HDPE. The degradation increased by increasing amount of manganese carboxylates. During accelerated weathering, the degradation took place more rapidly than during thermal treatment, particularly for HDPE containing manganese carboxylates. Photo-degradation and thermo-oxidative degradation took place simultaneously during accelerated weathering and allowed dramatic reductions of essential properties. Natural weathering has given similar effects with accelerated weathering. Manganese carboxylates has also shown the capabilities on enhancing degradation of HDPE in natural environment. Manganese stearate has shown a slightly greater effect in enhancing degradation of HDPE than manganese laurate and manganese palmitate during all treatments. Pure HDPE lost its elongation at break about 16 %; 65 % and 64 %, whereas HDPE containing 1% manganese stearate lost its elongation at break about 62 %; 96 % and 95 % for thermal treatment; accelerated weathering and natural weathering respectively. Tensile strength and tensile modulus also decreased proportionally with the decrease of elongation at break. Other properties have also been found to decrease including average molecular weight, thermal stability, and melting point. The MFI, carbonyl index and crystallinity were found to increase after all treatments. Generally, manganese carboxylates have demonstrated the capabilities on enhancing degradation of HDPE under all modes of treatments.

ABSTRAK

Penggunaan bahan plastik yang banyak sejak beberapa dekad yang lalu membawa kepada masalah alam sekitar yang disebabkan oleh kekurangan sifat keteruraian bahan plastik. Isu keteruraian bahan plastik telah memberi kesan dalam pembaharuan penghasilan plastik yang lebih cepat terurai. Kajian ini melibatkan penggunaan mangan karboksilat (mangan laurat, mangan palmitat and mangan stearat) dalam meningkatkan penguraian polietilena ketumpatan tinggi (HDPE). Mangan karboksilat dihasilkan melalui dua kaedah tindakbalas: (i) natrium karboksilat disintesiskan melalui tindakbalas natrium hidroksida dengan asid karboksilik, (ii) mangan karboksilat disintesiskan melalui tindakbalas mangan klorida dengan natrium karboksilat. Pencirian mangan karboksilat kemudiannya dapat dihasilkan. Gabungan mangan karboksilat sehingga 1% (w/w) ke dalam HDPE resin telah dijalankan dengan menggunakan mesin pengestrud skru berkembar yang kemudiannya melalui suntikan acuan untuk menghasilkan spesimen. Rawatan terma dilakukan pada suhu 70°C dengan masa maksima iaitu selama 1000 jam dalam menguji tahap penguraian HDPE tulen dan HDPE yang mengandungi mangan karboksilat. Pecutan penguasaan dijalankan sehingga 1000 jam yang menggabungkan pendedahan terhadap terma dan cahaya sinar UV. Penguasaan semulajadi dilakukan selama 24 minggu dengan keadaan cuaca di kawasan Gambang, Malaysia. Analisa kekuatan tensil, pemanjangan pada takat putus, spektrum FTIR, purata berat molekul, indeks aliran leburan(MFI), termogravimetri(TG), pembezaan imbasan kalorimetri(DSC), pembelauan sinar-X(XRD), imbasan mikroskop elektron(SEM) telah dijalankan untuk menilai perubahan yang berlaku semasa perawatan. Hasil ujikaji telah mendedahkan semua mangan karboksilat menunjukkan kestabilan terma yang mencukupi. Suhu lebur bagi mangan karboksilat tersebut dalam lingkungan 108-117°C. Mangan stearat menunjukkan kestabilan terma yang tertinggi dan takat lebur di antara mangan karboksilat sintesis yang lain-lain. Rawatan terma telah menyebabkan penguraian oksidatif terma bagi HDPE. Mangan karboksilat merupakan bahan penting dalam meningkatkan tahap penguraian HDPE. Penguraian akan bertambah dengan pertambahan kuantiti bahan mangan karboksilat. Semasa penguasaan pecutan, penguraian berlaku dengan lebih cepat berbanding semasa perawatan terma, terutama bagi HDPE yang mengandungi bahan mangan karboksilat. Penguraian foto dan penguraian oksidatif terma berlaku secara serentak semasa penguasaan pecutan dan membenarkan berlakunya keretakan pada sifat-sifat penting secara dramatik. Penguasaan semulajadi memberikan kesan serupa dengan penguasaan pecutan. Mangan karboksilat juga menunjukkan kebolehpayaan dalam meningkatkan tahap penguraian HDPE di persekitaran semulajadi. Mangan stearat menunjukkan kesan yang lebih baik dalam meningkatkan tahap penguraian berbanding mangan laurat dan mangan palmitat dalam semua perawatan. HDPE tulen kehilangan pemanjangan pada takat putus iaitu 16%, 65% dan 64% sedangkan HDPE yang mengandungi mangan stearat kehilangan pemanjangan pada takat putus iaitu 65%, 96%, dan 95% bagi perawatan terma, pecutan penguasaan dan penguasaan semulajadi. Kekuatan tensil dan modulus tensil juga menurun secara berkadaran dengan penurunan pemanjangan pada takat putus. Sifat-sifat lain juga didapati merosot termasuk purata berat molekul, kestabilan terma dan takat lebur. Nilai MFI, indek karbonil dan sifat penkristalan didapati ada peningkatan dalam semua perawatan. Secara umumnya, mangan karboksilat telah menunjukkan keupayaan dalam meningkatkan penguraian HDPE dalam semua kedah perawatan.

TABLE OF CONTENTS


	Page
TITLE	i
SUPERVISOR'S DECLARATION	ii
STUDENT'S DECLARATION	iii
DEDICATIONS	iv
ACKNOWLEDGEMENTS	v
ABSTRACT	vi
ABSTRAK	vii
TABLE OF CONTENTS	viii
LIST OF TABLES	xiii
LIST OF FIGURES	xiv
LIST OF SYMBOLS	xix
LIST OF ABBREVIATIONS	xx
CHAPTER 1 INTRODUCTION	
1.1 RESEARCH BACKGROUND	1
1.2 PROBLEM STATEMENT	5
1.3 OBJECTIVES OF RESEARCH	6
1.4 SCOPE OF RESEARCH	6
1.5 CONTRIBUTIONS OF RESEARCH	7
CHAPTER 2 LITERATURE REVIEW	
2.1 INTRODUCTION TO PLASTICS	8
2.2 POLYETHYLENE	9
2.2.1 Classification of Polyethylene	11

2.2.2	Properties of Typical Polyethylene and Their Applications	13
2.3	PROCESSING METHOD OF PLASTICS	14
2.3.1	Compounding	15
2.3.2	Injection Molding	15
2.4	POLYETHYLENE PROPERTIES AND TESTING	16
2.4.1	Fourier Transform Infrared Spectroscopy	16
2.4.1.1	Fourier Transform Infrared Examination Techniques	17
2.4.1.2	Fourier Transform Infrared Spectra	19
2.4.2	Tensile Properties	20
2.4.3	Molecular Weight	22
2.4.3.1	Average Molecular Weight	23
2.4.3.2	Method of Average Molecular Weight Measurement	24
2.4.4	Melt Flow Index	28
2.4.5	Thermal Stability	29
2.4.5.1	Thermogravimetry Analysis	29
2.4.5.2	Experimental Aspects of Thermogravimetry Analysis	30
2.4.5.3	Interpretation of Thermogravimetry Curve	31
2.4.6	Melting Temperature	34
2.4.6.1	Factors That Influence Melting Temperature	35
2.4.6.2	Differential Scanning Calorimetry	36
2.4.6.3	DSC Scan Analysis	38
2.4.7	Crystallinity	40
2.4.7.1	Crystallinity of Polymer from DSC Scan	41
2.4.7.2	Crystallinity of Polymer from XRD Trace	41
2.4.8	Surface Morphology	45
2.4.8.1	Scanning Electron Microscope	45
2.4.8.2	Specimen Preparation	46
2.5	DEGRADATION OF PLASTICS	47
2.5.1	Thermo-Oxidative Degradation	48
2.5.2	Photo Degradation	51
2.5.3	Accelerated Weathering Degradation	55

2.5.4	Natural Weathering Degradation	56
2.6	ADDITIVES FOR DEGRADABLE PLASTICS	58
2.7	EVALUATION OF DEGRADATION	60

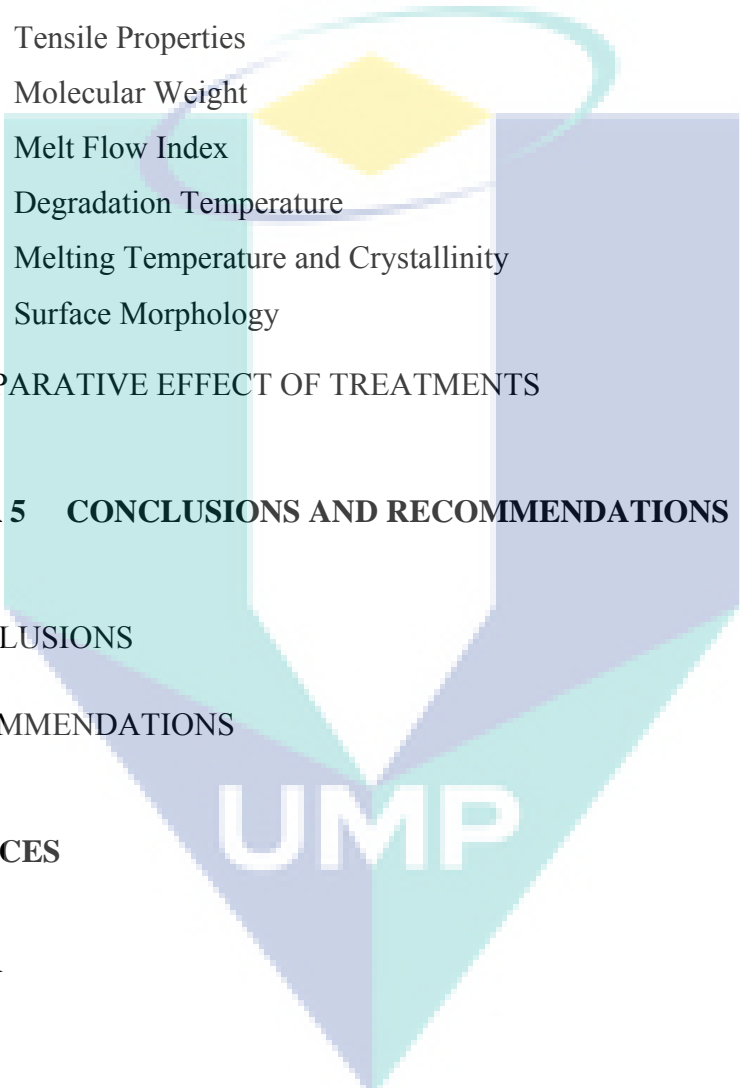
CHAPTER 3 METHODOLOGY

3.1	OVERALL RESEARCH WORKS	62
3.2	MATERIALS	64
3.3	SYNTHESIS OF MANGANESE CARBOXYLATES	64
3.4	CHARACTERIZATION OF MANGANESE CARBOXYLATES	65
3.4.1	Free Fatty Acid Content	65
3.4.2	Bulk Density	65
3.4.3	Solubility	66
3.4.4	Water and Ash Contents	66
3.4.5	Degradation Temperature	66
3.4.6	Melting Temperature	66
3.5	COMPOUNDING	67
3.6	INJECTION MOLDING	67
3.7	TESTING	68
3.7.1	Carbonyl Index	68
3.7.2	Tensile Properties	68
3.7.3	Average Molecular Weight	69
3.7.4	Melt Flow Index	70
3.7.5	Degradation Temperature	70
3.7.6	Melting Temperature	70
3.7.7	Crystallinity	71
3.7.8	Surface Morphology	71



3.8	TREATMENTS	71
3.8.1	Thermal Treatment	71
3.8.2	Accelerated Weathering Treatment	72
3.8.3	Natural Weathering Treatment	72
3.9	DEGRADATION EVALUATION	72
CHAPTER 4 RESULTS AND DISCUSSIONS		
4.1	SYNTHESIS AND CHARACTERIZATION OF MANGANESE CARBOXYLATES	74
4.1.1	Synthesis of Manganese Carboxylates	74
4.1.2	Characterization of Manganese Carboxylates	75
4.2	THERMO-OXIDATIVE DEGRADATION OF HIGH DENSITY POLYETHYLENE	80
4.2.1	Introduction	80
4.2.2	Infrared Spectra	80
4.2.3	Tensile Properties	82
4.2.4	Molecular Weight	90
4.2.5	Melt Flow Index	92
4.2.6	Degradation Temperature	93
4.2.7	Melting Temperature and Crystallinity	96
4.2.8	Surface Morphology	98
4.3	DEGRADATION OF HIGH DENSITY POLYETHYLENE UNDER ACCELERATED WEATHERING TREATMENT	101
4.3.1	Introduction	101
4.3.2	Infrared Spectra	101
4.3.3	Tensile Properties	104
4.3.4	Molecular Weight	112
4.3.5	Melt Flow Index	114
4.3.6	Degradation Temperature	114

4.3.7	Melting Temperature and Crystallinity	118
4.3.8	Surface Morphology	121
4.4	DEGRADATION OF HIGH DENSITY POLYETHYLENE UNDER NATURAL WEATHERING	123
4.4.1	Introduction	123
4.4.2	Infrared Spectra	124
4.4.3	Tensile Properties	127
4.4.4	Molecular Weight	135
4.4.5	Melt Flow Index	136
4.4.6	Degradation Temperature	137
4.4.7	Melting Temperature and Crystallinity	139
4.4.8	Surface Morphology	143
4.5	COMPARATIVE EFFECT OF TREATMENTS	144
CHAPTER 5 CONCLUSIONS AND RECOMMENDATIONS		
5.1	CONCLUSIONS	151
5.2	RECOMMENDATIONS	153
REFERENCES		154
Appendix A		162
Appendix B		165
Appendix C		166



LIST OF TABLES

Table No.	Title	Page
2.1	Main properties of typical polyethylene	14
3.1	Designation of samples	67
4.1	Properties of manganese carboxylates	77
4.2	Losses of tensile properties of samples after 1000 hours of thermal treatment	87
4.3	Degradation temperatures of samples, before and after 1000 hours of thermal treatment	95
4.4	Melting temperatures and crystallinities of samples before and after 1000 hours of thermal treatment	97
4.5	Losses of tensile properties of samples after 1000 hours of accelerated weathering	107
4.6	Degradation temperatures of HDPE samples before and after 1000 hours of accelerated weathering	117
4.7	Melting temperatures of HDPE samples and their crystallinities, before and after 1000 hours of accelerated weathering	119
4.8	Comparison of crystallinities obtained from DSC scan and XRD trace before and after 1000 hours of accelerated weathering	121
4.9	Gambang average weather	123
4.10	Losses of tensile properties after 24 weeks of natural weathering	130
4.11	Degradation temperatures of HDPE samples before and after 24 weeks of natural weathering	139
4.12	Melting temperatures of HDPE samples and their crystallinities before and after 24 weeks of natural weathering	141
4.13	Comparison of crystallinities obtained from DSC scan and XRD trace before and after 24 weeks of natural weathering	142
4.14	Degradation temperatures and activation energies of selected samples before and after three different treatments	146
4.15	Melting properties of selected samples before and after three different treatments	147

LIST OF FIGURES

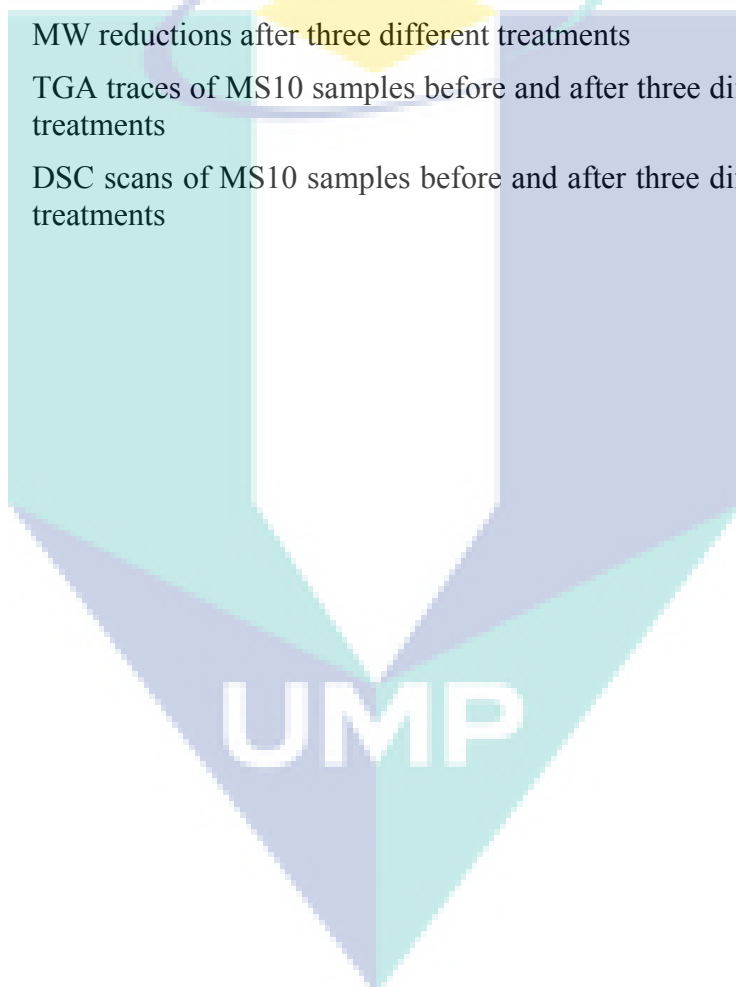
Figure No.	Title	Page
1.1	World plastics production 1950-2010	2
1.2	Plastics demand by converters 2010 in Europe: (a) breakdown by resin types, (b) breakdown by end use segments	2
1.3	Plastics demand in Malaysia 2010 breakdown by market segments of plastics products	3
2.1	Chemical structure of polyethylene	9
2.2	Molecular structure of polyethylene	10
2.3	Schematic of the molecular structure of different polyethylene (a) HDPE, (b) LDPE, and (c) LLDPE	12
2.4	The stress-strain behavior for brittle (curve A), plastics (curve B), and highly elastic (elastomeric) (curve C) polymers	22
2.5	Classification of thermogravimetry curves	32
2.6	Comparison TG curves and corresponding DTG curves	33
2.7	Temperature determination from a single-stage TG curve	33
2.8	Dependence of polymer properties as well as melting and glass transition temperatures on molecular weight	36
2.9	Schematic DSC curve for a polymeric sample	37
2.10	DTA curve of glass-ceramic sample	39
2.11	Polyolefin melting profiles	40
2.12	Plot of X-ray scattering intensity of linear-low density polyethylene	42
2.13	Three types of peak shapes in X-ray diffraction pattern (a) peak height proportional to peak area; (b) peak height not proportional to peak area; and (c) peak area overlapped by other peaks	43
2.14	Profile analysis of a diffractometer scan from polyethylene	44
2.15	Mechanism of thermo-oxidation of polyethylene	49
3.1	Flow chart of overall research	63
3.2	Dimension of specimen	69
4.1	TG traces of manganese carboxylates	77
4.2	DTG traces of manganese carboxylates	78
4.3	DSC scans of manganese carboxylates	79

4.4	FTIR spectra of ML10 samples, before (lower trace) and after (upper trace) thermal treatment	81
4.5	Carbonyl index of HDPE samples with various compositions during thermal treatment	82
4.6	Tensile strength of HDPE containing manganese laurate during thermal treatment	83
4.7	Tensile strength of HDPE containing manganese palmitate during thermal treatment	84
4.8	Tensile strength of HDPE containing manganese stearate during thermal treatment	84
4.9	Tensile modulus of HDPE containing manganese laurate during thermal treatment	86
4.10	Tensile modulus of HDPE containing manganese palmitate during thermal treatment	86
4.11	Tensile modulus of HDPE containing manganese stearate during thermal treatment	87
4.12	Elongation at break of HDPE containing manganese laurate during thermal treatment	88
4.13	Elongation at break of HDPE containing manganese palmitate during thermal treatment	89
4.14	Elongation at break of HDPE containing manganese stearate during thermal treatment	89
4.15	Average molecular weights of various samples during thermal treatment	91
4.16	MFI of various samples during thermal treatment	92
4.17	TG traces of pure samples, before and after 1000 hours of thermal treatment	93
4.18	DTG traces of pure samples, before and after 1000 hours of thermal treatment	94
4.19	TG traces of ML10 samples before and after 1000 hours of thermal treatment	94
4.20	DTG traces of ML10 samples, before and after 1000 hours of thermal treatment	95
4.21	Activation energy calculation for decomposition of pure sample	96
4.22	DSC scans of untreated and treated pure samples	97
4.23	DSC scans of untreated and treated ML10 samples	98
4.24	SEM image of samples (a) pure HDPE (b) ML10 (c) MP10 (d) MS10 before treatment	99
4.25	SEM image of samples (a) pure HDPE (b) ML10 (c) MP10	100

	(d) MS10 after 1000 hours of thermal treatment	
4.26	FTIR spectra of MP10 samples, before (lower trace) and after (upper trace) accelerated weathering	102
4.27	Carbonyl index of various samples during accelerated weathering	103
4.28	Tensile strength of HDPE containing manganese laurate during accelerated weathering	105
4.29	Tensile strength of HDPE containing manganese palmitate during accelerated weathering	105
4.30	Tensile strength of HDPE containing manganese stearate during accelerated weathering	106
4.31	Tensile modulus of HDPE containing manganese laurate during accelerated weathering	108
4.32	Tensile modulus of HDPE containing manganese palmitate during accelerated weathering	109
4.33	Tensile modulus of HDPE containing manganese stearate during accelerated weathering	109
4.34	Elongation at break of HDPE containing manganese laurate during accelerated weathering	110
4.35	Elongation at break of HDPE containing manganese palmitate during accelerated weathering	111
4.36	Elongation at break of HDPE containing manganese stearate during accelerated weathering	111
4.37	Molecular weight of various samples during accelerated weathering	113
4.38	MFI of samples during accelerated weathering	114
4.39	TG scans of pure samples before and after accelerated weathering	115
4.40	DTG scans of pure samples before and after accelerated weathering	116
4.41	TG scans of MP10 samples before and after accelerated weathering	116
4.42	DTG scans of MP10 samples before and after accelerated weathering	117
4.43	DSC scans of pure samples, before and after accelerated weathering	118
4.44	DSC scans of MP10 samples, before and after accelerated weathering	119
4.45	XRD traces of pure samples, before and after accelerated weathering	120

4.46	XRD traces of MP10 samples, before and after accelerated weathering	121
4.47	SEM image of samples (a) pure HDPE (b) ML10 (c) MP10 (d) MS10 after 1000 hours of accelerated weathering	122
4.48	FTIR spectra of MS10 samples before (lower trace) and after (upper trace) natural weathering	125
4.49	Carbonyl indexes of various samples during natural weathering	126
4.50	Tensile strength of HDPE containing manganese laurate during natural weathering treatment	128
4.51	Tensile strength of HDPE containing manganese palmitate during natural weathering treatment	129
4.52	Tensile strength of HDPE containing manganese stearate during natural weathering treatment	129
4.53	Tensile modulus of HDPE containing manganese laurate during natural weathering treatment	130
4.54	Tensile modulus of HDPE containing manganese palmitate during natural weathering treatment	131
4.55	Tensile modulus of HDPE containing manganese stearate during natural weathering treatment	131
4.56	Elongation at break of HDPE containing manganese laurate during natural weathering treatment	133
4.57	Elongation at break of HDPE containing manganese palmitate during natural weathering	134
4.58	Elongation at break of HDPE containing manganese stearate during natural weathering	134
4.59	Average molecular weight of samples during natural weathering	135
4.60	MFI of various samples during natural weathering	136
4.61	TG traces of pure samples, before and after 24 weeks of natural weathering	137
4.62	DTG traces of pure samples, before and after 24 weeks of natural weathering	138
4.63	TG traces of MS10 samples, before and after 24 weeks of natural weathering	138
4.64	DTG traces of MS10 samples, before and after 24 weeks of natural weathering	139
4.65	DSC scans of pure samples: before and after 24 weeks of natural weathering	140
4.66	DSC scans of MS10 samples: before and after 24 weeks of	141

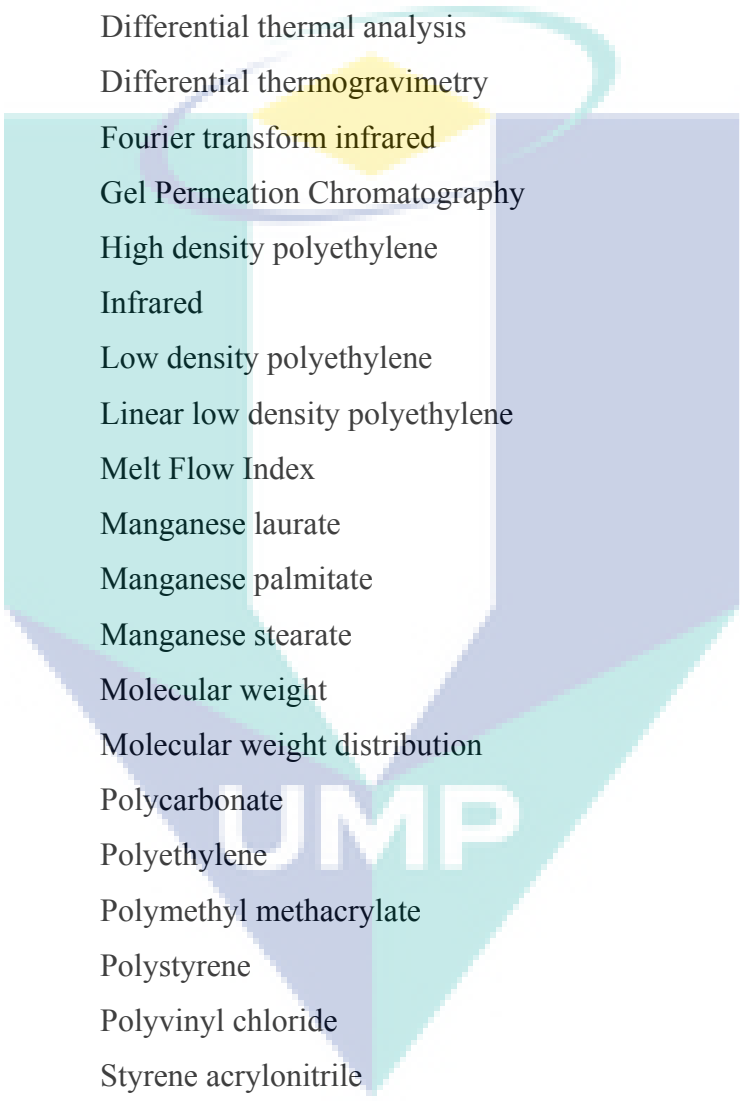
	natural weathering	
4.67	XRD traces of pure samples before and after natural weathering	142
4.68	XRD traces of MS10 samples before and after natural weathering	142
4.69	SEM image of samples (a) pure HDPE (b) ML10 (c) MP10 (d) MS10 after 24 weeks of natural weathering	143
4.70	Comparison of CI after three different treatments	145
4.71	Comparison of losses of elongations at break after three different treatments	145
4.72	MW reductions after three different treatments	146
4.73	TGA traces of MS10 samples before and after three different treatments	147
4.74	DSC scans of MS10 samples before and after three different treatments	148



LIST OF SYMBOL

C	Concentration
E_a	Activation energy, kJ/mol
M_v	Average molecular weight
M_n	Number average
M_w	Weight average
$[\eta]$	Intrinsic viscosity
η_{sp}	Specific viscosity
η_{rel}	Relative viscosity
T_m	Melting temperature, °C
T_g	Glass transition temperature, °C
λ	Wave length of X-ray
d	Interplanar spacing of crystalline material
θ	Diffraction angle
ΔH_f	Heat of fusion, J/g
X_{DSC}	Crystallinity index obtained from DSC scan, %
X_{XRD}	Crystallinity index obtained from XRD trace, %

UMP

LIST OF ABBREVIATION

ASTM	American Society for Testing and Materials
ATR	Attenuated total reflectance
COC	Cyclic olefin copolymer
DSC	Differential scanning calorimetry
DTA	Differential thermal analysis
DTG	Differential thermogravimetry
FTIR	Fourier transform infrared
GPC	Gel Permeation Chromatography
HDPE	High density polyethylene
IR	Infrared
LDPE	Low density polyethylene
LLDPE	Linear low density polyethylene
MFI	Melt Flow Index
ML	Manganese laurate
MP	Manganese palmitate
MS	Manganese stearate
MW	Molecular weight
MWD	Molecular weight distribution
PC	Polycarbonate
PE	Polyethylene
PMMA	Polymethyl methacrylate
PS	Polystyrene
PVC	Polyvinyl chloride
SAN	Styrene acrylonitrile
SEC	Size exclusion chromatography
SEM	Scanning electron microscopy
TGA	Thermogravimetric analysis
TG	Thermogravimetry
XRD	X-ray diffraction

CHAPTER 1

INTRODUCTION

1.1 RESEARCH BACKGROUND

Plastics have achieved almost irreplaceable role in many applications. Almost all aspects of life rely on the plastics. Recently, the usage of plastics increases significantly. Plastics have achieved an irreplaceable position in the packaging industry (Roy et al., 2006a). People rely to plastics in everyday activities, such as jugs, clothes, computer, etc (Bajer et al., 2007; Lokensgard, 2004). Plastics production systematically increases, thus, also amount of plastics waste grows (Bajer et al., 2007).

The world's annual production of polymer resins has experienced a steady growth since the beginning of the century, with growth predicted way into the 21st century. In developed countries, the growth in annual polymer production has diminished somewhat in recent years. However, developing countries in South America and Asia are now starting to experience tremendous growth (Osswald and Menges, 2003). From 2009 to 2010 the global plastics production increased by 15 million tonnes (6%) to 265 million tonnes, confirming the long term trend of plastics production growth of almost 5% per year over the past 20 years. Meanwhile in 2010 Europe accounted for 57 million tonnes (21.5%) of the global production and China overtook Europe as the biggest production region at 23.5% which mainly consisted of HDPE (11%), LDPE-LLDPE (17%), PP (18%) and PVC (8%). Figure 1.1 shows the growth of world plastics production from 1950-2010(PlasticsEurope, 2011).

There are over 18,000 different grades of polymers, available in the US alone. They can be divided into two general categories, thermosetting and thermoplastic polymers. In 1993, 90% of polymers produced in the United States were thermoplastics.

However, in a 1995 worldwide projection, thermoplastics account for 83% of the total polymer production (Osswald et al., 2006).

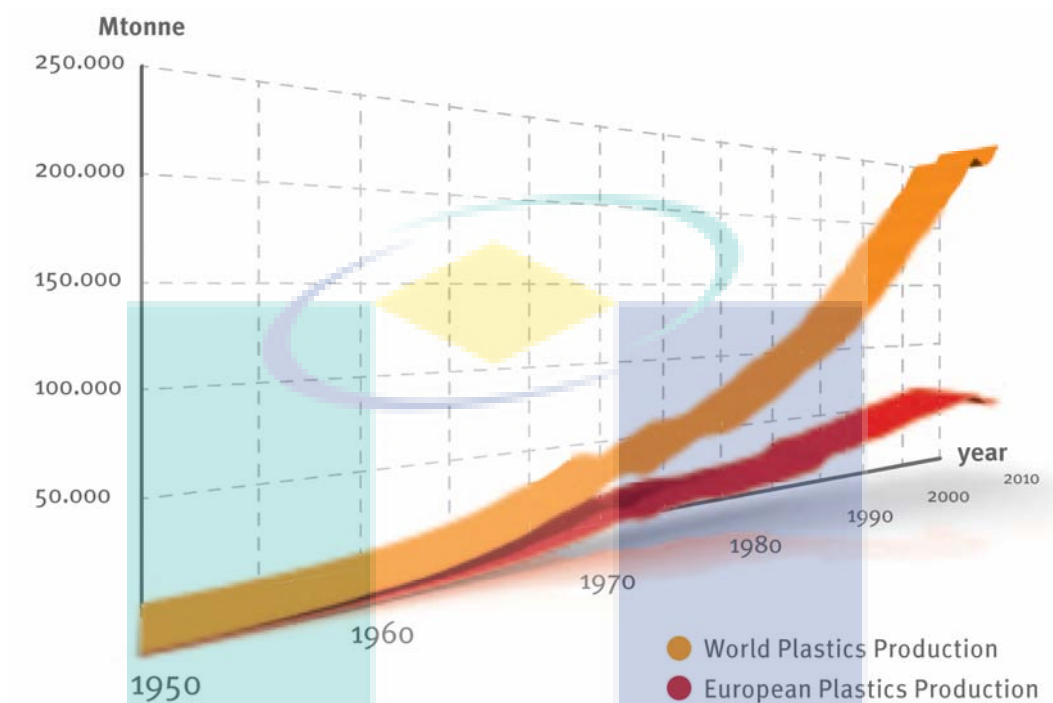


Figure 1.1 World plastics production 1950-2010 (PlasticsEurope, 2011)

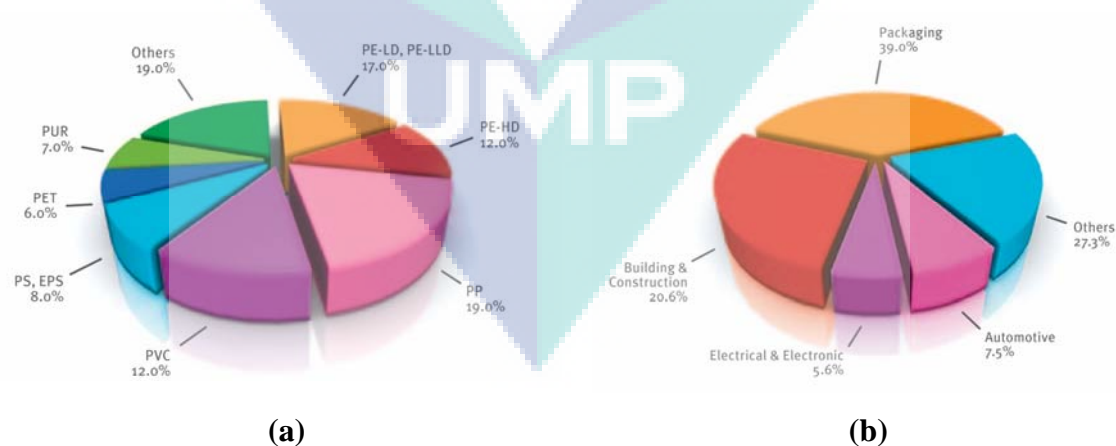


Figure 1.2 Plastics demand by converters 2010 in Europe: (a) breakdown by resin types, (b) breakdown by end use segments

There are five high-volume plastics families; polyethylene (including low density (LDPE), linear low density (LLDPE) and high density (HDPE)), polypropylene (PP), polyvinylchloride (PVC), polystyrene (solid PS and expandable EPS) and

polyethylene terephthalate (PET). Figure 1.2 shows plastics demand in Europe in 2010 (PlasticsEurope, 2011). Other data revealed that in 1999, the principal thermoplastic polymers (LDPE/HDPE, PP, PVC, PS, and PET) consumptions exceeded 28 millions tons in Western Europe, 79% of total plastic markets (thermoplastics and thermosets) in Western Europe and around 90% of total thermoplastics markets (Azapagic et al., 2003). In 2010 together the big five accounted for around 74% of all European plastics demands (PlasticsEurope, 2011).

In 2009 the total consumption of plastics resin in Malaysia accounted for 1.70 million metric tons (MT) (Boon, 2010). Previously total resin consumption accounted for 1.72 million MT in 2005, of which about 65% were polyolefins (PE & PP). Figure 1.3 represents the demand of plastics resin in Malaysia in 2005 by market segments. Packaging application accounted 36 % of total resin consumption (MPMA, 2005).

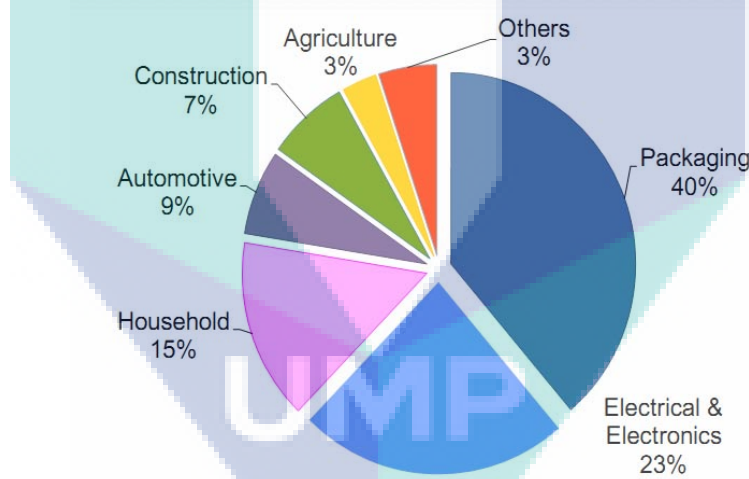


Figure 1.3 Plastics demand in Malaysia 2010 breakdown by market segments of plastics products.

Polyethylene is by far the most widely used polymeric material, accounting for 41% of the US plastic production (Osswald et al., 2006). Consumption of HDPE in United States was predicted that it would increase significantly (Lokensgard, 2004). In US, packaging accounts for over one-third of the captive use of thermoplastics, whereas construction, accounts for about half that number, and transportation account for only 4% of the total captive use of thermoplastics. On the other hand, 69% of the thermosets are used in building and construction, followed by used in transportation (Osswald and

Menges, 2003). Whereas in Europe, packaging remains the biggest end-use for plastics (40%) followed by electrical and electronic (23%), household (15%), automotive (9%), construction (7%), agriculture (3%) and others (3%) (PlasticsEurope, 2011).

Generally, most of packaging applications eventually end up as litter. Griffin (1993) reported that over 50% of the annual tonnages of all manufactured synthetic polymers are applied as packaging materials and that some 90% of this flow finishes as a component of urban garbage. The other report showed that the municipal solid waste stream in the U.S. totals nearly 160 metric tons per year and consists of about 7-11% by weight of post-consumer plastics (Andrady et al., 1993a). In 2001, plastics waste which mainly consisting of PE (above 40 wt %), PVC, PP, and poly-(ethylene terephthalate) had a total volume of 19.2 millions tons, accounting for about 8.4% of total municipal solid waste in the United States (Lei et al., 2007).

Plastic (polymers) is now being viewed as a serious worldwide environmental and health concern, especially for disposable application such as carrier and garbage bags. The increasing utilization of plastics has also caused concern for the role of plastics in environmental pollution (Lokensgard, 2004). Its character of being non-degradable is resulting in river pollution, choking in landfill, and is considered particularly undesirable and a hazard to animal life (Andrady et al., 1993a).

Some methods have been applied in order to reduce the effects of plastics on litter problem. In 1976, the Resource Conservation and Recovery Act (RCRA) promoted reuse, reduction, incineration, and recycling of materials. Recycling is a term generally reserved for post-consumer waste materials (Lokensgard, 2004). Most recycling programs accept plastics number 1 (PETE) and 2 (HDPE). The packaging of HDPE that appears in waste stream is only 25 percent of the total sales in 1993, 1,929,000 metric tons. The other products eventually find their way to landfills or incinerator (Lokensgard, 2004). However, the strategy of reduce, re-use, and recycling which have been introduced and applied widely, only overcome very small part of huge quantity of plastics waste.

1.2 PROBLEM STATEMENT

The growing environmental concern has made plastics a target of much criticism due to their lack of degradability (Albertsson et al., 1992). The large amounts of plastics ending up in the waste stream, has resulted in a trend towards manufacture and development of plastics with accelerated degradation time (Barr-Kumarakulasinghe, 1994).

Degradable polymers are designed to degrade in different ways and in different environments. An important distinction needs to be made between biodegradable plastics, i.e. those that capable of undergoing decomposition into carbon dioxide, methane, water, inorganic compounds, or biomass in which the predominant mechanism is the enzymatic action of microorganisms (bacteria, fungi, algae), and oxo-biodegradable plastics, which oxidize and embrittle in the environment and erode under the influence of ultraviolet (UV) light and heat (Excelplas, 2003).

The transition metals (Ti, V, Cr, Mn, Fe, Co, Ni, Cu, Zn) could be considered for use in initiating degradation of polymers (Griffin, 1993; Osawa et al., 1979; Poyner and Cakraborty, 1993). Many studies mostly utilized cobalt-based additives for LDPE or LLDPE (Bikiaris et al., 1997; Roy et al., 2006a; Roy et al., 2007a; Roy et al., 2006b; Roy et al., 2007b; Roy et al., 2007c). The other studies utilized other transition metals, such as iron and calcium (Pablos et al., 2010) and manganese (Erlandsson et al., 1997; Khabbaz et al., 1999; Sharma et al., 2001) for LDPE. Manganese is close to cobalt in periodic table, having almost same atomic number with cobalt. Manganese is more available in the nature and cheaper than cobalt (Hartman, 1992). Moreover, most studies on degradation have focused on LDPE.

The study on effects of manganese carboxylates i.e. manganese laurate, manganese palmitate and manganese stearate on the degradation of HDPE during accelerated weathering and natural weathering under weather conditions of Gambang, Malaysia especially, and generally Peninsular Malaysia, hasn't been existed yet. Malaysia represents tropical area. In addition, HDPE is also widely applied for post consumer products, like: packaging, plastic mulch, bottle etc. However, only few studies on degradation have focused on HDPE due to its high crystallinity, therefore it is

more difficult to degrade than one with low crystallinity. This research studies the synthesis of manganese carboxylates and the effects of manganese carboxylates on the degradation of HDPE. This study also compares the performances of manganese carboxylates i.e manganese laurate, manganese palmitate and manganese stearate on accelerating degradation of HDPE under accelerated weathering and natural weathering under weather conditions of Gampang, Malaysia.

1.3 OBJECTIVE OF RESEARCH

This research has objectives as listed below:

1. To synthesize manganese carboxylates and study their characteristics
2. To investigate the characteristics of manganese carboxylates-HDPE blends.
3. To study the effects of manganese carboxylates in accelerating degradation of HDPE under thermal treatment
4. To study the effect of manganese carboxylates on the degradation of HDPE during accelerated weathering treatment.
5. To study degradation behavior of HDPE containing manganese carboxylates during natural weathering, particularly in Gampang, Malaysia

1.4 SCOPE OF RESEARCH

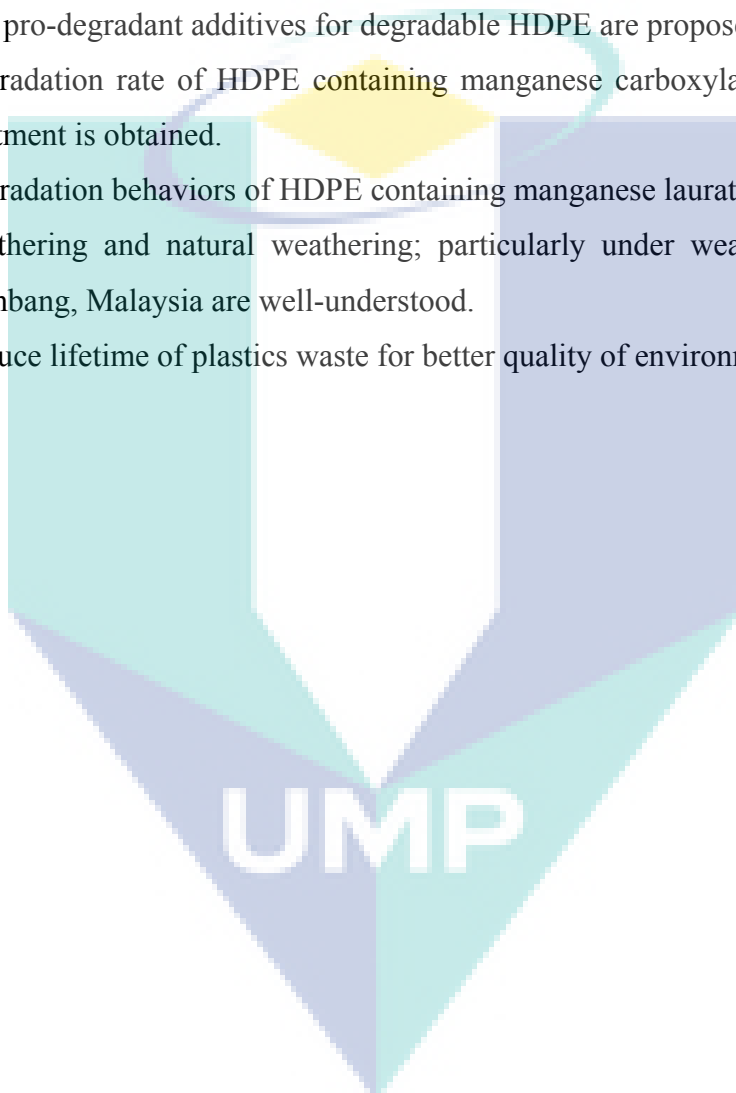
The scopes of this research consist of:

1. Synthesis of manganese carboxylates.
2. Characterization of manganese carboxylates.
3. Compounding of manganese carboxylates and HDPE resins.
4. Specimen molding (injection molding)
5. Investigate the effects of manganese carboxylates on properties of HDPE
6. Thermal treatment of HDPE containing manganese carboxylates and its effect on properties of HDPE.
7. Accelerated weathering of HDPE containing manganese carboxylates and its effect on properties of HDPE.
8. Natural weathering of HDPE containing manganese carboxylates and its effect on properties of HDPE.

1.5 CONTRIBUTION OF RESEARCH

The main outputs of this research are:

1. The synthesis methods of manganese carboxylates are developed.
2. Characterization of manganese carboxylates in terms of their physical and chemical properties is obtained.
3. The pro-degradant additives for degradable HDPE are proposed and developed.
4. Degradation rate of HDPE containing manganese carboxylates during thermal treatment is obtained.
5. Degradation behaviors of HDPE containing manganese laurate under accelerated weathering and natural weathering; particularly under weather conditions of Gombang, Malaysia are well-understood.
6. Reduce lifetime of plastics waste for better quality of environment.



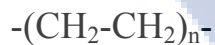
CHAPTER 2

LITERATURE REVIEW

2.1 INTRODUCTION TO PLASTICS

Plastics are polymeric materials with properties that are between those of elastomers and fibers. Elastomers are giant molecules possessing what is referred to as memory that they can be deformed, misshaped, and stretched, and after applied stressing force is removed, they return to their original, pre-stressed shape. Fibers possess high tensile strength and high modulus (high stress for small strains, i.e. stiffness) related to a relatively high degree of crystallinity. Plastics exhibit some flexibility and hardness and varying degrees of crystallinity (Carragher Jr., 2003).

Polymers are very large molecules (macromolecules) that are comprised or built up of smaller units or monomers. This monomer term is also used to indicate the basic chemical compound from which the polymer is polymerized. For example, the polymer polyethylene is produced from the monomer ethylene. It is usual to represent such a polymer in terms of its chemical repeat unit, as follows:



where n , which is the number of repeating units, can be large (ASM International, 2003; Painter and Coleman, 1997).

Polymers can be placed into thermoplastic, thermoset, or elastomer category. Thermoplastics are those polymers that solidify as they cooled no longer allowing the long molecules to move freely. When heated, these materials regain the ability to flow, as the molecules are able to slide past each other with ease. Thermosetting polymers solidify by being chemically cured. Here, the long macromolecules cross-link with each other during cure, resulting in a network of molecules that cannot slide past each other.

The formation of these networks causes the materials to lose the ability to flow even after reheating. Compared to thermosets, elastomers are only lightly cross-linked which permits almost full extension of the molecules. However, the links across the molecules hinder them from sliding past each other, making even large deformations reversible. They are very soft and very compliant elastic materials (Osswald and Menges, 2003).

Thermoplastic polymers are divided into two classes: amorphous and semi-crystalline polymers. The most common semi-crystalline thermoplastics are high density polyethylene, low density polyethylene, polypropylene, polytetrafluoroethylene, polyamide (Carragher Jr., 2003; Osswald and Menges, 2003). Amorphous polymers form large group of materials, including glassy, brittle polymers (such as polystyrene (PS), polymethyl methacrylate (PMMA), styrene acrylonitrile (SAN), and cyclic olefin copolymer (COC)) and ductile polymers (such as polyvinyl chloride (PVC) and polycarbonate (PC)). The characteristic that such polymers have in common is their “amorphous” structure, which means that they do not exhibit any crystalline structure in X-ray or electron scattering experiments (Michler, 2008)

2.2 POLYETHYLENE

Polyethylene (PE) (sometimes known as polythene) was discovered in 1933 by Reginald Gibson and Eric Fawcett at the British industrial giant. Imperial Chemical Industries (ICI) (Vasile and Pascu, 2005). In its simplest form a polyethylene molecule consists of a long backbone of an even number of covalently linked carbon atoms with a pair of hydrogen atoms attached to each carbon; chain ends are terminated by methyl groups. This structure is shown schematically in Figure 2.1 (Peacock, 2000), and the simple molecular structure is presented in Figure 2.2 (ASM International, 2003).

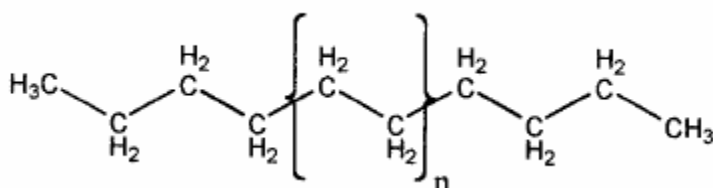


Figure 2.1 Chemical structure of polyethylene

Chemically pure polyethylene resins consist of alkanes with the formula $C_{2n}H_{4n+2}$, where n is the degree of polymerization, i.e. the number of ethylene monomers polymerized to form the chain. Unlike conventional organic materials, polyethylene does not consist of identical molecules. Polyethylene resins comprise chains with a range of backbone lengths. Typically the degree of polymerization is well in excess of 100 and can be as high as 250,000 or more, equating to molecular weights varying from 1400 to more than 3,500,000. Low molecular weight polyethylenes (oligomers) with a degree of polymerization between 8 and 100 are waxy solids that do not possess the properties generally associated with a plastic. When the degree of polymerization is less than 8, alkanes are gases or liquids at ordinary temperatures and pressures. Polyethylene molecules can be branched to various degrees and contain small amounts of unsaturation (Peacock, 2000).

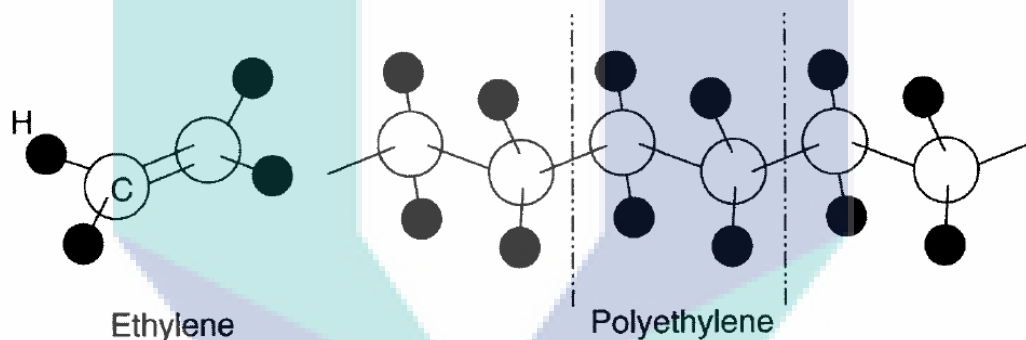


Figure 2.2 Molecular structure of polyethylene

Polyethylene is synthesized in several ways and resulting in different types of polyethylene. The branched polyethylene is called low density, high pressure polyethylene because of high pressure usually employed for its production; and because of the presence of the branches, the chains are not able to closely pack, leaving voids and subsequently producing a material that has a lower density in comparison to low-branched polyethylene. The other type of polyethylene is synthesized at much lower pressure and temperatures. This polyethylene has fewer branches and a higher softener temperature (above 100°C) (Carragher Jr., 2003).

2.2.1 Classification of Polyethylene

Many types of polyethylene exist, all having essentially the same backbone of covalently linked carbon atoms with pendant hydrogens; variations arise chiefly from branches that modify the nature of the material (Peacock, 2000). Branching interferes with intermolecular bonding and has a significant effect on rheology and crystallinity. Branching lowers dimensional stability and reduces the glass-transition temperature (T_g) with other major factors (i.e. MW and MWD) being constant. At a particular molecular weight, branching may also lead to a decrease in the melting temperature (T_m) of thermoplastics. Increased branching in polymers also decreases their ability to conduct heat. The increase in free volume from branching lowers the efficiency of thermal conduction due to a more tortuous path for heat conduction along primary valence bonds (ASM International, 2003).

Polyethylene (PE) is a good example of how branching influences properties of thermoplastics. There are a number of principal grades of polyethylene e.g. high density (HDPE), low density (LDPE), and linear low density (LLDPE). Structurally, these grades differ in the degree and type of branching on the main chain and in overall molecular weight (ASM International, 2003). Figure 2.3 shows the molecular structure of high density, low density, and linear low density polyethylene (Peacock, 2000).

High Density Polyethylene

High density polyethylene (HDPE) is chemically the closest in structure to pure polyethylene. It consists primarily of unbranched molecules with very few flaws to mar its linearity. With an extremely low level of defects to hinder organization, a high degree of crystallinity can be achieved, resulting in resins that have a high density (relative to other types of polyethylene). Some resins of this type are copolymerized with a very small concentration of 1-alkenes in order to reduce the crystallinity level slightly. High density polyethylene resins typically have densities falling in the range of approximately 0.94–0.97 g/cm³. Due to its very low level of branching, high density polyethylene is sometimes referred to as linear polyethylene (LPE) (Peacock, 2000). The high density polyethylene has between 5 and 10 short branches every 1000 carbon atoms (Osswald and Menges, 2003).

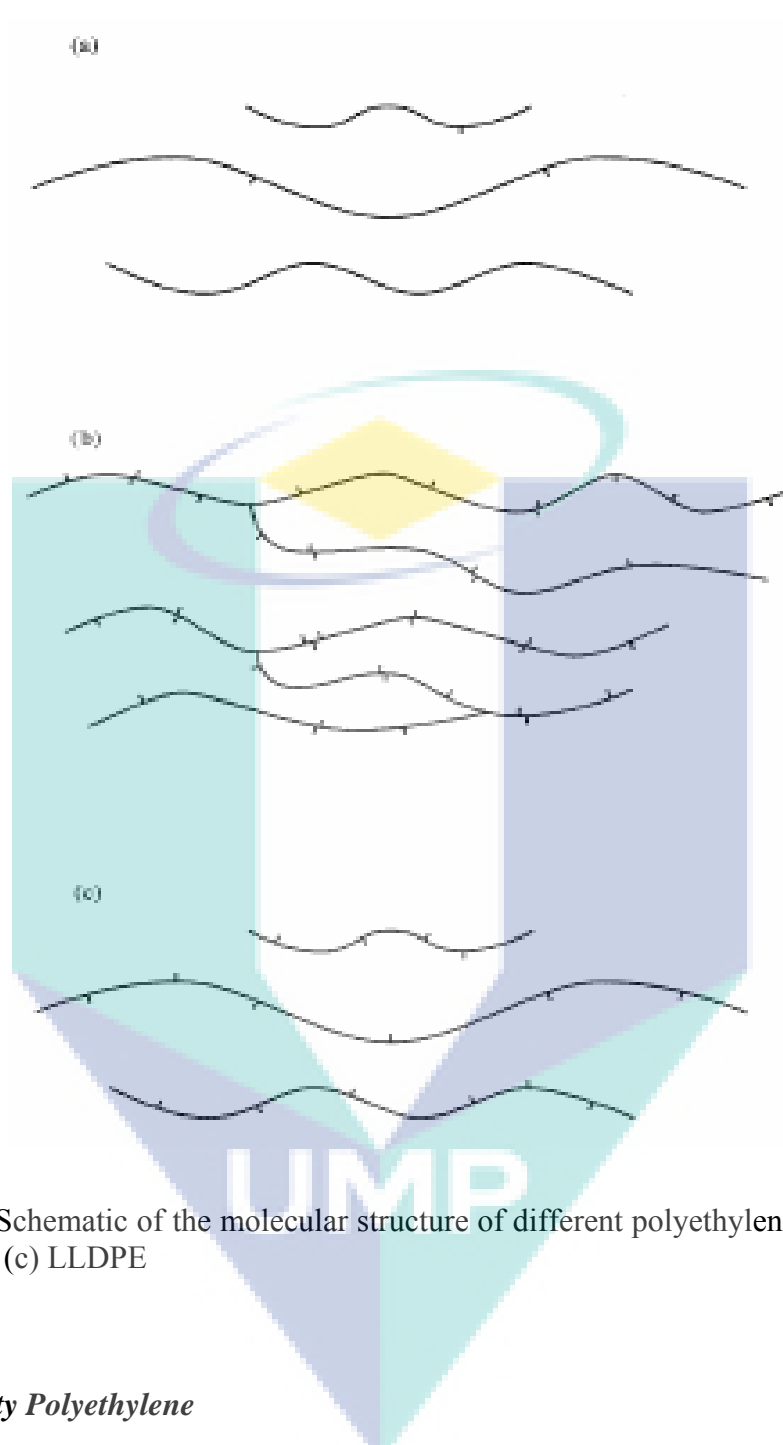


Figure 2.3 Schematic of the molecular structure of different polyethylene (a) HDPE, (b) LDPE, and (c) LLDPE

Low Density Polyethylene

Low density polyethylene (LDPE) is so named because such polymers contain substantial concentrations of branches that hinder the crystallization process, resulting in relatively low densities. The branches primarily consist of ethyl and butyl groups together with some long chain branches. Due to the nature of the high pressure polymerization process by which low density polyethylene is produced, the ethyl and butyl branches are frequently clustered together, separated by lengthy runs of unbranched backbone. Long-chain branches occur at random intervals along the length

of the main chain. The long-chain branches can themselves in turn be branched. The numerous branches characteristic of low density polyethylene molecules inhibit their ability to crystallize, reducing resin density relative to high density polyethylene. Low density polyethylene resins typically have densities falling in the range of approximately $0.90\text{--}0.94\text{ g/cm}^3$ (Peacock, 2000). The branches of low density polyethylene are mostly much longer than those of HDPE and are themselves usually branched (Osswald and Menges, 2003).

Linear Low Density Polyethylene

Linear low density polyethylene (LLDPE) resins consist of molecules with linear polyethylene backbones to which are attached short alkyl groups at random intervals. These materials are produced by the copolymerization of ethylene with 1-alkenes. The branches most commonly encountered are ethyl, butyl, or hexyl groups but can be a variety of other alkyl groups, both linear and branched. A typical average separation of branches along the main chain is 25–100 carbon atoms. Linear low density polyethylene resins may also contain small levels of long chain branching, but there is not the same degree of branching complexity as is found in low density polyethylene. Chemically these resins can be thought of as a compromise between linear polyethylene and low density polyethylene, hence the name. The branches hinder crystallization to some extent, reducing density relative to high density polyethylene. The result is a density range of approximately $0.90\text{--}0.94\text{ g/cm}^3$ (Peacock, 2000). The LLDPE has between 10 and 35 short chains every 1000 carbon atoms. Polymer chains with fewer and shorter branches can crystallize with more ease, resulting in higher density (Osswald and Menges, 2003).

2.2.2 Properties of Typical Polyethylene and Their Applications

Branching of the polymer chains influences the final structure, crystallinity, and properties of the polymer material (Osswald and Menges, 2003). At a particular molecular weight, branching leads to a decrease in T_m . Therefore, the orientation of high-molecular, linear chains can lead to an exceptionally high T_m . For example, ultra high molecular weight polyethylene (UHMWPE), with almost perfect chains, displays the highest T_m of the different PE grades with a T_m of about $150\text{ }^\circ\text{C}$ ($300\text{ }^\circ\text{F}$) and a crystallinity exceeding 70%. On the other extreme, LDPE has randomly displaced

branches and a T_m of about 100°C and crystallinity of less than 50% (ASM International, 2003). Properties of typical polyethylene are presented in Table 2.1 (Peacock, 2000).

Table 2.1 Main properties of typical polyethylene

Property	HDPE	LDPE	LLDPE
Density, (g/cm ³)	0.94-0.97	0.91-0.94	0.90-0.94
Degree of crystallinity (from calorimetry) (%)	55-77	30-54	22-55
Tensile yield stress (MPa)	17.92-31.02	8.96-19.30	7.58-19.30
Tensile strength at break (MPa)	22.06-31.02	8.27-31.02	13.10-44.81
Elongation at break (%)	10-1500	100-650	100-950
Melting temperature (°C)	125-132	98-125	100-125
Heat of fusion (cal/g)	38-53	21-37	15-43

The specific properties of polyethylene lead to their specific applications. The applications of HDPE comprise pipe and pipe fittings for water, petroleum tanks, toys, bowls, buckets, milk bottles, crates, films for packaging, blown bottle for foods, carrier bags, food wrapping material etc. LDPE is mostly applied as heavy duty sacks, general packaging, carrier bags, films or sheets for packaging, disposable goods, gloves, squeeze bottles. LLDPE is applied for packaging particularly film for bags and sheets, cable covering, lids, buckets and containers, pipe. Lower thickness (gauge) may be used compared to LDPE (Vasile and Pascu, 2005).

2.3 PROCESSING METHOD OF PLASTICS

Plastics processing is a form conversion process. The material that enters the process as plastic pellets or powder is basically the same material that exits the process as a plastic part. The plastic process converts the shape of the plastic material. However, this simple explanation of plastic processing needs to be slightly modified. Although the plastic entering the process is the same plastic exiting the process, the properties of the plastic material may be affected by the rigorous activities that occur during the process. The resulting properties of the plastic part may be different from the properties of the plastic material as defined by the plastic material manufacturer. Each processing method can have a different effect on the final properties (ASM International, 2003).

2.3.1 Compounding

The process of extrusion is similar to the squeezing of toothpaste or forming of spaghetti. As the viscosity of most plastic melt is high, extrusion requires the production of pressure in order to force the melt through the die. A screw pushes thermoplastic granules or powder through a heated cylinder, changing the plastic from solid to liquid and mixing the plastics as it moves through the barrel, then through the die which will give the plastic a constant cross section area. The plastic is melted in the barrel by the mechanical energy from the rotating screws and the heat, transferred from the high temperature barrels. There are two common types of extruders, single screw and double screw extruder. For single screw extruders, friction between the plastic and the rotating screw makes the resin rotate with the screw. The friction between the rotating resin and the barrel pushes the materials forward and generate heat. Single screw extruders are not positive displacement, so they are not effective mixing device (Beg, 2008; Todd, 2000).

A twin screw extruder is a compounding device to uniformly blend plasticizers, fillers etc. into the plastic melt. Twin screw extruders have intermeshing screws, the relative motion of the flight of one screw inside the channel of another, pushes the material forward with very low friction. Heat is controlled from an outside force and is not controlled by the speed (Todd, 2000).

2.3.2 Injection Molding

Injection molding is the most widely used polymeric fabrication process. A large force must be used to inject polymer into the hollow mould cavity. More melt must be packed into the mould during solidification to avoid shrinkage in the mould. Identical parts are produced through a cycle process involving the melting of pellet or powder resin followed by the injection of the polymer melt into the hollow mould cavity under higher pressure. Injection molding can be used to form a wide variety of products, for both thermosets and plastics. Complexity is virtually unlimited, sizes can vary and excellent tolerance is also possible (Beg, 2008).

Extrusion is used prior to injection molding when mixing of a thermoplastic, filler and additive is required. Pellets of the compounded mix are then fed into the hopper

are melted, the liquid melt is then injected into the closed mould cavity with a force. The melt is then allowed to cool and solidify before the mould is opened and the final product removed. The process can then be repeated (ASM International, 1988; Beg, 2008).

Advantages and disadvantages of injection molding are as follows (http://www.jobwerx.com/resources/injection_molding.html):

Advantages:

- High production rates
- Design flexibility
- Repeatability within tolerances
- Can process a wide range of materials
- Relatively low labor
- Little to no finishing of parts required
- Minimum scrap losses

Disadvantages:

- High initial equipment investment
- High start-up and running costs possible
- Part must be designed for effective molding
- Accurate cost prediction for molding job is difficult

2.4 POLYETHYLENE PROPERTIES AND TESTING

2.4.1 Fourier Transform Infrared Spectroscopy

Fourier transform infrared spectroscopy (FTIR) is the most widely used vibrational spectroscopic technique. FTIR is an infrared spectroscopy in which the Fourier transform method is used to obtain an infrared spectrum in a whole range of wavenumbers simultaneously (Leng, 2008). FTIR is commonly used in analysis of functional group of polymer. This method can detect the types of functionalities in the polymer structure e.g. (-CH₂), (-CH₃), or carbonyl (-C=O). Thus the changes of functionalities can be traced by using this analysis.

2.4.1.1 Fourier Transform Infrared Examination Techniques

There are two examination techniques in FTIR analysis, i.e. transmittance and reflectance (Gulmine et al., 2002; Leng, 2008). The technique used depends on the type of sample. The appropriate technique will result in an accurate spectrum.

Transmittance

The transmittance examination technique refers to the method of obtaining an infrared spectrum by passing an IR beam through a sample. It is most commonly used examination method in FTIR for two reasons. First, the transmittance technique generates high signal-to-noise ratios, and second, it is suitable for samples in any solid or liquid phases. Its main disadvantage is the thickness limitation of samples. A thick sample will absorb so much of the infrared radiation that detecting infrared transmission becomes impossible. Generally, for transmission examination, the sample thickness should not be more than 20 μm . On the other hand, sample that is too thin ($< 1 \mu\text{m}$) yields absorption bands too weak to be detected.

Solid samples for transmittance examination can be in one of two forms: thin film or powder. Thin film samples are mainly polymeric materials. Casting films with polymer solutions is commonly used method. Polymer films can also be made by mechanically pressing under elevated temperatures. Powder samples are made by grinding solid to powder and then diluting the powder with infrared-inert matrix materials. The common method for preparing powder samples is by making KBr pellets since KBr is transparent to infrared light. To make pellets, a solid sample and KBr are grinded together to obtain powder particles with size less than 2 μm diameter. Then, the powder mixture is die-pressed to form a pellet (Leng, 2008).

Reflectance

Reflectance examination techniques refer to methods for obtaining an infrared spectrum by reflecting IR radiation from a solid or liquid sample. The main advantage is that bulk and coating samples can be examined without destructive. These techniques are especially attractive for solid samples that are difficult to grind into powder and for

fast sample examination. However, reflectance techniques are less popular than transmission because of the following disadvantages. First, infrared radiation has limited penetration into the sample. A reflectance spectrum can only contain the infrared signals from the top 1 to 10 μm of a solid sample surface. This is a serious deficiency for sample with possible chemical change near its surface, and for quantitative analysis for which the exact pass-length of the infrared light in the sample must be known. Second, it is more difficult to capture reflected infrared light than transmitted light. A reflectance spectrum will show much more noise than the transmission spectrum for the same duration of examination. Third, reflectance techniques require special accessories, making the instrumentation more complicated and expensive (Leng, 2008).

Reflectance techniques may be used for samples that are difficult to analyze by the conventional transmittance methods. Reflectance methods can be divided into two categories. Internal reflectance measurements can be made by using an attenuated total reflectance cell in contact with the sample. There is also a variety of external reflectance measurements which involve an infrared beam reflected directly from the sample surface. There are three types of reflectance techniques: specular, diffuse and attenuated total reflectance (ATR). Specular reflectance is applied to samples with smooth and polished surfaces; diffuse reflectance is applied to samples with rough surfaces or powder (Leng, 2008; Stuart, 2005). ATR technique is suitable for examining thick samples e.g. sheet (Gulmine et al., 2002).

ATR is a type of internal reflection spectroscopy in which the sample is placed in contact with an internal reflection element (IRE) of high refractive index. Infrared radiation is focused onto the edge of the IRE, reflected through the IRE, and then directed to a suitable detector (Hind et al., 2001). The IRE is commonly called as ATR crystal. The crystals used in ATR cells are made from materials that have low solubility in water and are of a very high refractive index. Such materials include zinc selenide (ZnSe), germanium (Ge) and thallium-iodide (KRS-5) (Stuart, 2005).

ATR (attenuated total reflectance)-FTIR spectroscopy is a useful technique to study of samples showing large absorptivities in the mid-infrared spectral range. Due to

the low penetration depth of the radiation experienced with this technique mainly surface degradation can be studied (Gulmine et al., 2003).

2.4.1.2 Fourier Transform Infrared Spectra

For a molecule to show infrared absorptions it must possess a specific feature, i.e. an electric dipole moment of the molecule must change during the vibration. Infrared absorptions are not infinitely narrow and there are several factors that contribute to the broadening, e.g. collisions between molecules, Doppler effect (in which radiation is shifted in frequency when the radiation source is moving towards or away from the observer). The interactions of infrared radiation with matter may be understood in terms of changes in molecular dipoles associated with vibrations and rotations. Vibrations can involve either a change in bond length (stretching) or bond angle (bending). Some bonds can stretch in-phase (symmetrical stretching) or out-of-phase (asymmetric stretching). If a molecule has different terminal atoms such as HCN, ClCN or ONCl, then the two stretching modes are no longer symmetric and asymmetric vibrations of similar bonds, but will have varying proportions of the stretching motion of each group. In other words, the amount of coupling will vary. Bending vibrations also contribute to infrared spectra. It is best to consider the molecule being cut by a plane through the hydrogen atoms and the carbon atom. The hydrogens can move in the same direction or in opposite directions in this plane, here the plane of the page. For more complex molecules, the analysis becomes simpler since hydrogen atoms may be considered in isolation because they are usually attached to more massive, and therefore, more rigid parts of the molecule. This results in in-plane and out-of-plane bending vibrations (Stuart, 2005).

A FTIR spectrum represents absorbance arise from the material tested. An infrared spectrum converted from an interferogram by Fourier transform is called a single beam spectrum. A single beam spectrum includes both spectra from the sample and background. The background spectrum contains only the information from the instrument and atmosphere. The instrument contributions to background spectrum are from the detector, beam splitter, mirror and the IR source. The atmospheric contributions are mainly from water vapor and carbon dioxide. An FTIR spectrum is commonly expressed as a transmittance spectrum, in which vibration band peaks point

downward. It can also be expressed as an absorbance spectrum, in which vibration band peaks point upward (Leng, 2008).

The infrared spectrum can be divided into three main regions: the far infrared ($<400\text{ cm}^{-1}$), the mid-infrared ($4000\text{--}400\text{ cm}^{-1}$) and the near-infrared ($13000\text{--}4000\text{ cm}^{-1}$). Many infrared applications employ the mid-infrared region, but the near- and far-infrared regions also provide important information about certain materials. Generally, there are less infrared bands in the $4000\text{--}1800\text{ cm}^{-1}$ region with many bands between 1800 and 400 cm^{-1} . Sometimes, the scale is changed so that the region between 4000 and 1800 cm^{-1} is contracted and the region between 1800 and 400 cm^{-1} is expanded to emphasize features of interest (Stuart, 2005).

FTIR spectrum of polyethylene has main absorptions: CH_2 asymmetric stretching (2919 cm^{-1}); CH_2 symmetric stretching (2851 cm^{-1}); CH_2 bending deformation (1473 and 1463 cm^{-1}); CH_3 symmetric deformation (1377 cm^{-1}) (Gulmine et al., 2002) or (1375 cm^{-1}) (Andrady et al., 1993b), wagging deformation (1366 and 1351 cm^{-1}); twisting deformation (1306 cm^{-1}); wagging deformation (1176 cm^{-1}); and (rocking deformation ($731\text{--}720\text{ cm}^{-1}$) (Gulmine et al., 2002).

2.4.2 Tensile Properties

Several different types of mechanical properties are used to characterize polymers, but three important properties of load-bearing polymers (plastics) are usually stiffness, strength, and toughness (ASM International, 2003). The presence of crystalline phase enables polyethylene to retain its mechanical strength over a large temperature range. Probably the most important and significant single mechanical measurement to be made on PE is the determination of elastic modulus or stiffness. Highly branched PE possesses lower modulus than the linear one (Vasile and Pascu, 2005). The crystallinity level has a pronounced effect on the stiffness (Peacock, 2000). Yield strength, tensile strength, and elongation at break are mechanical properties that are particularly important in terms of practical applications. These are commonly determined from stress-strain curves (Vasile and Pascu, 2005).

Tensile testing is one of the most common forms of physical testing performed on polyethylene samples. The data available from such testing are extremely informative with regard to both applications and fundamental knowledge. It should be recognized that, due to the variety of morphologies associated with polyethylene, there is no typical force versus elongation curve applicable to all samples (Peacock, 2000).

Plastics are viscoelastic materials, in which mechanical deformation can be very dependent on temperature as well as time. The time dependence can be broken down in terms of the rate at which a stress is applied, the duration of the applied stress, and the overall stress history. The short-term tensile test (ASTM D 638 and ISO 517) is one of the most widely used mechanical tests of plastics for determining mechanical properties such as tensile strength, yield strength, yield point, and elongation. The stress-strain curve from tension testing is also a convenient way to classify plastics (ASM International, 2003).

Three typically different types of stress–strain behavior are found for polymeric materials, as represented in Figure 2.4. Curve *A* illustrates the stress–strain character for a brittle polymer, it fractures while deforming elastically. The behavior for a plastic material, curve *B*, is similar to that for many metallic materials; the initial deformation is elastic, which is followed by yielding and a region of plastic deformation. Finally, the deformation displayed by curve *C* is totally elastic; this rubber-like elasticity (large recoverable strains produced at low stress levels) is displayed by a class of polymers termed the elastomer. The mechanical characteristics of polymers are much more sensitive to temperature changes near room temperature. The influence of strain rate on the mechanical behavior may also be important. In general, decreasing the rate of deformation has the same influence on the stress–strain characteristics as increasing the temperature; that is, the material becomes softer and more ductile (Callister and Rethwisch, 2011).

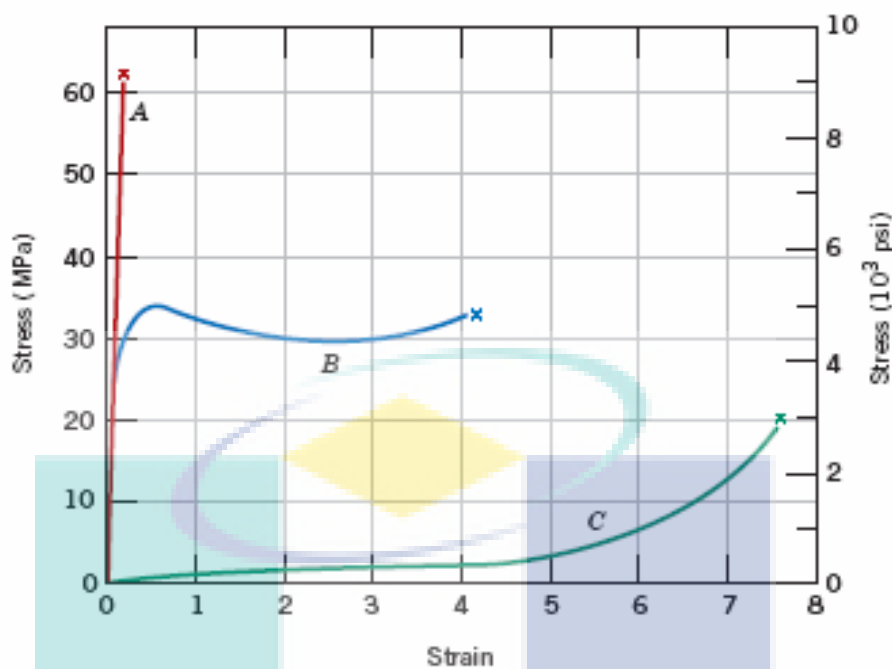


Figure 2.4 The stress-strain behavior for brittle (curve A), plastics (curve B), and highly elastic (elastomeric) (curve C) polymers.

The elongation at break of a polyethylene sample is reported as the observed strain (ϵ), percent strain. Ideally the elongation at break would be measured directly with an extensometer. However, it is more common to assume that all deformation occurs within the gauge region of the sample and to calculate the elongation based upon crosshead displacement as a function of the initial gauge length (Peacock, 2000).

2.4.3 Molecular Weight

Pure low-molecular-weight organic compounds are monodisperse, i.e. all the molecules in any sample of pure material have identical molecular weight (M). In contrast, polydispersity is a characteristic of most macromolecules (Seymour, 1971). A typical synthetic polymer sample contains with a wide distribution of chain lengths. This distribution is seldom symmetric and contains some molecules of very high molecular weight. The exact breadth of molecular weight distribution depends upon the specific conditions of polymerization (Fried, 1995). Hence, the polymer scientist is usually concerned with an average molecular weight (\bar{M}). It is necessary to define an average molecular weight to characterize an individual polymer sample (Fried, 1995; Seymour, 1971).

In general, properties such as density, refractive index, and hardness of high polymers are essentially independent of molecular weight. However, properties of amorphous polymers, such as melt viscosity, softening temperature, tensile and impact strengths, and heat resistance, are related to the length of polymer chain. Tensile and impact strength properties increase rapidly as the chain length increases. The melt viscosity continues to increase rapidly as the molecular weight increases. Since polymers with very high molecular weight are difficult to process and fabricate, an appropriate compromise is usually made between maximum physical properties and processibility (Seymour, 1971). Polyethylene has a wide range of molecular weight, depending on its type. For example, the molecular weight of some types of HDPE is in a range of $1-5 \times 10^5$ (Liang et al., 2008), whereas LDPE has average molecular weight up to 60,000 (Bashford, 1997).

2.4.3.1 Average Molecular Weight

There are several important molecular-weight averages, namely: number average molecular weight, weight average molecular weight, and viscosity average molecular weight. For a discrete distribution of molecular weights, an average molecular weight, \bar{M} , may be defined as

$$\bar{M} = \frac{\sum_i N_i M_i^\alpha}{\sum_i N_i M_i^{\alpha-1}} \quad (2.1)$$

Where N_i indicates the number of moles of molecules with molecular weight of M_i and the parameter α is a weighing factor that defines a particular average of the molecular-weight distribution. The molecular weight averages that are important in determining polymer properties are the number average, \bar{M}_n ($\alpha=1$) and the weight average, \bar{M}_w ($\alpha=2$) (Fried, 1995).

$$\bar{M}_n = \frac{\sum_{i=1}^N N_i M_i}{\sum_{i=1}^N N_i} \quad (2.2)$$

$$\overline{M}_w = \frac{\sum_{i=1}^N N_i M_i^2}{\sum_{i=1}^N N_i M_i} \quad (2.3)$$

The average molecular weight values (\overline{M}_v) obtained by viscosity techniques are between the number average (\overline{M}_n) and weight average (\overline{M}_w) and closer to the latter. The number average molecular weight (\overline{M}_n) or arithmetic mean may be obtained by actually counting the molecules (Seymour, 1971).

A measure of the breadth of molecular weight distribution is given by the ratios of molecular weight averages. For this purpose, the most commonly used ratio is $\overline{M}_w/\overline{M}_n$, which is called the polydispersity index or PDI. The PDIs of commercial polymers vary widely. For example, commercial grades of polystyrene with a \overline{M}_n of over 100,000 have polydispersities indices between 2 and 5, while polyethylene may have a PDIs as high as 30 (Fried, 1995).

2.4.3.2 Method of Average Molecular Weight Measurement

Since commercial synthetic polymers have broad distributions of molecular weight and it is therefore necessary to report an average molecular weight when characterizing a sample. Absolute values of \overline{M}_n and \overline{M}_w can be obtained by primary characterization methods of osmometry and scattering, respectively. There are a number of secondary methods by which average molecular weight can be determined. The most important of secondary methods is gel-permeation chromatography (GPC), sometimes called size-exclusion chromatography (SEC). Another widely-used secondary method is the determination of intrinsic viscosity from which the viscosity-average molecular weight can be determined (Fried, 1995).

Osmometry

Osmometry technique is conducted by measuring osmotic pressure of polymer solution and solvent. Basically osmometer consists of a membrane semipermeable held between two compartments equipped with glass capillaries and supply standpipes. In operation, pure solvent and a dilute solution of polymer in the same solvent are placed

on opposite sides of a semipermeable membrane. Thus the solvent passes through the semipermeable membrane until a specific hydrostatic head is established in the capillary tube. The difference in liquid heights in the two capillaries (Δh) is related to osmotic pressure or activity (Fried, 1995; Seymour, 1971).

The difference in height Δh may be converted to osmotic pressure π by multiplying by gravity g and solution density ρ in the equation 2.4. Since the unrestricted capillary rise in a dilute solution is a function of concentration (C), one may employ a modified van't Hoff equation (equation 2.5) to determine the molecular weight \bar{M}_n . When $1/RT$ multiplied by the reduced osmotic pressure π/C is plotted against C , the intercept is $1/\bar{M}_n$ (Seymour, 1971).

$$\pi = \Delta h \rho g \quad (2.4)$$

$$\pi = \frac{RT}{\bar{M}_n} C + BC^2 \quad (2.5)$$

Light Scattering Method

The weight average molecular weight can be obtained directly by scattering experiments. The technique is light scattering from dilute polymer solution. The light-scattering techniques were developed by Debye in 1944 for the determination of the molecular weight (\bar{M}_w) of uncharged polymers. Light passing through a solution produces an induced oscillatory dipole between the electrons in the polymer and those in the solvent. The resultant oscillation reradiates the energy as scattered light. This scattering, which is readily observable as turbidity (τ) is related to the size of the molecules and the difference between the index of refraction of the polymer and the solvent (Fried, 1995; Seymour, 1971). According to Debye, the turbidity τ or scattered flux, i.e., the energy scattered per second, is related to the heterogeneity of the system and the molecular dimensions, as well as the average molecular weight \bar{M}_w (Seymour, 1971).

Gel Permeation Chromatography

One of the most widely used methods for routine determination of molecular weight and molecular weight distribution is gel permeation chromatography (GPC), which employs the principle of size exclusion chromatography (SEC) to separate

samples of polydisperse polymers into fractions of narrower molecular weight distribution. Basic instrumentation for GPC analysis consists of several small-diameter columns which are packed with small, highly porous beads.

During GPC operation, pure prefiltered solvent is continuously pumped through the columns at a constant flow rate, usually 1 to 2 mL min⁻¹. Then, a small amount (1 to 5 mL) of a dilute polymer solution (<0.2 g.dL⁻¹) is injected by syringe into the solvent stream and carried through the columns. Polymer molecules can then diffuse from this mobile phase into the stationary phase composed of solvent molecules occupying the pore volumes. The smallest polymer molecules are able to penetrate deeply into the interior of the bead pores, but the largest molecules may be completely excluded by the smaller pores or only partially penetrate the larger ones. As pure solvent elutes the columns after injection, the largest polymer molecules pass through and finally out of the packed columns. These are followed by the next largest molecules, then the next largest, and so on, until all the polymer molecules have been eluted out of the column in descending order of molecular weight.

The concentration of polymer molecules in each eluting fraction can be monitored by means of a polymer-sensitive detector, such as an infrared or ultraviolet device. Usually, the detector is a differential refractometer, which can detect small differences in refractive index between pure solvent and polymer solution. A signal from the detector is recorded as function of time, which for a fixed flow-rate is directly proportional to the elution volume, V_r . For a given polymer, solvent, temperature, pumping rate, and column packing and size, V_r is related to molecular weight. The form of this relation can be found only by comparing elution volumes with those of known molecular weight and narrow molecular-weight distribution, under identical conditions (Fried, 1995).

Intrinsic Viscosity Measurement

Another method widely used for routine molecular-weight determination is based upon the determination of the intrinsic viscosity, $[\eta]$, of a polymer in solution through measurements of solution viscosity. Molecular weight is related to $[\eta]$ by the Mark-Houwink-Sakurada equation given as

$$[\eta] = K \overline{M}_v^a \quad (2.6)$$

where, \overline{M}_v is the viscosity-average molecular weight defined for a discrete distribution of molecular weights as

$$\overline{M}_v = \frac{\sum_{i=1}^N N_i M_i^{1+a}}{\sum_{i=1}^N N_i M_i} \quad (2.7)$$

Both K and a are empirical (Mark-Houwink) constants that are specific for a given polymer, solvent, and temperature (Fried, 1995).

Intrinsic viscosity is implicitly expressed by the Huggins equation:

$$\frac{\eta_{sp}}{C} = [\eta] + k'[\eta]^2 C \quad (2.8)$$

Where k' is a constant (the Huggins coefficient) for a specified polymer, solvent, and temperature. As indicated from Equation (2.8), the $[\eta]$ can be obtained from the intercept of a plot of η_{sp}/C , which commonly called as the reduced viscosity, versus C . The parameter η_{sp} is called specific viscosity.

$$\eta_{sp} = \eta_{rel} - 1 \quad (2.9)$$

$$\eta_{rel} = \frac{\eta_{solution}}{\eta_{solvent}} \quad (2.10)$$

In actual practice, reduced viscosity is obtained at different concentrations by measurement of the time required for a dilute solution (t) and pure solvent (t_s) to fall from a fiducial mark to another in small glass capillary.

$$\eta_{sp} = \frac{\eta_{solution} - \eta_{solvent}}{\eta_{solvent}} = \frac{t - t_s}{t_s} \quad (2.11)$$

The efflux times are measured using capillary viscometers. The capillary viscometers may be either Ostwald-Fenske or Ubbelohde types (Fried, 1995; Higiroy et al., 2006; Huggins, 1942).

Polyethylene is soluble in xylene at elevated temperature (Muthana and Mark, 1949). For this reason, molecular weight of polyethylene can be determined by measuring viscosity of polyethylene-xylene solution at 105 °C. Molecular weight can be calculated by using intrinsic viscosity-molecular weight relation (Roy et al., 2007a).

2.4.4 Melt Flow Index

One of the most common physical properties routinely reported on manufacturer resin data sheets or product bulletins is the melt index (MI) (for polyethylene) or melt flow rate (MFR) (for all other thermoplastic resins, alloys, and composites)(ASM International, 2003). The melt index (MI)—also known as the “melt flow index” (MFI)—of a polyethylene resin refers to the rate at which it extrudes from a capillary die under a standard set of conditions. The melt index of a polyethylene resin depends on its molecular characteristics, primarily average molecular weight, molecular weight distribution, and branching characteristics—short chain versus long chain, concentration, and distribution (Peacock, 2000).

ASTM D 1238-98 cites the average flow (g/10 min) of a thermoplastic material through a standardized orifice under standardized conditions (temperature and dead load). The actual steady-shear rate for many materials is about 5 reciprocal seconds. ASTM D 3364-94 is similar to ASTM D 1238-98 but it uses a capillary die that is three times longer. Again, the measured flow is only an indirect indication of the molecular weight, which is inversely proportional to the measured flow of the thermoplastic material. The lower the molecular weight of the polyethylene, for example, the greater the melt index. The lower the melt flow rate of the resin, the higher the molecular weight or bulk-average molecular weight of many resins blended together. The MI or MFR is only an inverse indication of the “overall” molecular weight and does not indicate anything about the equally important molecular weight distribution (ASM International, 2003).

The melt index of a polyethylene resin is sometimes equated with its weight-average molecular weight, there being an approximately inverse relationship between the two values. Care must be exercised when applying such relationships because they hold true only for series of resins that have very similar molecular characteristics, e.g. high density polyethylene resins made with the same catalyst system or high pressure products from a given reactor. There is no universal relationship between the melt index and molecular weight applicable to all resins. The various conversion processes for manufacturing finished goods from base resin require different ranges of melt index for optimum performance; i.e. a balance of material properties and processability (Peacock, 2000).

2.4.5 Thermal Stability

Thermal stability of a material is stability against degradation upon exposure to elevated temperatures in an inert environment. Polymers are often exposed to high temperatures during processing and/or use. Thus, thermal stability is among the most important properties of polymers for a wide range of applications (Bicerano, 1996). Thermal stability is often assessed by thermogravimetric analyzer (TGA), which is also commonly called as thermogravimetry (TG). This can be done to obtain relative comparisons between different materials or as an accelerated means for lifetime predictions (ASM International, 2003). The TG technique is simple but effective for assessing thermal stability and chemical reactions by monitoring mass change in materials. Several reactions involve mass change, including dehydration, desorption, decomposition and oxidation (Leng, 2008). Thermal stability is characterized by degradation temperature; the temperature at which a material is decomposed.

2.4.5.1 Thermogravimetry Analysis

Thermogravimetry (TG) is a technique for measuring mass change of a sample with temperature. A sample to be measured is placed in a furnace and its mass change is monitored by a thermobalance. The main application of TG is to analyze material decomposition and thermal stability through mass change as a function of temperature in scanning mode or as a function of time in the isothermal mode. TG curves are plotted as mass change expressed in percent versus temperature or time. Decomposition of a

sample is represented by two characteristic temperatures: T_i and T_f . T_i is the lowest temperature when the onset of mass change is detected and T_f is the lowest temperature when the mass change is completed. The TG thermobalance structure includes a microbalance, furnace, temperature programmer and computer. The key component is the microbalance, which measures the mass change. A typical microbalance is able to measure mass change of $\pm 1\mu\text{g}$ with maximum mass of 100 mg (Leng, 2008).

2.4.5.2 Experimental Aspects of Thermogravimetry Analysis

Samples

Sample mass, volume and form are important for recording accurate and reproducible TG curves. Reliable TG curves rely on minimization of deviation between sample temperature and programmed temperature. Deviation typically results from either endothermic or exothermic reactions in the sample and subsequent heat transfer between heat source and sample. Sample mass is the most important parameter affecting TG curves. In general, small sample mass is better than large mass for minimizing temperature deviation. TG sample mass is usually about several milligrams. The low limit of sample mass depends on the resolution limit of the microbalance. Samples can be in block, flake, fiber or powder form. Sample form is the second most important parameter affecting TG curves. For example, decomposition of the powdered PMMA sample occurs at lower temperature than it does with other forms. A block sample should be ground or sliced to obtain a suitable form for TG examination. We should avoid excessive force during such mechanical processing, because mechanical deformation of the sample may also affect the TG (Leng, 2008).

Atmosphere

TA can be run in either a reactive or non-reactive atmosphere. Reactive atmospheres include corrosive, oxidizing and reducing gases. Non-reactive atmospheres should be an inert gas with little water vapor. Dry Ar and N_2 are commonly used for non-reactive atmospheres. Gas flows through the furnace tube around the sample and carries volatile products out.

Heating Rate

The heating rate affects thermogravimetry (TG) curves considerably, similar to DTA and DSC. For example, with endothermic decomposition, a high heating rate will increase the starting and finishing temperatures of decomposition. Also, the temperature range from start to finish will be wider at a higher heating rate than a lower heating rate. There are two reasons for heating rate effects. First, high heating rate is more likely to generate a temperature difference between the sample and thermocouple junction. The real sample temperature may lag behind that of the thermocouple. Second, in decomposition with volatile products, it takes time for those products to diffuse out of the sample and to be carried away by flowing gas. A low heating rate is more likely to generate thermal equilibrium and give a reproducible result for the analysis. A heating rate of about $5\text{--}10\text{ }^{\circ}\text{C}\cdot\text{min}^{-1}$ is recommended for TG examination (Leng, 2008).

2.4.5.3 Interpretation of Thermogravimetry Curve

TG curves can be classified into seven types as illustrated in Figure 2.5 (Leng, 2008). Type (i) is a nearly horizontal line that indicates there is no decomposition with mass loss of volatile products over the temperature range. Use of other types of TA techniques may be necessary to find out whether a thermal event has occurred in the temperature range. Type (ii) indicates a rapid mass loss at the initial stage of a TA curve. It is likely that the sample has gone through drying or desorption. Type (iii) is a one-stage decomposition curve which is typical in TG curves. It can define the stability limit of a sample. Type (iv) is a curve of multi-stage decomposition with stable intermediates. Type (v) is also a curve of multi-stage decomposition, but there is no stable intermediate. Type (v) may be a high heating-rate version of type (iv). Rerunning a TG analysis of a sample showing a type (v) curve with a low heating rate is necessary. Type (vi) indicates that a chemical reaction with mass gain has occurred in the sample. A typical example is oxidation of metal samples. Type (vii) indicates a mass-gain reaction occurs and then a mass loss reaction occurs at a higher temperature in the sample, which is rarely seen. A slope change of a TG curve is the main feature used to analyze a sample. Sometimes, the slope change is uncertain; in this case, a derivative TG curve can be used. The derivative TG (DTG) curve is a plot of dm/dT versus temperature. Figure 2.6 (Leng, 2008) shows comparison of TG and corresponding DTG curves. A

peak in a DTG curve represents a maximum of mass change rate. DTG does not contain any new information other than the original TG curve; however, it clearly identifies the temperature at which mass loss is at a maximum.

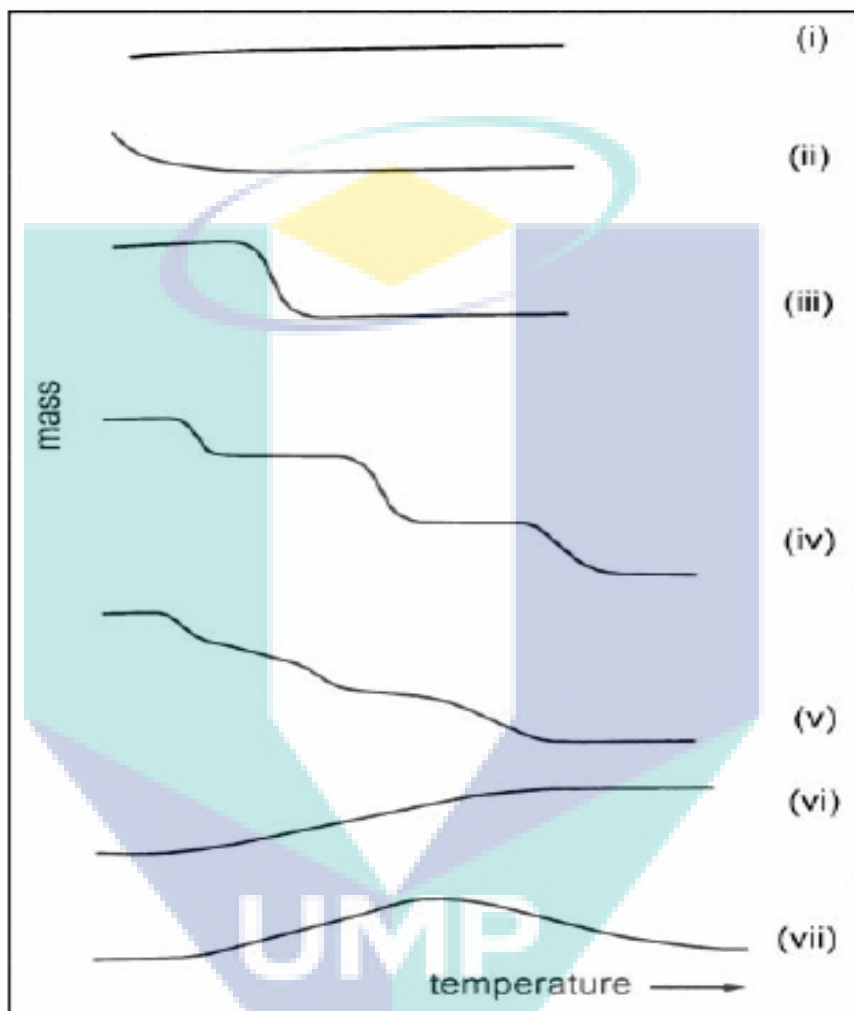


Figure 2.5 Classification of thermogravimetry curves

The determination of characteristic temperatures in TG curves is similar to that in DTA and DSC curves. As illustrated in Figure 2.7 (Leng, 2008), the temperature at which decomposition starts is defined as the intersection of initial line tangent and tangent of line portion when the slope changed. The finishing temperature of decomposition is defined in a similar manner. A mid-point temperature between the starting and finishing temperature can be defined as T_B .

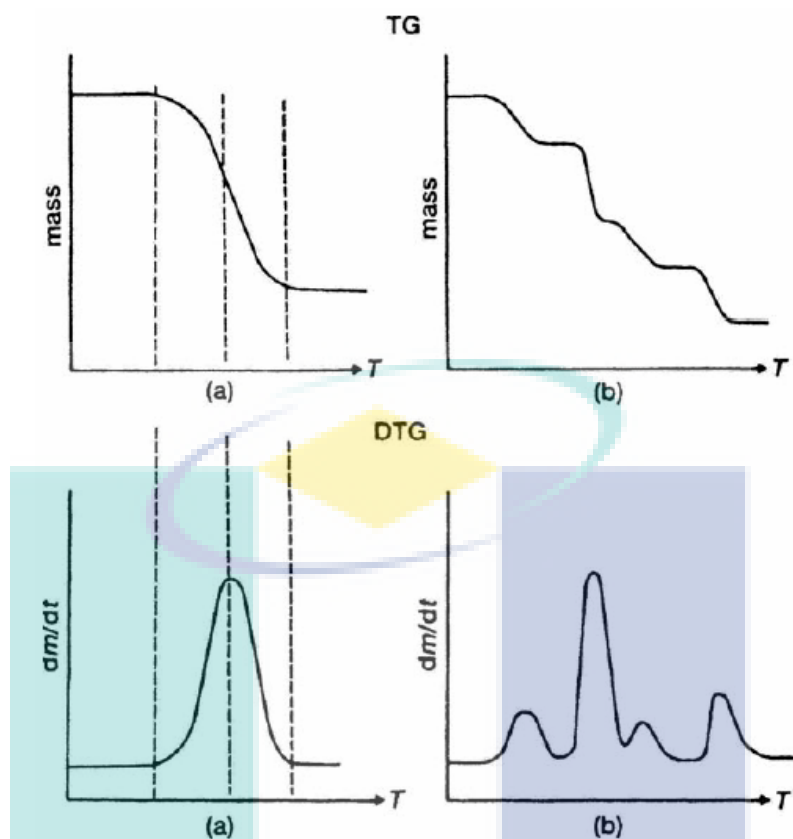


Figure 2.6 Comparison TG curves and corresponding DTG curves

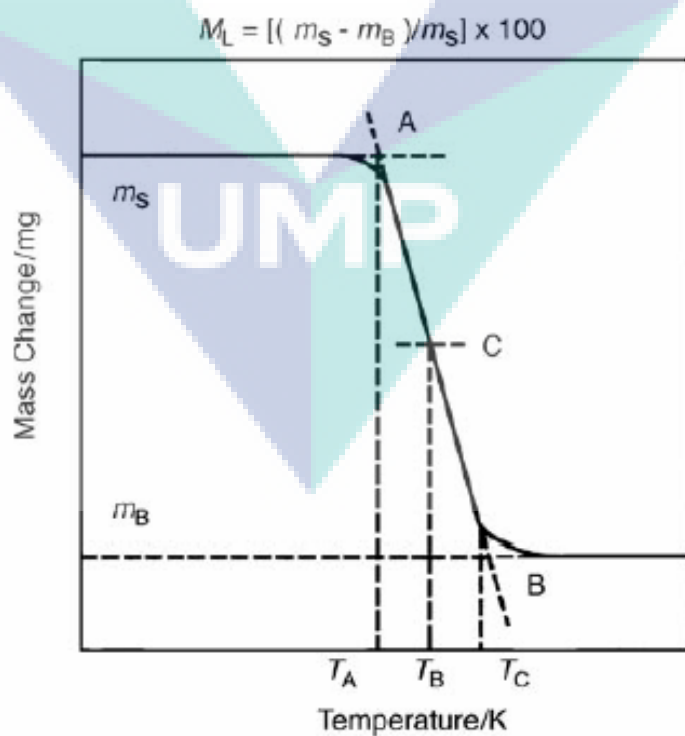


Figure 2.7 Temperature determination from a single-stage TG curve

Kinetic parameters for the various stages of thermal degradation could be determined from the TGA graphs using the Broido equation below (Beg and Pickering, 2008; Broido, 1969).

$$\ln\left(\ln\frac{1}{y}\right) = -\frac{E_a}{RT} + \ln\left(\frac{RZ}{E_a\beta}T_{\max}^2\right) \quad (2.12)$$

where y is the fraction of non-volatilized material not yet decomposed, T_{\max} is the temperature of maximum reaction rate, β is the heating rate, Z is the frequency factor, and E_a is the activation energy. The activation energies, E_a , determined from the slopes of these plots.

2.4.6 Melting Temperature

Three phenomena that are important with respect to the design and processing of polymeric materials are crystallization, melting, and the glass transition. Crystallization is the process by which, upon a cooling, an ordered (i.e. crystalline) solid phase is produced from liquid melt having a highly random structure. The melting of a polymer crystal corresponds to the transformation of a solid material having an ordered structure of aligned molecular chains, to a viscous liquid in which the structure is highly random. This phenomenon occurs, upon heating, at the melting temperature, T_m . Melting of polymers takes place over a range of temperatures. In addition, the melting behavior depends on the history of the specimen, in particular at which it crystallized. The apparent melting behavior is a function of the rate of heating; increasing this rate results in an elevation of the melting temperature. The glass transition occurs in amorphous (or glassy) and semicrystalline polymers and is due to a reduction in motion of large segments of molecular chains with decreasing temperature. Upon cooling, the glass transition corresponds to gradual transformation from liquid to rubbery material and finally to a rigid solid. The temperature at which the polymer experiences the transition from rubbery to rigid states is termed the glass transition temperature, T_g . Of course, this sequence of events occurs in the reverse order when a rigid glass at a temperature below T_g is heated. In addition, abrupt changes in other physical properties accompany this glass transition: for example, stiffness, heat capacity, and coefficient of thermal expansion (Callister and Rethwisch, 2011).

2.4.6.1 Factors That Influence Melting Temperature

During melting of a polymer there will be a rearrangement of the molecules in the transformation from ordered to disordered molecular states. Molecular chemistry and structure will influence the ability of the polymer chain molecules to make these rearrangements and, therefore, will also affect the melting temperature.

Chain stiffness, which is controlled by the ease of rotation about the chemical bonds along the chain, has a pronounced effect. The presence of double bonds and aromatic groups in the polymer backbone lowers chain flexibility and causes an increase in T_m . Furthermore, the size and type of side groups influence chain rotational freedom and flexibility; bulky or large side groups tend to restrict molecular rotation and raise T_m . For example, polypropylene has a higher melting temperature than polyethylene (175 °C versus 125 °C); the CH₃ methyl side group for polypropylene is larger than the H atom found on polyethylene. The presence of polar groups (Cl, OH, and CN) even though not excessively large, leads to significant intermolecular bonding forces and relatively high T_m . This may be verified by comparing the melting temperatures of polypropylene (175 °C) and poly-(vinyl chloride) (212 °C).

The melting temperature of a polymer will also depend on molecular weight. At relatively low molecular weights, increasing \bar{M} (or chain length) raises T_m as shown in Figure 2.8. Furthermore, the melting of a polymer takes place over a range of temperatures, and, thus, there will be a range of T_m rather than a single melting temperature. This is because every polymer will be composed of molecules having a variety of molecular weights, and because T_m depends on molecular weight. For most polymers, this melting temperature range will normally be on the order of several degrees Celsius. Those melting temperatures mentioned earlier are near the high ends of these ranges. Degree of branching will also affect the melting temperature of a polymer. The introduction of side branches introduces defects into the crystalline material and lowers the melting temperature. High-density polyethylene, being a predominately linear polymer, has a higher melting temperature than low density polyethylene which has some branching (Callister and Rethwisch, 2011).

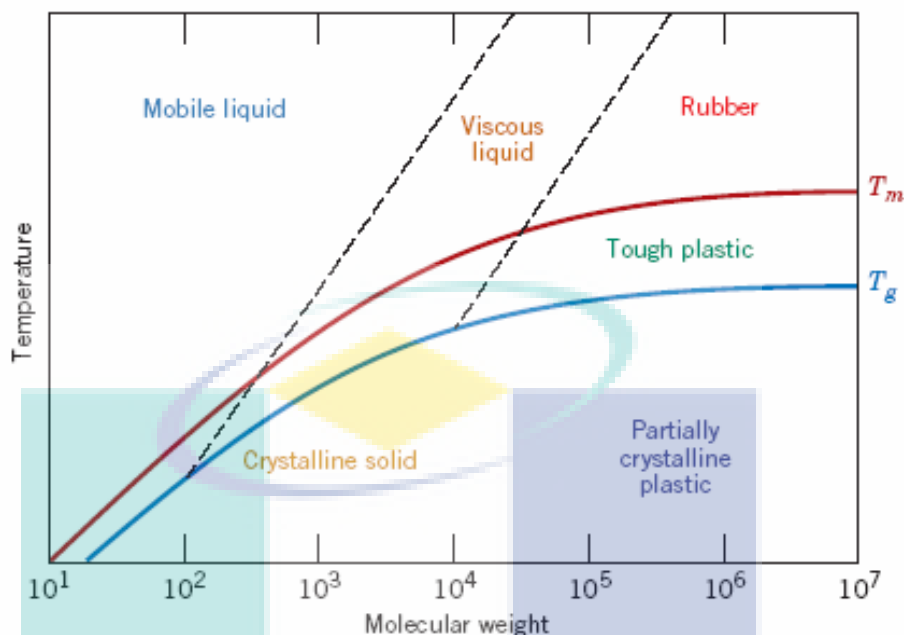


Figure 2.8 Dependence of polymer properties as well as melting and glass transition temperatures on molecular weight.

2.4.6.2 Differential Scanning Calorimetry

Differential scanning calorimetry (DSC) measures the energy absorbed (endotherm) or produced (exotherm) as a function of time or temperature. It is used to characterize melting, crystallization, resin curing, loss of solvents, and other processes involving an energy change. Differential scanning calorimetry may also be applied to processes involving a change in heat capacity, such as the glass transition. An experimental analysis related to DSC is differential thermal analysis (DTA), in which temperature differentials are measured. This information is on relative heat capacities, presence of solvents, changes in structure (that is, phase changes, such as melting of one component in a resin system), and chemical reactions. However, heat flow is not measured by the DTA method. In the DSC method, the sample and reference are placed in thin metal (aluminum) pans, with the thermocouple sensors below the pans. Differential scanning calorimetry measurements can be made in two ways: by measuring the electrical energy provided to heaters below the pans necessary to maintain the two pans at the same temperature (power compensation) or by measuring the heat flow (differential temperature) as a function of sample temperature (heat flux).

In the DTA method, the sensor thermocouple is placed either directly in the sample or close to the sample (ASM International, 2003).

Although DTA and DSC are similar in thermal event measurements and instrumentation, they are different in the following aspects. DTA is a qualitative technique because measured temperature differences do not provide any quantitative data for energy. In contrast, DSC is a quantitative technique because measured heat flow provides enthalpy changes in the sample during a thermal event. DTA can operate over a wider temperature range than DSC. The DTA can reach a temperature of greater than 1500 °C, while the power-compensated DSC is restricted to a maximum temperature of about 750 °C. This DTA feature is important for examining materials with high melting temperature such as ceramics and some metals (Leng, 2008).

A DSC curve is illustrated in Figure 2.9 (Leng, 2008) in which heat flow is plotted versus temperature. The heat flow has a unit of energy per unit time per unit mass, usually in units of Wg^{-1} . The DSC curves are commonly recorded over a temperature range by heating or cooling a sample with a constant rate. Commonly, heat flow into a sample is indicated as an upward feature of the DSC curve. However, it can be customized either an upward or a downward feature.

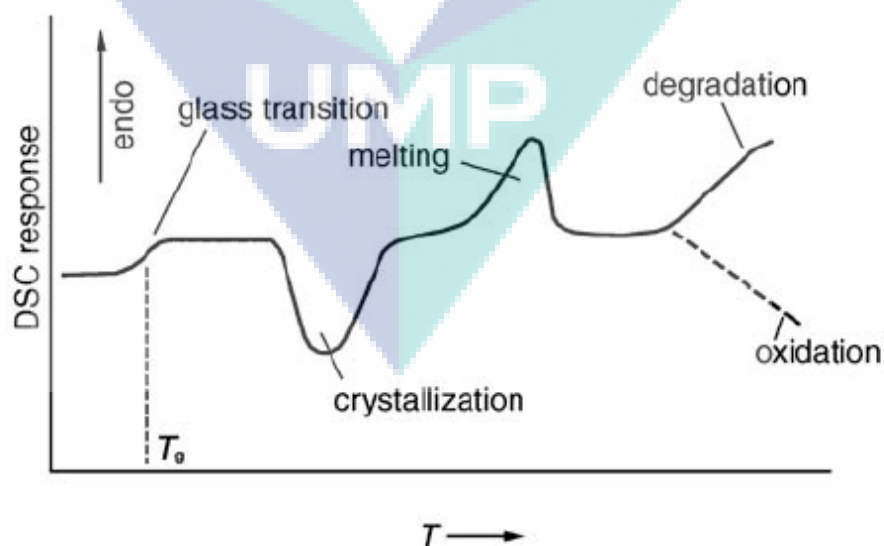


Figure 2.9 Schematic DSC curve for a polymeric sample

2.4.6.3 DSC Scan Analysis

Measuring transition temperatures is the primary task of DTA and DSC. The common transitions are melting, crystallization and glass transition. Figure 2.16 demonstrates how to determine the temperatures of thermal events from a DTA or a DSC curve. The DTA curve of a glass–ceramic sample shown in Figure 2.10 exhibits three thermal events during heating: glass transition, crystallization (or devitrification) and melting. Melting and crystallization exhibit endothermic and exothermic peaks, respectively. The glass transition exhibits only a change in the slope of the curve. The glass transition temperature (T_g) can be determined at the point where the curve deviates from the linearity of the sample baseline. For DSC curves which are not linear, T_g should be determined at the temperature where the curve deviates from the interpolated sample baseline, known as the onset temperature. T_g can more reliably be defined as the intersection between two tangents to the sample baselines before and after slope change when the point of the curve deviating from the sample baseline. The temperature of the first-order phase transition such as crystallization temperature (T_c) and melting temperature (T_m) should be defined at the intersection of the tangent to the maximum rising slope of the peak and the extrapolated sample baseline. The method to define T_m or T_c can be understood by analyzing the change of sample temperature during DTA scanning at a constant heating rate. When a solid melts, the sample temperature (T_s) remains at the melting temperature while the reference temperature (T_r) continuously increases with heating. Thus, $\Delta T (=T_s - T_r)$ starts to decrease, deviating from the baseline, until melting is completed; thus, ΔT reaches a minimum. The temperature of the melting peak represents the temperature of melting completion. Analysis of melting temperature of DTA scan is similar to that of DSC scan. The only difference is that the heat flow in DSC replaces temperature change in DTA (Leng, 2008).

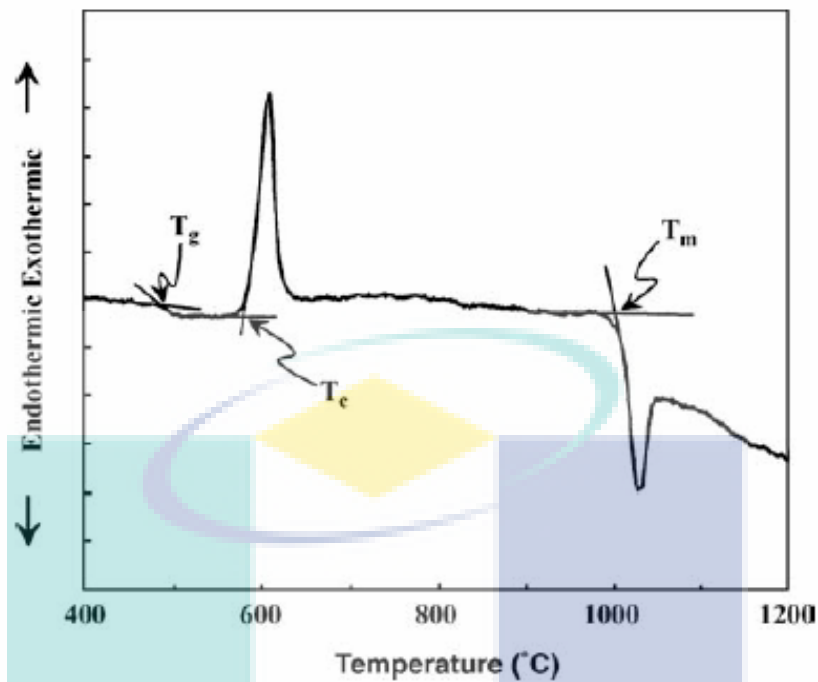


Figure 2.10 DTA curve of glass-ceramic sample

The enthalpy change of phase transformation can be directly measured from the corresponding peak area of a DSC curve. The DSC is commonly plotted as $\frac{dH}{dT}$ per mass unit versus temperature. The total enthalpy change ΔH should be proportional to the peak area (A_p).

$$\Delta H/mass = K_c \cdot A_p \quad (2.13)$$

where K_c is a calibration factor that includes contributions from the experimental conditions and the thermal conductivity of the system. We can obtain K_c by measuring the peak area of the standard sample, for which we know enthalpy change, for instance; Indium (commonly used standard material for calibration) has melting temperature 156.61 °C and enthalpy change of melting 28.71 J/g. For the power-compensated DSC, K_c is virtually independent of temperature. For the heat flux DSC, K_c becomes temperature dependent and has to be determined at a temperature close to that of the peak to be measured. The A_p measurement relies on interpolation of the sample baseline (Leng, 2008). Figure 2.11 shows the typical DSC scans of polyelofins and their melting points and enthalpy of fusion (enthalpy changes of melting) (ASM International, 2003).

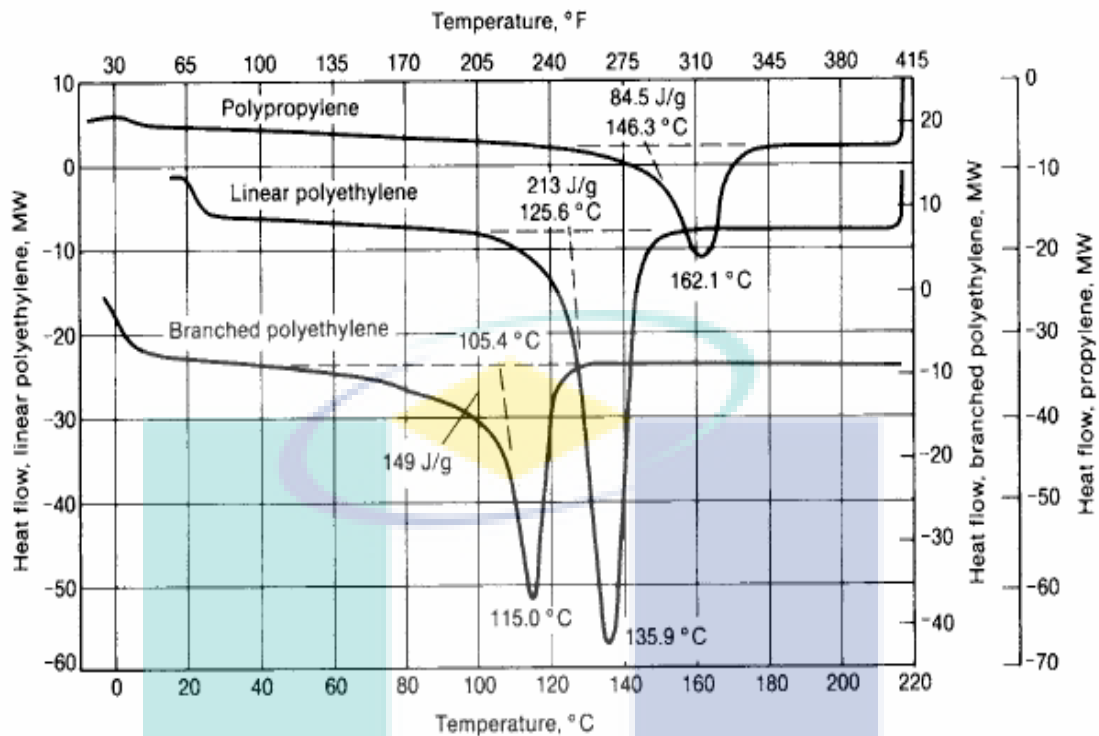


Figure 2.11 Polyolefin melting profiles (ASM International, 2003)

DTA and DSC curves are sensitive to the first-order transition, which exhibits an enthalpy change. First-order transitions include melting and solid-state phase transformations. The curve peaks of DTA and DSC readily reveal solid-state phase transformations over a temperature range. Polymeric materials are more sensitive to temperature than metals and ceramics. A large number of polymers exhibit physical and chemical property changes with changes in temperature. Besides determining the temperatures of glass transition, crystallization and melting, we can also determine special properties of polymers such as crystallinity, curing status, polymer content and stability (Leng, 2008).

2.4.7 Crystallinity

Polymer molecules are often only partially crystalline (or semicrystalline), having crystalline regions dispersed within the remaining amorphous material. Any chain disorder or misalignment will result in an amorphous region, a condition that is fairly common, since twisting, kinking, and coiling of the chains prevent the strict ordering of every segment of every chain. The degree of crystallinity may range from completely amorphous to almost entirely (up to about 95%) crystalline. The density of a

crystalline polymer will be greater than an amorphous one of the same material and molecular weight, since the chains are more closely packed together for the crystalline structure (Callister and Rethwisch, 2011). Polyethylene is one of semicrystalline polymers. The regularity of chain relates to crystallinity of polyethylene. The branching in polyethylene diminishes the crystallinity. High density polyethylene has crystallinity of 55-77%, LDPE 30-54 %, and LLDPE 22-54 % (Peacock, 2000).

2.4.7.1 Crystallinity of Polymer from DSC Scan

The enthalpy of fusion of DSC scans also reveals the degree of crystallinity. A large number of polymeric materials have both amorphous and crystalline structures. The melting temperature is that of a crystalline solid to liquid transformation. The degree of crystallinity, X_C , is determined from the ratio of the heat of fusion of a polymer sample, ΔH_{SC} , and the enthalpy of fusion of a 100% crystalline sample, ΔH_C (Leng, 2008; Osswald et al., 2006). The formula is presented in equation (2.14). The enthalpy of fusion of 100% crystalline of HDPE is 293 J/g (Lei et al., 2007; Liang et al., 2004).

$$X_C = \frac{\Delta H_{SC}}{\Delta H_C} \quad (2.14)$$

2.4.7.2 Crystallinity of Polymer from XRD Trace

X-ray diffraction is used for analyzing crystalline phases in solid materials, determining the extent of crystallinity, and identifying crystalline structure. The crystalline state of a thermoplastic material affects the ultimate strength, the thermomechanical properties, and the end-use performance. The extent of crystallinity can be altered by the processing or thermal history of the plastic (ASM International, 2003). Crystalline polymers can be characterized by their XRD patterns. X-ray diffraction analysis is needed when the percent crystallinity may be related to field problems. The crystalline portion of a polymer will diffract when exposed to x-rays, for example, CuK-alpha at 1.542 Å. Crystal diffraction follows Bragg's law:

$$n\lambda = 2d \sin \theta \quad (2.15)$$

where n is a constant (usually 1), λ is the wavelength of the x-ray, d is the interplanar spacing of the crystalline material, and $\sin \theta$ is the experimental diffraction angle (ASM International, 2003).

XRD Pattern

Wide-angle X-ray diffraction (WAXRD), also known as wide-angle X-ray scattering (WAXS), refers to the scattering of X-rays over a range of angles (θ) from about 2° to 180° . When discussing X-ray diffraction, it is customary to refer to the scattering angle in terms of 2θ . The precise range of scattering angles depends on the wavelength of the incident X-rays and the separation of the scattering planes. In the case of polyethylene irradiated with nickel-filtered copper $K\alpha$ X-rays (a commonly used X-ray source), the most useful information is available in the range of 2θ angles from 5° to 50° . This corresponds to a range of atomic spacings on the order of 2 to 20 Å. This range spans the major planes in the crystalline unit cell and the intermolecular separations in the non-crystalline regions. Figure 2.12 represents XRD pattern of linear low density polyethylene (Peacock, 2000). Spectra of polyethylene exhibit diffraction peaks at around angle of $2\theta=21.5^\circ$ representing (110) diffraction plane and 23.9° representing (200) diffraction plane (Lei et al., 2007; Li and Weng, 2009; Yuan et al., 2010). The sharp peaks are due to the scattering from the crystalline regions and the broad underlying 'hump' is due to scattering from non-crystalline areas. The larger underlying 'hump' in spectrum means the lower crystallinity (Li and Weng, 2009).

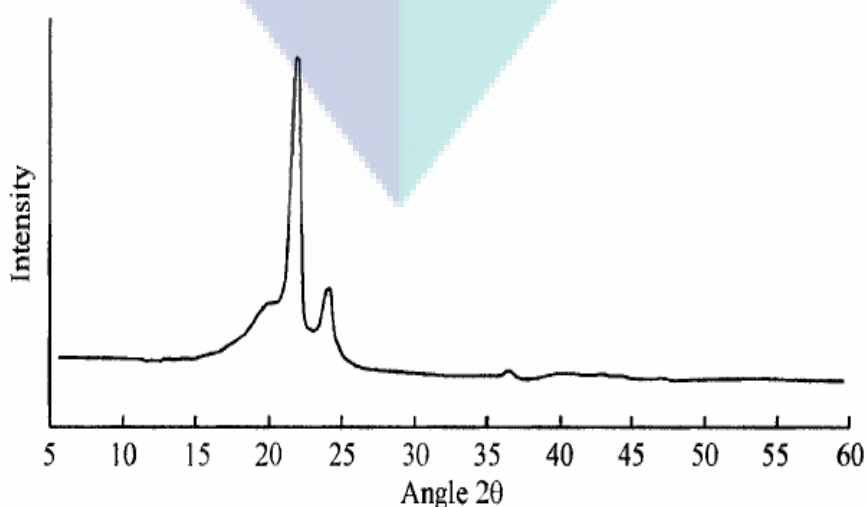


Figure 2.12 Plot of X-ray scattering intensity of linear-low density polyethylene

Ideally, a Bragg diffraction peak is a line without width. In reality, diffraction from a crystal specimen produces a peak with a certain width as shown in Figure 2.13. The peak width can result from instrumental factors and the size effect of the crystals. Small crystals cause the peak to be widened due to incompletely destructive interference (Leng, 2008).

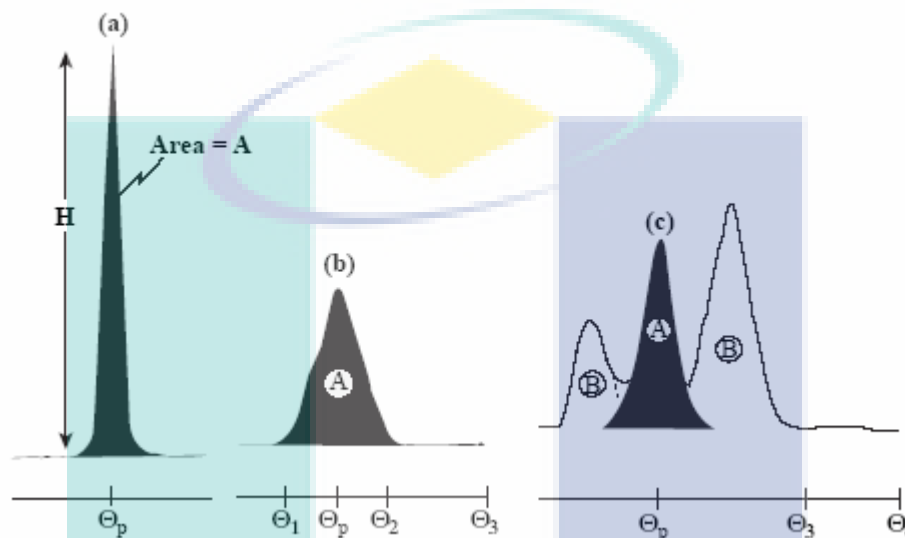


Figure 2.13 Three types of peak shapes in X-ray diffraction pattern (a) peak height proportional to peak area; (b) peak height not proportional to peak area; and (c) peak area overlapped by other peaks

Quantitative Analysis

A polymer can be considered partly crystalline and partly amorphous. The crystallinity parts give sharp narrow diffraction peaks and the amorphous component gives a very broad peak (halo). The ratio between these intensities can be used to calculate the amount of crystallinity in the material.

Wide-angle X-ray diffraction can be used to measure the degree of crystallinity of a complete range of polyethylenes, including some that contain fillers. In addition it can provide information about unit cell dimensions. Balanced against this, samples analyzed with a goniometer must be either a fine powder or unoriented and flat. Deconvolution of the scattering pattern may be subjective, and the model of morphology is two-phase. The accuracy of results is similar to that from differential scanning calorimetry, i.e., approximately $\pm 5\%$. Experimental limitations largely

preclude the application of wide-angle X-ray diffraction to manufactured items other than films, sheets, and fibers (Peacock, 2000).

Figure 2.14 (Murthy and Minor, 1990) represents XRD scan of polyethylene. The crystallinity index of polyethylene was determined by calculating the ratio of area under the peak at angle of 21.62° and 23.94° representing crystalline part, with total area. Total area comprises crystalline part (peak intensity of 21.62° and 23.94°) and amorphous part (peak intensity of 20.06°). The corresponding method for crystallinity determination from XRD scans has also been developed by Yao (1992). Roy et al. (2007a) have found crystal peaks of LDPE at 21.5° , 24.7° , and 36.07° in X-ray diffraction pattern, which correspond to inter-lamellar spacing of 4.1, 3.6, and 2.49\AA , respectively, and also reported determination of crystallinity of LDPE by using those peaks.

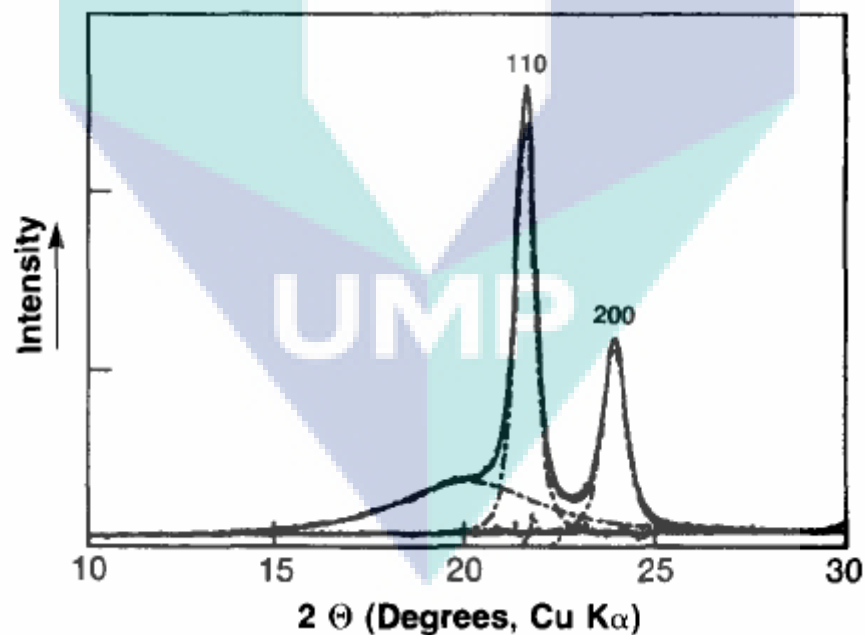


Figure 2.14 Profile analysis of a diffractometer scan from polyethylene

2.4.8 Surface Morphology

Many analytical analyses are available for the study and characterization of surfaces. These techniques provide data about the physical topography, physical properties, chemical composition, and chemical structure of the surfaces under study. Most of these techniques are based on bombarding the surface with photons, x-rays, ions, neutrons, or electrons and analyzing the radiation emitted and/or reflected from the surface. Other techniques use other interactions, such as physical probing of the surface. Analyzing the chemistry and topography of failure surfaces is an important part of failure analysis (ASM International, 2003).

The scanning electron microscope (SEM) is the most widely used to examine microscopic structure by scanning the surface of materials, similar to scanning confocal microscopes but with much higher resolution and much greater depth of field. An SEM image is formed by a focused electron beam that scans over the surface area of a specimen. Perhaps the most important feature of an SEM is the three-dimensional appearance of its images because of its large depth of field. For example, the depth of field can reach the order of tens of micrometers at $10^3\times$ magnifications and the order of micrometers at $10^4\times$ magnifications. An SEM is relatively easily operated and maintained. In addition, an SEM system enables us to obtain chemical information from a specimen by using various techniques, including by equipping the X-ray energy dispersive spectrometer (EDS)(Leng, 2008).

2.4.8.1 Scanning Electron Microscope

A scanning electron microscope consists of an electron gun and a series of electromagnetic lenses and apertures. The electron gun for generating an electron beam is either thermoionic or field emission type guns. Thermoionic emission gun includes the *tungsten filament gun* and the *lanthanum hexaboride*(LaB₆) gun. The filament (cathode) is heated by electrical current (*filament current*) to high temperature (~2800 K) enabling the conduction electrons in the filament to leave the surface. The electrons are accelerated by a high electric voltage between the filament and anode to a high energy level. Field emission gun does not need to provide thermal energy for electrons to overcome the surface potential barrier of electrons. Electrons are pulled out by

applying a very high electric field to a metal surface. The field emission gun generates the highest intensity electron beam, 10^4 times greater than that of the tungsten filament gun and 10^2 times greater than that of the LaB_6 gun. There are two kinds of field emission guns: thermal guns, work at about 1600–1800 K and cold guns, works at room temperature. Advanced SEM systems use a field emission gun because of its high beam brightness. Because electron energy determines the wavelength of electrons and wavelength largely determines resolution of the microscope, the acceleration voltage determines the resolution to a large extent. The acceleration voltage for generating an electron beam is in the range 1–40 kV (Leng, 2008).

An SEM optical path goes through several electromagnetic lenses, including condenser lenses and one objective lens in a SEM. The deflection system moves the probe over the specimen surface along a line and then displaces the probe to a position on the next line for scanning, so that a rectangular raster is generated on the specimen surface. Probe scanning is operated by a beam deflection system incorporated within the objective lens in an SEM. The signal electrons emitted from the specimen are collected by a detector, amplified, and used to reconstruct an image. An SEM is able to provide image magnification from about $20\times$ to greater than $100,000\times$.

2.4.8.2 Specimen Preparation

For topographic examination, minimal preparation of specimens should be done in order to preserve features of their surfaces. The preparation should involve only sizing the specimens to fit a SEM specimen holder and removing surface contaminants. The specimen holder of an SEM varies with manufacturer. Common contaminants on the specimen surfaces are hydrocarbons from oil and grease, because an electron beam decomposes any hydrocarbon and leaves a deposit of carbon on the surface. The deposit generates an artifact of a dark rectangular mark in SEM images. A dark mark is readily seen on a hydrocarbon-containing specimen at lower magnification after examining the same location at higher magnification. The carbon deposition is formed quickly under a higher magnification because of the higher exposure rate of electron beam. Surfaces with oil or grease contamination should be cleaned by an organic solvent such as methanol or acetone in an ultrasonic cleaner. It is also important to avoid touching the

cleaned specimen with bare hands because fingerprints contain volatile hydrocarbon compounds (Leng, 2008).

2.5 DEGRADATION OF PLASTICS

Degradability is the ability of materials to break down, by bacterial (biodegradable), thermal (oxidative) or ultraviolet (photodegradable) action (Andrady et al., 1993a; Excelplas, 2003). It is well known that polymeric materials, especially plastics, are degraded by action of heat, light, and air (Poyner and Cakraborty, 1993). A variety of environmental factors may affect polymer degradation: oxygen, temperature, sunlight, water, stress, living organisms and pollutants. The rate of degradation is also governed by properties of the material itself such as surface/volume ratio and additives (Albertsson et al., 1992). Degradation under exposure to the outdoor environment might take place predominantly due to chemical changes in material. Degradation will therefore affect the average molecular weight, the polydispersity, and the chemistry of polymer (Andrady et al., 1993a).

Some polymers have specific sensitivity to certain factors, resulting new term of degradable polymer. Oxo-degradable polymers are those that undergo controlled degradation through the incorporation of pro-degradant additives (additives that can trigger and accelerate the degradation process). These polymers undergo accelerated oxidative define degradation initiated by natural daylight, heat and/or mechanical stress, and embrittle in the environment and erode under the influence of weathering (Excelplas, 2003). Photodegradable polymers are those that break down through the action of ultraviolet (UV) light, which degrades the chemical bond or link in the polymer or chemical structure of the plastic. This process can be assisted by the presence of UV-sensitive additives in the polymer (Bajer et al., 2007; Excelplas, 2003). Polymer can also undergo thermal degradation by action of heat or thermal conditions. Polyolefins are known to be sensitive to thermal oxidation, due to the impurities generated during their manufacture at high temperature (Khabbaz et al., 1999; Singh and Sharma, 2008).

2.5.1 Thermo-oxidative Degradation

Under normal conditions, photochemical and thermal degradations are similar and are classified as oxidative degradation. The main difference between the two is the sequence of initiation steps leading to auto-oxidation cycle. Other difference includes that thermal reactions occur throughout the bulk of the polymer sample, whereas photochemical reactions occur only on the surface. Thermal degradation of polymers occurs through random and chain degradation (depolymerization reaction) initiated by thermal (Singh and Sharma, 2008).

Many studies have been conducted on thermo-oxidative degradation of polyethylene, particularly low density polyethylene (LDPE). Saccani et al. (2011) have studied ageing of LDPE and coated-LDPE in air-circulated oven at 95°C. LDPE was found to be more brittle than LDPE with coating after ageing process. Bikiaris et al. (1997) studied the effect of methyl methacrylate-butadiene-styrene copolymer on the thermo-oxidation of LDPE/plasticized starch blends. Roy et al. (2007b) investigated the effect of cobalt carboxylates on the thermo-oxidative degradation of LDPE films. The studies indicate that films containing these additives susceptible to thermo-oxidative degradation. In other study, Sharma et al. (2001) conducted a study on the effect of pro-oxidant, i.e. manganese stearate, on the thermo-oxidative degradation of sago starch filled polyethylene. It was found that incorporation of manganese stearate had accelerated the thermo-oxidative degradation of LLDPE. Those studies conducted in the air circulated oven at temperature of 70 °C.

Johnston and Morrison (1996) proposed the mechanism of thermo-oxidation of polyethylene as presented in Figure 2.15. The mechanism construes series of reactions e.g. radicals forming, hydroperoxide forming, cleavage of hydroperoxide. Those processes lead to chain scission.

Thermal degradation of polymers may follow either chain end degradation or random degradation route. The chain end degradation initiates from the end of the chain and successively releases the monomer units (Murata et al., 2002; Singh and Sharma, 2008). Random degradation occurs at any random point along the polymer chain. This

is reverse to polycondensation process where the polymer degrades to lower molecular weight fragments (Singh and Sharma, 2008).

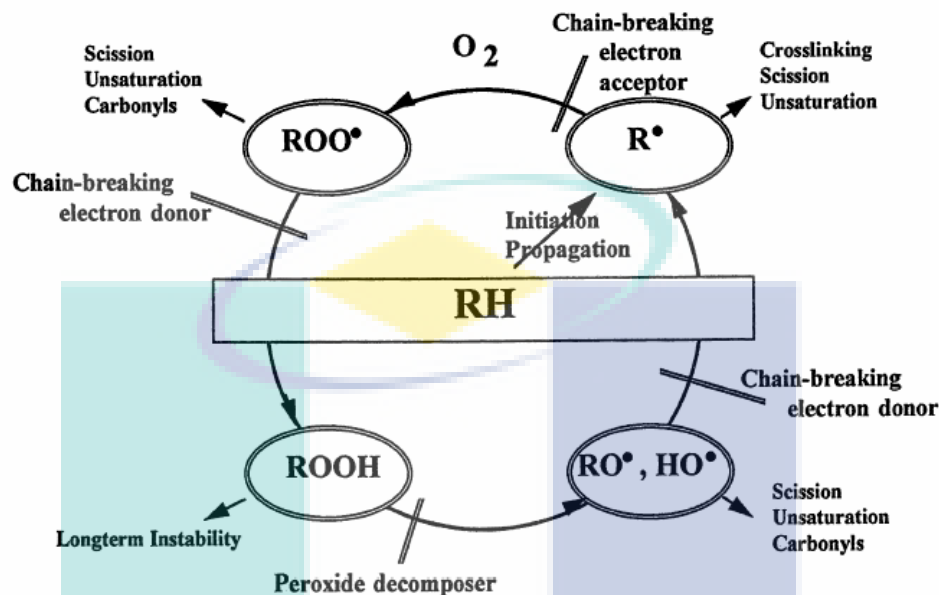
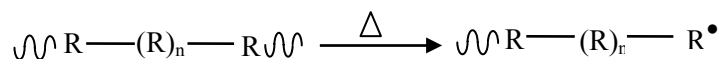


Figure 2.15 Mechanism of thermo-oxidation of polyethylene

During thermo-oxidative aging, heat and oxygen will initiate free radical reactions to degrade polyethylene (Albertsson et al., 1987; Albertsson et al., 1994). The initiation of the thermo-oxidative process of polyethylene may follow the ways of the formation of alkyl free radicals from the polymer (RH) (Johnston and Morrison, 1996) or direct formation of hydroperoxide groups (Wiles, 2005a). Once the alkyl radicals are formed, they may react rapidly with oxygen and generate alkylperoxy free radicals (ROO^\bullet). The peroxy free radicals may then abstract hydrogen from the polymer substrate to form hydroperoxides (ROOH) (Johnston and Morrison, 1996). The formation of alkyl radicals can be presented in Scheme 2.1 (Singh and Sharma, 2008).



Scheme 2.1 Formation of alkyl radicals

On the other hand, Scheme 2.2 shows the direct formation of hydroperoxide groups (ROOH) attached to carbon atom in the polymer backbone under the effect of

heat and air i.e. oxygen. The hydroperoxide groups readily cleave and forming radicals (Wiles, 2005a).

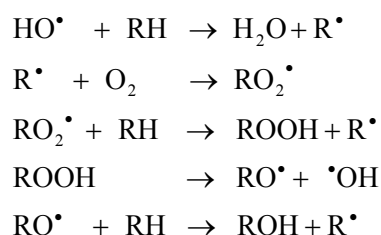


Scheme 2.2 Reaction of hydroperoxides formation and cleavage

At the elevated temperatures, hydroperoxides rapidly cleave to form alkoxy and hydroxyl radicals. These compounds may in turn rapidly abstract hydrogen from the polymer substrate to form more alkyl radicals (Johnston and Morrison, 1996). The alkoxy radical (RO^\bullet) is exceedingly unstable. It will decompose spontaneously to form ketones and aldehydes (depending on the structure of the 'parent' hydroperoxide group) and these carbonyl compounds will undergo further oxidation to produce acids and esters (Wiles, 2005a).

The mechanism of the transition metal-catalyzed degradation of PE has been described as a free radical mechanism proceeding from the formation of hydroperoxides along the polymer back bone through reaction of the polymer with molecular oxygen (Sharma et al., 2001). The presence of metal compound will catalyze the hydroperoxide decomposition step of the oxidation mechanism (Albertsson et al., 1994; Bikiaris et al., 1997; Sharma et al., 2001).

The radicals formed during initial stage of thermo-oxidation will attack polymer backbone. They initiate the oxidation of polyethylene by following the mechanism shown in Scheme 2.3 (Erlandsson et al., 1997). While oxidation proceeds in the polymeric chains, the chain scissions predominate (Bikiaris et al., 1997).



Scheme 2.3 Oxidation of polyethylene

2.5.2 Photo Degradation

Composition of the solar radiation reaching the earth's surface is mainly made up of radiation in the visible and infrared areas of the electromagnetic spectrum. Approximately 43% of solar radiation is in the infrared region and has a wavelength of greater than 700 nm – this radiation does little to most plastics apart from heating the material. Approximately 52% of solar radiation is in the visible region and has a wavelength of between 400 and 700 nm – this radiation both heats the plastic and can also start photochemical reactions. The last 5% of the radiation is in the ultraviolet (UV) region and has a wavelength of between 400 and 290 nm. UV radiation can be classified as near, far or extreme UV but it is also possible to classify UV radiation in terms of UVA, UVB and UVC types of radiation where UVA is made up of wavelengths from approximately 320 to 400 nm, UVB is made up of wavelengths from approximately 280 to 320 nm and UVC is made up of wavelengths from approximately 100 to 280 nm. Only UVA and UVB ultraviolet rays reach the earth's surface because the ozone layer blocks the UVC radiation (Zeus, 2010).

However, sufficient radiation in the 280 to 400 nm range reaches the earth's surface and affects many organic compounds. This ultraviolet radiation causes yellowing and embrittlement of many organic polymers. The energy in the 280 to 400 nm range (100 to 72 kcal) is sufficient to cleave covalent bonds. Trace impurities present in commercial polymers may catalyze the degradation. This degradative process is related to the polymer structure. Linear polymers are more resistant than branched chains, and the rate of deterioration is proportional to surface area exposed (Seymour, 1971).

Photo-oxidative degradation is the process of decomposition of the material by the action of light, which is considered as one of the primary sources of damage exerted upon polymeric substrates at ambient conditions. Most of the synthetic polymers are susceptible to degradation initiated by UV and visible light. Normally the near-UV radiations (290–400 nm) in the sunlight determine the lifetime of polymeric materials in outdoor applications. Polymer degradation occurs mainly in the ether parts of the soft-segments, where photo-irradiation generates ester, aldehyde, formate and propyl end groups. UV radiations have sufficient energy to cleave C–C bond. The most damaging

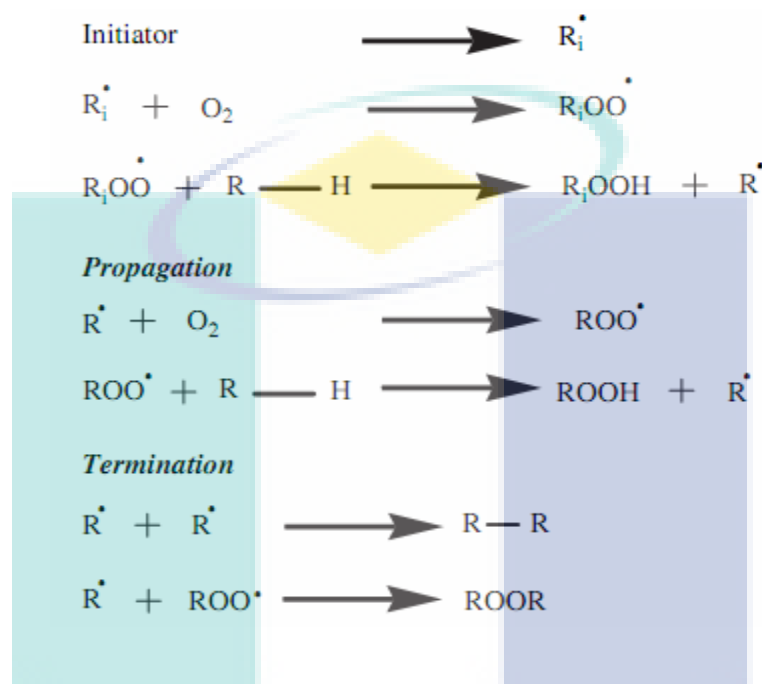
UV wavelength for a specific plastic depends on the bonds present and the maximum degradation therefore occurs at different wavelengths for different types of plastics, e.g. it is around 300 nm for polyethylene (PE) and around 370 nm for polypropylene (PP). Photo-degradation changes the physical and optical properties of the plastic. The most damaging effects are the visual effect (yellowing), the loss of mechanical properties of the polymers, the changes in molecular weight and the molecular weight distribution for the same. PE and PP films when exposed to solar UV radiation readily lose their extensibility, mechanical integrity and strength along with decrease in their average molecular weight (Singh and Sharma, 2008).

The mechanisms of the degradation and oxidation reactions are determined by the extraneous groups and/or impurities in the polymer, which absorb light quanta and form excited states. Excited states may cleave the polymer chains and form radical pairs by following Norrish Type I reaction or form pairs of saturated and unsaturated chain ends by hydrogen transfer by following Norrish Type II reaction (Peacock, 2000; Singh and Sharma, 2008).

The polymer radicals may add molecular oxygen to peroxy radicals, which abstract hydrogen and form hydroperoxide groups, which absorb UV light or become excited by energy transfer, the weak O–O bonds break and pairs of alkoxy and hydroxyl radicals are formed which may react in various ways, e.g. by hydrogen abstraction, chain scission, rearrangement, etc. and accelerate photo-degradation. Double bonds may add excited oxygen molecules in singlet state. In this reaction, the double bond is shifted to an adjacent C–C bond and a hydroperoxide group is formed. Some synthetic polymers, e.g. aromatic polyesters and polyamides, have inherent absorption of UV light, causing excitation, radical formation, oxygen addition, splitting off small molecules, chain scission, etc. Some of these polymers are auto-stabilized towards photo-degradation by formation of an oxidized surface layer with high absorption of near UV and visible light of short wavelengths, preventing further penetration of light into deeper layers (Singh and Sharma, 2008).

The absorption of UV light that has sufficient energy to break the chemical bonds in the main polymer chain leads to the initiation of mechanism responsible for

polymer degradation. It involves a radical chain mechanism or the formation of initial radical. Different initiation steps under varied conditions have been undertaken in different polymers. The photo-oxidative degradation mechanism comprises some steps as shown in Scheme 2.4 (Singh and Sharma, 2008).

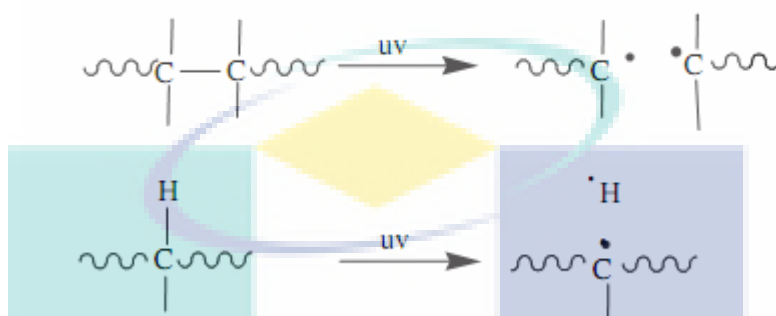


Scheme 2.4 Mechanism of photo-oxidative degradation

UV light exposure at certain level can directly initiate radicals' formation of polymer. Dissociation energy of C-C bond (375 kJ/mol) and C-H bond (420 kJ/mol) is equivalent to UV radiation of 320 nm and 290 nm. Thus, direct photolysis of C-C and C-H bond is possible and the radical formed in these reactions become a source of initiation radicals as shown in Scheme 2.5 (Singh and Sharma, 2008).

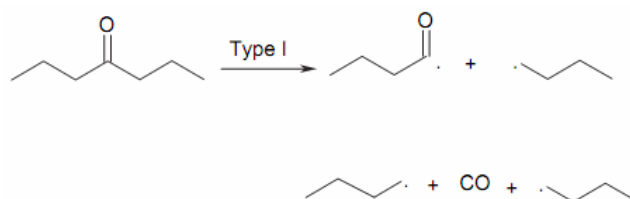
In the initiation of reaction, hydroperoxides are formed as result of oxidation. Hydroperoxides are commonly the major products of oxidative degradation and are potentially powerful initiators of further degradation (Roy et al., 2007a). Since hydroperoxides are very sensitive to UV light, especially in the presence of transitions metals, the hydroperoxides formed during UV radiation have probably decomposed very quickly into radicals (Erlandsson et al., 1997). Other functionalities introduced during degradation include carbonyl groups, which are basically a result of

hydroperoxide decomposition. The products of hydroperoxides decomposition generally consist of ROO^\bullet , RO^\bullet and H_2O (Albertsson et al., 1994). The carbonyl groups absorb UV radiation readily and get excited to singlet and triplet states which further decompose via Norrish reactions of type I, II and III.

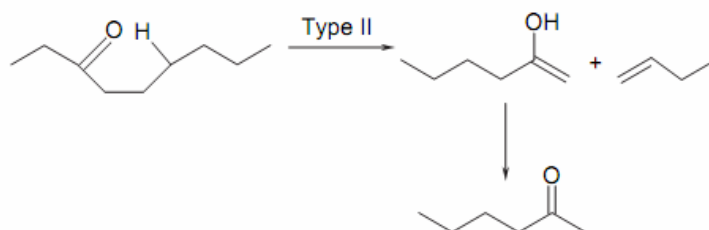


Scheme 2.5 Direct photolysis

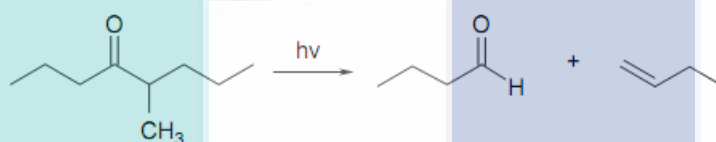
Norrish type I reaction (Scheme 2.6) is a radical cleavage of the bond between the carbonyl group and α C-atom (α -scission), and is followed by formation of CO. Norrish type II reaction (Scheme 2.7), a non-radical, intramolecular process occurs via the formation of a six membered cyclic intermediate. Abstraction of hydrogen from the γ carbon results in its subsequent decomposition into an unsaturated polymer chain end, and a polymer chain with an end carbonyl group. Norrish type III reaction (Scheme 2.8) is also a non-radical chain scission; however, it involves the transfer of β hydrogen atom and leads to the formation of an olefin and an aldehyde. The activation energy of Norrish type reactions are different; the probability of Norrish II ($E_a = 0.85$ kcal/mol) is higher than that of Norrish I ($E_a = 4.8$ kcal/mol); the latter is however more probable at higher temperature (Roy et al., 2007a).



Scheme 2.6 Norrish type I reaction



Scheme 2.7 Norrish type II reaction



Scheme 2.8 Norrish type III reaction

Some studies of photo-degradation of polyethylene utilized artificial UV light instead of solar UV light. Roy et al. (2006b) studied effect of cobalt carboxylates on the photo-oxidative degradation of low-density polyethylene by using 40W UV-B lamps generating energy between 280 and 370 nm with maxima at 313 nm. The other studies utilized 40 W sunlamps generating energy between 280 and 350 nm for photo-degradation of LDPE (Albertsson et al., 1992; Erlandsson et al., 1997). The studies showed that LDPE degraded at different stages according to compositions under UV exposure.

2.5.3 Accelerated Weathering Degradation

The long-term behavior of materials due to environmental influences can be evaluated by the real time observations of the materials exposed to natural conditions for several years. However, research program lasting 10 years or more are rare for organizational and economic reasons. Accelerated aging tests seem to be useful for this purpose. The accelerated tests of specimens or elements subjected to special conditions in which, after a short time, the results obtained are equivalent to natural long-term

exposure and are applied with moderate success. Accelerated tests are composed of different actions or cycles of actions, which should produce measurable and appreciable effects after a certain number of hours, days or months. Typically, they do not exceed a few weeks or months of steady action or a certain number of cycles (Brandt, 2009). However, during accelerated weathering measured variables can include exposure time, UV exposure as radiant energy over a specific wavelength range, and water exposure as number of cycles or time. To allow better comparison between studies it is recommended that performance after weathering be reported after a specific radiant exposure, the time integral of irradiance (Beg, 2008).

Pure laboratory testing involves using environmental chambers and artificial light sources to approximately replicate outdoor conditions but with a greatly reduced test time under highly controlled conditions. Laboratory testing can quickly assess the relative stability of plastics but has the major disadvantage that the quicker the test the lower the correlation to real behavior in the field (Singh and Sharma, 2008). Accelerated weathering test combines factors that affect degradation in natural weathering e.g. sunlight exposure, rain, humidity, condensation, heat or temperature etc.

Beg and Pickering (2008) have studied accelerated weathering of unbleached and bleached Kraft wood fiber reinforced polypropylene composites using QUV tester with UVA lamp (340 nm) at irradiance 0.68 W/m^2 . This study was conducted up to 1000 hours. Attwood (2006) has also studied accelerated weathering of polyolefin blend (LDPE, HDPE, PP, and carbon black masterbatch) using QUV accelerated weathering tester at irradiance of 0.68 W/m^2 and 340 nm (UVA lamp). The duration of test was up to 5000 hours. Espi et al.(2007) have conducted study on accelerated weathering of LDPE using weathering device which utilize a xenon lamp.

2.5.4 Natural Weathering Degradation

For the most part, degradation takes place in the presence of oxygen, resulting in its gradual incorporation into the polymer molecules by a series of autocatalytic reactions. The most common degradative environment encountered by polyethylene products is weathering in outdoor situations. Under these circumstances the primary factor is exposure to ultraviolet (UV) radiation, with thermal effects playing a secondary

role. Prolonged exposure to high temperature in the absence of light is sufficient to cause degradation, but polyethylene's relatively poor mechanical performance at elevated temperatures ensures that such conditions are rarely encountered in normal service. Temperatures in excess of the crystalline melting point are inevitably encountered during processing, but exposure to such harsh conditions is generally short-lived, and generally little harm comes to the physical properties of adequately stabilized resins. Electrical properties, which are sensitive to small concentrations of contaminants, may be adversely affected by even short exposures to molding temperatures in the presence of oxygen. During the weathering process it is quite conceivable that temperatures sufficient to promote the photo-oxidation process will be encountered. Significant levels of high energy radiation and mechanical and chemical stresses are rarely encountered in common use, but may promote degradation of various types when they are present (Peacock, 2000).

The amount of UV present in the incident solar radiation varies dramatically with location and is particularly high near the equator. Weathering due to UV radiation can vary dramatically depending on the location of the product in the world and the intended application location should always be specified at the earliest stage. Temperature also plays a role in weathering. Since degradation process is temperature dependent, it will occur more rapidly at higher temperatures. The general rule is that for every 10°C increase in temperature the reaction rate will double. Tropical areas therefore suffer not only from increased UV exposure but also faster reaction rates because of the increased temperatures. Humidity is also important to be considered in natural degradation. Most weathering processes are considerably slower in hot dry climates than in hot wet climates (Zeus, 2010).

Outdoor exposure can be performed on samples mounted on testing racks, oriented under standard conditions to expose the material to the full radiation spectrum besides the temperature and humidity of that location (Singh and Sharma, 2008). Ojeda et al. (2011) have studied natural weathering of PP, LLDPE, HDPE and LLDPE/HDPE blend. The samples was put on the platforms that were built with an angle of 30° to the ground, facing the equator, in Porto Alegre, RS (Brazil), 30°02'S; 51°12' W. The results

showed that PP and the HDPE/LLDPE with pro-oxidant additives blend are rapidly degrading materials, whereas HDPE and LLDPE degrade more slowly.

Basfar and Idris Ali (2006) have studied natural weathering tests of LDPE and LLDPE films which were placed on the rack facing southward at an angle of 45° with the plane of the earth. Sheikh et al. (2006) studied a formulation of photosensitized polyethylene under weathering conditions of Tehran, Iran. The sample films were also placed at an angle of 45° to the southerly direction. Andrady et al. (1993a) also studied direct weathering outdoors of LDPE at several locations in US, in which samples were exposed on plywood backing at an angle of 45° facing south.

2.6 ADDITIVES FOR DEGRADABLE PLASTICS

It is necessary to obtain formulations of degradable plastics. Photodegradable compositions are useful, for example, for making agricultural mulching film which can be used to protect seeds and seedlings but which rapidly degrades so that it does not interfere with ripening, harvesting or replanting. Such compositions are also useful to prevent the accumulation of litter (Poyner and Cakraborty, 1993). Enhanced degradability afforded by photodegradable plastics and consequent shortening of the outdoor lifetimes of plastics litter, is expected to be environmentally desirable (Andrady et al., 1993a).

Wiles (2005b) reported that the use of pro-degradant additives speeds up degradation processes dramatically. Many compounds have been utilized as pro-degradant or pro-oxidant additives. Some methods used to accelerate the degradation process are the addition of transition metal pro-oxidants or carbon monoxide polymer, both of which are designed to catalyze photo-degradation and thermal degradation (Barr-Kumarakulasinghe, 1994).

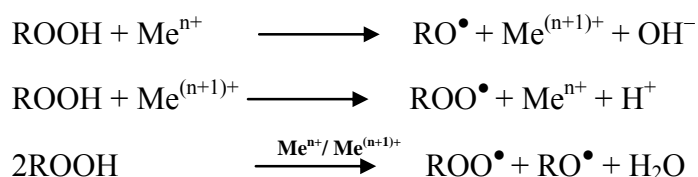
Transition metal salts are preferred as pro-oxidants for degradable compositions. The transition metal salts used in preferred embodiments are salts formed by combining transition metals with organic acids of sufficiently high molecular weight to give salt

soluble in the host polymer blends used (Griffin, 1993). Typical transition metals whose salts and complexes do feature in such applications are Ce, Zn, Cu, Ag, Ni, Co, Fe, Mn, Cr, and V (Griffin, 1993; Poyner and Cakraborty, 1993).

Many studies on pro-oxidant additives for polyethylene have been conducted. Osawa et al.(1979) have investigated the effect of a series transition metal (Ti, V, Cr, Mn, Fe, Co, Ni, Cu, Zn) stearates on the photo degradation of a high-density polyethylene. Poyner and Cakraborty (1993) used β -diketones, which have a cyclic structure, and their metal complexes as pro-degradant for LDPE. The preferred metals are those that give pale-colored complexes e.g. Zn and Mn. The amount of the pro-degradant diketone that is used is preferably 0.05 to 5%, more preferably 0.05 to 1%.

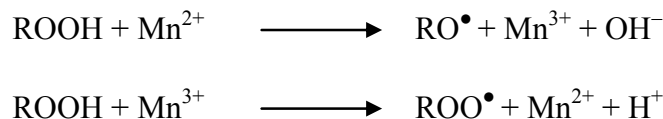
The capability of cobalt stearate as pro-oxidant additive of LDPE has been widely studied. Cobalt stearate was found to be effective in enhancing degradation of low density polyethylene (Bikiaris et al., 1997; Roy et al., 2006a; Roy et al., 2007a; Roy et al., 2006b; Roy et al., 2007b; Roy et al., 2007c). Pablos et al. (2010) studied comparative effect of Fe and Ca-stearates as pro-oxidant additives for polyethylene, i.e. LDPE and LLDPE. Polyethylene with Fe-stearate was found to degrade faster than pure polyethylene and polyethylene with Ca-stearate.

Utilization of manganese stearate as pro-oxidant additive for LDPE has also been studied. The results showed capability of manganese stearate in accelerating degradation of polyethylene (Erlandsson et al., 1997; Khabbaz et al., 1999; Sharma et al., 2001). Albertsson et al. (1994) reported that the presence of trans-metal in the degrading polymer catalyzed decomposition of hydroperoxides as shown in Scheme 2.9.



Scheme 2.9 Metal catalyst reaction with hydroperoxides

In analogy, the manganese compound catalyzes oxidation by following the mechanism shown in Scheme 2.10.



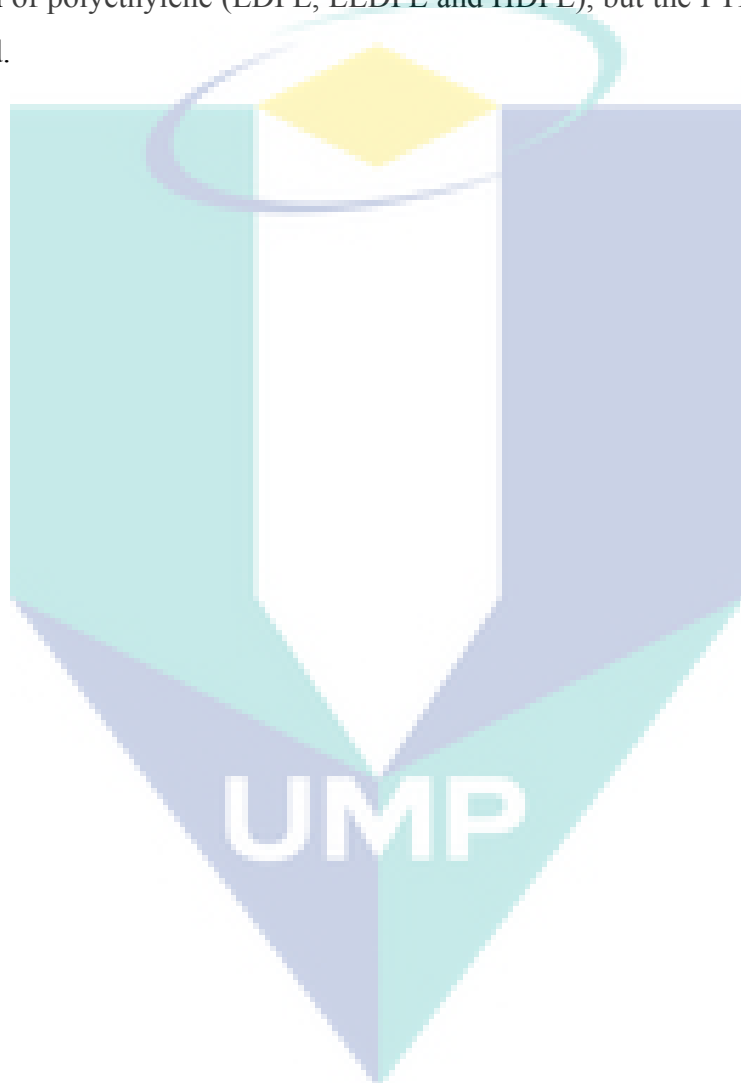
Scheme 2.10 Manganese catalyst reaction with hydroperoxides

2.7 EVALUATION OF DEGRADATION

The initiation of the degradation process is accompanied by loss of useful tensile properties (Andrady et al., 1993a; Barr-Kumarakulasinghe, 1994). Mechanical properties are the most sensitive to changes occurring during degradation, with percentage elongation being the most sensitive; percentage elongation is itself more sensitive in the direction transverse to machine extrusion of the film (Barr-Kumarakulasinghe, 1994). Among physical test methods commonly used for evaluating the oxidative stability of polymers are tensile strength and elongation at break, and impact strength. Elongation is more useful measure of oxidative degradation than tensile strength (Hamid et al., 1992).

In order to observe the aging of the material, it is characterized with respect to mechanical properties (elongation at break, tensile properties or impact strength) and visible characteristics, such as crack formation, chalking, and changes in color. The alterations in the polymeric materials on exposure can be characterized with FTIR spectroscopy and ultra violet/visible (UV/vis) spectroscopy (Singh and Sharma, 2008). Osawa et al. (1979) used carbonyl index to confirm the degradation of HDPE which took place. For plastic films used in bags, mulch film, or in six-pack carrier applications, tensile properties, tear properties, dynamic mechanical properties, puncture resistance, and other relevant measurement might be used to monitor disintegration (Andrady et al., 1993a).

Furthermore, number of characterizations or testing are carried out to observe the degradation taking place, e.g. molecular weight, thermal stability(TGA), melting temperature(DSC), crystallinity(XRD), surface morphology (SEM) as reported by Roy (Roy et al., 2007a). Colom et al.(2003) have used FTIR study, DSC test and SEM in monitoring degradation of polypropylene-polyethylene copolymer. Gulmine et al. (2003) have used FTIR, DSC, SEM, density and hardness analyses to monitor degradation of polyethylene (LDPE, LLDPE and HDPE), but the FTIR analysis is more emphasized.



CHAPTER 3

METHODOLOGY

3.1 OVERALL RESEARCH WORKS

The study of additive-assisted degradation of HDPE comprised some experimental laboratory activities. The main activities were preparation of additives of manganese carboxylates namely manganese laurate, manganese palmitate, and manganese stearate, compounding of resin and additives, treatments of samples and degradation evaluation.

The overall experimental works carried out can be seen in Figure 3.1. The initial step of research synthesized manganese carboxylates, namely manganese laurate, manganese palmitate, and manganese stearate. Following step was characterization of manganese carboxylates to obtain their important properties.

Compounding was carried out to mix additives and HDPE resin in various compositions. The compounds were then molded by injection molding machine to produce dumbbell specimens of samples. The properties of samples were observed. Treatments namely thermal treatment, accelerated weathering treatment, and natural weathering treatment, were applied to all samples of compounds and pure samples. The treatments represented artificial and natural treatments. The changes of properties of samples due to degradation were observed by comparing properties of samples, before and after treatments. The certain extent of changes of properties could be considered as certain level of degradation.

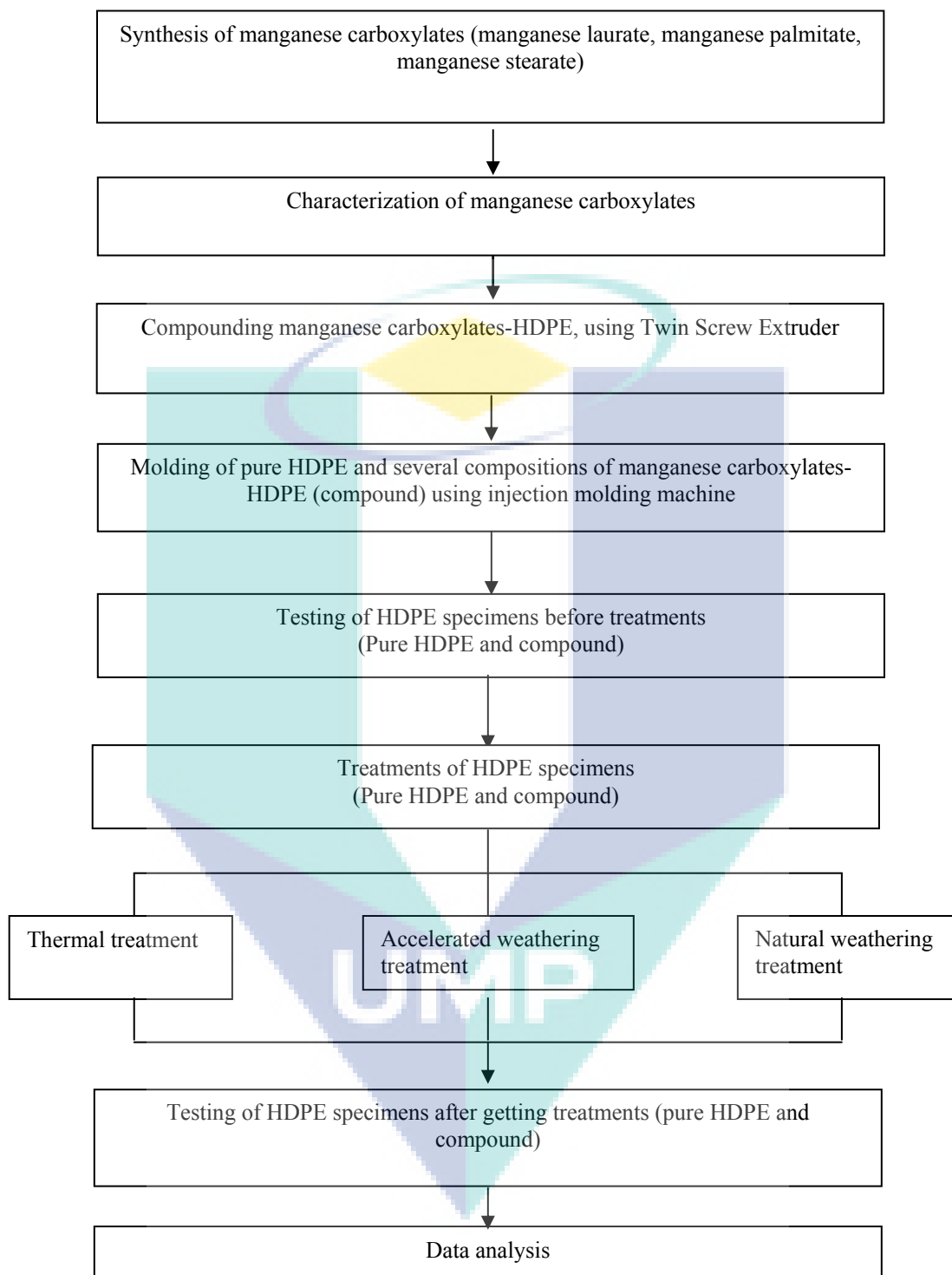


Figure 3.1 Flow chart of overall research

3.2 MATERIALS

Materials used in this study were manganese chloride tetrahydrate (System), sodium hydroxide, lauric acid, palmitic acid, stearic acid (Merck), ethanol (industrial grade), acetone, n-hexane (R&M Chemicals), cyclohexane, benzene (Merck), and toluene (System). They were used without any treatments. Deionized water was used for all processes. High density polyethylene, Etilinas HD5301AA, manufactured by Polyethylene Malaysia Sdn. Bhd., was used to prepare samples. The HDPE had a density of 0.951 kg/m^3 and melt flow index (MFI) 0.081 g/10 min at temperature of 190°C and a load of 2.16 kg.

3.3 SYNTHESIS OF MANGANESE CARBOXYLATES

Manganese carboxylates were synthesized following methods of synthesis of cobalt (II) linolenat, cobalt (II) oleat. Cobalt (II) linolenat and cobalt (II) oleat could be synthesized by metathesis reaction of cobalt salt solutions and the sodium salt of the organic acid (Grant, 1993).

Manganese carboxylates, namely manganese laurate, manganese palmitate, and manganese stearate, were synthesized through two steps of reactions. The first is reaction of carboxylic acid and sodium hydroxide and the second is reaction of sodium carboxylate and manganese (II) chloride. Carboxylic acids used were lauric acid, palmitic acid, and stearic acid with carbon chain of 12, 16, and 18, respectively. All of them were long-straight chain saturated carboxylic acid, which were in solid phase at the room temperature. The melting point of carboxylic (lauric, palmitic, and stearic) acids are in the range $44\text{-}69^\circ\text{C}$. Carboxylic acid (lauric acid, palmitic acid and stearic acid) and sodium hydroxide, in stoichiometric ratio and liquid phase, were reacted to produce sodium carboxylate (sodium laurate, sodium palmitate and sodium stearate, respectively). Carboxylic acid was mixed with water and heated up until carboxylic acid melted. Temperature maintained at $80\text{-}85^\circ\text{C}$. Sodium hydroxide 0.25M was added gradually, and maintained to be agitated for two hours. The lower temperature would make reaction take place slowly and reactants were not mixed homogenously. The higher temperature which closes to boiling point of mixture would cause formation of foam. Perfect agitation was needed to ensure mixture in well-mixed condition.

The second step, manganese chloride tetrahydrate solution 0.20 M was added gradually into the product of first step reaction containing sodium laurates, sodium palmitate, and sodium stearate to obtain manganese laurate, manganese palmitate, and manganese stearate respectively. Temperature was still maintained at 80-85°C, and kept to be continuously stirred. The stoichiometric ratios between reactants were used. The low concentration of manganese chloride was favorable since reaction would take place well in low concentration. The low concentration of manganese chloride would make the lower ratio between solid and liquid. Thus, mixing process would run well and complete reaction could be reached.

Manganese laurate, manganese palmitate, and manganese stearate in solid phase which were produced in second step were filtered and washed repeatedly with hot water to separate sodium chloride. Finally, manganese laurate, manganese palmitate, and manganese stearate were dried in the oven at temperature of 60 °C for 2 hours.

3.4 CHARACTERIZATION OF MANGANESE CARBOXYLATES

The characterization was done to determine the important properties of manganese carboxylates. The characterization comprised properties of bulk density, solubility, water content, ash content, melting point, and degradation temperature.

3.4.1 Free Fatty Acid Content

Free fatty acid content was observed by titration method. Manganese carboxylates were mixed with hot neutral-alcohol and samples were titrated with NaOH solution with phenolphthalein indicator. The volume of sodium hydroxide solution needed was recorded and weight of free fatty acid could be determined. The free fatty acid content was determined from weight of fatty acid divided by weight of sample.

3.4.2 Bulk Density

Bulk density test was performed using volumetric cylinder. The cylinder with known volume (25mL) was filled with the sample of manganese carboxylates. The excess material on top of the measuring cylinder was scraped off. The bulk density was determined by dividing the net weight of sample by volume of cylinder.

3.4.3 Solubility

The solubility was tested in water with various solvents e.g. ethanol, n-hexane, cyclohexane, acetone, benzene, and toluene. Solubility testing was conducted by pouring 2 g of manganese carboxylates (manganese laurate, manganese palmitate, or manganese stearate) in Erlenmeyer flask containing 100 ml solvent. Erlenmeyer flask was then shaken at 100 rpm at room temperature for 2 hours. The change of mixture was observed during being shaken. The mixture of manganese carboxylate and solvent was filtered to separate insoluble manganese carboxylate. The manganese carboxylate retained insoluble was weighed to check the weight change.

3.4.4 Water and Ash Content

Water content test was performed by putting crucible porcelain containing 5 g of manganese carboxylates in oven operated at 105°C, followed by weighing the sample periodically until there was no change on the weight of samples. The difference of weights, before and after heating in the oven, was calculated and compared with initial weight of sample to obtain water content value. Ash content was determined by heating up crucible porcelain containing sample up to 600°C in the furnace for 2 hours, and weighed the residue.

3.4.5 Degradation Temperature

Evaluation of degradation temperatures were performed using thermogravimetric analyzer (TGA) (MODEL: TA Instruments Q500). The applied heating rate was 20°C/min from room temperature up to 1000°C under nitrogen atmosphere, and ramp method. Platinum pans were used for this test (Bajer et al., 2007; Rimez et al., 2008).

3.4.6 Melting Temperature

Melting points were investigated using differential scanning calorimeter (DSC) (MODEL: TA Instruments Q1000). The applied heating rate was 10 °C/min in temperature range 30-200°C under nitrogen atmosphere at flow rate of 50 mL/min.

3.5 COMPOUNDING

The compounding of HDPE with manganese laurate manganese palmitate, and manganese stearate were carried out using co-rotating twin screw extruder (MODEL: Lab Tech Engineering with L/D 40) at temperature 200 °C. Prior to extrusion, HDPE and manganese laurate, manganese palmitate, and manganese stearate were dried in the oven at 80°C for 6 hours and followed by dry mixing. Mixing was conducted by putting resin and manganese carboxylates in the plastic bag, and then shaken manually for several minutes. The mixture of resin-manganese carboxylate was fed into extruder hopper gradually. Following extrusion, the material was pelletized with 2-3mm size.

3.6 INJECTION MOLDING

The pellet obtained from extruder was then dried in the oven at 80°C for 2 hours, and injection molded into specimens for tensile testing using a Nissei NS20-2A injection molder at temperature of 200°C. Samples' dimension was 63.5 x 9.80 x 3.16 mm (overall length x overall width x thickness), and dimension at the narrow section was 10.00 x 3.68 x 3.16mm (length x width x thickness), following type V sample of ASTM D638-08: Standard Test Method for Tensile properties of Plastics. The samples were labeled in accordance with percentage of manganese laurate loaded as listed in Table 3.1.

Table 3.1 Designation of samples

Sample label	Additive loaded (% , w/w)		
	Manganese laurate	Manganese palmitate	Manganese stearate
Pure	0		
ML02	0.2		
ML04	0.4		
ML06	0.6		
ML08	0.8		
ML10	1.0		
MP02		0.2	
MP04		0.4	
MP06		0.6	
MP08		0.8	
MP10		1.0	
MS02			0.2
MS04			0.4
MS06			0.6
MS08			0.8
MS10			1.0

3.7 TESTING

Testing was performed on samples to investigate mechanical properties, carbonyl index, molecular weight, MFI, thermal properties, crystallinity, and surface morphology. Detailed tests are described below. The initial properties of samples were necessary to examine for comparing with properties after treatments.

3.7.1 Carbonyl Index

Functional groups changes were observed using Fourier transforms infrared spectroscopy (FTIR) (MODEL: Thermo Nicolet Avatar 370). ATR technique was applied with 64 scans and resolution of 4 cm^{-1} . Smart performer part was used to collect background and samples spectra. The thin slices of samples' surface were taken and analyzed under the smart performer accessories of FTIR. The Ge crystal was used in this equipment. The tests were repeated three times for each sample to get consistent results.

The growth of the carbonyl absorption band at around 1718 cm^{-1} was monitored. To take into account variations in sample thickness, the ratio of the carbonyl absorption band to that of a band at 1375 cm^{-1} attributed to $-\text{CH}_3$ bending was used in the analysis. The latter peak is not affected by degradation (Andrady et al., 1993b). This latter band also known as an internal thickness band; i.e. a band that depends only on the quantity of the material exposed to the beam and remains unchanged during chemical changes. So by using this band, it compensated for the thickness differences among the samples (Bikiaris et al., 1997).

3.7.2 Tensile Properties

Tensile testing was carried out according to ASTM D638-08: Standard Test Method for Tensile Properties of Plastics. The dumbbell shape of specimens was used with dimension of $63.5 \times 9.80 \times 3.16\text{ mm}$ (overall length x overall width x thickness), and dimension at the narrow section was $10.00 \times 3.68 \times 3.16\text{ mm}$ (length x width x thickness) as shown in Figure 3.2. The specimens were placed in conditioning room at $23 \pm 3^\circ\text{C}$ for 40 hours prior to tensile testing according to ASTM D618-99: Standard Practice for Conditioning Plastics for Testing. Following conditioning process, the

specimens were tested using a universal testing machine (MODEL: Shimadzu AG-X) with a 5 kN load cell operated at a crosshead speed of 10 mm/min and gauge length (grip-to-grip) 25.4mm. Five samples were tested for each batch and average value was reported. The values reported were tensile strength, tensile modulus and elongation at break. These tests were carried out at 25°C.

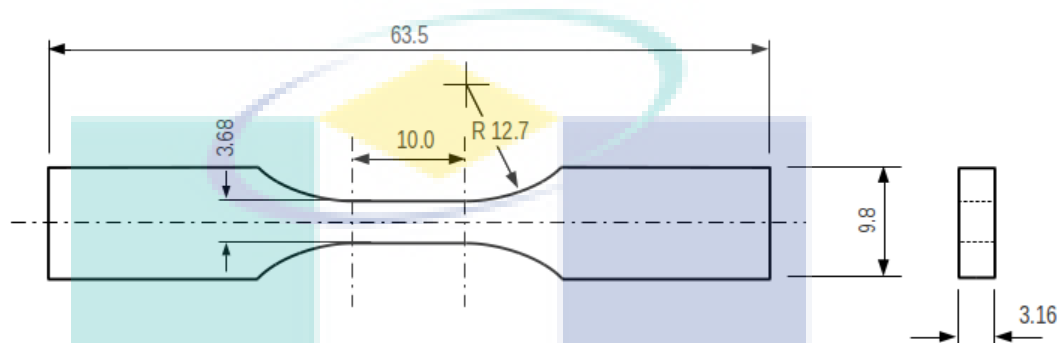


Figure 3.2 Dimension of specimen

3.7.3 Average Molecular Weight

The average molecular weights of samples were observed to reveal the degradation process. The method used was intrinsic viscosity-average molecular weight relationship or known as The Mark-Houwink-Sakurada equation. It is found that for polyethylene with xylene solvent at temperature of 105°C, the empirical constants are $K = 16.5 \times 10^{-3}$ ml/g and $a = 0.83$ (Fried, 1995; Kurata and Tsunashima, 1999; Roy et al., 2006b). The Mark-Houwink-Sakurada equation which relates intrinsic viscosity and average molecular weight of polyethylene can be presented as below.

$$[\eta] = 1.65 \cdot 10^{-3} \cdot \overline{M}_v^{0.83} \quad (3.1)$$

where $[\eta]$ = intrinsic viscosity and \overline{M}_v = average molecular weight.

The intrinsic viscosity was determined by The Huggins' Equation (Higiro et al., 2006; Huggins, 1942). Samples of HDPE in various conditions were dissolved in xylene at temperature of 105°C. The solutions must be dilute with concentration of solute in the range of 0.01-0.05 g/dl. Relative viscosity was obtained from the ratio of efflux time of

dilute solution with efflux time of pure solvent. The measurements of efflux times of pure solvent and dilute solutions were performed using Ostwald capillary viscometer. During measurement, the viscometer was immersed in constant temperature oil bath controlled at 105°C.

The plot of reduced viscosity against concentration of dilute solution was made. The intercept of linear regression line with y axis was considered as intrinsic viscosity. The average molecular weight can be then obtained by using the Mark-Houwink-Sakurada equation.

3.7.4 Melt Flow Index (MFI)

MFI was measured according to ASTM D1238-94a: Standard Test Method for Melt Flow Rates of Thermoplastics by Extrusion Plastometer using melt indexer (MODEL: Dynisco LMI 4000) at temperature of 190°C and using an applied load of 2.16 kg. Three measurements were carried out for each batch.

3.7.5 Degradation Temperature

Evaluation of degradation temperatures were performed using thermogravimetric analyzer (TGA) (MODEL: TA Instruments Q500). The applied heating rate was 20°C/min from room temperature up to 750°C under nitrogen atmosphere. The tests were carried out using platinum pan.

3.7.6 Melting Temperature

Melting point tests were carried out using Differential Scanning Calorimeter (DSC) (MODEL: TA Instruments Q1000). The DSC was operated at an applied heating rate of 10°C/min in nitrogen atmosphere, at gas flow rate of 50 mL/min, and temperature range of 35-170°C. Three consecutive run of DSC (Khabbaz et al., 1999) or the heat-cool-heat method was applied in this test. The first cycle, samples were heated up from 35°C up to 170°C; the second cycle, cooled down from 170°C to 35°C, and the third cycle, heated up to 170°C again. Melting peak temperature, onset melting temperature and heat of fusion could be obtained from the DSC scan curve.

3.7.7 Crystallinity

Crystallinity of samples was observed before and after treatments, comprised pure and additive-loaded samples. The crystallinity was investigated using DSC scan endothermic curves. The value of crystallinity was determined by comparing heat of fusion of samples with heat of fusion of fully crystalline of HDPE, 293 J/g.

$$\text{Crystallinity, } \chi_{DSC} = \frac{\Delta H_f \text{ samples}}{293} \quad (3.2)$$

For selected samples, crystallinity was also confirmed by X-ray diffraction test. XRD test was carried out using a Philip's X-ray diffractometer with a current of 15 mA and a voltage of 54 kV using Cu-K α radiation and a graphite monochromator with the range of $2\theta = 12-80^\circ$.

3.7.8 Surface Morphology

Surface morphology study was conducted to examine the changes in the surface morphology due to the treatments. This study was conducted using scanning electron microscope (SEM) (MODEL: Seizz, Evo 50) operated at 10kV and magnification of 250 \times . The tests were performed without coating.

3.8 TREATMENTS

Number of treatments was performed to investigate the performances of manganese laurate, manganese palmitate, and manganese stearate in accelerating degradation of HDPE. The treatments consisted of artificial (thermal and accelerated weathering) and natural (sunlight exposure and natural weathering) treatments.

3.8.1 Thermal Treatment

Thermal treatment was carried out using oven. Samples were incubated with circulated air at temperature of 70°C (Bikiaris et al., 1997; Roy et al., 2007b; Sharma et al., 2001) for the duration of 100, 200, 400, 600, 800 and 1000 hours. Five samples were taken for tensile testing and five additional samples at certain periods for other tests e.g. MFI, molecular weight, DSC, TGA, SEM.

3.8.2 Accelerated Weathering Treatment

Accelerated weathering treatments was carried out using an accelerated weathering tester (MODEL: Q-LAB QUV/spray with solar eye irradiance control) following ASTM G154-06: Standard Practice for Operating Fluorescent Light Apparatus for UV Exposure of Nonmetallic Materials, using UVA 340 lamps at an irradiance of 0.68 W/m^2 (Attwood et al., 2006; Beg and Pickering, 2008). Every cycle comprises 3 steps: 8 hours UV exposure 0.68 W/m^2 at 60°C , 0.25 hour water spray and 3.75 hours condensation at 50°C . The samples were submitted to the aging process for durations of 100, 200, 400, 600, 800 and 1000 hours. The samples positions were turned every 50 hours to ensure UV light reaching both sides of sample's surfaces. Five samples were taken for tensile testing and five additional samples at certain periods for other tests e.g. MFI, molecular weight, DSC, TGA, SEM.

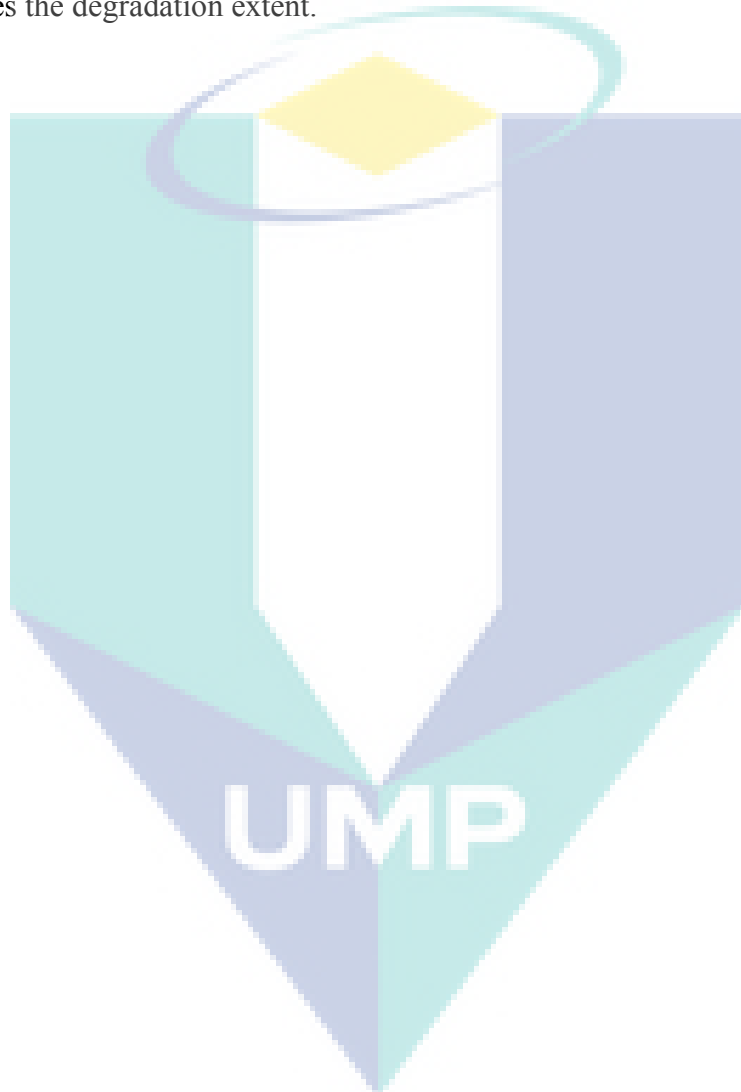
3.8.3 Natural Weathering Treatment

Natural weathering treatment of samples was carried out on the open rack facing at an angle of 45° to south (Basfar and Idriss Ali, 2006; Sheikh et al., 2006). Samples were mounted on the rack, exposed directly to outdoor natural environment. Natural weathering treatment was conducted during September 2009-March 2010 in Gambang, Malaysia. The samples were submitted to treatment for the duration of 2, 4, 6, 8, 10, 12, 16, 20, and 24 weeks. The samples positions were turned every week to ensure sunlight reaching both sides of sample's surfaces. Five samples were taken for tensile testing and five additional samples at certain periods for other tests e.g. MFI, molecular weight, DSC, TGA, SEM.

3.9 DEGRADATION EVALUATION

The degradation was observed by determining the changes of properties of samples, before and after treatments. Testing was done to samples after getting treatments. The properties of samples (compounds and pure samples) after treatments were recorded. The tests performed were same with tests before treatments, consisted of mechanical properties, carbonyl index, average molecular weight, MFI, thermal stability, melting temperature, crystallinity and surface morphology. Tensile tests were

done for all samples. For other tests, only selected samples were tested. For instance, surface morphology studies were only performed before and after longest duration of treatments. For MFI, data were taken at 200, 600, and 1000 hours of either thermal treatment or accelerated weathering treatment, at 6, 12, and 24 weeks of natural weathering treatment. All of measured properties of samples in every treatment were recorded and plotted in graphic. The comparisons of changes of properties would be used to assess the degradation extent.



CHAPTER 4

RESULTS AND DISCUSSION

4.1 SYNTHESIS AND CHARACTERIZATION OF MANGANESE CARBOXYLATES

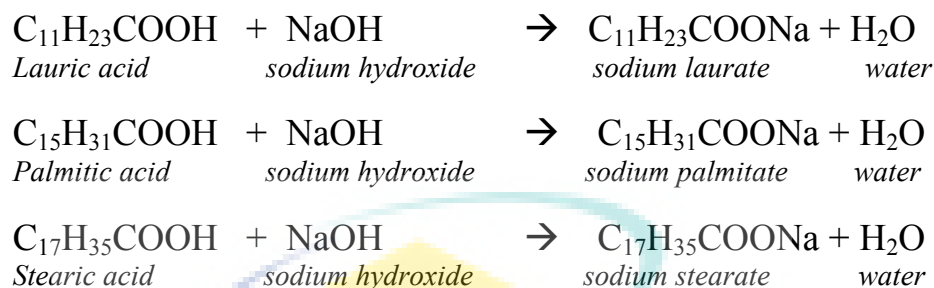
The objective of this study was to examine the effects of manganese carboxylates in accelerating the degradation of HDPE under weathering conditions. Since manganese carboxylates are the core substances in this study and to ensure consistent manganese carboxylates quality, it was decided to synthesis the manganese carboxylates in house. Furthermore, manganese laurate, manganese palmitate, and manganese stearate are not commonly used in industry, hence, are very difficult to find suppliers for such products. However, this study focuses on utilization of manganese carboxylates as pro-degradant additives for HDPE, hence; the synthesis is not deeply investigated. The synthesis is aimed just to get the products i.e. manganese laurate, manganese palmitate and manganese stearate. However characterization of products has been done to make sure that the products are manganese carboxylates and also to obtain the properties of manganese carboxylates.

4.1.1 Synthesis of Manganese Carboxylates

Synthesis of manganese carboxylates, namely: manganese laurate, manganese palmitate and manganese stearate, has been carried out following the similar procedure of synthesis of cobalt (II) oleate and cobalt (II) linolenate which comprises two steps of reactions.

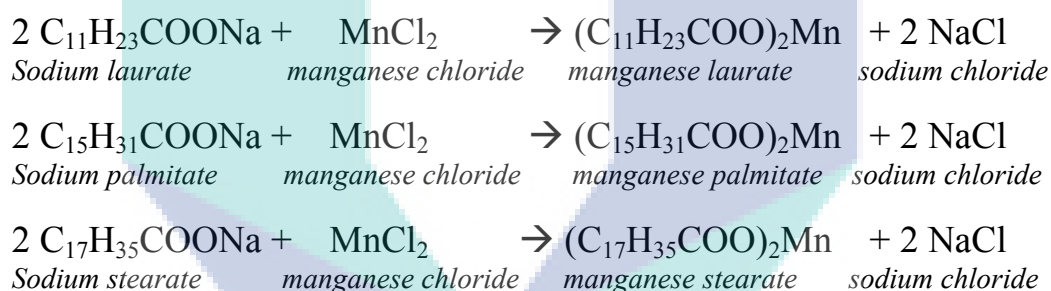
The first step comprised reactions between (a) sodium hydroxide and lauric acid, (b) sodium hydroxide and palmitic acid, and (c) sodium hydroxide and stearic acid that

produce sodium carboxylates, namely sodium laurate, sodium palmitate, and sodium stearate. Those reactions can be stated as shown in Scheme 4.1.



Scheme 4.1 Sodium carboxylates synthesis

The second step comprised reactions between manganese chloride and sodium carboxylates namely sodium laurate, sodium palmitate, and sodium stearate, that could be written as shown in Scheme 4.2.



Scheme 4.2 Manganese carboxylates synthesis

The yields of reactions were calculated from the real amount of final products compared to the theoretical amount of the final products. The yields of reactions were found to be not significantly different for different carboxylic acids, i.e. manganese laurate (ML) 99.35 %, manganese palmitate (MP) 98.92% and manganese stearate (MS) 99.09%.

4.1.2 Characterization of Manganese Carboxylates

Characterization was carried out for manganese carboxylates which have been synthesized in the laboratory. Characterization of manganese carboxylates was performed in order to observe the essential properties to be a polymer additive. The characteristics of manganese carboxylates observed include free fatty acid content, bulk

density, water content, ash content, solubility, degradation temperature, and melting point. Thermal properties are very important since polymer processing take place at a relatively high temperature.

Analysis of free fatty acid (FFA) on the manganese carboxylates concluded that the manganese carboxylates were free from FFA, even with batches of lower than 100% yield. The reason behind this was the fact that the unreacted carboxylic acids flew as filtrate during filtration or washed up by hot water during washing process.

The solubility of manganese carboxylates in several solvents have been investigated in water and several types of solvents namely ethanol, n-hexane, cyclohexane, acetone, benzene, and toluene. All manganese carboxylates were insoluble in water and also in all other solvents used. All manganese carboxylates exhibited same properties in solubility.

The bulk densities of manganese carboxylates and other essential properties are reported in Table 4.1. All of manganese carboxylates are in the form of powder and have low densities. The water contents of manganese carboxylates are almost similar, in the range of 2.3 to 2.7%. The ash content of manganese laurate is the highest among manganese carboxylates. This is due to the highest content of manganese which retain as residue during heating. The trend shows that ash contents of manganese carboxylates increase with decreasing chain length of carboxylates. It can be explained by the content of manganese in every one gram of manganese carboxylates. The manganese content was 12.1 % per gram manganese laurate, 9.7 and 8.8 % for manganese palmitate and manganese stearate, respectively.

Thermal stability of manganese carboxylates was investigated using Thermogravimetric Analyzers (TGA). Figure 4.1 and 4.2 represent TG and DTG traces of manganese carboxylates. The corresponding data have been reported earlier in Table 4.1. Degradation temperature was determined from extreme decrease of weight during heating process. It is shown by steep slope of the curve in TGA test result. Manganese carboxylates lost more than 80% of their weight during degradation process. The

maximum degradation points were determined from the peaks of curves of relations between derivative weight change and temperature.

Table 4.1 Properties of manganese carboxylates

Property	Manganese Laurate	Manganese Palmitate	Manganese Stearate
Bulk density, g/cm ³	0.376	0.227	0.201
Water content, %	2.70	2.31	2.39
Ash content, %	18.84	16.87	14.34
Degradation temperature, °C			
T _{onset}	275.59	285.42	287.98
T _{maximum}	319.81	335.48	347.72
T _{final}	406.68	408.63	411.73
Melting temperature, °C			
T _{onset}	104.95	111.27	114.69
T _{m (peak)}	108.11	115.09	117.66

TGA test results have revealed a single step degradation of all manganese carboxylates. The degradation temperatures of manganese carboxylates increase with increasing chain length of molecule, from manganese laurate (ML) with 12 carbon atoms, manganese palmitate (MP) with 16 carbon atoms, and manganese stearate (MS) with 18 carbon atoms respectively. The decrease in the decomposition temperatures is associated with shorter carbon chain. The shorter chain of manganese carboxylates gives the lower thermal stability.

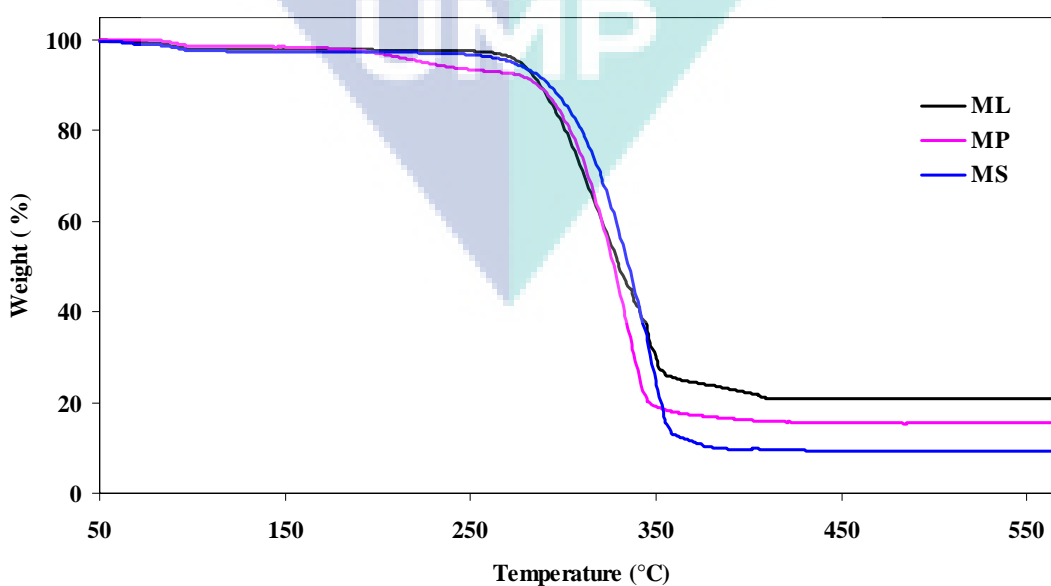


Figure 4.1 TG traces of manganese carboxylates

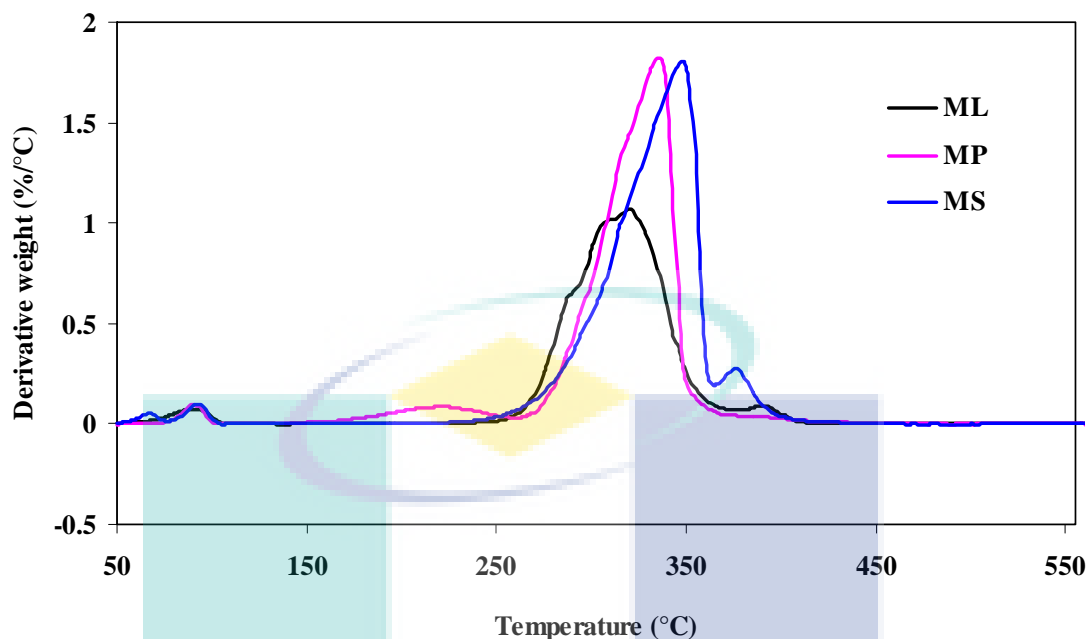


Figure 4.2 DTG traces of manganese carboxylates

Manganese laurate starts to degrade at temperature of 275.59 °C. Manganese palmitate and stearate have higher degradation temperatures than manganese laurate. All manganese carboxylates have good thermal stability, especially in application for polyethylene, since the temperature of polyethylene processing is much lower than their degradation temperatures.

Tests have been done using Differential Scanning Calorimeters (DSC) to determine melting point of manganese carboxylates. The DSC test results can be seen in Figures 4.3. The melting points of manganese laurate, manganese palmitate, and manganese stearate were determined from the peak of endothermic melting transition. In the calorimetric study performed by DSC, the melting onset temperature (T_o) and the melting peak temperature (T_p) of material could be obtained as reported by Colom *et al.* (2003). Melting points of manganese carboxylates were summarized as listed in Table 3 below.

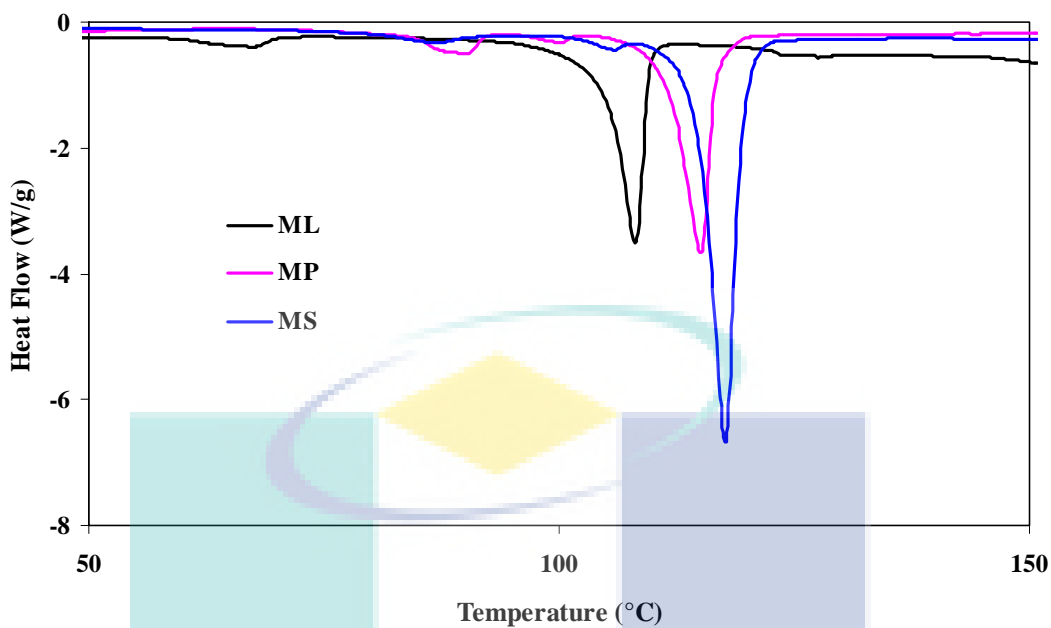


Figure 4.3 DSC scans of manganese carboxylates

Melting points of manganese carboxylates increased with increasing carbon chain length of carboxylates. The increase of melting points is not linear as increasing chain length. As discussed in section of thermal stability, melting points of manganese carboxylates show the similar behavior with polymeric material. The shorter chains of molecules of manganese carboxylates give the lower melting point.

4.2 THERMO-OXIDATIVE DEGRADATION OF HIGH DENSITY POLYETHYLENE

4.2.1 Introduction

Thermo-oxidative degradation of HDPE with manganese carboxylates have been studied at temperature of 70°C in the air-circulated oven. Thermo-oxidative degradation tests are mostly conducted instead of composting condition. During composting, the temperature can reach 70°C. There are factors that affect composting process; however temperature is the most influencing factor. Some characteristics have been monitored in considering thermo-oxidative degradation including infrared spectra, tensile strength, tensile modulus, elongation at break, average molecular weight, melt flow index, degradation temperature, melting temperature, crystallinity and surface morphology.

4.2.2 Infrared Spectra

The oxidation of polyethylene resulting products with carbonyl groups was monitored by measuring the existence of carbonyl peaks. Generally, some carbonyl groups (1700 cm^{-1}) are usually detected by infrared spectroscopy in all unexposed polymers. Some groups grew during aging (Seymour, 1971). Figure 4.4 shows the FTIR spectra of treated and untreated sample of ML10. As mentioned earlier, the bands of around 1718 and 1375 cm^{-1} are used as basis of carbonyl index calculation. Nevertheless, the region of $1700\text{-}1800\text{ cm}^{-1}$ seems to consolidate and also region of $1350\text{-}1400\text{ cm}^{-1}$. Sometimes it is hard to distinguish certain peaks, since they are overlapped by other peaks (Bikiaris et al., 1997; Khabbaz et al., 1999), so they appear to be one peak. However, the difference of traces was obviously exhibited by the presence of absorbance peak at around 1718 cm^{-1} . The peak evidenced the process of oxidation. Before treatment peaks around 1718 cm^{-1} did not obviously appear, but grew during incubation. It has been observed that for degraded polyethylene, the absorption band around 1714 cm^{-1} (Gulmine et al., 2003) or 1718 cm^{-1} (Andrady et al., 1993b), which can be assigned to the C=O stretching vibration of a ketone group, grows in intensity with extended aging, and at the same time new bands begin to appear. These absorption bands indicate that more than one oxidation product is formed. The carbonyl bands were assigned to C=O stretching vibrations in aldehydes and/or esters (1733 cm^{-1}) carboxylic acid groups (1700 cm^{-1}) and γ -lactone (1780 cm^{-1}) (Gulmine et al., 2003).

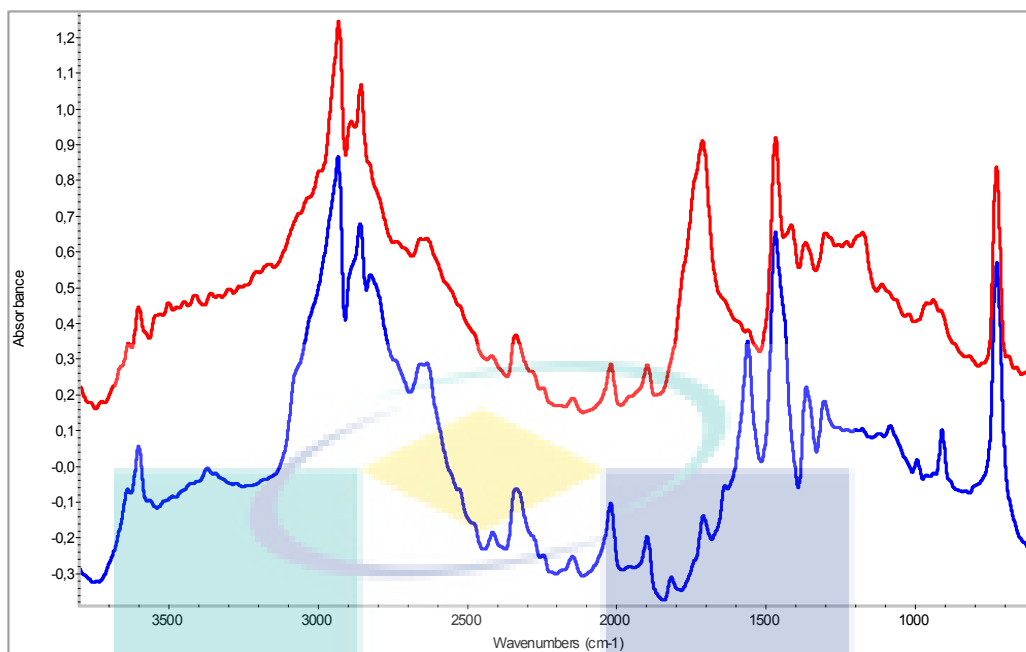


Figure 4.4 FTIR spectra of ML10 samples, before (lower trace) and after (upper trace) thermal treatment

The absorbances at some regions were also found to increase. The regions were at $3300\text{--}3500\text{ cm}^{-1}$ (hydroxyl groups), $1000\text{--}1300\text{ cm}^{-1}$ (ether groups), and $900\text{--}1000\text{ cm}^{-1}$ (vinyl groups). However, those increases are not significant. The peak at around 1560 cm^{-1} appeared in untreated samples and faded during treatment. This peak is assigned to manganese carboxylates. As reported in previous study, the presence of absorbance at 1560 cm^{-1} was due to asymmetric vibration stretching of the carboxylic group coordinated to metal ion (Roy et al., 2006b). The manganese carboxylates decomposed when acting as catalyst in decomposing of hydroperoxides.

Figure 4.5 shows the carbonyl index (CI) of samples during treatment. In the early periods of treatment, CI slightly increased, after 200 hours of treatment, the CI increased more significantly. Samples containing manganese carboxylates experienced much more increase of CI than pure sample as the result of higher degradation level. For instance, the CI of pure samples increased from initial value of 0.022 to 3.015 after 1000 hours of thermal treatment and from initial value of 0.095–0.102 to 12.459–14.432 in the end of treatment for samples with additives (1% w/w). This result is consistent with previous studies which have recorded the increase of CI of polyethylene containing pro-oxidant additives during thermo-oxidative aging (Khabbaz et al., 1999; Roy et al., 2007b).

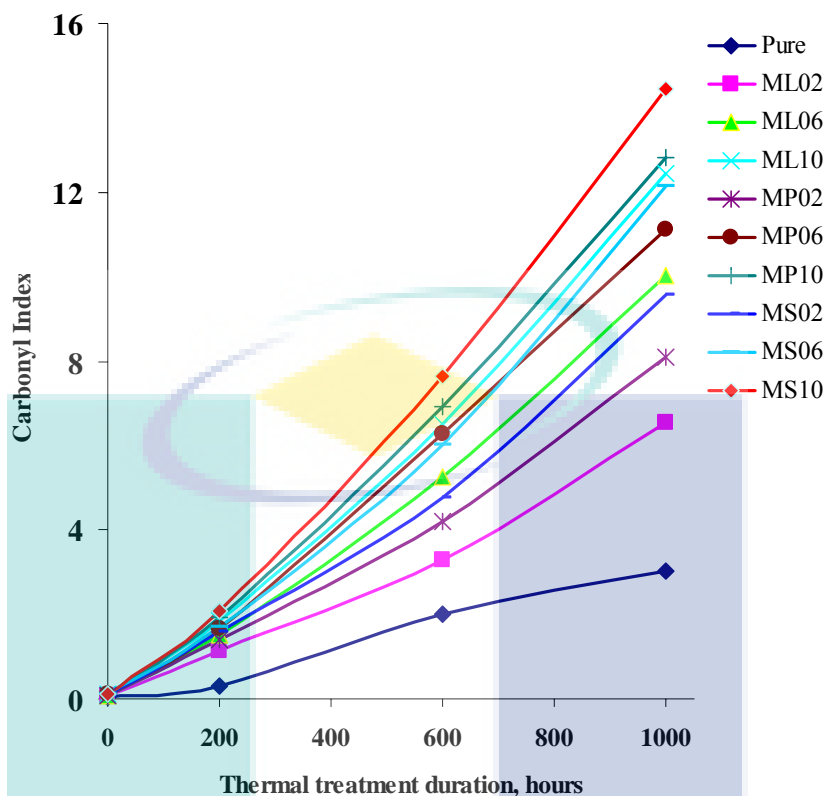


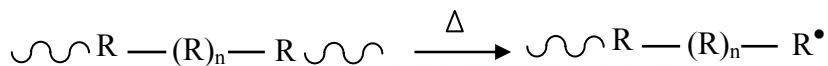
Figure 4.5 Carbonyl index of HDPE samples with various compositions during thermal treatment

4.2.3 Tensile Properties

Tensile properties of samples were observed during thermal treatment. The observations comprised tensile strength, tensile modulus and elongation at break. Little differences were found for tensile strength of pure sample and samples containing manganese carboxylate at initial condition i.e. before treatments. This result indicates that there is no significant effect of incorporation of manganese carboxylate on the tensile strength of HDPE. Figures 4.6–4.8 represent the changes in tensile strength during thermal treatment. Tensile strength of pure sample increased in the early period of thermal treatment and followed by slowly decreased after 200 hours of treatment. In the early period, crosslinking of HDPE might have occurred (Vasile and Pascu, 2005), resulting the higher tensile strength observed (Roy et al., 2006b). Crosslinking of polyethylene has occurred as result of coupling of alkyl radicals (Johnston and Morrison, 1996) due to thermal treatment. The mechanism of thermo-oxidative degradation of HDPE can be written as shown in Scheme 4.3 following model proposed

by Singh and Sharma(2008). The mechanism comprised three steps namely initiation, propagation and termination. The coupling of alkyl radicals took place during termination.

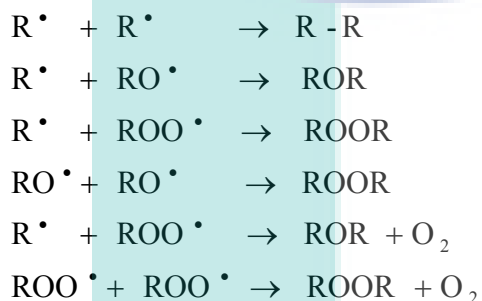
Initiation



Propagation



Termination



Scheme 4.3 Mechanism of thermo-oxidative degradation

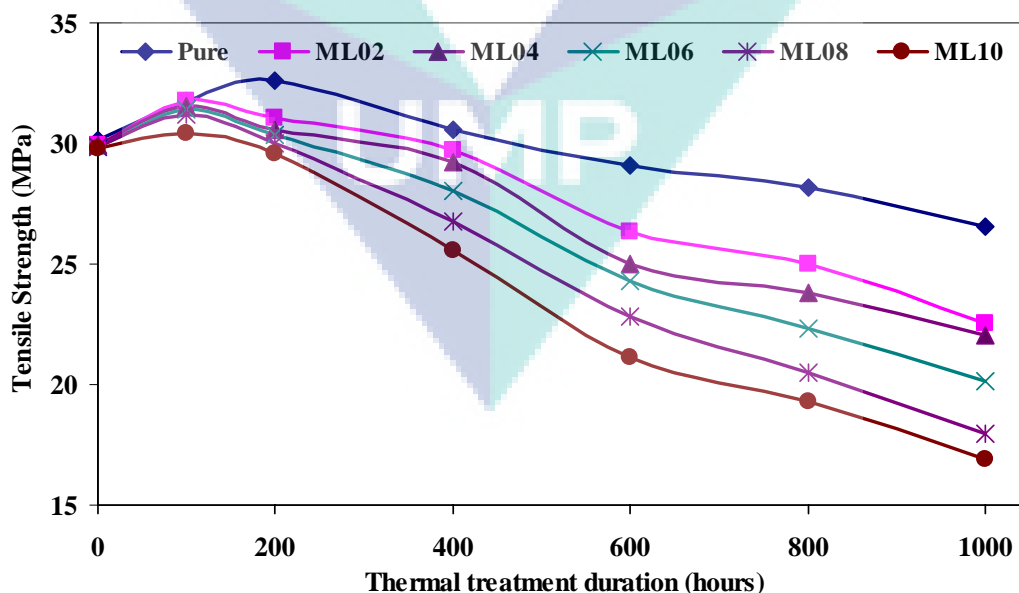


Figure 4.6 Tensile strength of HDPE containing manganese laurate during thermal treatment

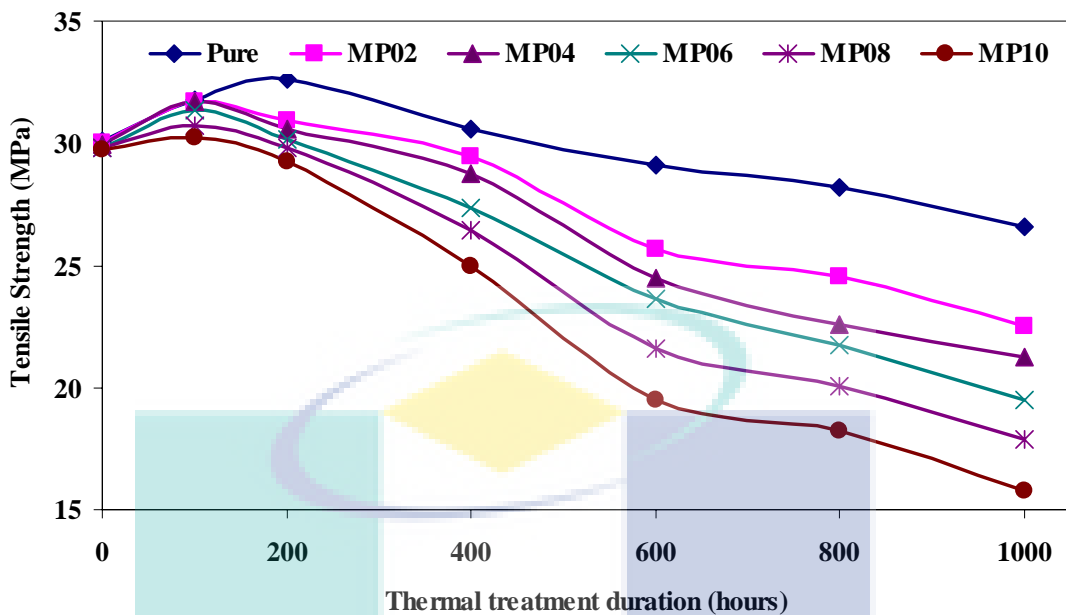


Figure 4.7 Tensile strength of HDPE containing manganese palmitate during thermal treatment

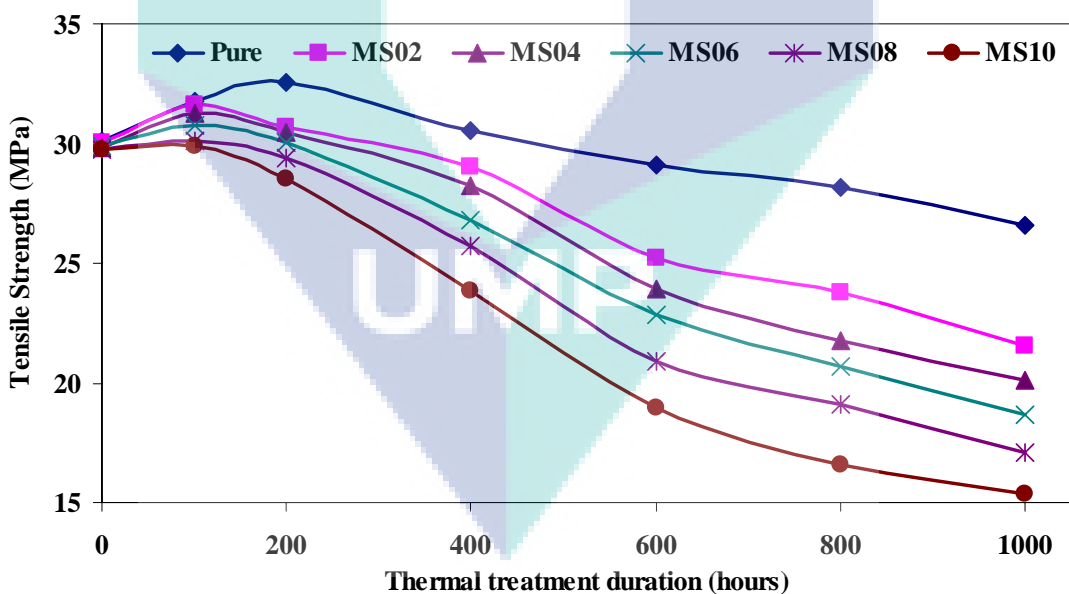


Figure 4.8 Tensile strength of HDPE containing manganese stearate during thermal treatment

However, chain scissions due to thermal treatment lead to the decrease of tensile strength. Pure samples lost about 11.74% of their tensile strength after 1000 hours of thermal incubation. On the other hand, the tensile strengths of samples containing

manganese carboxylates showed the significant amount of lowering during thermal treatment.

The tensile strength of ML02, MP02 and MS02 samples slightly increased in the first hundred hours and thereafter decreased gradually. Meanwhile the tensile strengths of ML10, MP10, and MS10 samples were relatively constant until a hundred hours and then decreased. In the early hours of incubation, the crosslinking phenomenon probably took place, while the oxidation might have not occurred yet, so that tensile strength appeared to rise with a minor scale. At the initial stage, if the higher concentrations of manganese laurate were loaded, the increasing of tensile strength did not obviously occur.

After 200 hours of thermal treatment, tensile strength of samples containing manganese laurate, manganese palmitate, and manganese stearate started to decrease. This suggested that oxidation was initiating to take place on the polyethylene and then resulting in the chain scissions of polyethylene. With the increasing amount of manganese laurate, resulted in the decrease of the tensile strength observed. After 1000 hours of thermal treatment, tensile strength decreased for ML02 and ML10 samples as much as 24.80% and 43.33%, respectively. The losses of tensile strengths of selected samples are presented in Table 4.2. Samples with manganese stearate experienced the largest decrease of tensile strength. This result indicates that the manganese carboxylates play a role for increasing the rate of degradation of HDPE. Simply, the degree of tensile strength decreasing is in accordance with manganese carboxylate loading.

The changes of tensile modulus of samples have shown the similar trends with those of tensile strength. The decreases of tensile modulus occurred proportionally with the decreases of tensile strength. However the decreases of tensile modulus were lesser than those of tensile strength. Figures 4.9-4.11 represent tensile modulus of samples during thermal treatment, and the losses of tensile modulus for selected samples are presented in Table 4.2.

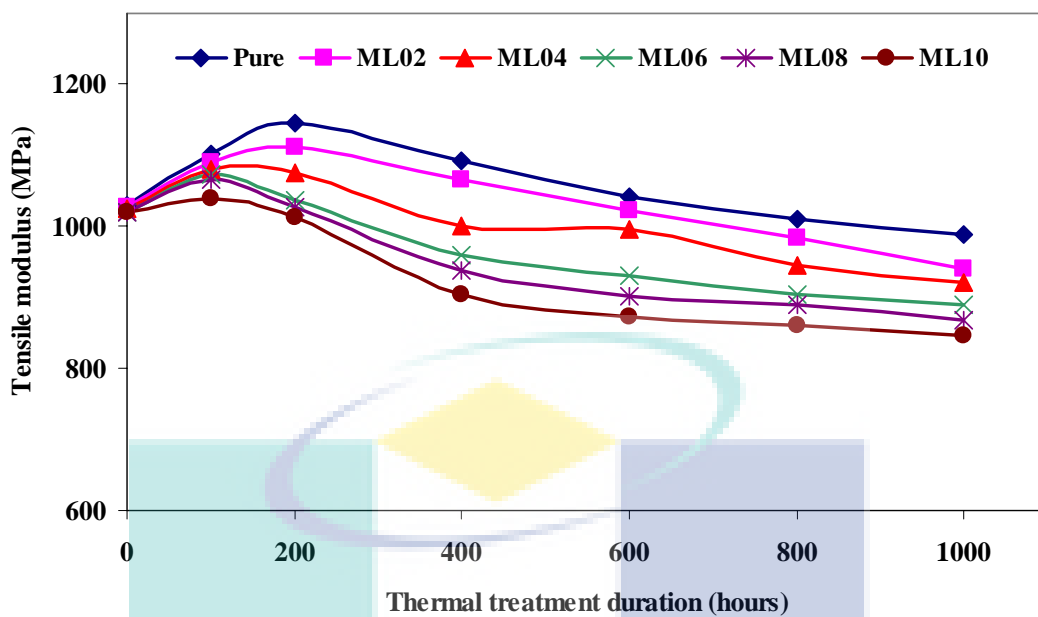


Figure 4.9 Tensile modulus of HDPE containing manganese laurate during thermal treatment

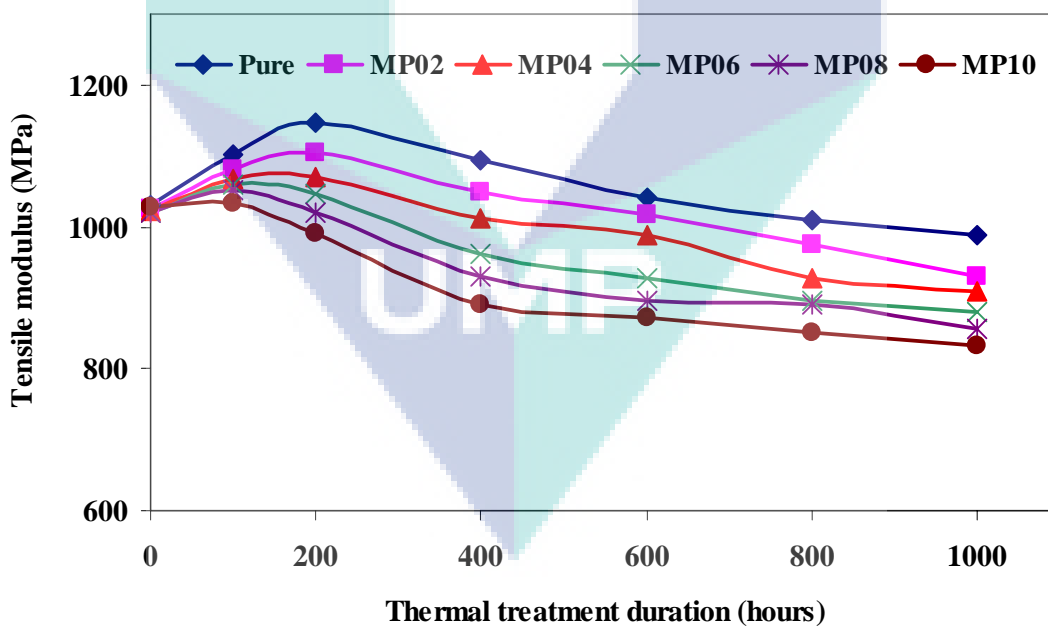


Figure 4.10 Tensile modulus of HDPE containing manganese palmitate during thermal treatment

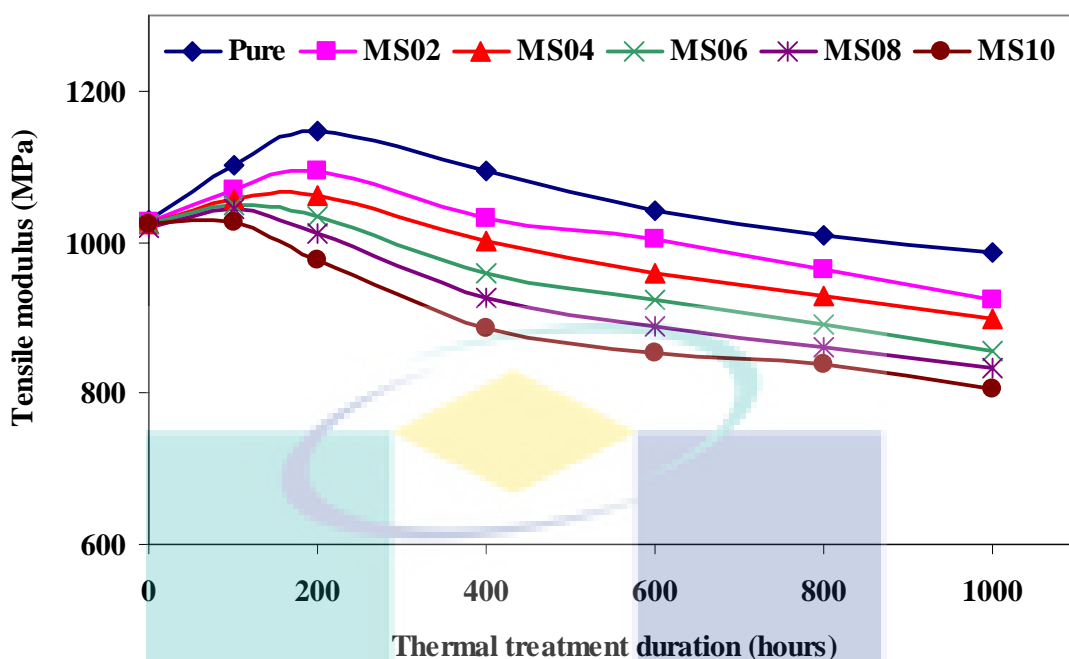


Figure 4.11 Tensile modulus of HDPE containing manganese stearate during thermal treatment

Table 4.2 Losses of tensile properties of samples after 1000 hours of thermal treatment

Samples	Loss of tensile strength, %	Loss of tensile modulus, %	Loss of elongation at break, %
Pure	11.74	5.13	16.21
ML02	24.80	8.38	36.07
ML10	43.33	17.04	55.85
MP02	25.04	9.37	39.42
MP10	47.00	18.91	58.42
MS02	28.12	10.12	42.04
MS10	48.38	21.40	62.11

Figures 4.12–4.14 reveal the changes in elongation at break of samples during treatment. There was no significant decrease of elongation at break for pure samples; however, the significant lowering was observed for the manganese carboxylate-containing samples. Despite the increase in tensile strength of all samples with different levels, at the first hours of thermal treatment, elongation at break tended to decrease from the beginning of treatment. When crosslinking underwent, specimens grew to be harder and more brittle, so that the elongation at break decreased. Elongation at break

proceeded to decrease more rapidly when the chain scissions took place in the oxidation stage of degradation.

The decrease of strains at break is rising by increasing the amount of all types of manganese stearate loading in HDPE. For comparison, pure samples lost 16.21% of the initial strain at the break, while 42.04% for MS02 samples and 62.11% for MS10 samples, after 1000 hours of treatment as shown in Table 4.2. Manganese stearate showed the highest lowering of elongation at break among manganese carboxylates used, followed by manganese palmitate and manganese laurate. The order of effects follows the chain length of manganese carboxylate. Manganese stearate (C_{18}) has longest chain, followed by manganese palmitate (C_{16}) and manganese laurate (C_{12}). Chain length plays a vital role in degradation. When the chain length increases, the carboxylate is capable of blending easily with the base polymer resulting in its increased capability to act as pro-oxidant, as reported by Roy et al. (2006b). It is due to similar structure of the long carbon chain of stearate with structure of polyethylene.

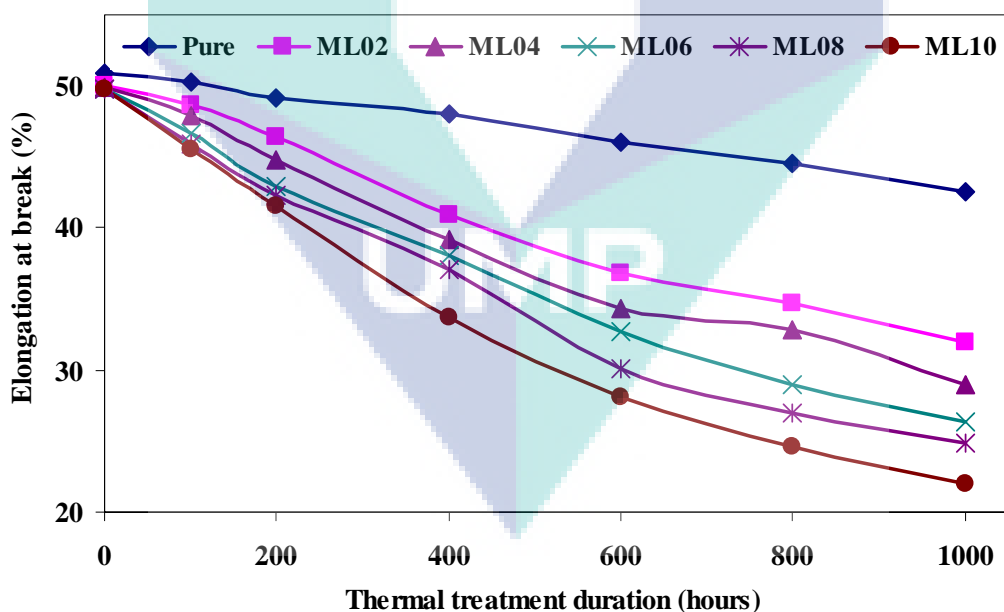


Figure 4.12 Elongation at break of HDPE containing manganese laurate during thermal treatment

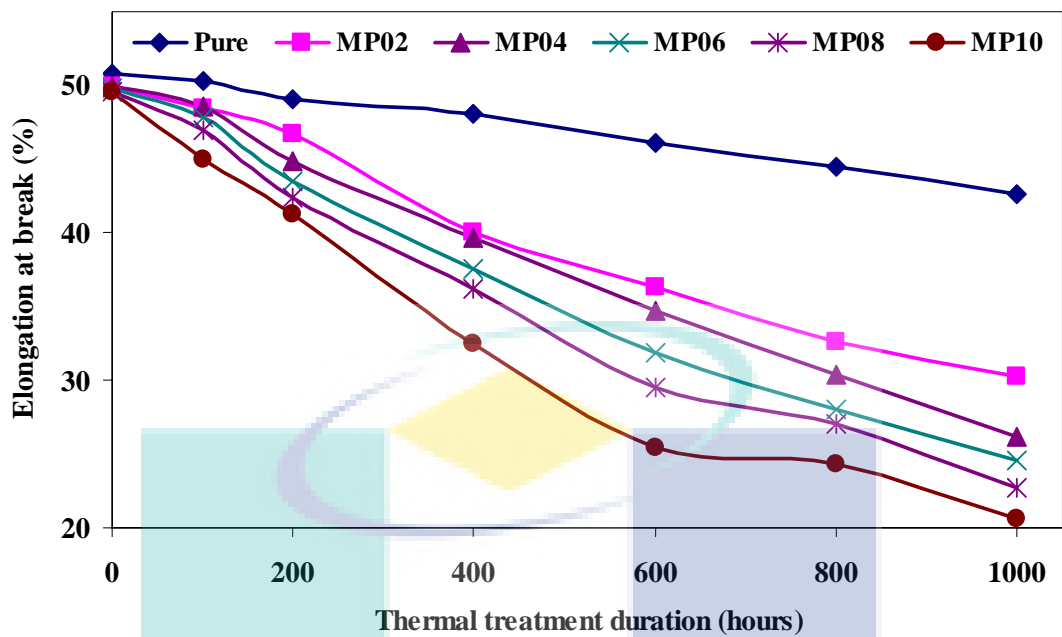


Figure 4.13 Elongation at break of HDPE containing manganese palmitate during thermal treatment

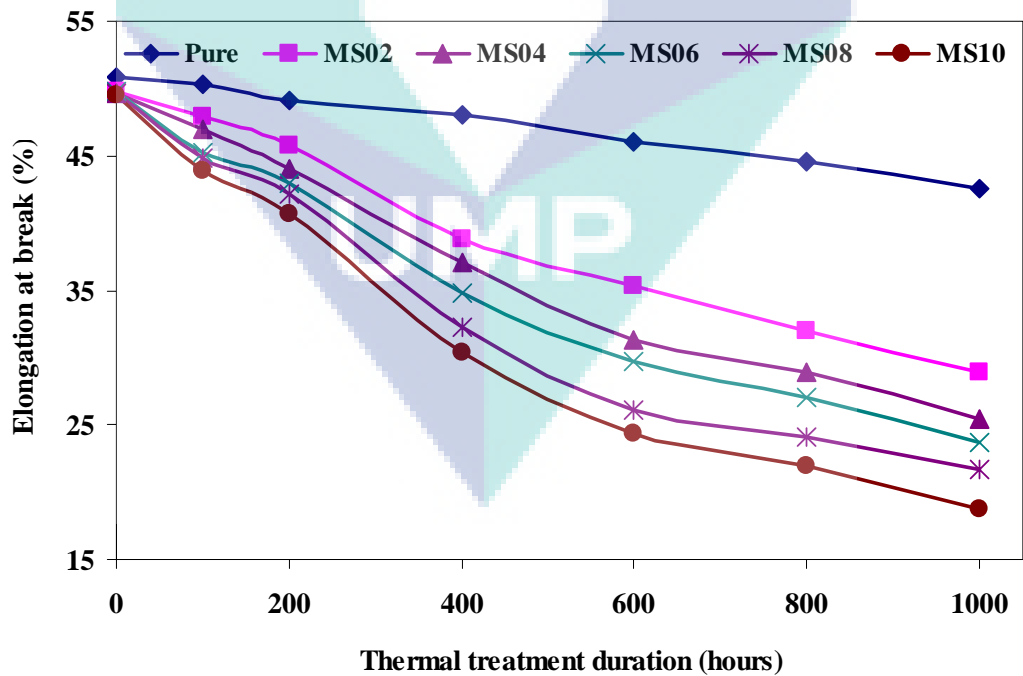


Figure 4.14 Elongation at break of HDPE containing manganese stearate during thermal treatment.

Mechanical properties depend strongly on molecular weight and more precisely on molecular weight distribution. There was a significant decrease in mechanical properties during the course of thermal incubation. The reason is that the concentration of high-molecular-weight chains, which contribute to the most of the mechanical properties, is decreasing during the oxidation as a result of chain scission (Bikiaris et al., 1997).

In the previous study, Sharma et al. (2001) conducted thermo-oxidative aging of LLDPE containing manganese stearate. They found that the manganese stearate improved the degradation process of LLDPE resulting in the dramatic loss of elongation and tensile properties during thermal exposure. The blend of LLDPE (LLDPE with 6 % of starch, 6 % of epoxidized rubber and 600 ppm (0.06 %) of manganese stearate) has lost about 29 % of its initial tensile strength and 30 % of its initial elongation at break after 4 weeks (672 hours) of thermal treatment. On the other hand, HDPE with 0.2 % of manganese stearate has lost 20.74 % of its initial tensile strength and 35.86 % of its initial elongation at break after 800 hours of thermal treatment. Thus HDPE samples containing manganese stearate showed lesser amount of loss of tensile and elongation at break compared with LLDPE containing manganese stearate. This was due to the stability against aging of HDPE is higher than LDPE and LLDPE as reported in literature (Gulmine et al., 2003) and also due to different length of carboxylic chain of manganese salt. Winslow (1977) and Iring et al. (1986) have also reported that branched polyethylene is more readily oxidized than the linear analogues due to the presence of tertiary C-H site at each branch point.

4.2.4 Molecular Weight

Average molecular weight is a direct measure of chain scissions process resulting lower chain length of molecules. Shorter chains of polymers mean lower molecular weights. The average molecular weight (\overline{M}_v) obtained by viscometry method are presented in Figure 4.15.

As observed in Figure 4.15, upon thermal treatment \overline{M}_v of all samples decreased accordingly including pure HDPE. The \overline{M}_v of pure samples decreased

gradually. Pure sample only experienced \overline{M}_v lowering of 16.12%. In contrary, the \overline{M}_v of samples with manganese carboxylate decreased significantly during thermal treatment. Increasing the amount of manganese carboxylate resulted in greater decrease of molecular weight. It can be seen in the plot at different amount of manganese carboxylates loading. For example, sample with 0.2 % of manganese stearate (MS02) experienced lowering of \overline{M}_v as much as 54.27 %, while the lowering values of \overline{M}_v for MS06 and MS10 were 63.23 % and 69.49 %, respectively as shown in Figure 4.12. Sample containing 1% manganese stearate (MS10) experienced the greatest lowering of \overline{M}_v . That is greater than those samples containing 1% manganese laurate (ML10) and manganese palmitate (MP10) with values of 67.51 and 68.38 %, respectively.

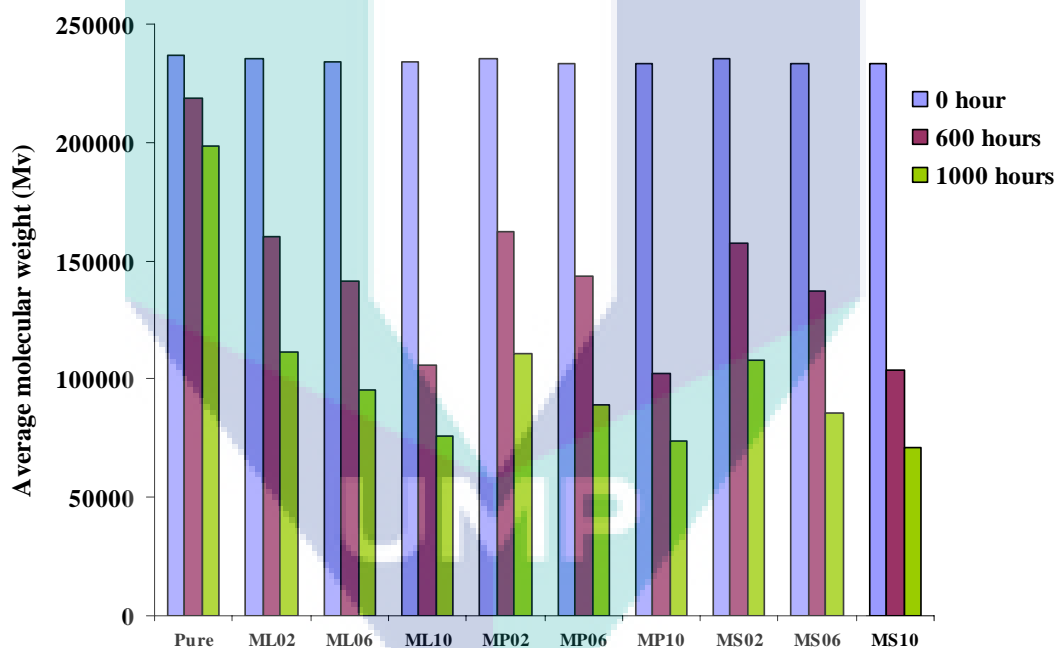


Figure 4.15 Average molecular weights of various samples during thermal treatment

There is little bit different among manganese carboxylates effects on average molecular weight. However, in general, manganese stearate gave the highest effect on molecular weight of HDPE among manganese carboxylates. It is due to capability manganese stearate to blend easily with polymer compared with manganese palmitate and manganese laurate, as mentioned previously. The samples containing manganese carboxylates showed the decrease of molecular weight paralleled to the reduction of mechanical properties i.e. tensile strength and elongation at break. This is the evidence

of the chain scission took place during treatment. This result is in agreement with that of Erlandsson et al. (1997) who found that polyethylene containing pro-oxidant experienced a much larger decrease of molecular weight than the pure one during thermal aging.

4.2.5 Melt Flow Index

Melt flow index (MFI) is indirectly a measure of molecular weight (Bikiaris et al., 1997). Molecular weight can be reflected in the mechanical properties. Reduction of mechanical properties reflects reduction of molecular weight (Bikiaris et al., 1997; Sung and Nikolov, 1992). Measuring MFI gives supporting evidence on the degradation which has taken place.

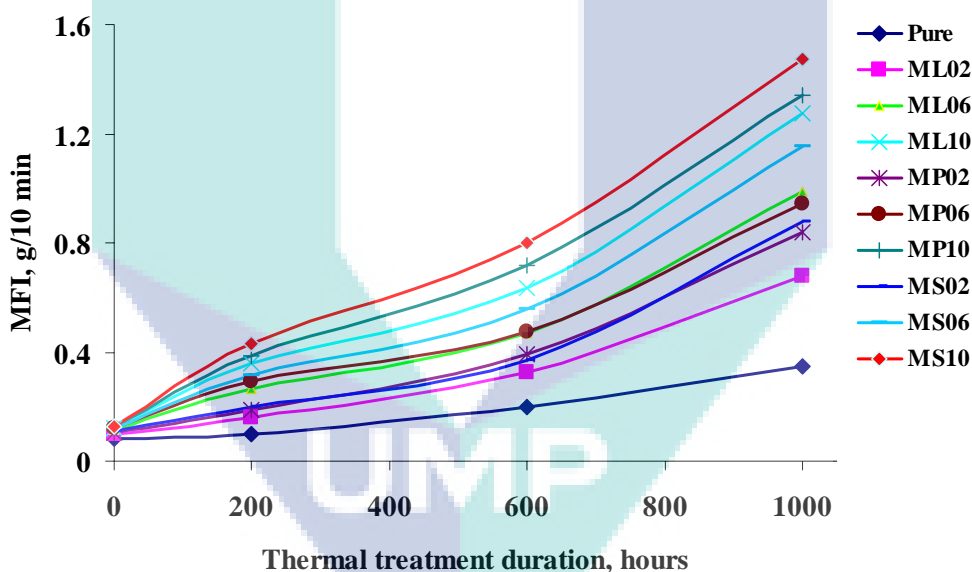


Figure 4.16 MFI of various samples during thermal treatment

Loading of manganese carboxylate resulted in an increase in MFI of the samples during treatment as shown in Figure 4.16. The MFI of samples containing manganese carboxylate increased slowly at the beginning period, and faster in the end period, while pure samples experienced gradual increase. Samples with higher amount of loaded-manganese carboxylate experienced higher increase of MFI. Manganese stearate was found to result in highest increase of MFI of samples. With the increase of MFI confirmed the molecular weight decrease as result of chain scission that produced lower

molecular weight macromolecules. The MFI also increased with increasing the duration of thermal treatment, whereas molecular weight decreased.

4.2.6 Degradation Temperature

Degradation temperature constitutes a measure of thermal stability of samples. Some information can be gained in TG or DTG trace regarding thermal stability of sample. For example, TG and DTG traces of pure sample and ML10 sample are presented in Figure 4.17–4.20, and the corresponding data are listed in Table 4.3. The plot showed that TG and its derivative (DTG) traces shifted to lower temperatures after getting thermal treatment for 1000 hours. TG traces of pure HDPE samples were also shifted to lower temperature after 1000 hours thermal treatment.

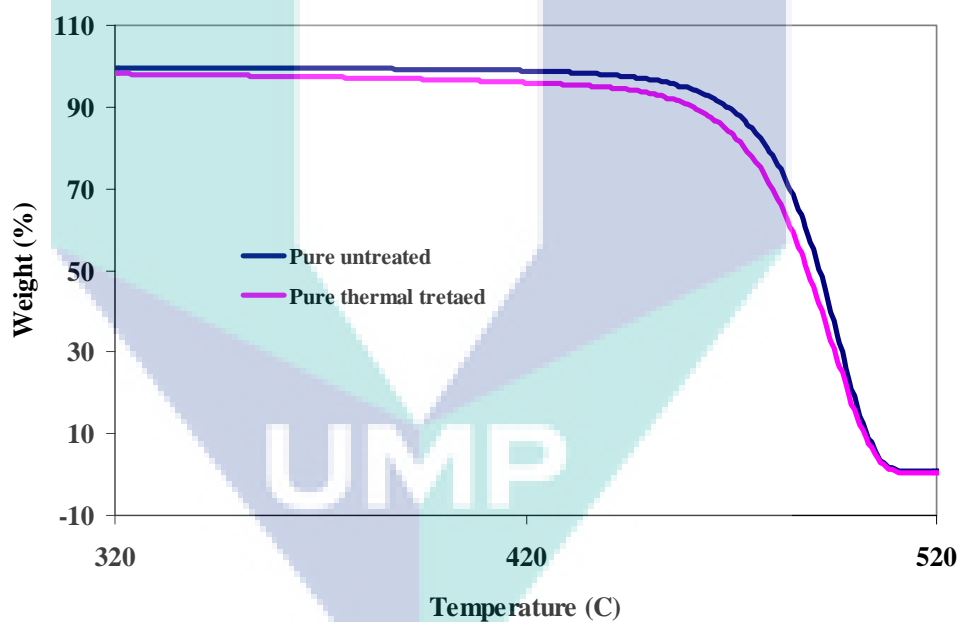


Figure 4.17 TG traces of pure samples, before and after 1000 hours of thermal treatment

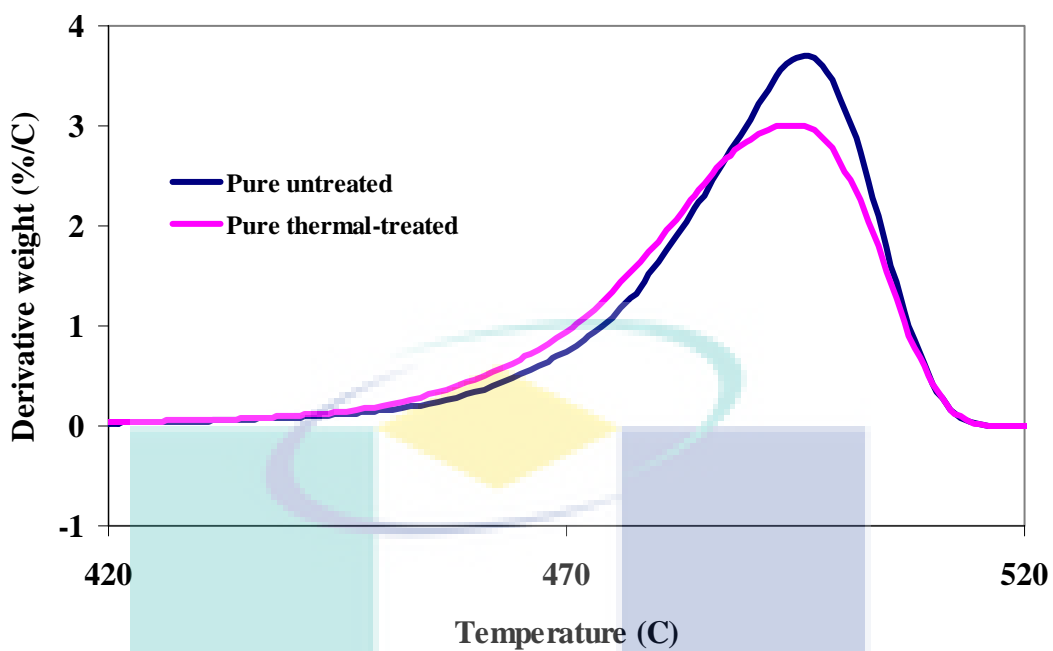


Figure 4.18 DTG traces of pure samples, before and after 1000 hours of thermal treatment

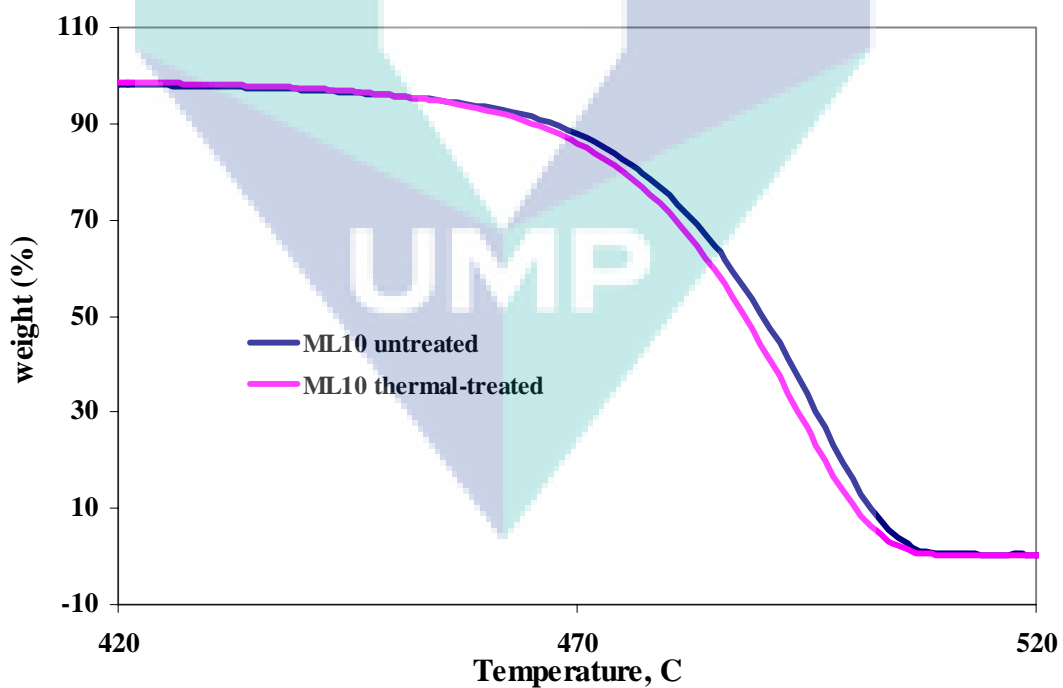


Figure 4.19 TG traces of ML10 samples before and after 1000 hours of thermal treatment

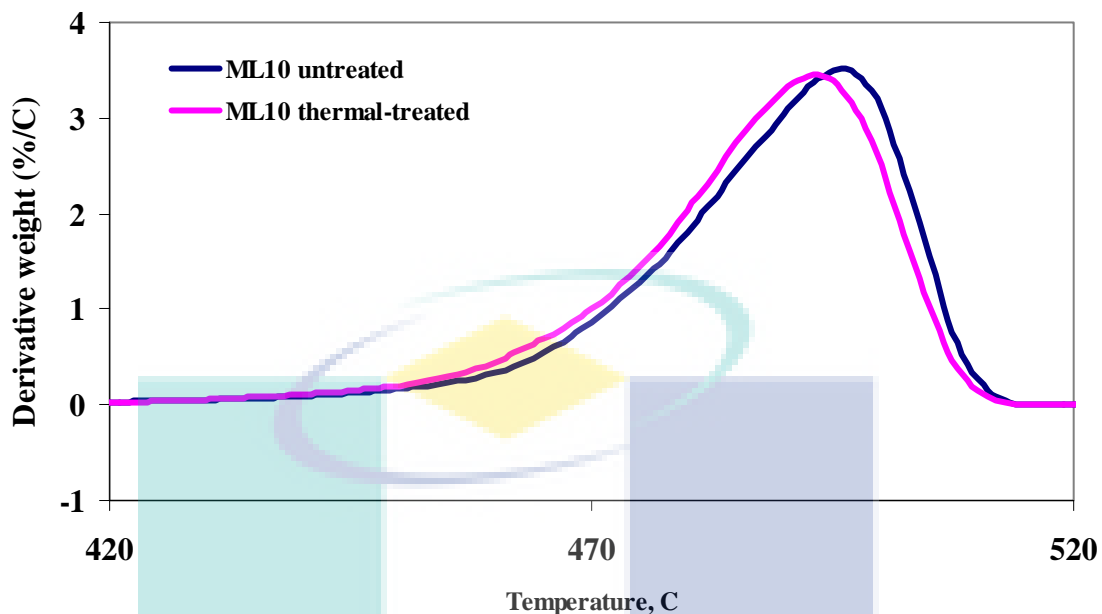


Figure 4.20 DTG traces of ML10 samples, before and after 1000 hours of thermal treatment

Table 4.3 also shows comparison of thermal stability among manganese carboxylates. Both pure sample and ML10 sample experienced reduction of thermal stability. It was due to lower molecular weight products of chain scissions, as evidenced by molecular weight measurement. However, ML10 samples underwent a slightly greater reduction than pure one, indicates that manganese laurate plays a role in lowering degradation temperature. Manganese palmitate and manganese stearate have also demonstrated similar performance in lowering degradation temperature. However manganese stearate has performed a most influential effect in lowering degradation temperature of HDPE.

Table 4.3 Degradation temperatures of samples, before and after 1000 hours of thermal treatment

Sample	Before thermal treatment					After thermal treatment				
	T _{onset} °C	T _{maximum} °C	T _{final} °C	Residue %	Ea kJ/mol	T _{onset} °C	T _{maximum} °C	T _{final} °C	Residue %	Ea kJ/mol
Pure	470.15	496.03	518.29	1.04	332.72	464.27	495.16	518.22	0.47	295.97
ML10	470.02	495.82	518.12	0.44	317.80	463.23	493.26	516.36	0.28	276.00
MP10	470.75	495.16	516.43	0.71	328.49	463.31	493.10	516.36	0.38	278.18
MS10	469.15	495.33	517.32	0.55	311.04	459.80	491.87	514.43	0.43	282.01

Activation energy of decomposition process was calculated using Broido equation (Broido, 1969). Initially, plots of $\ln(\ln(1/y))$ versus $1/T$ for decomposition stages were drawn, such as in Figure 4.21 and generally found to be linear, suggesting good agreement with the Broido equation. The activation energies, E_a , were determined from the slopes of these plots. The activation energy decreased for pure sample and samples with manganese carboxylates after getting thermal treatment for 1000 hours.

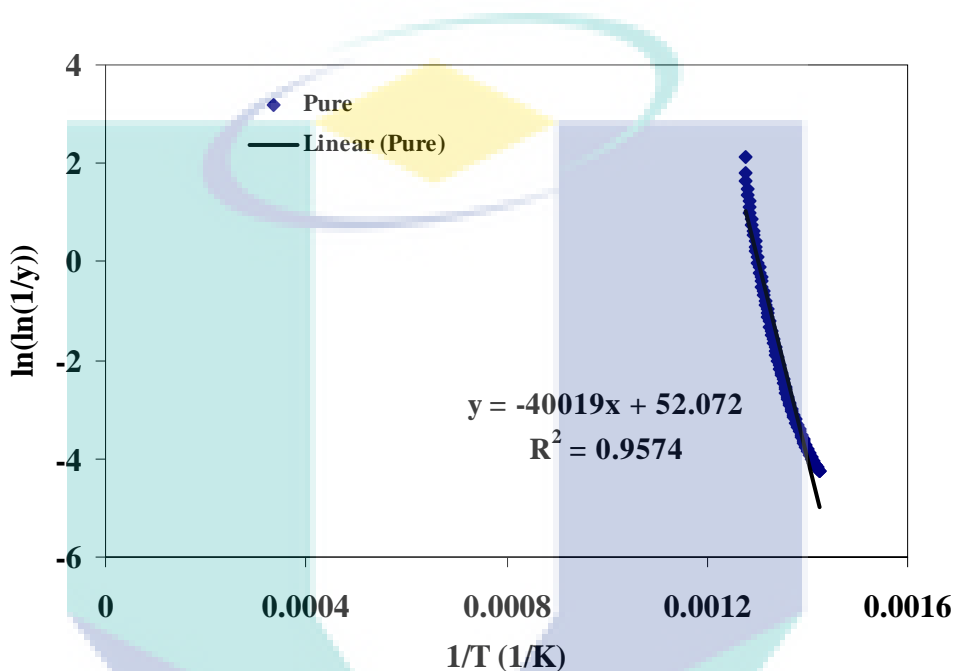


Figure 4.21 Activation energy calculation for decomposition of pure sample

4.2.7 Melting Temperature and Crystallinity

The DSC tests were done in order to investigate melting point and crystallinity. Endothermic curve of DSC scan gives information about melting temperature and degree of crystallinity. The DSC scans of pure samples and samples containing manganese laurate, for treated and untreated samples, are plotted in Figures 4.22 and 4.23, and the relating data are summarized in Table 4.4.

Figures 4.22 and 4.23 showed that the melting temperatures of both pure samples and samples containing manganese carboxylates underwent slight reduction after 1000 hours of thermal treatment. However, samples containing pro-oxidant have lower T_m than pure samples either before or after thermal treatment. The reduction of T_m could be due to the breakdown of HDPE chains and molecular weight reduction. As

reported by Colom et al. (2003), the decreases of the decomposition and melting temperatures are associated with shorter polymeric chains and a lower thermal stability of the material.

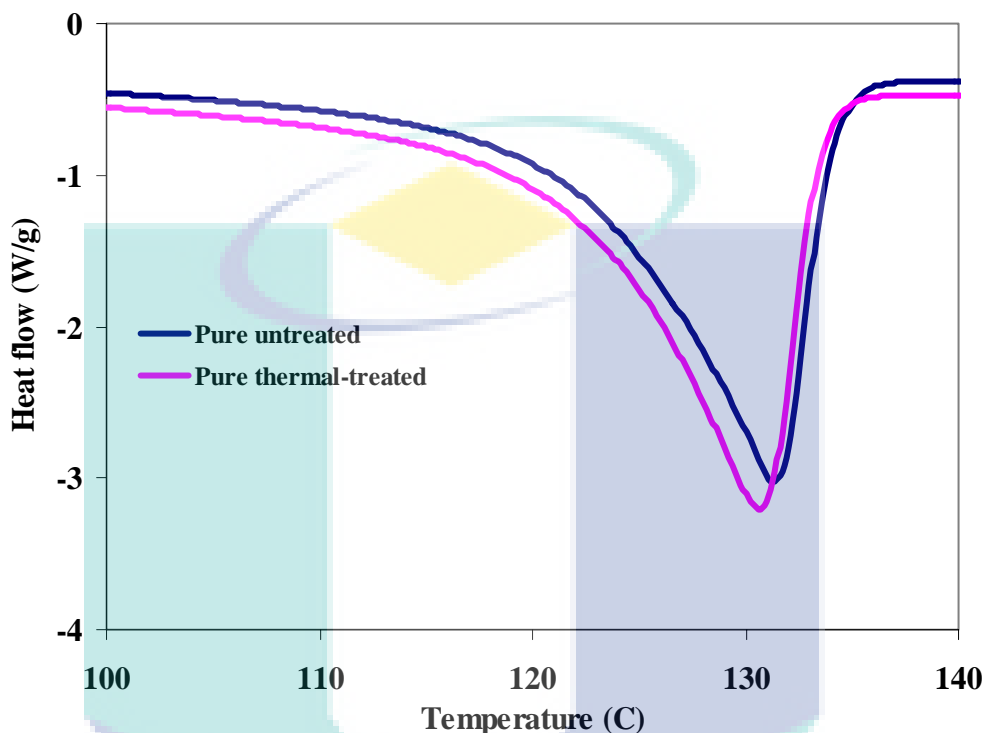


Figure 4.22 DSC scans of pure samples before and after 1000 hours of thermal treatment

Table 4.4 Melting temperatures and crystallinities of samples before and after 1000 hours of thermal treatment

Sample	Before thermal treatment				After 1000 hours of thermal treatment			
	T_o , °C	T_m , °C	ΔH_f , J/g	X_{DSC}	T_o , °C	T_m , °C	ΔH_f , J/g	X_{DSC}
Pure	122.64	131.35	140.8	48.04	121.75	130.65	143.7	49.03
ML10	122.42	130.95	143.2	48.86	121.64	130.29	152.0	51.86
MP10	122.19	130.70	143.7	49.03	121.43	130.03	156.4	53.36
MS10	122.18	130.72	141.5	48.28	121.31	129.96	157.8	53.84

T_o : melting point (onset), T_m : melting point (peak), °C; ΔH_f : heat of fusion, J/g; X_{DSC} : crystallinity index obtained from DSC scan(%)

The crystallinity index is obtained from DSC scans and showed the increasing nature during thermal treatment. The crystallinity of pure samples increased around 1%, from 48.04 to 49.03%, whereas ML10, MP10 and MS10 samples underwent higher increases, about 3%, 4.33% and 5.56 %, respectively. However, all samples have initial crystallinity index in the range of 48-49%, and the rest part of material is in amorphous

or non crystalline states which allow absorbing oxygen. As reported in literature (ASM International, 2003), thermo-oxidative degradation occurs with presence of oxygen which is absorbed by the amorphous region of polyethylene.

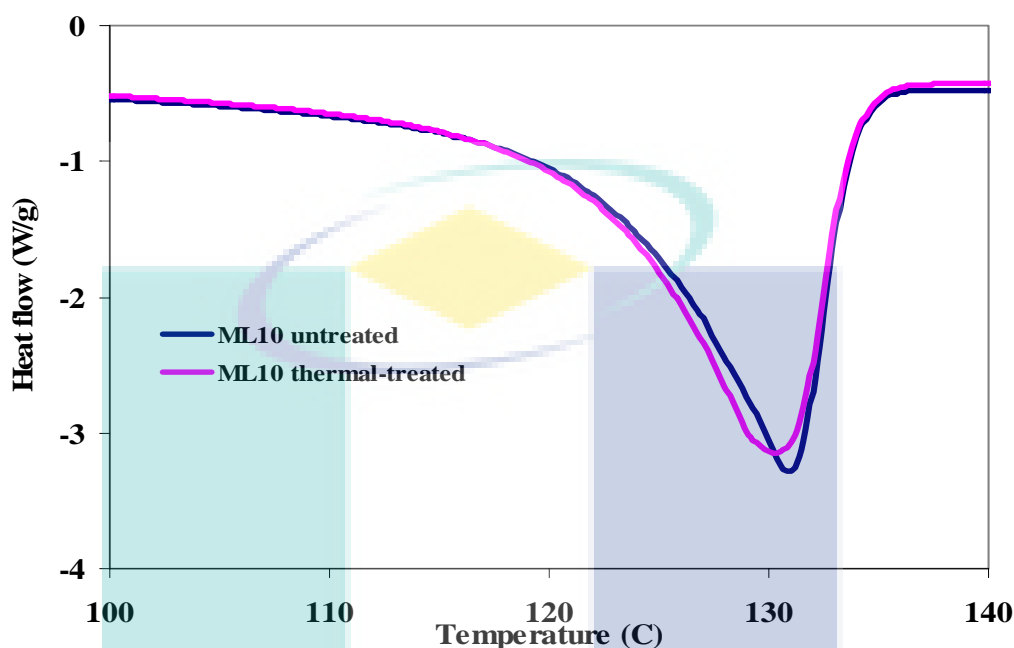


Figure 4.23 DSC scans of ML10 samples before and after 1000 hours of thermal treatment

The increase of crystallinity is due to chain scission along the amorphous regions. The chain scission allows the freed segments resulted to crystallize (Khabbaz et al., 1999). The creation of new intermolecular polar bonds, due to carbonyl groups also lead to this effect (Khabbaz et al., 1999; Sebaa et al., 1992). Furthermore the increases of crystallinity of samples containing manganese carboxylates, give supporting evidence on the role of manganese carboxylates in accelerating degradation process of HDPE during thermal treatment.

4.2.8 Surface Morphology

Surface morphology study was done on selected samples using scanning electron microscope (SEM) at magnification of 250 \times . Figure 4.24 and 4.25 represent the SEM image of pure, ML10, MP10, and MS10 samples, before and after thermal treatment for 1000 hours. The pure sample and all other samples have smooth surface at the initial condition. After getting 1000 hours of thermal treatment, the surface texture

of pure sample did not exhibit noticeable difference. The thermal treatment did not significantly affect surface texture of pure sample. Yet ML10 sample showed the existence of ruggedness during thermal treatment. The developed samples defects and cracks on the surface were also observed. Thus manganese laurate contributed on deterioration of surface texture of HDPE. This also occurred on samples with manganese palmitate and manganese stearate. Their surface textures were found to have a powdery white deposit. It appeared on a thin outer surface of samples, particularly samples with high amount of additive loading.

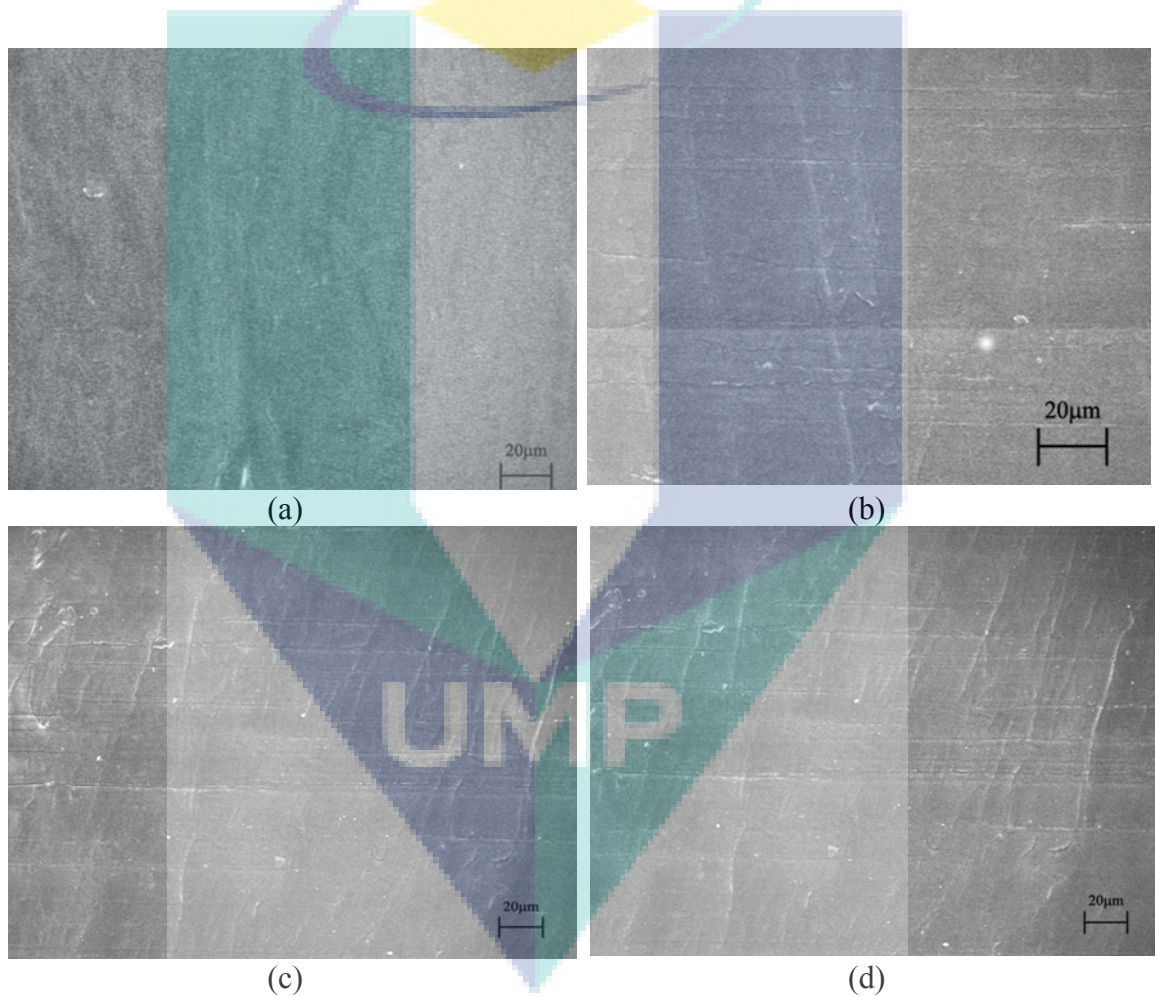


Figure 4.24. SEM image of samples (a) pure HDPE (b) ML10 (c) MP10 (d) MS10 before treatment

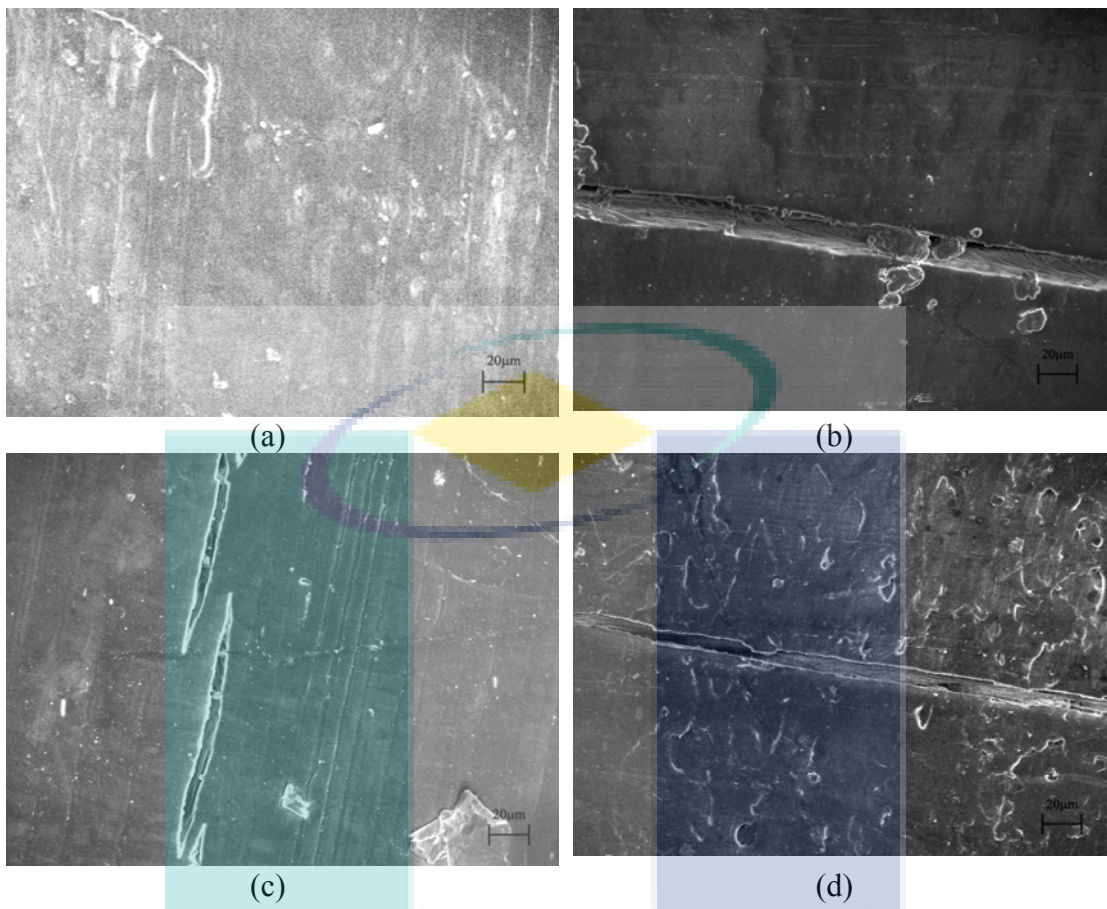


Figure 4.25. SEM image of samples (a) pure HDPE (b) ML10 (c) MP10 (d) MS10 after 1000 hours of thermal treatment

4.3 DEGRADATION OF HIGH DENSITY POLYETHYLENE UNDER ACCELERATED WEATHERING TREATMENT

4.3.1 Introduction

Accelerated weathering treatment has been conducted in QUV accelerated weathering tester that combined thermal, UV light, condensation, and water spray in a test cycle. The cycle of test consisted of three consecutive steps: 8 hours UV exposure 0.68 W/m^2 at 60°C , 0.25 hour water spray and 3.75 hours condensation at 50°C . Those steps were simulating sunlight, rainfall, and humidity (wetness). The irradiance of UV light at 0.68 W/m^2 and wavelength of 340 nm is recognized as peak natural daylight standard according to International Society for Illumination (Novak, 2006).

Pure HDPE samples and HDPE samples with various compositions of manganese carboxylates (manganese containing ML, MP and MS) were exposed to accelerated weathering. The duration of weathering was up to 1000 hours. The changes of characteristics of HDPE samples are reported below in order to assess degradation occurred.

4.3.2 Infrared Spectra

During accelerated weathering, thermal and UV light exposure can play simultaneous effects on HDPE samples. Thermal exposure leads to thermo-oxidative degradation, whereas UV light exposure leads to photo-degradation. The UV light gives the major contribution on the degradation of HDPE.

As the carbonyl groups are generated during degradation, they arise in the FTIR spectra of sample after accelerated weathering. Carbonyl groups generated comprises ketonic, ester, carboxylic, aldehyde, and lactone. Consequently carbonyl index of samples rise during accelerated weathering. Figure 4.26 shows the FTIR spectra of MP10 samples before and after accelerated weathering. The absorbance in the region of $1700\text{-}1800 \text{ cm}^{-1}$ which is the region of carbonyl groups, increases after accelerated weathering. The region of carbonyl groups normally comprises peaks of some compounds. However, they consolidate in one wide peak as happen on FTIR spectra of ML10 sample after thermal treatment.

A small increase in the region of 3300-3500 was detected. This region is attributed to hydroxyl groups. This result is consistent with results of previous studies. In the degradation of polyethylene, Bikiaris et al. (1997) observed absorbance at 3450 cm^{-1} and 3380 cm^{-1} that are attributed to formation of alcoholic groups and hydroperoxides groups respectively. Albertson and Karlsson (1990) reported that in pure LDPE degraded in accelerated environment, alcoholic compounds, i.e. butanol, pentanol, were found in degradation products. Other small increase is also observed in the region of 1000 $^{-1}$ -1300 cm^{-1} . This region is attributed to ether (C-O) bond (Bajer et al., 2007). An increase in absorbance is also observed at the region between 940 and 970 cm^{-1} , where vinyl groups absorb (Bikiaris et al., 1997). During water spray and condensation, some degradation products on the sample surface might be leached as they are water soluble, allowed UV light to penetrate deeper and resulted in further photo-degradation.

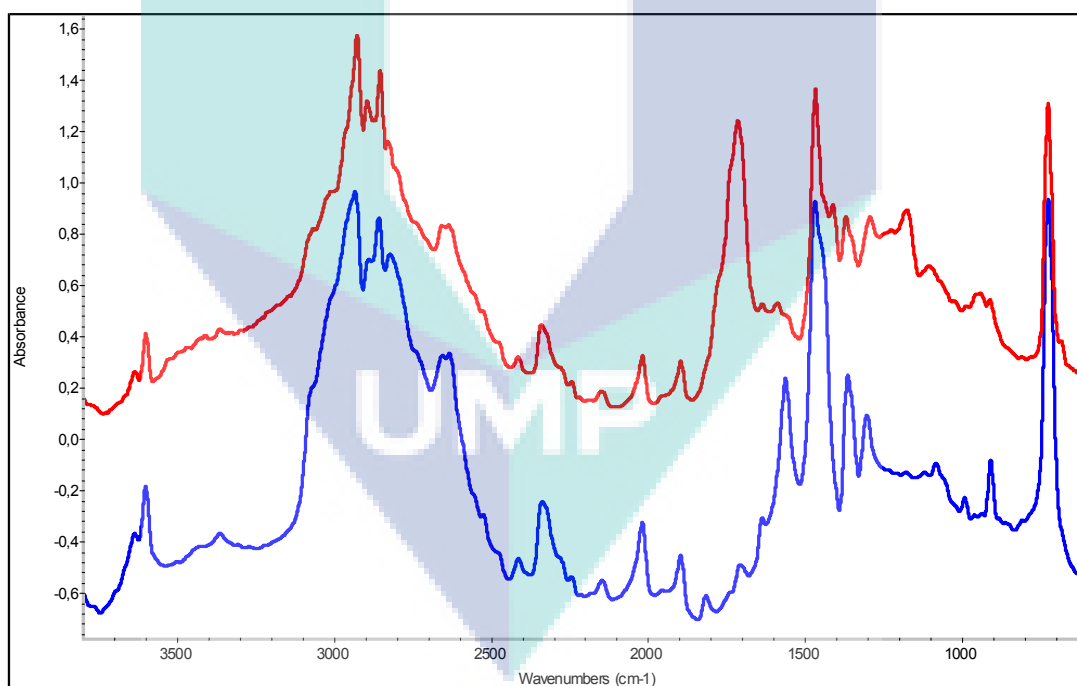


Figure 4.26 FTIR spectra of MP10 samples, before (lower trace) and after (upper trace) accelerated weathering

In study of photo-degradation of polyethylene with cobalt carboxylates as pro-oxidant additives, Roy et al. (2006b) reported that on absorption of energy in the form of light, the cobalt carboxylates undergo decarboxylation leading to the formation of

free radicals. These generate radicals on the main chain of the polymer matrix leading to chain scission which finally affects the mechanical properties. This phenomenon also happens on manganese carboxylates in HDPE matrix during accelerated weathering. It is indicated by disappearing of absorbance peak of around 1560 cm^{-1} , the peak of metal-organic salt.

Figure 4.27 represents the changes of carbonyl index of various samples during accelerated weathering. It can be noted that the initial carbonyl index is not significantly affected by the incorporation of manganese carboxylates. Pure samples demonstrate a slow increase of carbonyl index, whereas samples with additives i.e. manganese laurate, palmitate and stearate, demonstrate rapid increases of carbonyl index.

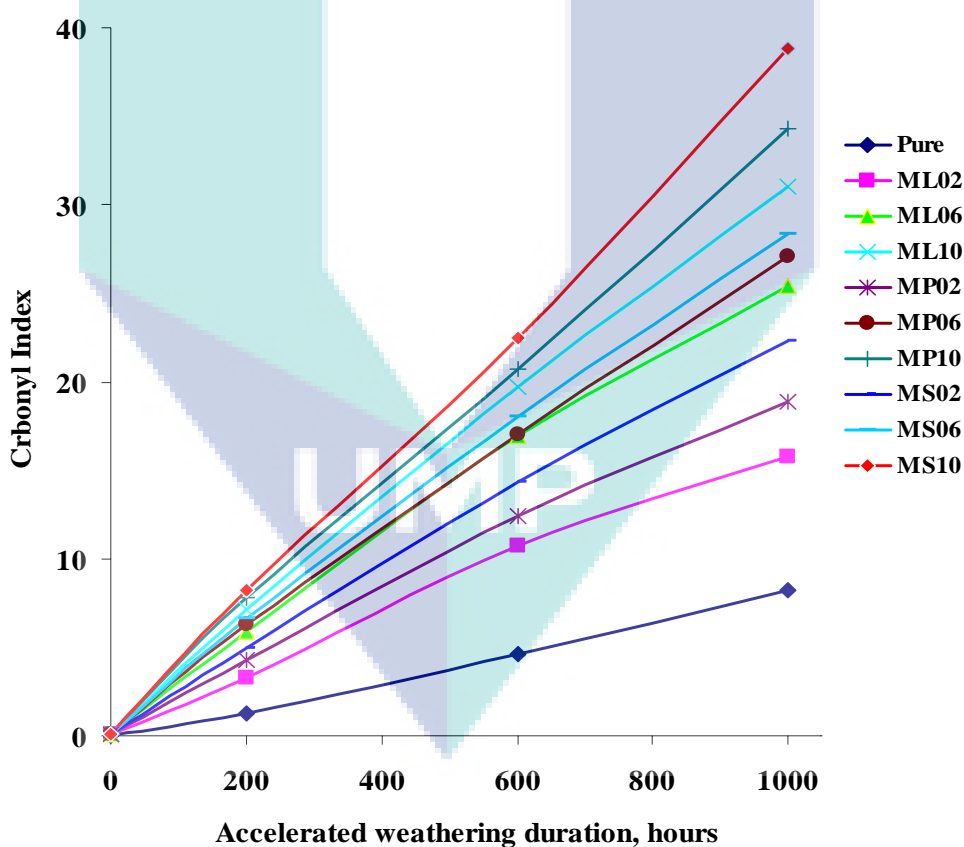


Figure 4.27 Carbonyl index of various samples during accelerated weathering

The carbonyl index also increased by increasing the amount of additives incorporated. The carbonyl index of pure sample increased from initial value of 0.022 to 8.197 after 1000 hours of accelerated weathering. The initial carbonyl index of samples

with manganese carboxylates (1%) were ~ 0.095 - 0.102 , and increased to ~ 34.013 - 38.791 in the end of accelerated weathering. This result is different with that of Erlandsson et al. (1997) who observed the slow increase of carbonyl index of LDPE and LDPE containing masterbatch (starch and pro-oxidant) either during UV exposure or thermal exposure at 65°C . This is due to simultaneous effect of thermal and UV light during accelerated weathering that lead to rapid degradation of HDPE, especially HDPE containing manganese carboxylates. Thus, photo-degradation and thermo-oxidative degradation take place together at the same time resulting in rapid oxidation of HDPE, and consequently resulting in high carbonyl index.

4.3.3 Tensile Properties

Tensile properties namely tensile strength, tensile modulus and elongation at break were monitored during accelerated weathering treatment to assess degradation process. Progressive lowering of tensile strength during accelerated weathering is presented in Figure 4.28–4.30. Tensile strength of pure samples increased in the beginning of accelerated weathering treatment, and reached the peak at 100 hours of treatment. After 200 hours, the strengths started to decrease gradually. In contrary, samples containing additives i.e. manganese carboxylates demonstrated rapid decrease during accelerated weathering. Samples of ML02, MP02 and MS02 showed rapid decreases of tensile strength since the beginning of accelerated weathering treatment. It was due to simultaneous effects of thermal and UV exposure. However, the decreases were not as rapid as those of ML10, MP10 and MS10. The decreases occurred more rapidly by increasing the amount of manganese carboxylates incorporated.

It is interesting to note that pure HDPE has lost as much as 41.77 % of its tensile strength after 1000 hour of accelerated weathering, whereas ML02 and ML10 samples have lost 55.43 and 70.39 % respectively. The samples with other additives showed similar behavior with ML samples, but relatively higher in loss of tensile strength. The detailed data is listed in Table 4.5. The tensile strength loss increased with increasing of loading of manganese carboxylates and also with duration of treatment. Manganese stearate was generally found to demonstrate better performance in lowering tensile

strength than manganese laurate and manganese palmitate. However, the differences were not too significant.

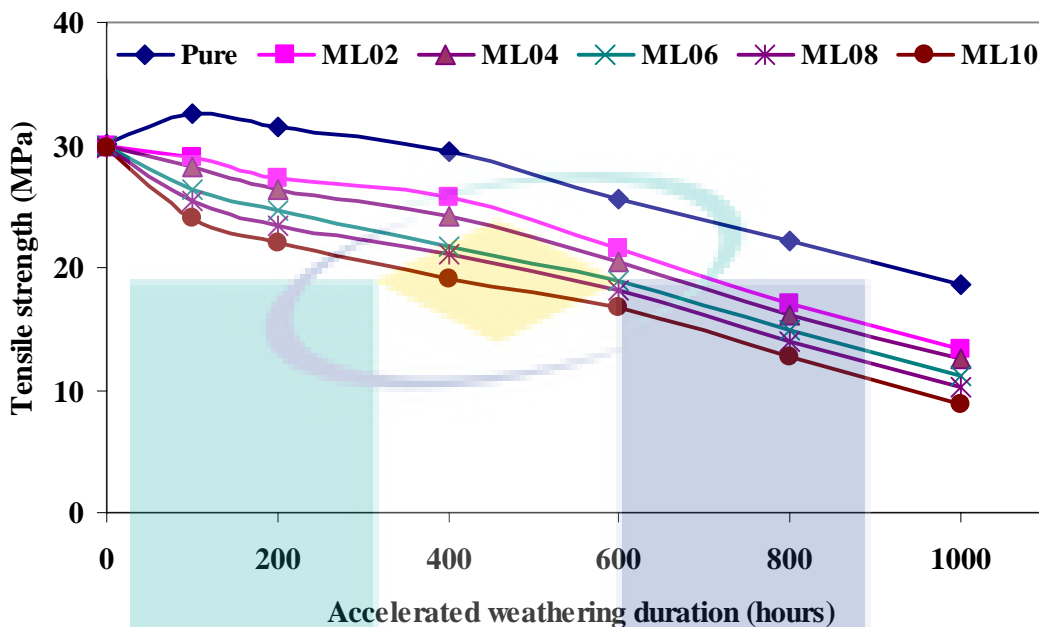


Figure 4.28 Tensile strength of HDPE containing manganese laurate during accelerated weathering

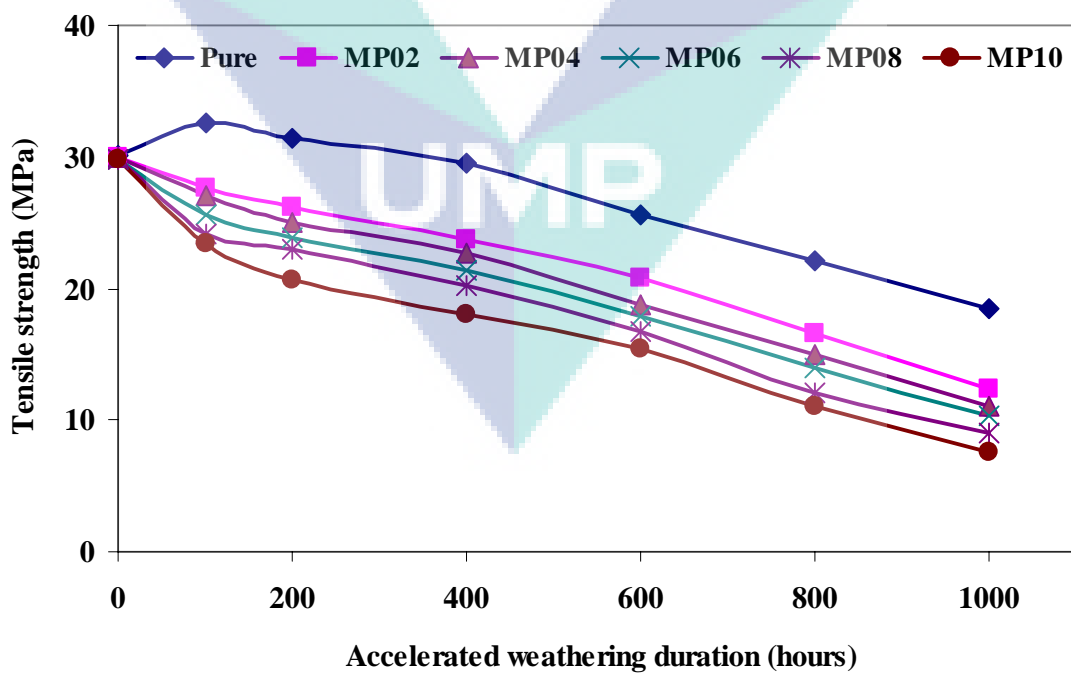


Figure 4.29 Tensile strength of HDPE containing manganese palmitate during accelerated weathering

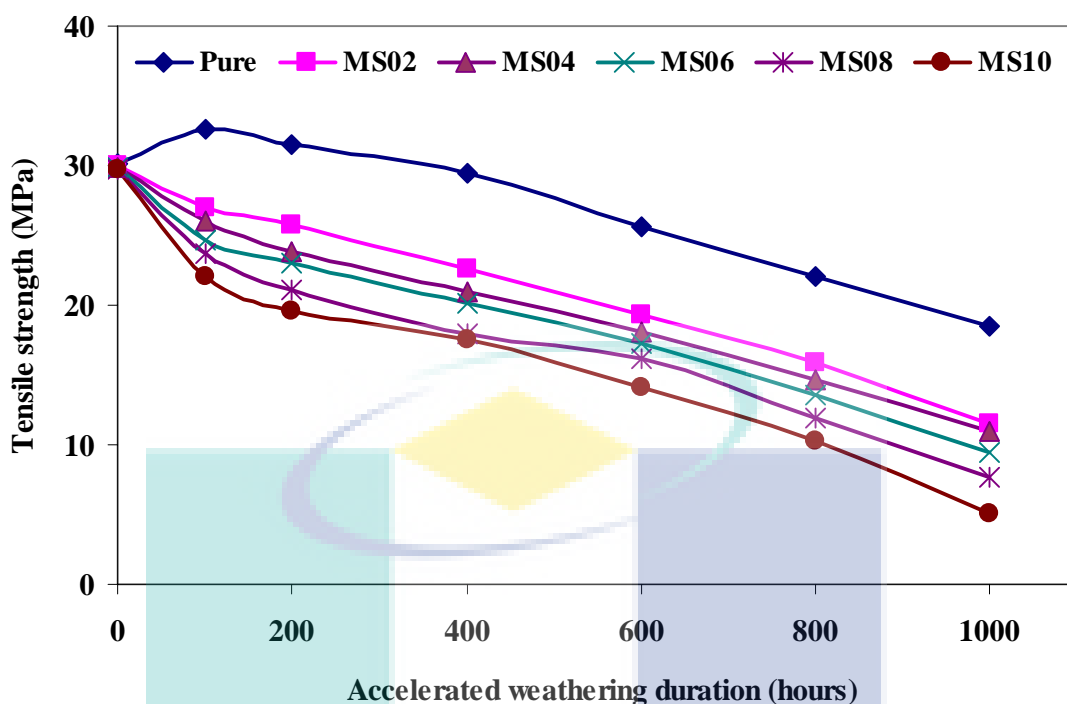
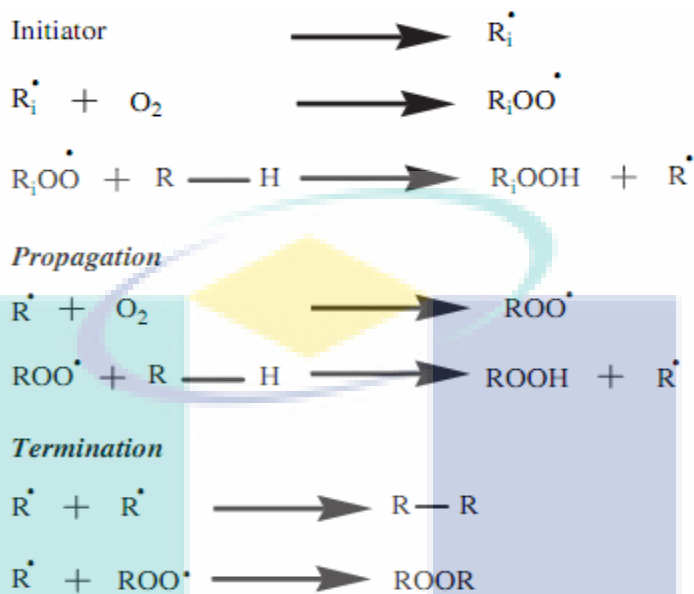


Figure 4.30 Tensile strength of HDPE containing manganese stearate during accelerated weathering

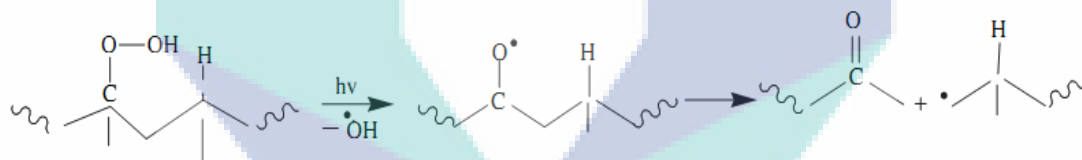
The increase of tensile strength of pure samples in early periods of treatment suggested the phenomena of crosslinking taking place. As explained in previous section (see section 4.2), thermal treatment alone could result in crosslinking. In accelerated weathering, the presence of UV light and thermal/heat give simultaneous effects, and initiate crosslinking that result in higher tensile strength. When UV and thermal exposure continue, chain scission took place as indicated by the decrease of tensile strength of pure samples after 200 hours of treatment. Chain scission could happen when oxidation of polymer took place.

The thermo-oxidative degradation and photo-degradation have occurred simultaneously during accelerated weathering. Mechanism of photo degradation of HDPE during accelerated weathering could be explained following the mechanism proposed by Singh and Sharma(2008) as shown in Scheme 4.4. The mechanism comprises steps namely initiation, propagation and termination. The coupling of alkyl radicals step has led to crosslinking in the beginning period of treatment. Hydroperoxide species generated in propagating step lead to backbone degradation through cleavage of

hydroperoxide O–O bond followed by β -scission as presented in Scheme 4.5. Backbone degradation leads to loss of tensile properties.



Scheme 4.4 Mechanism of photo-oxidative degradation



Scheme 4.5 Backbone scission

Table 4.5 Losses of tensile properties of samples after 1000 hours of accelerated weathering

Samples	Loss of tensile strength, %	Loss of tensile modulus, %	Loss of elongation at break, %
Pure	38.45	20.15	65.19
ML02	55.43	33.83	82.51
ML10	70.39	47.76	92.82
MP02	58.80	38.26	84.75
MP10	74.49	51.21	94.19
MS02	61.74	39.89	85.79
MS10	83.05	54.50	96.33

Samples with ML, MP and MS additives demonstrated the decrease of tensile strength at various levels since the beginning of accelerated weathering treatment. It suggested chain scission took place since the beginning of accelerated weathering. In the initial stage of accelerated weathering, tensile strength of ML,MP and MS samples decreased rapidly, and going slower in the end period of treatment. Photo-degradation and thermo-oxidative degradation might take place simultaneously during accelerated weathering, led to rapid loss of mechanical properties i.e. tensile strength, tensile modulus and elongation at break. UV light effect may play major role in accelerated weathering and assisted by thermal effect.

Figures 4.31–4.33 represent the changes of tensile modulus of HDPE samples that contain manganese carboxylates in various compositions during accelerated weathering treatment. It was found that the changes of tensile modulus of samples were similar with the changes of tensile strength of samples. However the changes of tensile modulus were lesser than those of tensile strength.

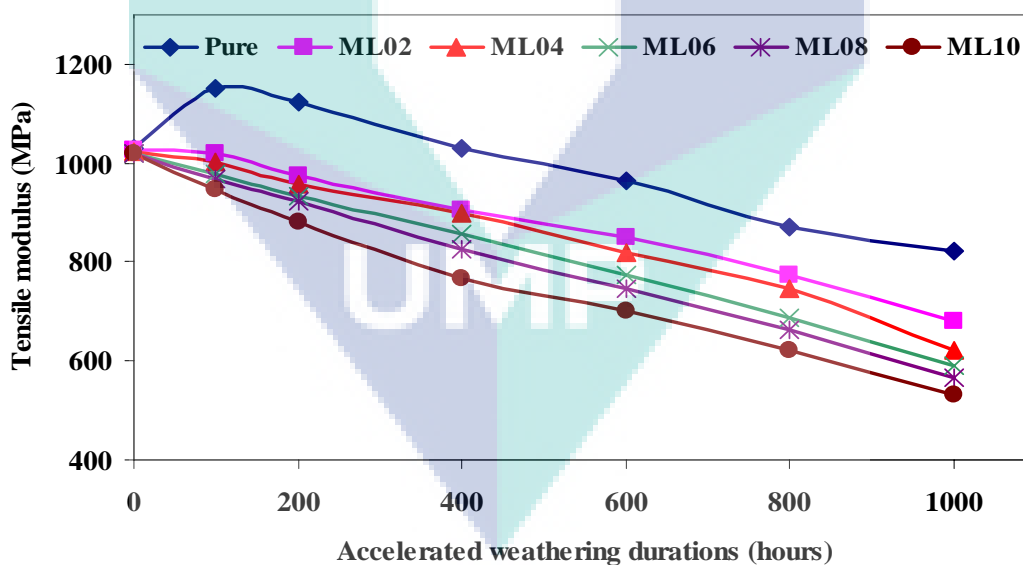


Figure 4.31 Tensile modulus of HDPE containing manganese laurate during accelerated weathering

Pure samples experienced the increase of tensile modulus in the first 100 hours of accelerated weathering treatment, and then started to decrease gradually after 200 hours, while all samples containing manganese carboxylates experienced the decrease of tensile modulus since the beginning of accelerated weathering treatment. The losses

of tensile modulus of selected samples after 1000 hours of accelerated weathering are presented in Table 4.5.

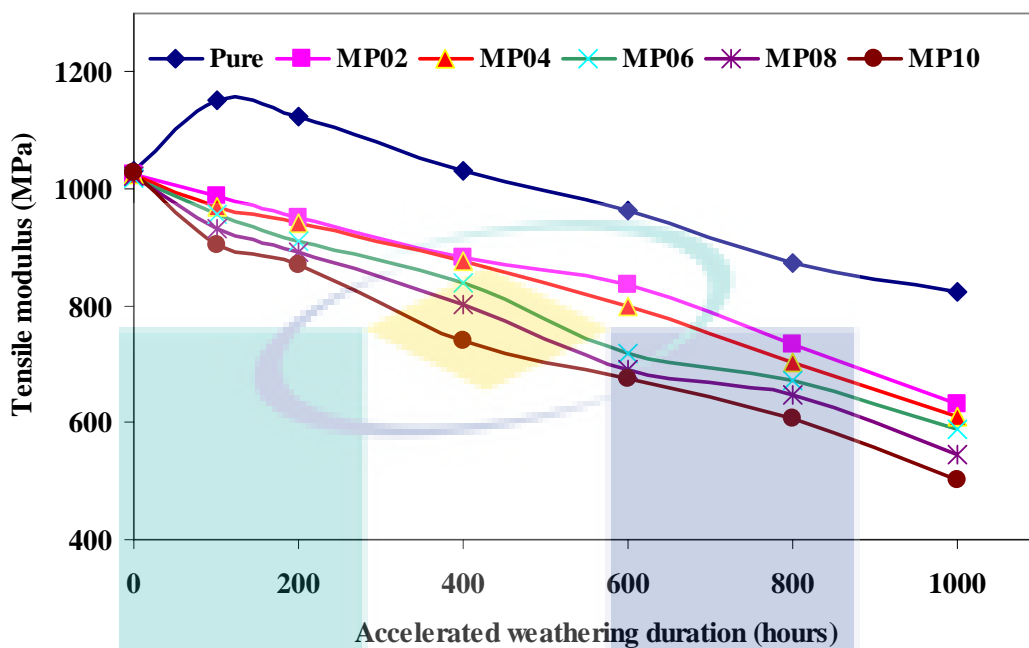


Figure 4.32 Tensile modulus of HDPE containing manganese palmitate during accelerated weathering

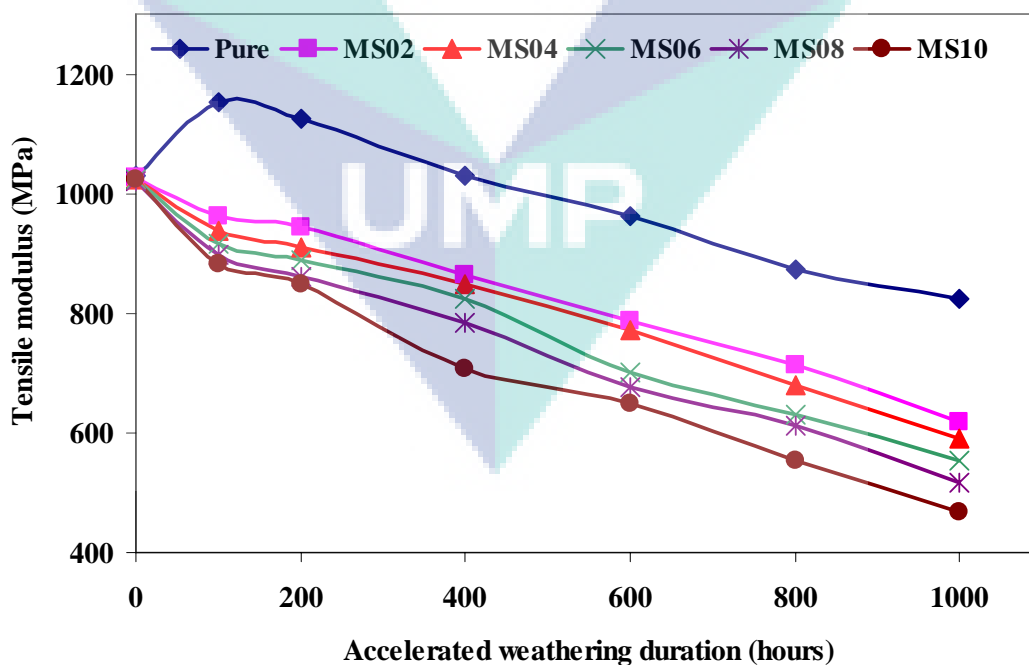


Figure 4.33 Tensile modulus of HDPE containing manganese stearate during accelerated weathering

Figures 4.34–4.36 reveal the changes of elongation at break of various samples during accelerated weathering. Pure samples experienced gradual decrease of elongation at break since the beginning of accelerated weathering. Despite the increase of tensile strength in the beginning of accelerated weathering, the elongation at break decreased systematically during treatment. Even, the tensile strength of pure samples decreased faster in the early periods than in the end periods of accelerated weathering. The crosslinking happened in the beginning of accelerated weathering led samples to be more brittle and lowering elongation at break. When accelerated weathering continued, it led to chain scission and decreasing tensile strength continuously.

However, all samples containing manganese carboxylates underwent decrease of elongation at break much faster than pure samples. The elongation at break decreased rapidly since accelerated weathering started. They demonstrated faster decrease of elongation at break in the beginning of accelerated weathering than in the end periods. Manganese laurate, manganese palmitate and manganese stearate show similar behaviors of elongation at break decrease. Nevertheless, manganese stearate demonstrates the highest effect on lowering both tensile strength and elongation at break of HDPE.

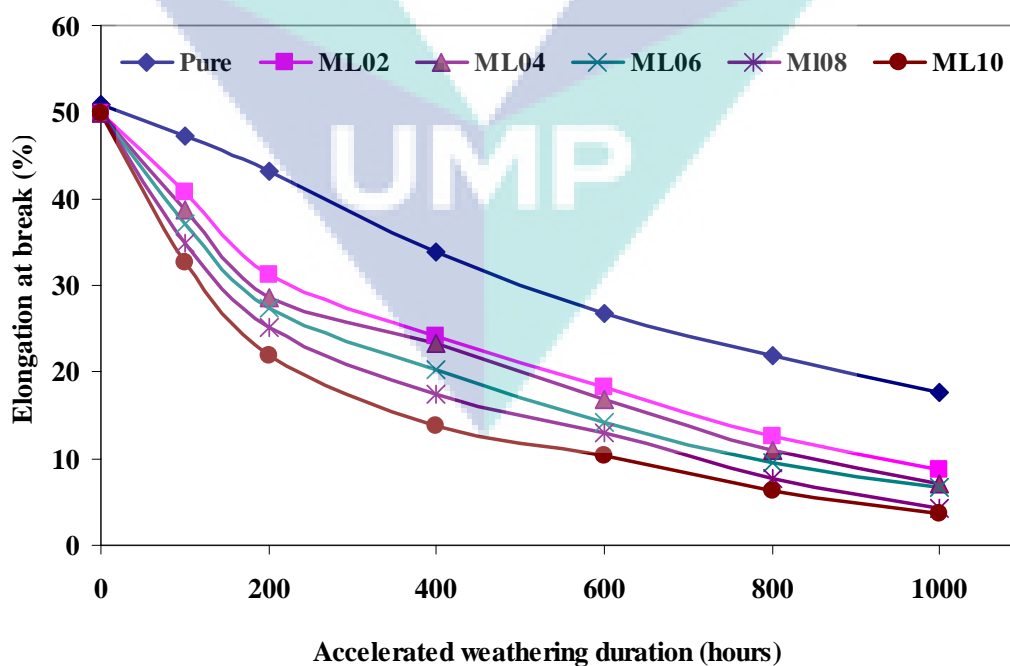


Figure 4.34 Elongation at break of HDPE containing manganese laurate during accelerated weathering

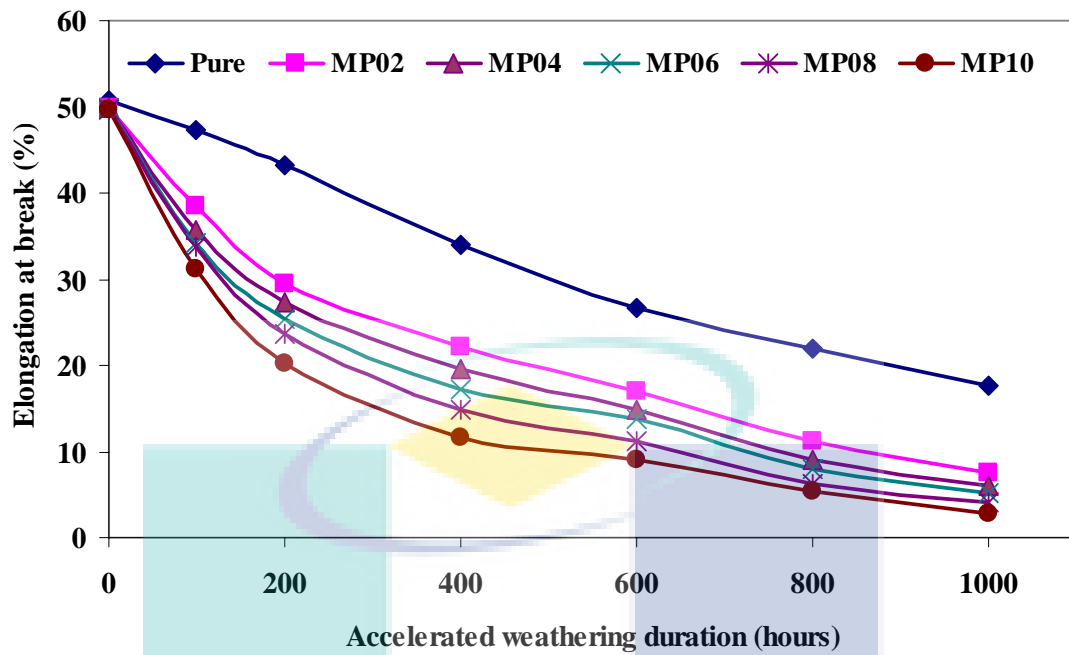


Figure 4.35 Elongation at break of HDPE containing manganese palmitate during accelerated weathering

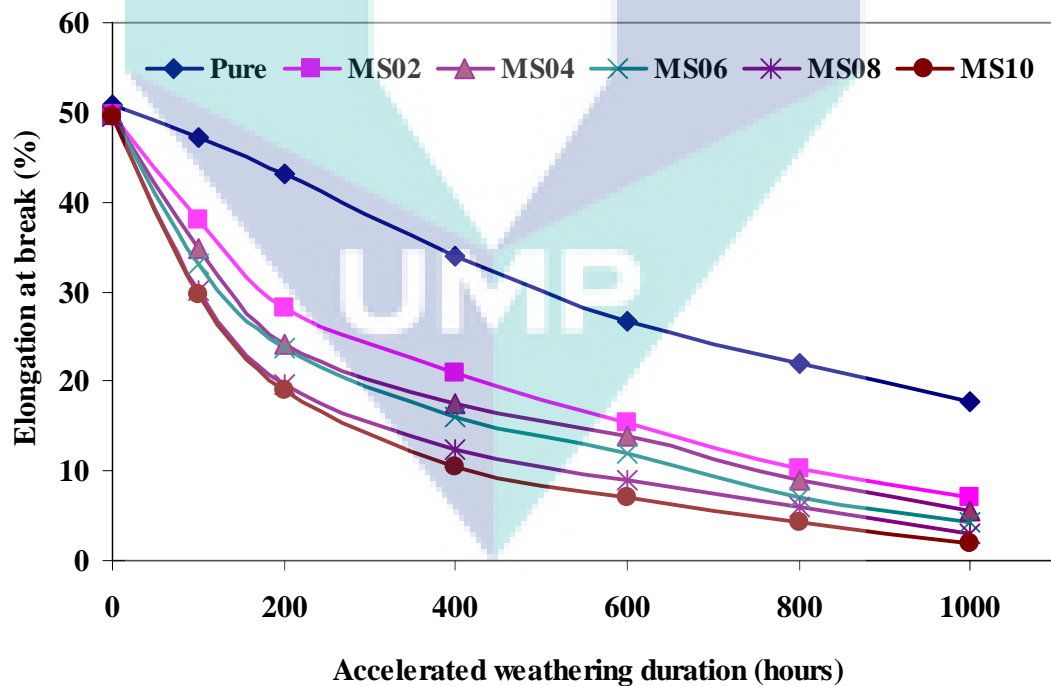


Figure 4.36 Elongation at break of HDPE containing manganese stearate during accelerated weathering

After 1000 hours of accelerated weathering, the cross section of samples containing manganese carboxylates showed that the surface of samples experienced the worse deterioration compare to inner part. It suggests that accelerated weathering, which dominated by UV light effect (photo-degradation) rather than thermal effect (thermo-oxidative degradation), mostly affected the surface of samples. It is due to the limited penetration of UV light into the inner part of samples, particularly for thick samples. Water spray also contributes in leaching degradation products and prevents some products to block UV penetration into deeper surface. However, it only affects on thin surface of sample. It is confirmed by the rapid decrease of tensile strength of samples in the beginning periods of accelerated weathering, and going slower in the end periods of accelerated weathering. Further effect on tensile strength is contributed by thermal effect or thermo-oxidative degradation only.

In the previous study of photo-degradation of polyethylene, Roy et al (2007a; 2006b) have found that LDPE films underwent very rapid decrease of tensile strength during treatment. Those results slightly differ with results of this study in which rapid decrease of tensile strength happened in the early periods of weathering, and became slower in the end periods. This was due to different thickness of sample. This study used specimen with thickness of 3.16 mm, while the previous study used the thin samples (70 μm) which ensured the UV light penetrates into inner part of samples.

4.3.4 Molecular Weight

Figure 4.37 represents the changes of average molecular weight (\overline{M}_v) of pure sample and various compositions of samples during accelerated weathering. The \overline{M}_v of pure sample significantly decreased during accelerated weathering. The \overline{M}_v of pure sample reduced 42.53% of its initial value. On the other hand, the \overline{M}_v of the samples with manganese carboxylate decreased dramatically during accelerated weathering. However, this result reveals that HDPE is quite sensitive to UV exposure; moreover it is worsened with the presence of manganese carboxylates as pro-degradant additives. The greater reduction of \overline{M}_v occurs by increasing the amount of incorporated manganese carboxylates. For example, MP02 sample underwent a reduction of 70.32% of its initial value, and 88.49% for MP10 sample, while ML10 and MS10 samples experienced

reduction of 87.34% and 90.48 % of their initial values, respectively. Sample containing manganese stearate demonstrated greatest reduction of molecular weight. However, the differences were not too significant.

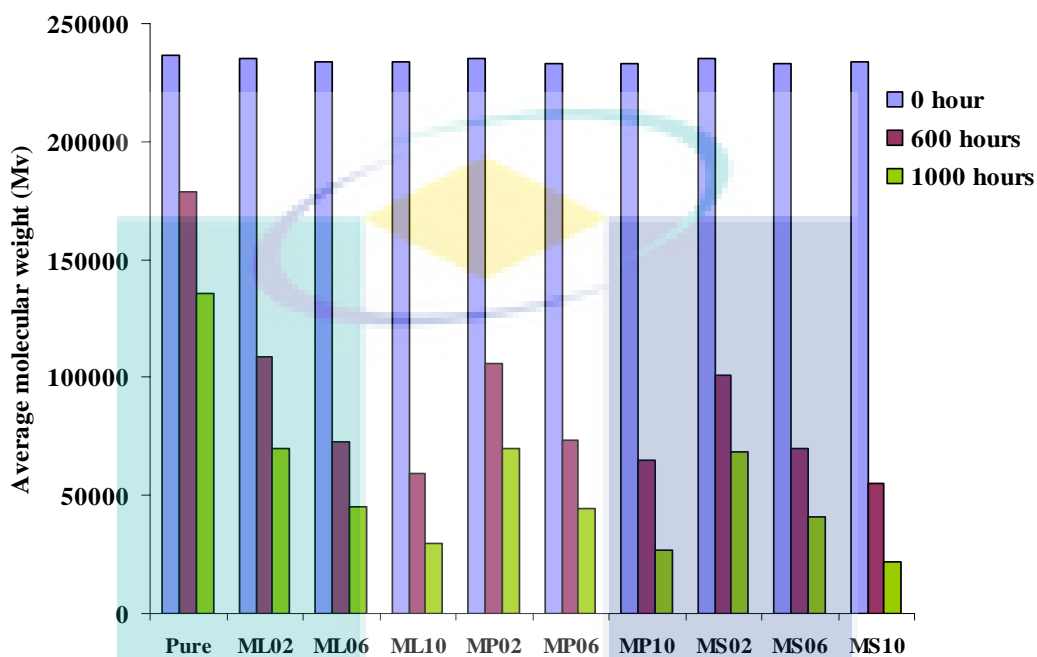


Figure 4.37 Molecular weight of various samples during accelerated weathering

Generally, the reductions of molecular weight at period of 0 to 600 hours of accelerated weathering are greater than those of period of 600 to 1000 hours. Simply, it suggests a faster degradation in the beginning period of weathering than in the end period. The result is in agreement with that of Roy et al. (2006b) who studied molecular weight of LDPE containing cobalt-based pro-oxidant additives during UV exposure for maximum duration of 600 hours. Pure LDPE experienced a slower decrease of molecular weight than LDPE containing pro-oxidant additives. It was also found that the decrease of molecular weight is similar with the decrease of mechanical properties i.e. tensile strength and elongation at break for the same composition. It suggests that chain scissions lead to lower molecular weight and lowering mechanical properties.

4.3.5 Melt Flow Index

Melt flow index of various compositions of samples is depicted in Figure 4.38. That figure reveals that the incorporation of manganese carboxylates results in increasing MFI of samples significantly during accelerated weathering. Pure sample underwent small increase of MFI, from 0.081g/10min initially to 0.817 g/10min after 1000 hours of accelerated weathering. For comparison, MFI of ML10 sample increased from 0.123 to 2.465 g/10min, whereas for MP10 sample and MS10 sample were from 0.125 to 2.548 g/10 min and from 0.126 to 2.659 correspondingly. It is also found that MFI of samples containing additives are affected by amount of additives incorporated and duration of weathering. MFI shows that there is reduction of molecular weight. As mentioned earlier, lower MFI indicates a lower molecular weight, and a lower molecular weight means shorter chain of HDPE. It is caused by chain scission during accelerated weathering.

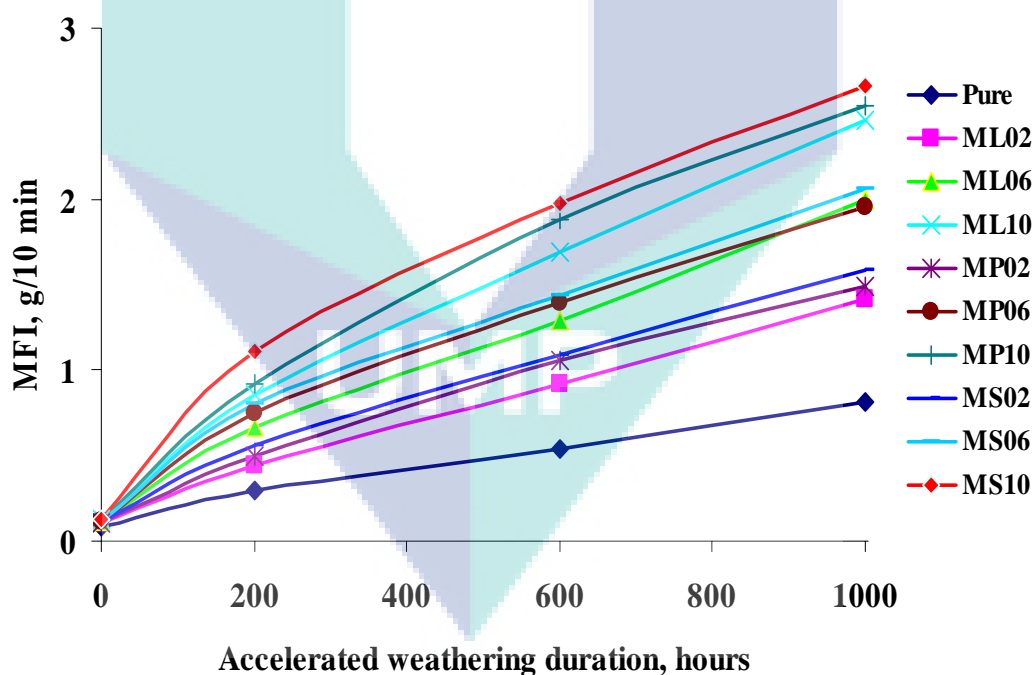


Figure 4.38 MFI of samples during accelerated weathering

4.3.6 Degradation Temperature

Selected samples namely pure, ML10, MP10 and MS10 were analyzed using TGA, since those samples have shown the greatest reductions of properties e.g. tensile

strength, elongation at break, average molecular weight (\overline{M}_v) and MFI. Figure 4.39–4.42 represents TG and DTG of pure sample and MP10 sample, before and after accelerated weathering. The TG and DTG traces after 1000 hours of accelerated weathering shifted to lower temperatures for both pure sample and MP10 sample. It also happened to MP10 and MS10 samples. All samples demonstrated a single stage of decomposition process. Thermal stabilities of samples which are indicated by degradation temperature are summarized in Table 4.6. All samples containing manganese carboxylates have shown lower degradation temperature than pure sample. After getting accelerated weathering, the decreases of degradation temperature of samples with manganese carboxylates were found to be greater than that of pure sample. As mentioned earlier, lower degradation temperatures of sample indicate the lower molecular weight. It conforms to the decrease of average molecular weight during accelerated weathering which has been presented earlier.

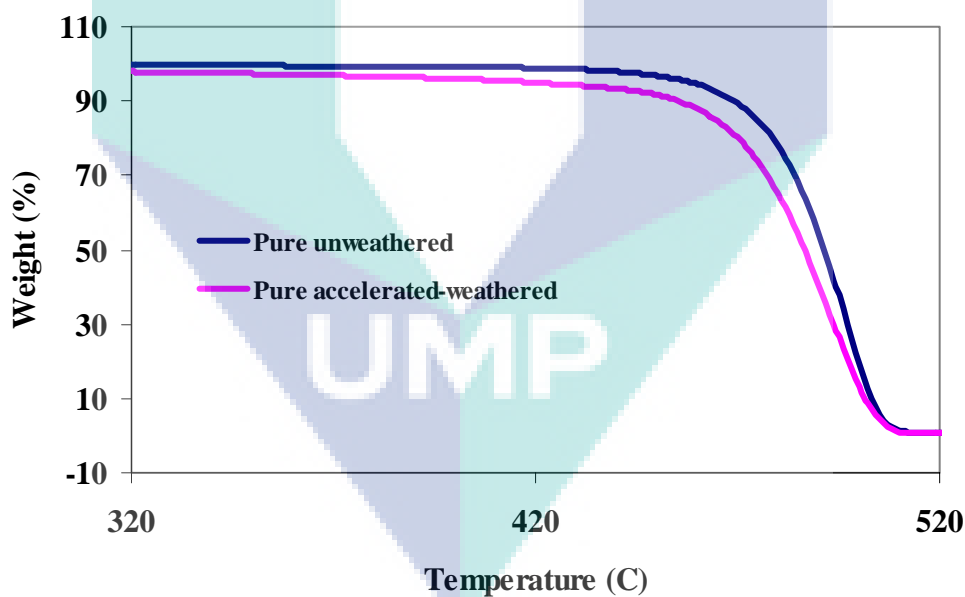


Figure 4.39 TG scans of pure samples before and after 1000 hours of accelerated weathering

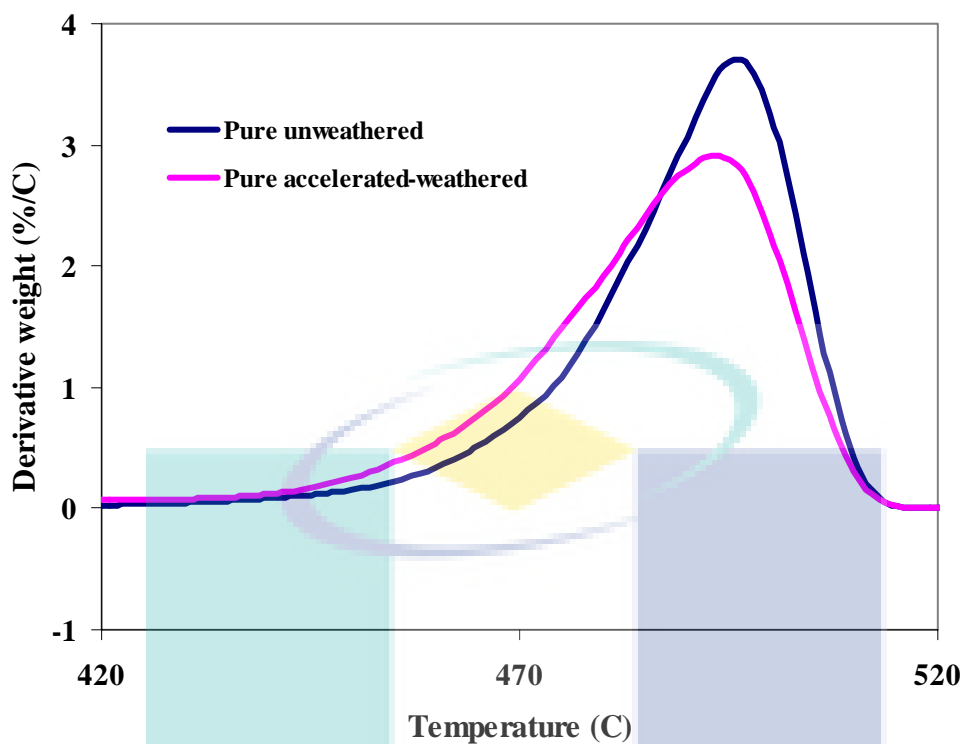


Figure 4.40 DTG scans of pure samples before and after 1000 hours of accelerated weathering

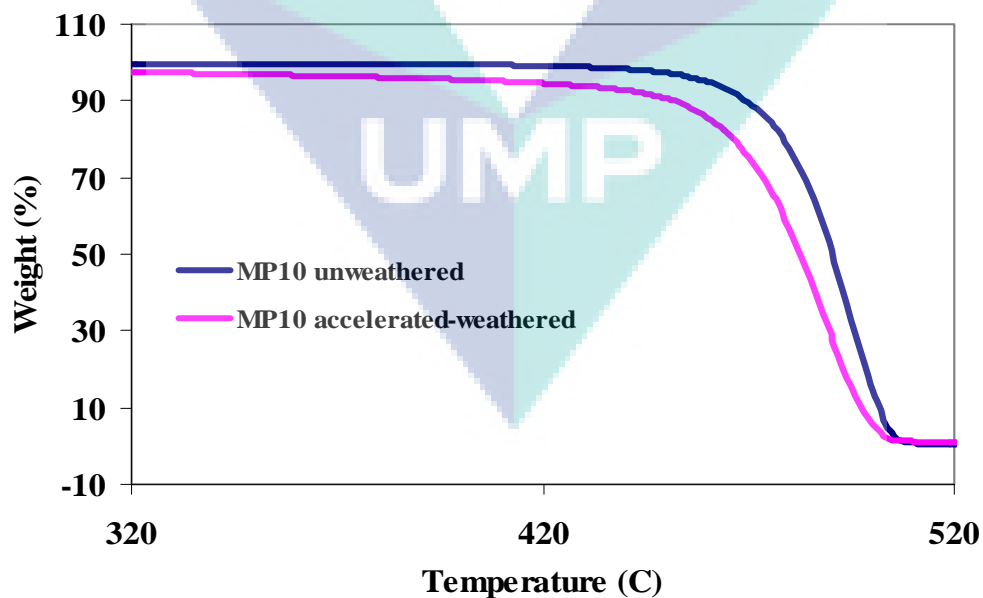


Figure 4.41 TG scans of MP10 samples before and after 1000 hours of accelerated weathering

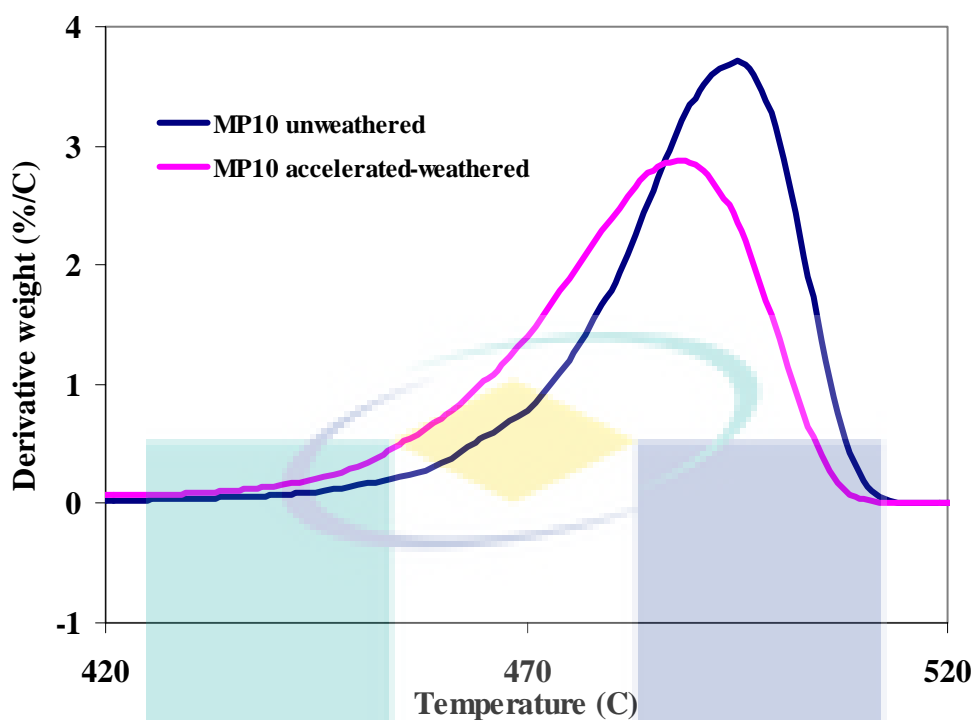


Figure 4.42 DTG scans of MP10 samples before and after 1000 hours of accelerated weathering

The activation energy is also found to be decreased after 1000 hours of accelerated weathering. Yet there is no change in residue. The results are similar with that of Beg and Pickering (2008) who observed effect of accelerated weathering on pure polypropylene (PP) and PP composite. They found that pure PP experienced a reduction of thermal stability indicated by decrease of degradation temperature and activation energy after 1000 hours of accelerated weathering.

Table 4.6 Degradation temperatures of HDPE samples before and after 1000 hours of accelerated weathering

Sample	Before accelerated weathering					After accelerated weathering				
	T _{onset} °C	T _{maximum} °C	T _{final} °C	Residue %	Ea kJ/mol	T _{onset} °C	T _{maximum} °C	T _{final} °C	Residue %	Ea kJ/mol
Pure	470.15	496.03	518.29	1.04	332.72	462.00	493.80	516.36	0.78	253.37
ML10	470.02	495.82	518.12	0.44	317.80	458.24	490.39	515.39	0.94	250.08
MP10	470.75	495.16	516.43	0.71	328.49	457.21	488.54	513.46	0.85	234.89
MS10	469.15	495.33	517.32	0.55	311.04	451.94	486.90	511.53	0.45	233.42

4.3.7 Melting Temperature and Crystallinity

Selected samples namely pure, ML10, MP10 and MS10 were analyzed using DSC, based on the same reason with choosing samples in TGA analysis. The results are summarized in Table 4.7. For illustration of the results, DSC scans of pure sample and MP10 sample, before and after 1000 hours of accelerated weathering, are depicted in Figures 4.43 and 4.44, Figures 4.43 and 4.44 shows that DSC traces of both pure and MP10 samples shifted to lower temperature after 1000 hours of accelerated weathering. This phenomenon also happened on ML10 and MS10 samples. After 1000 hours of accelerated weathering, the melting temperature (T_m) of MP10 sample decreased significantly from 130.70°C initially to 127.91°C, on the other hand the T_m of pure sample slightly decreased from initial value of 131.35°C to 130.19°C. It happened due to breakdown of HDPE chains with lower molecular weight took place during degradation, as mentioned previously. The measurement of average molecular weight and MFI has obviously showed that the lower molecular weight of HDPE and other compounds were produced as the results of photo-degradation and thermo-oxidative degradation during accelerated weathering.

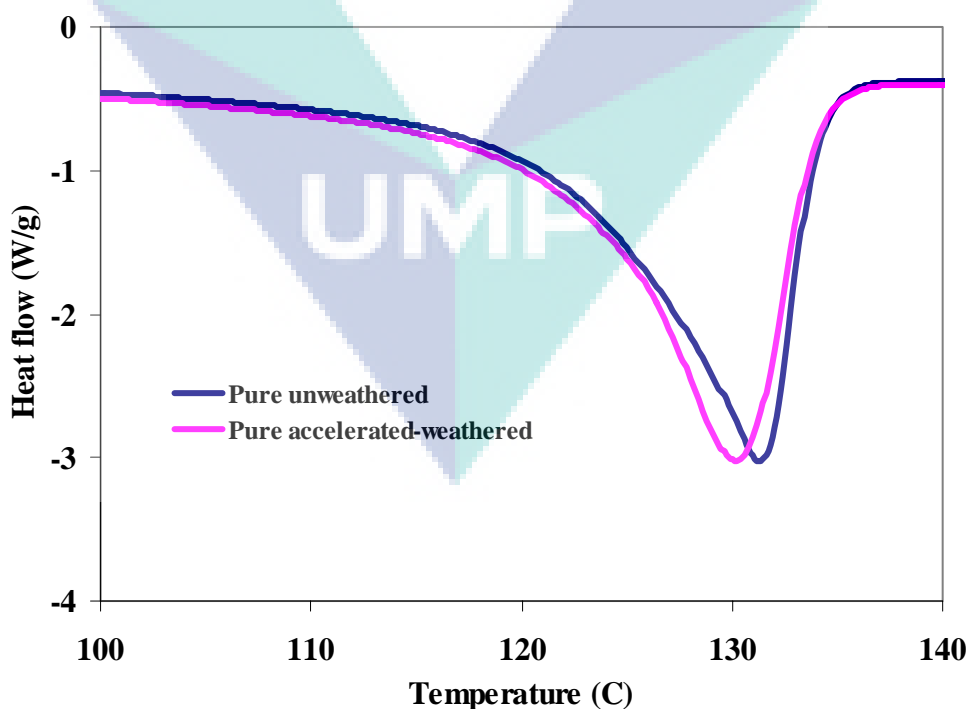


Figure 4.43 DSC scans of pure samples, before and after 1000 hours of accelerated weathering

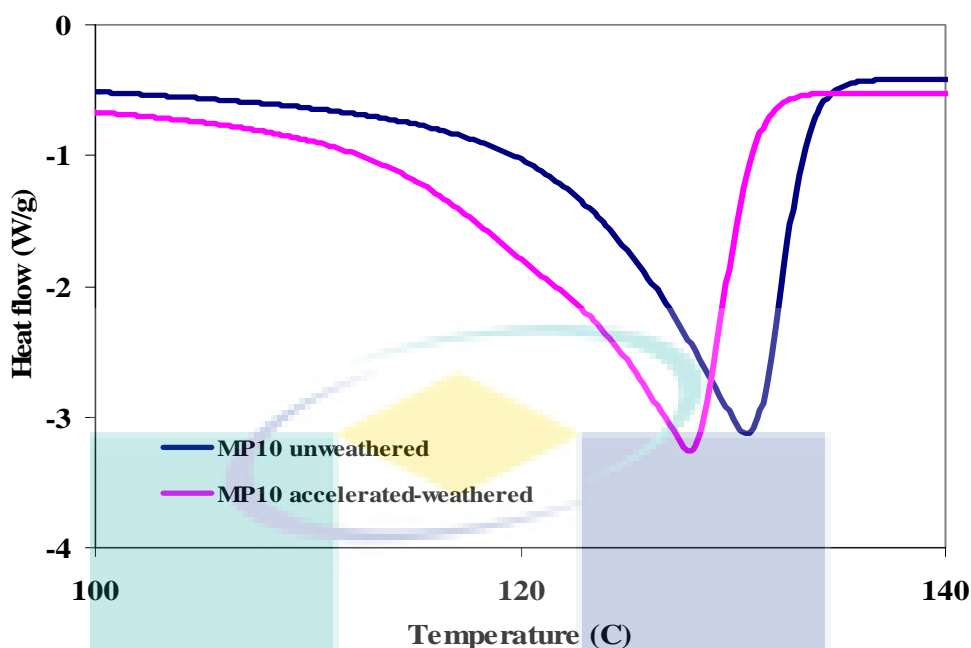


Figure 4.44 DSC scans of MP10 samples, before and after 1000 hours of accelerated weathering

Table 4.7 Melting temperatures of HDPE samples and their crystallinities, before and after 1000 hours of accelerated weathering

Sample	Before accelerated weathering				After accelerated weathering			
	T_o , °C	T_m , °C	ΔH_f , J/g	X_{DSC}	T_o , °C	T_m , °C	ΔH_f , J/g	X_{DSC}
Pure	122.64	131.35	140.8	48.04	121.50	130.19	150.8	51.45
ML10	122.42	130.95	143.2	48.86	118.18	127.94	164.7	56.19
MP10	122.19	130.70	143.7	49.03	117.59	127.91	170.3	58.10
MS10	122.18	130.72	141.5	48.28	117.20	127.69	168.4	57.45

T_o : melting point (onset), T_m : melting point (peak), °C; ΔH_f : heat of fusion, J/g; X_{DSC} : crystallinity index obtained from DSC scan(%)

The crystallinity index obtained from DSC scans increases during accelerated weathering. The crystallinity of pure samples increased from 48.04% to 51.45%, whereas ML10, MP10 and MS10 samples underwent higher increases as presented in Table 4.7. As discussed earlier, the oxidation attacked amorphous part of HDPE resulting shorter chain products which rearranged and crystallized (Khabbaz et al., 1999; Sebaa et al., 1992).

The crystallinity observation is supported by XRD scans as depicted in Figure 4.45 and 4.46. The intensity of pure sample was found to be higher after 1000 hours of accelerated weathering. The intensity of MP10 sample was found to increase much

higher than that of pure sample. ML10 and MS10 also experienced the same phenomena with MP10 sample. It suggests the increase of crystallinity after accelerated weathering. Generally, the XRD patterns of samples show the hump at 2θ -angle of 20.6° which is recognized as the amorphous hump, and crystalline peaks which are found at 2θ angle of around 21.9° , 24.2° , and 36.7° . The crystallinity of sample from XRD patterns was determined from the ratio of area under crystalline peaks to the total area of amorphous and crystalline peaks (Murthy and Minor, 1990; Roy et al., 2007a). The crystallinities of samples obtained from XRD patterns (X_{XRD}) and their comparison with those obtained from DSC scan (X_{DSC}) are presented in Table 4.8.

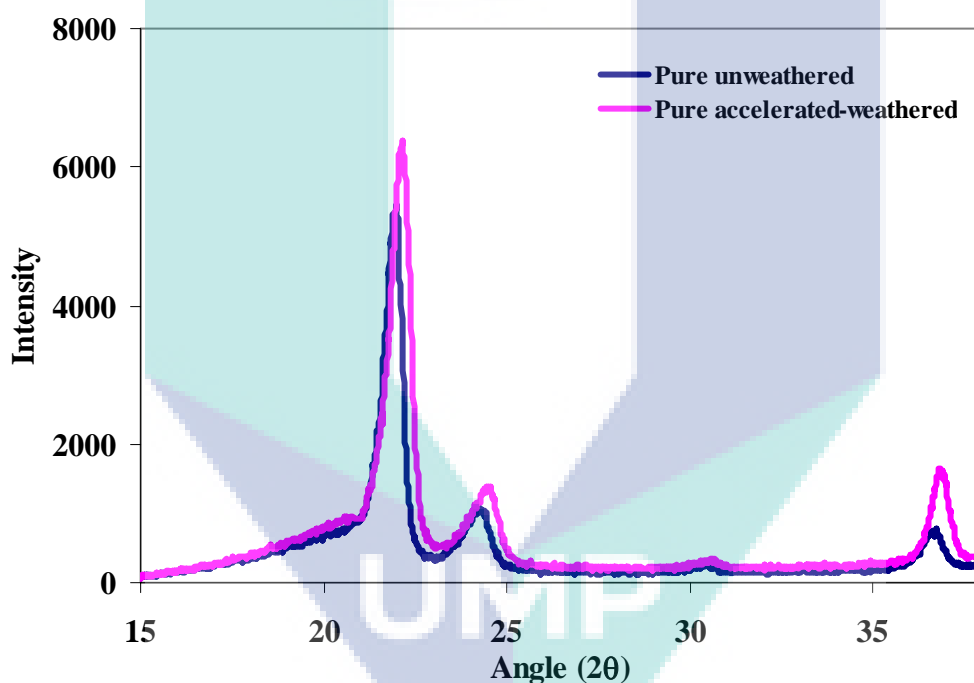


Figure 4.45 XRD traces of pure samples, before and after 1000 hours of accelerated weathering

The X_{XRD} is generally found to be higher than X_{DSC} for corresponding sample. However, the X_{XRD} has shown similar behavior with X_{DSC} in which it increased after 1000 hours of accelerated weathering. Furthermore the significant increases of crystallinity of samples containing manganese carboxylates, has evidenced the significant role of manganese carboxylates in enhancing degradation process of HDPE during accelerated weathering.

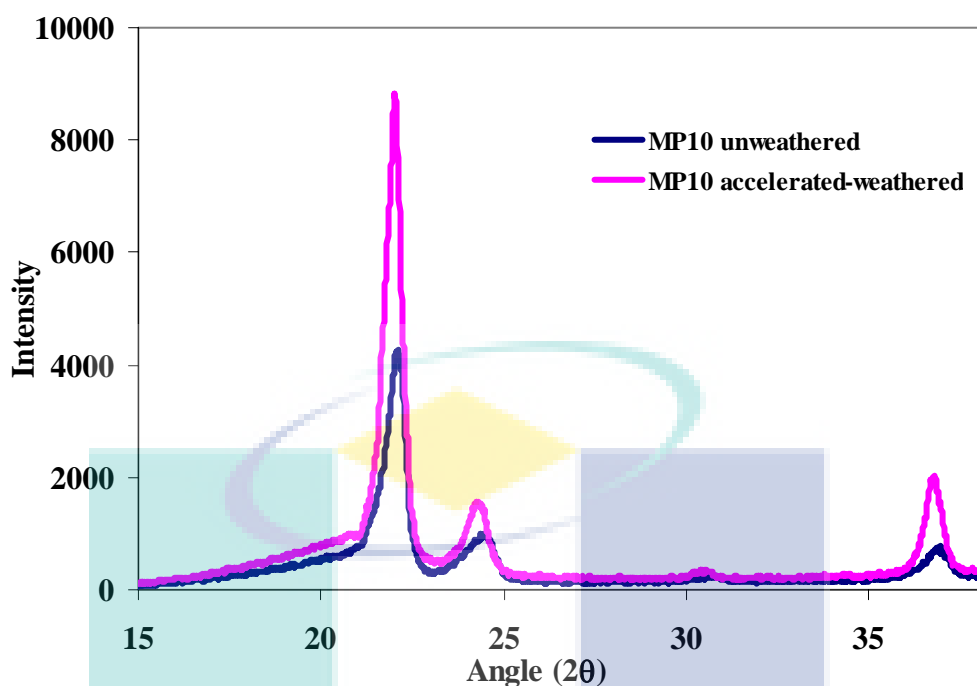


Figure 4.46 XRD traces of MP10 samples, before and after 1000 hours of accelerated weathering

Table 4.8 Comparison of crystallinities obtained from DSC scan and XRD trace before and after 1000 hours of accelerated weathering

Sample	Before accelerated weathering		After accelerated weathering	
	X_{DSC}	X_{XRD}	X_{DSC}	X_{XRD}
Pure	48.04	54.31	51.45	56.86
ML10	48.86	54.74	56.19	61.37
MP10	49.03	55.76	58.10	62.92
MS10	48.28	55.48	57.45	64.97

X_{DSC} : crystallinity index obtained from DSC scan (%);

X_{XRD} : crystallinity index obtained from XRD scan (%)

4.3.8 Surface Morphology

Figure 4.47 shows the surface texture of pure sample and samples with manganese carboxylates after 1000 hours of accelerated weathering. The surface of pure sample was found to be slightly affected after 1000 hours of accelerated weathering, as opposed to samples containing manganese carboxylates. The surface texture of all samples containing manganese carboxylates exposed to the accelerated weathering

strongly deteriorated, in the form of ruggedness and deposition of white powdery material on the surface. As degradation mostly occurred on amorphous part at the surface of sample, the degraded part of HDPE crystallizes and results in a higher crystallinity. It leads to shrinkage of sample. Spray water and condensation lead to leaching of some degradation products on the surface. This leads to further degradation process. Meanwhile the inner part of sample is less affected. The difference between inner part and surface may lead to contraction and result in surface cracks as reported by Beg (2008). The surface cracks which are found may lead to lower mechanical properties i.e. tensile strength and elongation at break.

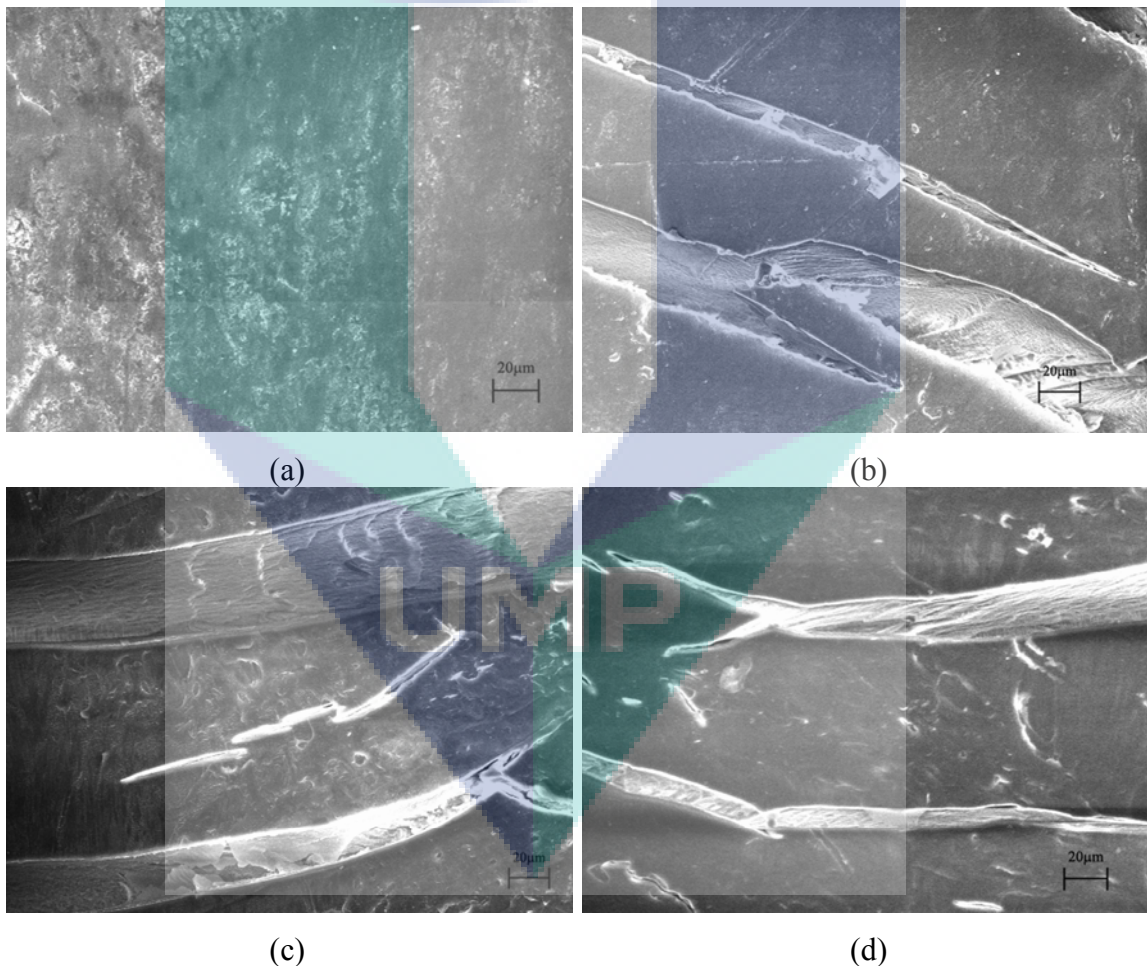


Figure 4.47. SEM image of samples (a) pure HDPE (b) ML10 (c) MP10 (d) MS10 after 1000 hours of accelerated weathering

4.4 DEGRADATION OF HIGH DENSITY POLYETHYLENE UNDER NATURAL WEATHERING TREATMENT

4.4.1 Introduction

Natural weathering or outdoor exposure of various compositions of HDPE sample was done in Gambang, Malaysia (latitude: 3°43'07"N and longitude: 103°07'16"E). Generally, this site is tropical area with relatively high rainfall, high temperature and high intensity of sunlight. In Peninsular Malaysia, the minimum range of mean relative humidity varying from a low 80% in February to a high of only 88% in November. April and May are the months with the highest average monthly temperature in most places and December and January are the months with the lowest average monthly temperature as reported by Malaysian Meteorological Department (MMD, 2010). The temperature and rainfall are summarized in Table 4.9.

Table 4.9 Gambang average weather
(<http://www.meoweather.com/history/Malaysia/na/3.7166667/103.1/Gambang.html>)

Month	Temperature (°C)				Average rainfall (mm)	
	Average		Absolute		Daily	Monthly
	Max	Min	Max	Min		
January	29.5	22.5	36.1	11.5	8.8	274.3
February	30.8	22.5	35.2	18.5	6.1	170.3
March	31.8	23.1	39.4	19.2	5.9	181.7
April	32.9	23.7	38.8	20.3	4.6	138.8
May	33.3	23.9	38.6	13.7	6.2	193.4
June	32.9	23.7	36.4	21.5	5.5	165.4
July	32.6	23.5	37.5	20.6	5.8	180.2
August	32.7	23.4	36.6	13.5	7.3	227.5
September	32.6	23.3	35	14.9	6.5	196.0
October	32.0	23.3	35.6	21.0	9.0	279.2
November	30.7	23.2	35.0	14.8	13.2	395.9
December	29.5	22.9	34.2	20.2	21.8	674.5

On average, Malaysia receives from 4.21 to 5.56kWh/m² of solar radiation a year. The maximum solar radiation receive is 5.56 kWh/m² mostly in Northern region of Peninsular Malaysia and Southern region of East Malaysia. The highest solar radiation is estimated at 6.8 kWh/m² in August and November while the lowest is 0.61 kWh/m² in December (Azhari et al., 2008). The natural weathering treatment was conducted for maximum duration of 24 weeks during September 2009 to March 2010. The weathering was started when solar radiation and temperature are high and in the middle of treatment

the rainfall increased, as opposite sunlight intensity and temperature decreased. The final period of treatment, temperature and solar radiation increased, while rainfall decreased.

4.4.2 Infrared Spectra

In the natural environment, the degradation process is complex due to the presence of sunlight, wind, rain, pollutants, non-isothermal conditions (Sheikh et al., 2006), and also humidity. However, sunlight and temperature may dominate the influencing factors. Sunlight or solar radiation are composed of a number of spectra, including infrared (IR), visible light, and UV; however UV radiation is the most influential. The degradation process occurs as the result of combined factors working simultaneously. Some climatic variables affect to light-induced degradation of polymer. Andrady et al (2006) have reported that increase in solar UV radiation is the most influential light on light-induced degradation of polymer, followed by the increase in temperature, humidity and pollutants, respectively.

The degradation under solar UV radiation (photo-degradation) is initiated by formation of radicals, followed by formation of hydroperoxide (Singh and Sharma, 2008). The high ambient temperature plays role in enhancing hydroperoxide decomposition since hydroperoxides rapidly cleave to form alkoxy and hydroxyl radicals at elevated temperature (Johnston and Morrison, 1996; Wiles, 2005). High temperature may also directly initiate thermo-oxidative degradation. The mechanisms of thermo-oxidative degradation and photo-degradation have been discussed earlier (see Section 4.2.3 and Section 4.3.3). Both photo-degradation and thermo-oxidative degradation usually generate carbonyl, hydroxyl and vinyl groups, and eventually result in chain scissions of polymer. Al-Madfa et al. (1998) have also observed that two competitive processes are occurring simultaneously during weather ageing of the LDPE: oxidative degradation and cross-linking. Under any set of conditions one will dominate. The decomposition of the hydroperoxide formed usually leads to chain splitting, recombination of free radicals products can lead to cross-linking in polyethylene. The presence of manganese carboxylates as pro-degradant additives has promoted the more rapid degradation process by catalyzing the decomposition of hydroperoxide (Albertsson et al, 1992, Bikiaris et al, 1997).

Figure 4.48 represents the FTIR trace of MS10 samples due to natural weathering for 24 weeks. It shows the increases of absorbance at 3300-3500 cm^{-1} attributed to hydroxyl groups, 1700–1800 cm^{-1} attributed to carbonyl groups, and 1000-1300 cm^{-1} attributed to ether groups, and 900–1000 cm^{-1} attributed to vinyl groups after 24 weeks of natural weathering. However, the absorbance of carbonyl groups that comprise ketonic, ester, carboxylic, aldehyde, and lactone is the most changed. The absorbances of other groups slightly increase. This result is similar to that of Sheikh et al. (2006) who observed the significant changes in hydroxyl (3200–3600 cm^{-1}), carbonyl (1715–1720 cm^{-1}) and unsaturated (800–1000 cm^{-1}) groups regions as a function of the exposure time under the natural and accelerated conditions.

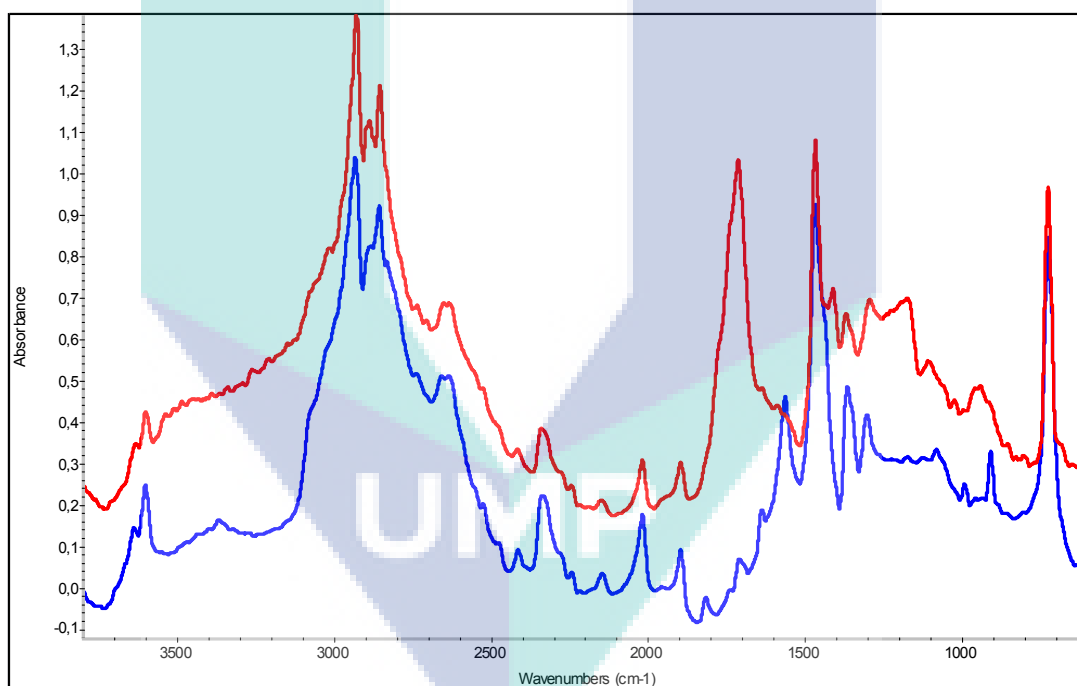


Figure 4.48 FTIR spectra of MS10 samples before (lower trace) and after (upper trace) natural weathering

As carbonyl groups generated during natural weathering, consequently CI rises. Figure 4.49 shows the change of CI of various samples during natural weathering. It shows the obvious difference between pure HDPE and HDPE with manganese carboxylates. HDPE with additives undergoes more significant increase of CI than pure HDPE. In the first weeks, the increases of CI are larger than those at end period of

treatment. It is due to rapid photo-degradation process since the solar radiation in the first weeks is quite high. It leads to rapid formation of carbonyl groups. Andrady et al. (2003) have reported that the increase in ambient temperatures could play an important role in enhancing the rates of photo-degradation in materials exposed to sunlight. During solar ultraviolet radiation, the greater temperature would contribute higher effect on degradation of plastics than the greater humidity. The degradation takes place slower by the increasing rainfall and the reduced solar radiation. It is shown by the small increase of CI from the middle to end period of natural weathering.

Generally, MS gives the greatest effect on enhancing natural photo-degradation of HDPE, indicated by the greatest increase of CI after 24 weeks of natural weathering. As discussed previously, it was due to the long carbon chain of manganese stearate that has similar structure with HDPE. Hence, it was easy to mix with HDPE and effectively act as pro-degradant.

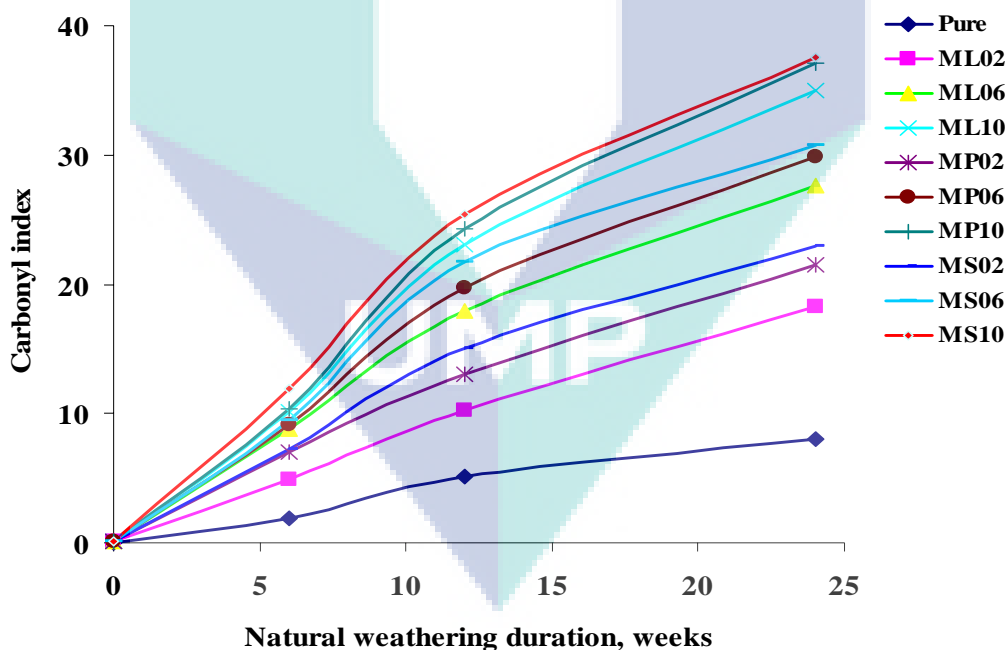


Figure 4.49 Carbonyl indexes of various samples during natural weathering

4.4.3 Tensile Properties

Tensile strength of samples containing manganese carboxylates during natural weathering treatment are depicted in Figures 4.50–4.52. Generally, all samples exhibit decreases of tensile strength with increasing weathering duration. However, HDPE with additives degrade more rapidly than pure HDPE. Furthermore, the higher amount of additive in HDPE results in the faster degradation. It is interesting to note that pure sample showed an increase of tensile strength at 2 weeks of natural weathering treatment and it was relatively constant until 4 weeks of treatment. It is due to crosslinking process, consequently tensile strength increases. After 6 weeks of treatment, tensile strength of pure HDPE hereafter gradually decreased until end of treatment. Further sunlight exposure lead to chain scissions, subsequently tensile strength decreases gradually.

During first 8 weeks of natural weathering treatment (September-October), the intensity of sunlight is relatively high that leads to photo-oxidative degradation. The high temperature plays secondary effect on enhancing degradation. Andrady et al.(1993a) have reported that during outdoor exposure of polyethylene, the disintegration obtained is a consequence of both photo-degradation (photo-initiated autooxidation) as well as thermo-oxidative reactions. At some locations temperature plays an important role in determining the rate of disintegration.

The initial degradation process of pure HDPE is characterized by radical and hydroperoxide formations and normally crosslinking takes place. The mechanism of degradation including crosslinking process has been discussed previously (see Section 4.2.3 and 4.3.3). Crosslinking leads to increasing tensile strength of HDPE. While sunlight exposure continues, it results in further degradation of HDPE. Eventually, the chain scissions predominate rather than crosslinking process, and subsequently result in decreasing tensile strength. As shown in Figures 4.50–4.52, the tensile strengths of samples containing 0.2–0.4%(w/w) of manganese carboxylates were relatively constant until 4 weeks of treatment, and then decreased systematically with increasing duration of natural weathering. The samples containing higher amount of manganese carboxylates 0.6–1.0% (w/w) experienced decreases of tensile strength during entire

period of treatment. However, the rapid degradation of samples containing additives (0.6–1.0%) occurs in the first weeks of natural weathering due to environment conditions. It is consistent with findings of Al-Madfa et al. (1998) who have reported that the loss in mechanical properties (yield strength and ductility) in the first week of ageing (outdoor weathering) could be attributed to the material oxidation taking place in the air and accelerated by the UV.

The second period during November-December (week 9–16), the condition is high rainfall, low temperature and low sunlight intensity. It leads to slower degradation since photo-degradation take place slower due to lower solar radiation, as indicated by the deflection of curves at week 10. It suggests the changes in the rate of degradation. The third period, during January – March, the rainfall is going lower, the temperature and sunlight intensity are higher. The degradation remains at slow rate. The deposition of degradation products on the surface of sample absorbs sunlight. It retards penetration of sunlight into inner part of sample, and lets inner part slightly affected. However, thermo-oxidative degradation keeps taking place and allows samples undergoing tensile strength decrease.

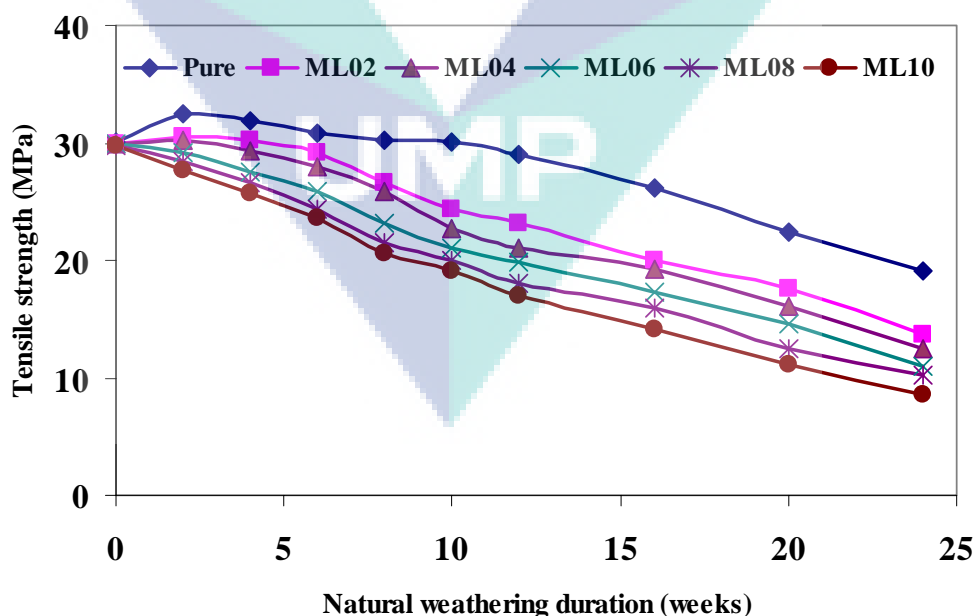


Figure 4.50 Tensile strength of HDPE containing manganese laurate during natural weathering

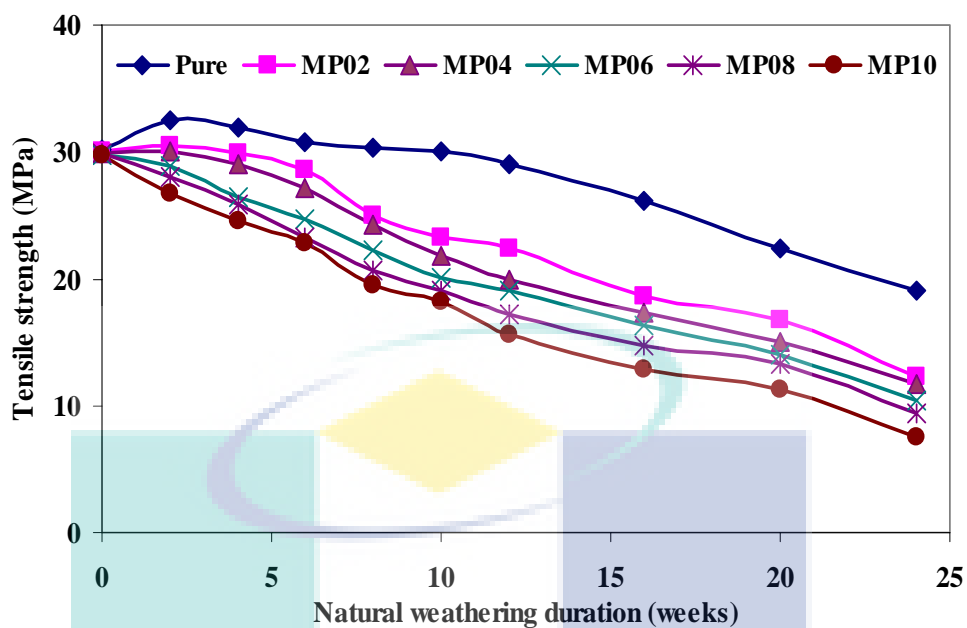


Figure 4.51 Tensile strength of HDPE containing manganese palmitate during natural weathering

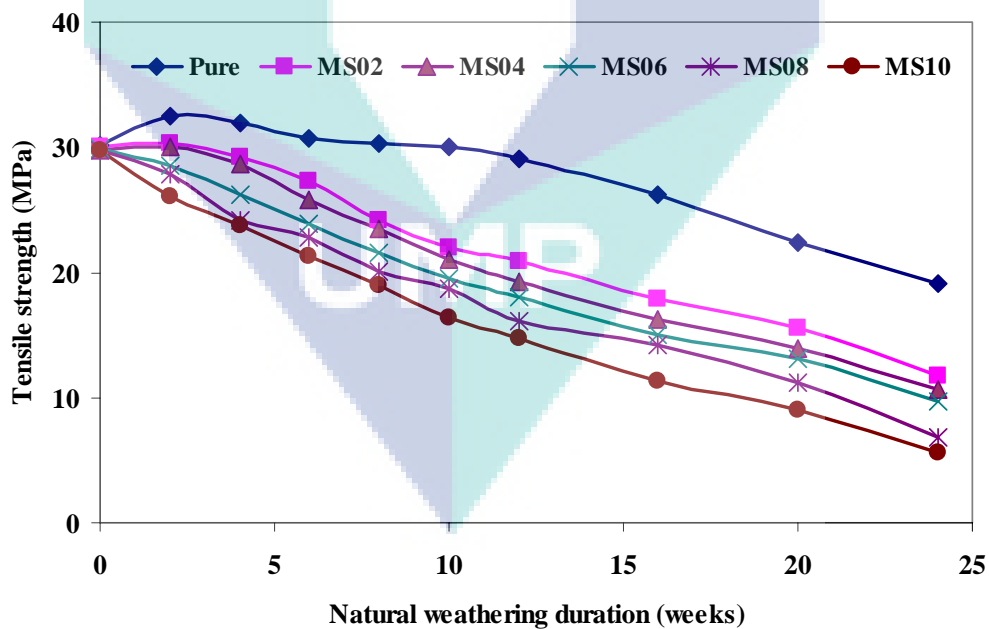


Figure 4.52 Tensile strength of HDPE containing manganese stearate during natural weathering

Tensile modulus of all samples containing manganese carboxylates decreased during natural weathering. Pure samples experienced an increase of tensile modulus in

the first 2 weeks of natural weathering, and decreased after 4 weeks. The changes of tensile modulus of samples have shown the similar trends with those of tensile strength. However the decreases of tensile modulus were lesser than those of tensile strength. Figures 4.53-4.55 represent tensile modulus of samples during natural weathering treatment, and the losses of tensile modulus for selected samples are presented in Table 4.10.

Table 4.10 Losses of tensile properties of samples after 24 weeks of natural weathering

Samples	Loss of tensile strength, %	Loss of tensile modulus, %	Loss of elongation at break, %
Pure	36.67	19.26	64.54
ML02	54.07	32.27	82.90
ML10	71.33	47.57	93.02
MP02	59.26	36.74	84.04
MP10	74.68	50.86	94.80
MS02	61.05	39.02	85.56
MS10	81.08	53.55	95.74

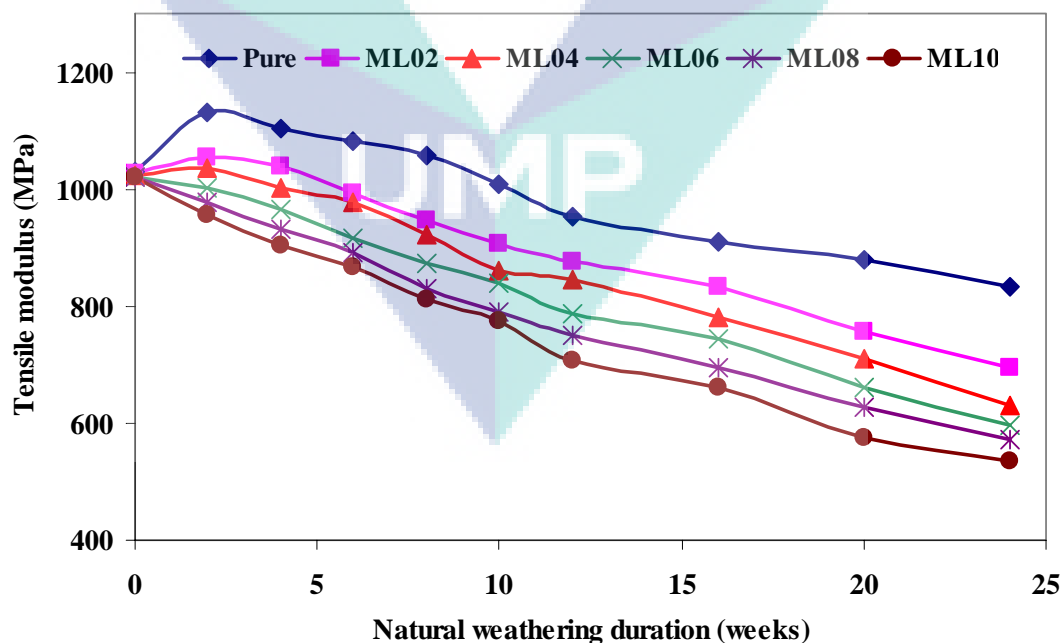


Figure 4.53 Tensile modulus of HDPE containing manganese laurate during natural weathering

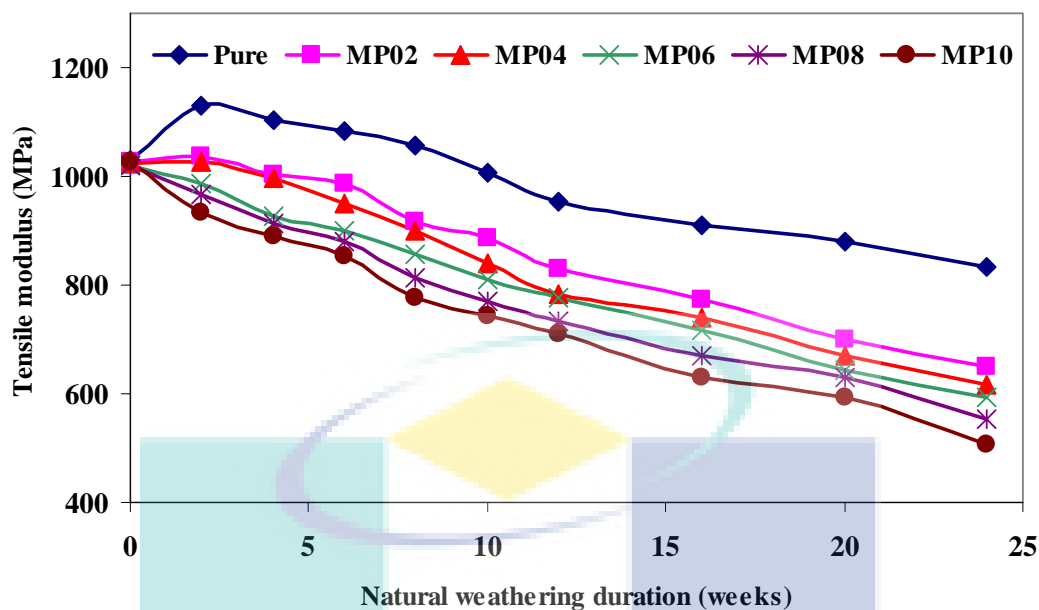


Figure 4.54 Tensile modulus of HDPE containing manganese palmitate during natural weathering

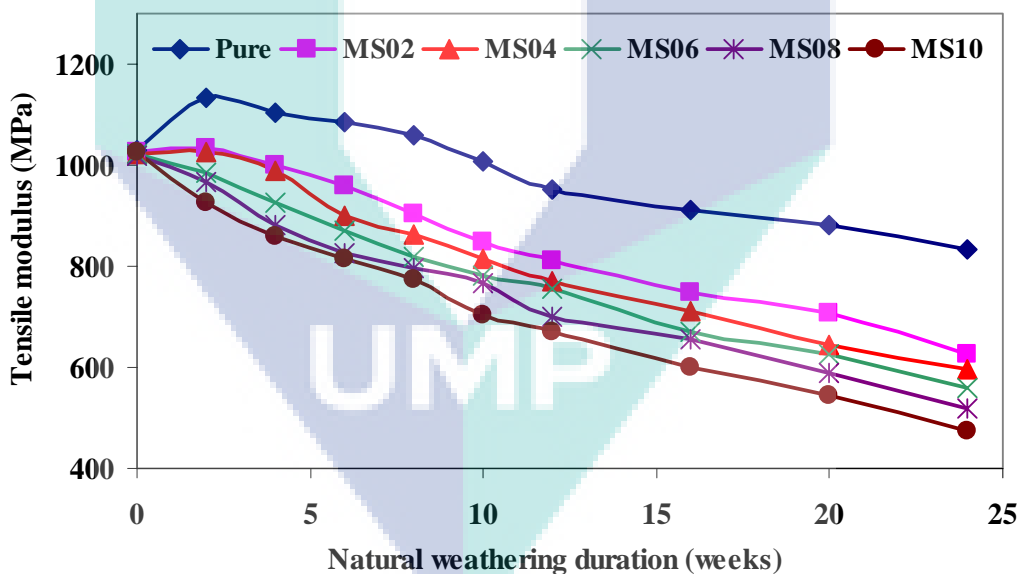


Figure 4.55 Tensile modulus of HDPE containing manganese stearate during natural weathering

Figures 4.56–4.58 represent the change of elongation at break during natural weathering treatment. The changes in elongation at break give more obvious indication on degradation than the changes in tensile strength. All samples undergo the decreasing elongation at break. However, elongations at break of HDPE containing additives decreased more rapidly than pure HDPE. Despite the increase of tensile strength in the

first weeks, pure HDPE underwent the decrease of elongation at break during entire period of natural weathering exposure. These figures also obviously show that the elongation at break of HDPE with manganese carboxylates decrease rapidly in the first 8 weeks of treatment. That indicates the rapid degradation has occurred. As explained earlier, it is due to high solar radiation that induces rapid photo-degradation supported by effect of high temperature. This result is consistent with that of previous study by Hamid (cited in (Andrady et al., 2003)) who compared the weathering of polyethylene agricultural mulch films under high-UV outdoor exposure conditions at ambient temperature and at 25°C inside a controlled temperature UV-transparent chamber. Under ambient conditions, in Dhahran (Saudi Arabia), the surface temperature of the plastic rose as high as 60 °C depending on color and thickness, because of the absorption of solar IR wavelengths. The average elongation at break of the polyethylene was periodically measured; this property is particularly sensitive to degradation in this type of material. The rate of light-induced breakdown of the polyethylene under comparable UV exposure was slower by a factor of four when the temperature was controlled at the lower temperature of 25 °C.

At around week 10–12, the rates of degradation changes dramatically as indicated by extreme deflection of curves, and changes hereafter from high to low slope until end of treatment. Moreover, the end part of curves is found to be flat, indicating very slow degradation. The rain water may leach the degradation products on the surface of sample and lets solar radiation to penetrate deeper. Nevertheless, the lower intensity of solar radiation and lower temperature during high rainfall period lets degradation remaining slow. In the end of treatment, solar radiation increases, as the rainfall decrease. Yet the photo-degradation has been retarded by degradation products on the surface, and thermo-oxidative degradation induced by temperature may play secondary effect that allows the overall degradation keep taking place very slowly. It is also found that the deleterious effect of degradation during natural weathering mostly occurs on the surface of sample. It suggests the photo-degradation, which is stimulated by solar radiation, predominates in the overall degradation.

Figures 4.50–4.58 describe that increasing amount of additives i.e. manganese carboxylates results in increasing degradation. For example, pure HDPE loses 36.67 % of its initial tensile strength and 64.54% of its initial elongation at break after 24 weeks of natural weathering exposure. Meanwhile, MS 02 and MS10 samples lose 61.05 and 81.08 of their initial tensile strength and 85.56 and 95.74 of their elongation at break, respectively. Generally, MS give the most influential effect among other additives i.e. ML and MP as obviously shown in Table 4.10.

The result is in agreement with that of Sheikh et al. (2006) who have compared degradation of commercial LDPE and photosensitized LDPE which contains ferric stearate under weathering condition of Tehran. They have found that photosensitized LDPE films deteriorate more rapidly than commercial LDPE as indicated by the decrease of tensile properties. It has also been reported that polyethylene films exposed to solar UV-B radiation readily lose their extensibility and strength (Andrady et al., 1998; Hamid et al., 1992). Ojeda et al. (2011) have also reported the similar results on natural weathering of PP, HDPE, LLDPE and LLDPE/HDPE blend. All samples experienced decrease of elongation at break by increasing exposure time.

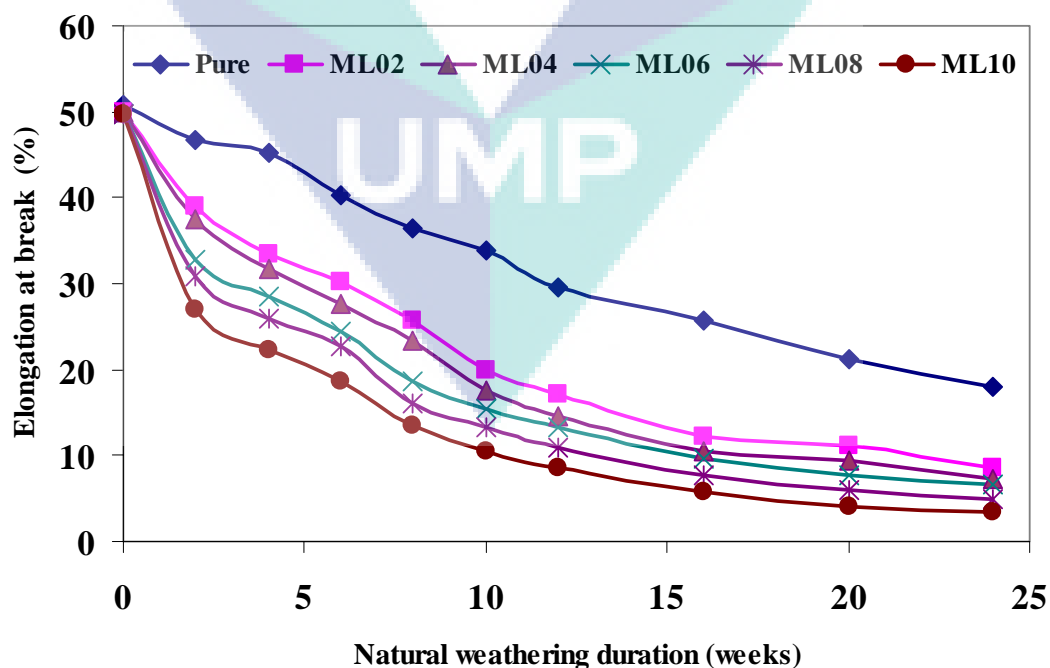


Figure 4.56 Elongation at break of HDPE containing manganese laurate during natural weathering

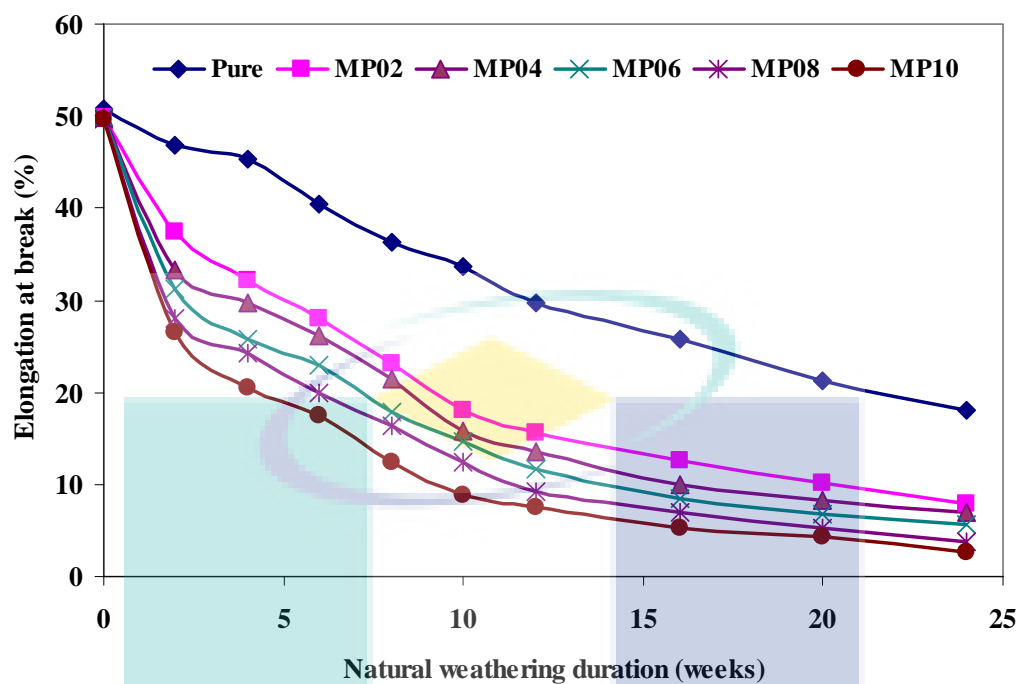


Figure 4.57 Elongation at break of HDPE containing manganese palmitate during natural weathering

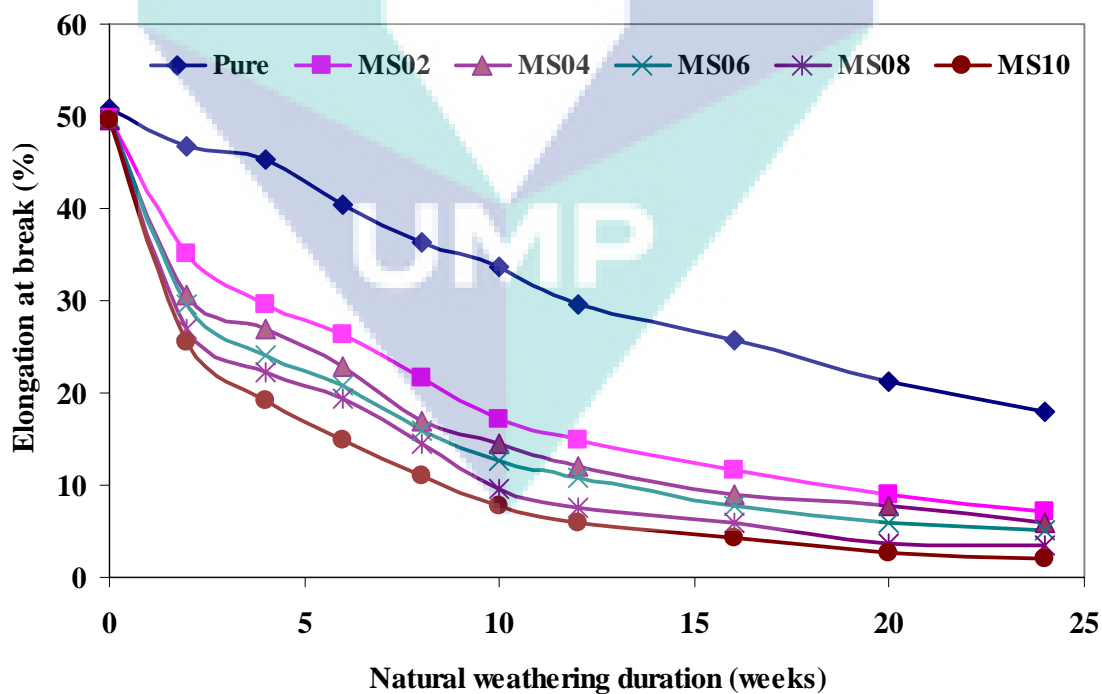


Figure 4.58 Elongation at break of HDPE containing manganese stearate during natural weathering

4.4.4 Molecular Weight

Figure 4.59 represents the changes of average molecular weight of pure HDPE and various compositions of HDPE during natural weathering. All samples exhibit decrease of average molecular weight during natural weathering. HDPE is sensitive to solar radiation, especially solar UV radiation. However, HDPE with additives i.e. ML, MP and MS experience much more significant decrease of molecular weight than pure HDPE. Average molecular weight of pure HDPE decreases about 40 % of its initial value after 24 weeks of natural weathering. The incorporation of manganese carboxylates as pro-degradant additives has enhanced the degradability of HDPE. The average molecular weight decreases more significantly when the amount of incorporated additives increases. For example, MS02 sample undergoes a reduction of 69.02% of its initial value, and 85.82% for MS10 sample after 24 weeks of natural weathering. HDPE containing manganese stearate has demonstrated greatest reduction of molecular weight. This result is in agreement with previous study by Andrady et al. (1993b) who has observed that polyethylene films exposed to solar UV radiation experience decreasing the average molecular weight.

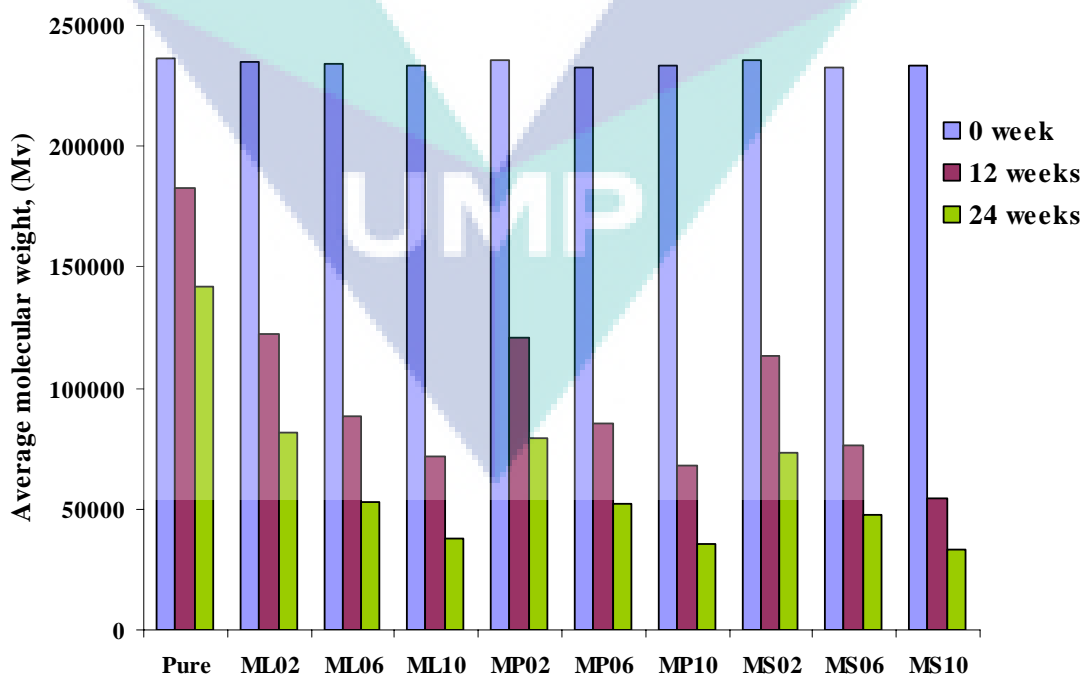


Figure 4.59 Average molecular weight of samples during natural weathering

In general, the reductions of molecular weight in the first 12 weeks of natural weathering are greater than those of 12 weeks later. In other words, the degradation takes place faster in the beginning than the end of natural weathering. It parallels to the decrease of elongation at break of samples during natural weathering. It has proved that chain scissions occurred during natural weathering consequently result in lowering average molecular weight as well as decrease of mechanical properties i.e. elongation at break and tensile strength.

4.4.5 Melt Flow Index

Figure 4.60 represents MFI of various compositions of HDPE samples during natural weathering. It shows that MFI of all samples increase with increasing duration of natural weathering. Pure HDPE have experienced a slight increase of MFI after 24 weeks of natural weathering, from initial value of 0.081 to 0.779 g/10min. The presence of manganese carboxylates in HDPE has significantly raised the MFI. The MFI of MS10 has been found to increase from 0.126 to 2.604 g/10min. This is the greatest increase compared with ML10 and MP10 samples: from 0.123 to 2.451g/10min and from 0.125 to 2.498g/10min respectively. The increasing amount of additives results in higher MFI. The higher MFI indicates the lower average molecular weight. It reconfirms that shorter chain of HDPE has been formed during natural weathering.

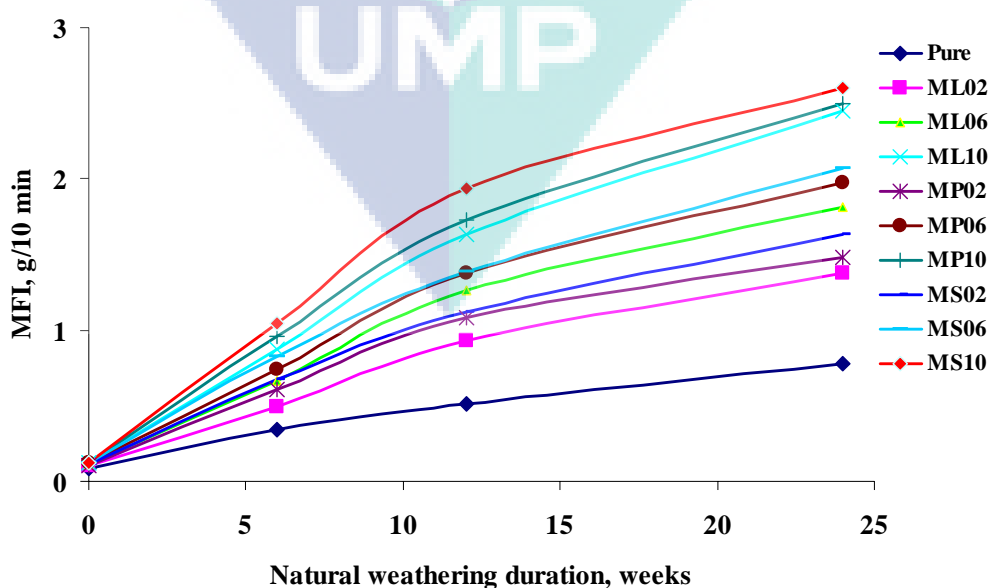


Figure 4.60 MFI of various samples during natural weathering

4.4.6 Degradation Temperature

Figures 4.61-4.64 represent TG and DTG of pure sample and MS10 sample, before and after 24 weeks of natural weathering. The corresponding data are summarized in Table 4.11. The TG and DTG traces after 24 weeks of natural weathering shifted to lower temperatures for both pure sample and MS10 sample. It also happened to ML10 and MP10 samples. The figures also show that all samples demonstrate a single stage of decomposition process. However, samples containing manganese carboxylates show greater changes in degradation temperature than pure sample. The greatest change has been performed by MS10 sample. The lower degradation temperature is corresponding to the lower molecular weight. This result is in agreement with the decrease of average molecular weight during natural weathering due to chain scissions.

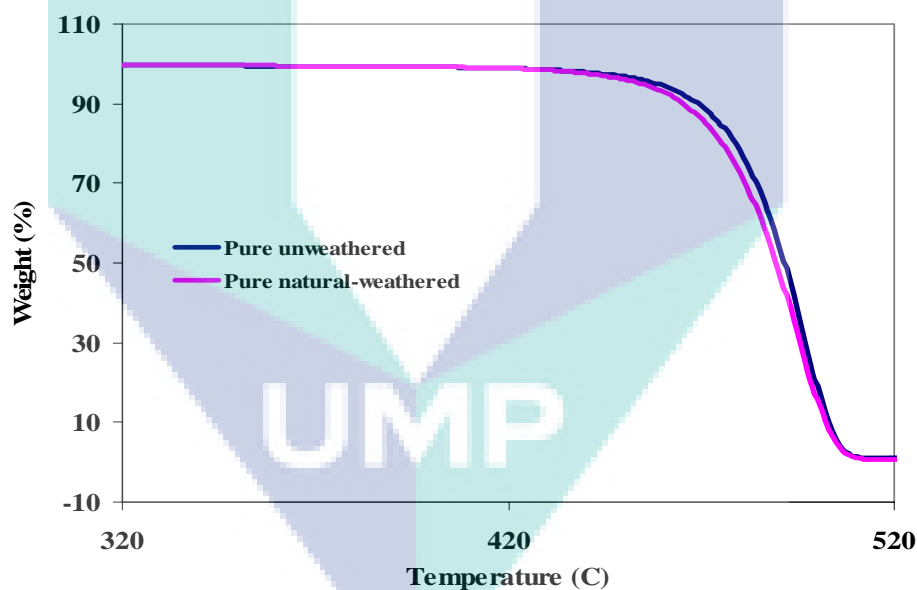


Figure 4.61 TG traces of pure samples, before and after 24 weeks of natural weathering

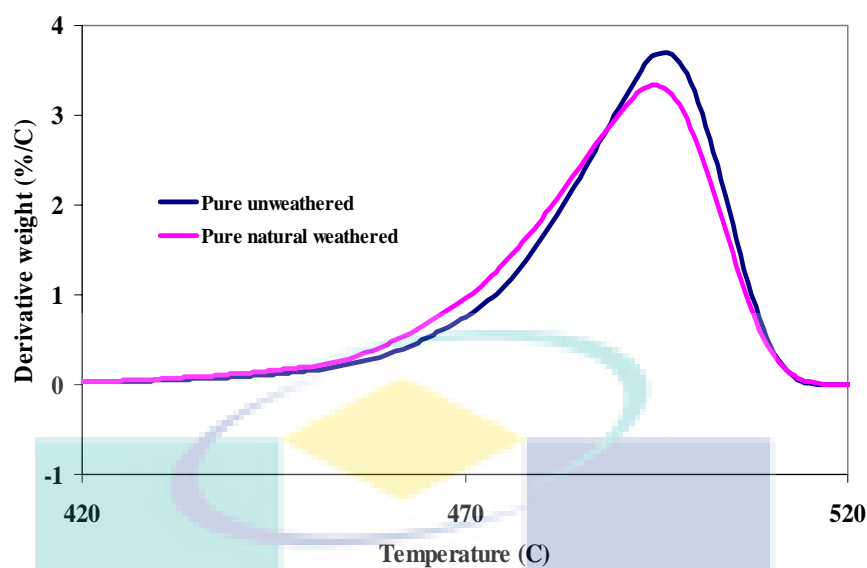


Figure 4.62 DTG traces of pure samples, before and after 24 weeks of natural weathering

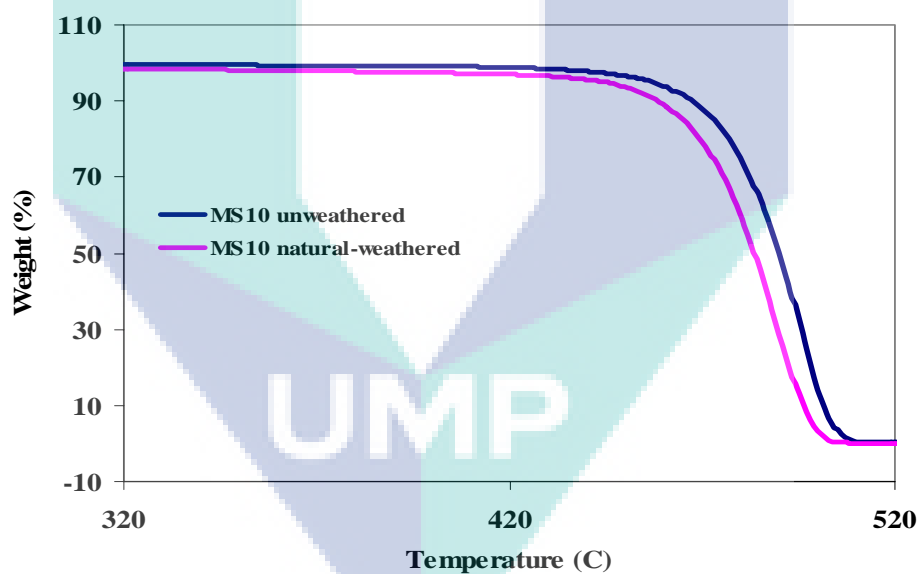


Figure 4.63 TG traces of MS10 samples, before and after 24 weeks of natural weathering

Generally, the activation energies of all samples have been found to be reduced after 24 weeks of natural weathering. Nevertheless, the presences of manganese carboxylates have led to enhancing the reduction of activation energy. Low activation energies for the degradation processes have been reported as evidence of degradation

during outdoor weathering enhanced by temperature (Hamid, cited in Andrady et al., 2003). The residues have not changed significantly.

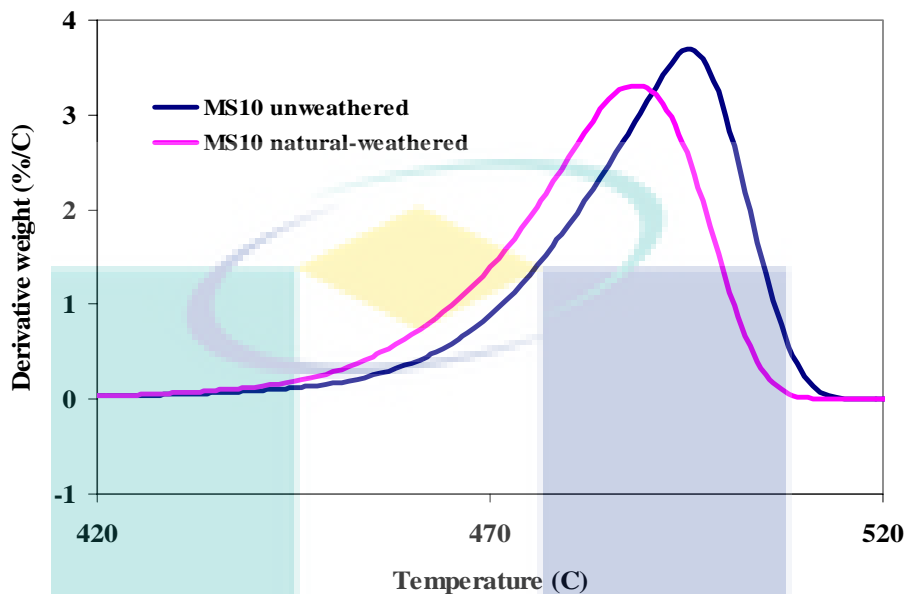


Figure 4.64 DTG traces of MS10 samples, before and after 24 weeks of natural weathering

Table 4.11 Degradation temperatures of HDPE samples before and after 24 weeks of natural weathering

Sample	Before natural weathering					After natural weathering				
	T _{onset} °C	T _{maximum} °C	T _{final} °C	Residue %	Ea kJ/mol	T _{onset} °C	T _{maximum} °C	T _{final} °C	Residue %	Ea kJ/mol
Pure	470.15	496.03	518.29	1.04	332.72	464.67	494.83	517.22	0.85	283.86
ML10	470.02	495.82	518.12	0.44	317.80	459.33	491.01	515.20	0.25	270.33
MP10	470.75	495.16	516.43	0.71	328.49	460.68	490.37	515.38	0.59	231.76
MS10	469.15	495.33	517.32	0.55	311.04	460.97	488.88	513.32	0.29	248.14

4.4.7 Melting Temperature and Crystallinity

Melting behaviors of various samples of HDPE have been observed by using DSC, before and after natural weathering treatment. Figures 4.65 and 4.66 represent the DSC scans of pure sample and MS10 sample, before and after 24 weeks of natural weathering treatment. The corresponding data are summarized in Table 4.12. The DSC scans show similar phenomena with those of TG/DTG traces. They shift to lower

temperature after 24 weeks of natural weathering treatment due to the presence of lower molecular weight of degradation products. The presence of lower molecular weight fraction has been proven by average molecular weight measurement as discussed previously. After 24 weeks of natural weathering, the melting temperature (T_m) of pure sample slightly decreased from 131.35°C initially to 130.47°C, whereas the melting temperature of MS10 sample more significantly decreased from initial value of 130.72°C to 128.44°C. The HDPE samples containing manganese carboxylates have also shown the lower melting temperature than pure HDPE after exposed to natural weathering for 24 weeks.

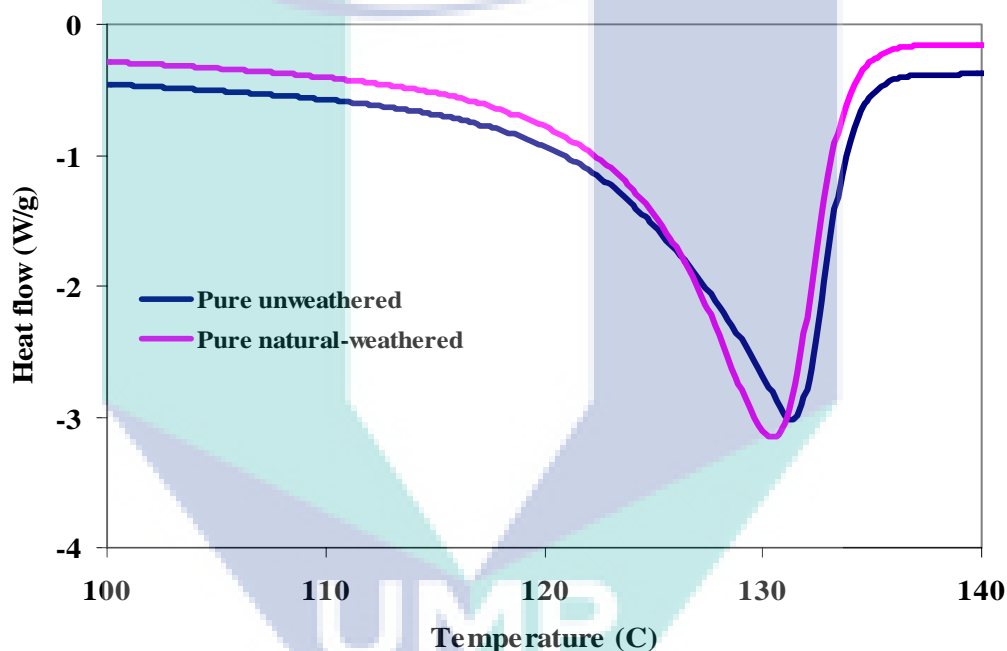


Figure 4.65 DSC scans of pure samples before and after 24 weeks of natural weathering

The crystallinity indexes obtained from DSC scan (X_{DSC}) have been found to increase during natural weathering treatment for all samples. Pure HDPE have experienced less significant increase of crystallinity than HDPE with either ML or MP or MS. The crystallinity of MS10 sample has increased from 48.28% to 56.29%, whereas pure sample has increased from 48.04% to 51.83%. It is due to crystallization of degradation products that commonly have shorter chain (Khabbaz et al., 1999; Sebaa et al., 1992).

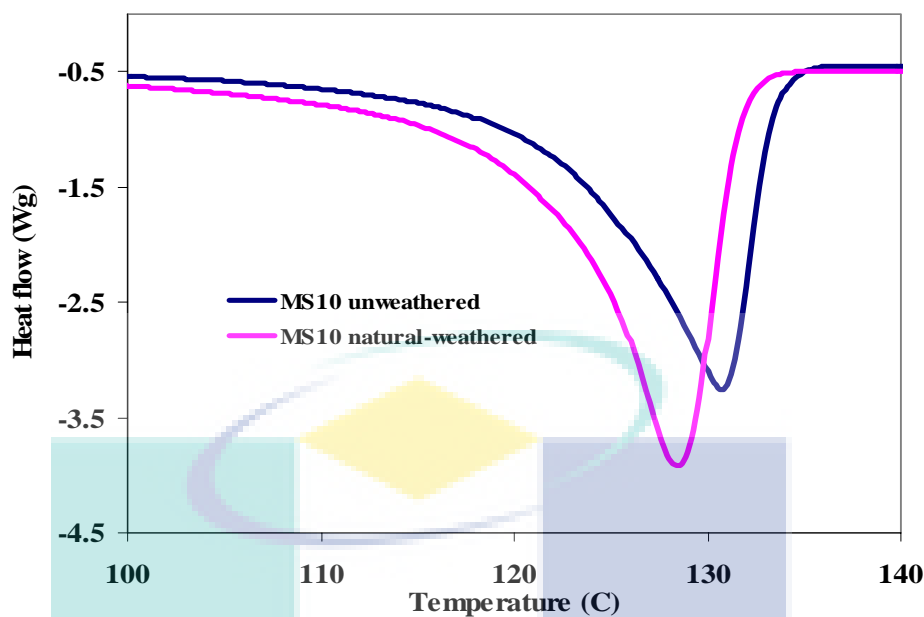


Figure 4.66 DSC scans of MS10 samples before and after 24 weeks of natural weathering

Table 4.12 Melting temperatures of HDPE samples and their crystallinity before and after 24 weeks of natural weathering

Sample	Before natural weathering				After natural weathering			
	T_o , °C	T_m , °C	ΔH_f , J/g	X_{DSC}	T_o , °C	T_m , °C	ΔH_f , J/g	X_{DSC}
Pure	122.64	131.35	140.8	48.04	121.77	130.47	151.9	51.83
ML10	122.42	130.95	143.2	48.86	121.34	129.27	157.9	53.87
MP10	122.19	130.70	143.7	49.03	121.43	128.39	163.1	55.65
MS10	122.18	130.72	141.5	48.28	121.12	128.44	165.0	56.29

T_o : melting point (onset), T_m : melting point (peak), °C; ΔH_f : heat of fusion, J/g; X_{DSC} : crystallinity index obtained from DSC scan(%)

The XRD test has reconfirmed crystallinity observation by DSC scan. The XRD scans of pure HDPE and MS10 sample, before and after natural weathering treatment are presented in Figures 4.67 and 4.68. Both pure HDPE and MS10 samples show the increases of intensities that indicates the increase of crystallinity. The determination of crystallinity of sample has been discussed previously. The crystallinities of samples obtained from XRD patterns (X_{XRD}) and their comparison with those obtained from DSC scan (X_{DSC}) are presented in Table 4.13. Generally, X_{XRD} are greater than X_{DSC} for corresponding samples.

Table 4.13 Comparison of crystallinities obtained from DSC scan and XRD trace before and after 24 weeks of natural weathering

Sample	Before natural weathering		After natural weathering	
	X_{DSC}	X_{XRD}	X_{DSC}	X_{XRD}
Pure	48.04	54.31	51.83	56.17
ML10	48.86	54.74	53.87	58.99
MP10	49.03	55.76	55.65	60.64
MS10	48.28	55.48	56.29	61.32

X_{DSC} : crystallinity index obtained from DSC scan (%);
 X_{XRD} : crystallinity index obtained from XRD scan (%)

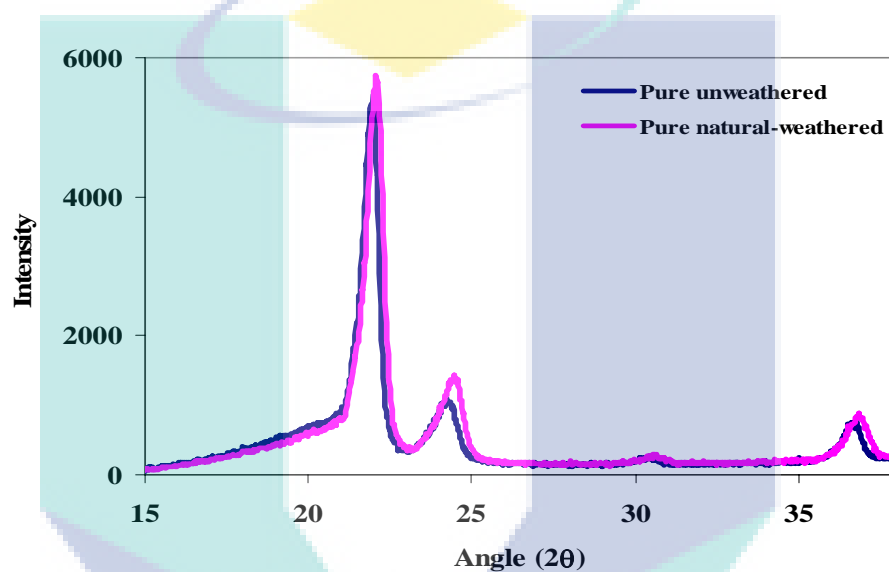


Figure 4.67 XRD traces of pure samples before and after natural weathering

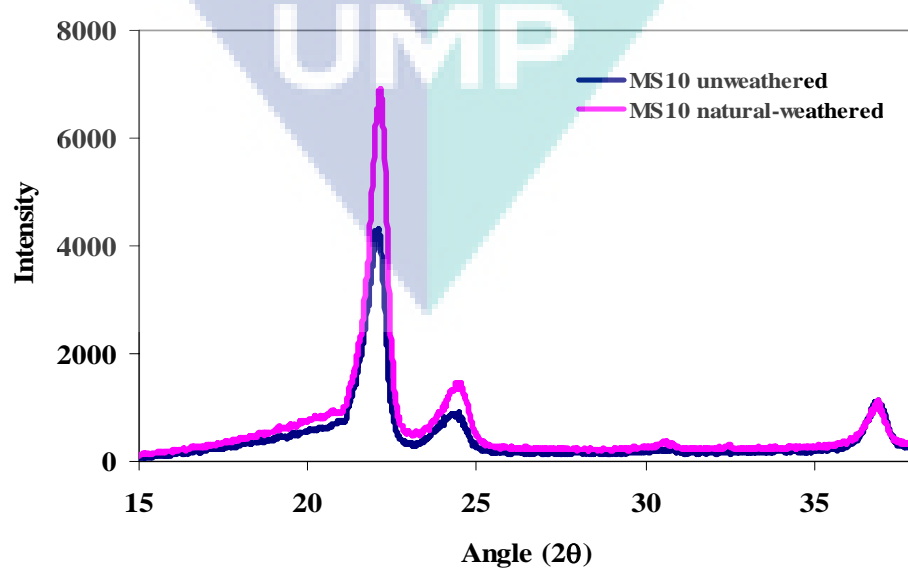


Figure 4.68 XRD traces of MS10 samples before and after natural weathering

4.4.8 Surface Morphology

The changes of surfaces of samples were observed by using SEM. Figure 4.69 shows SEM image of samples after 24 weeks of natural weathering. The surfaces of samples containing manganese carboxylates show the noticeable changes after exposed to natural weathering for 24 weeks. The changes are characterized by ruggedness, surface cracks or defects, and chalking on the surface of samples. In contrast, pure HDPE only experienced a little change on surface texture. It has been observed that surface of thick sample is the most affected during degradation induced by UV radiation and the surface cracks have arisen as the result of surface contraction. The cracks may lead to reduction of tensile property (Beg, 2008; Schoolenberg and Meijer, 1991).

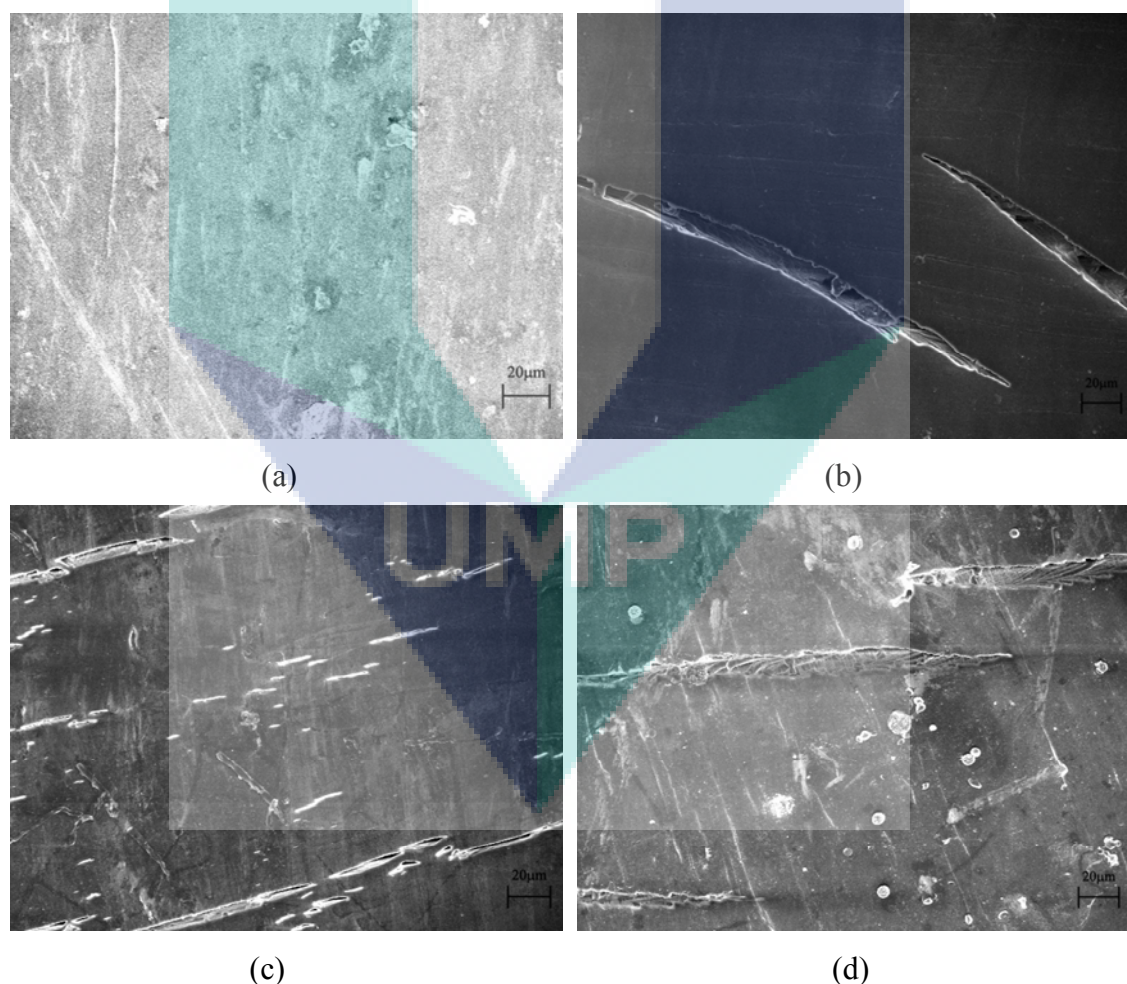


Figure 4.69. SEM image of samples (a) pure HDPE (b) ML10 (c) MP10 (d) MS10 after 24 weeks of natural weathering

4.5 COMPARATIVE EFFECT OF TREATMENTS

Three different treatments i.e. thermal treatment, accelerated weathering, and natural weathering have been conducted and the results have been presented above. Pure HDPE and HDPE containing manganese have shown different behaviors of degradation during those treatments. However, during those treatments HDPE containing manganese carboxylates i.e. ML, MP, and MS have performed the faster degradation than pure HDPE.

The FTIR test has shown that peaks at some regions have grown during all treatments. The regions are $3300\text{-}3500\text{ cm}^{-1}$ (hydroxyl groups), $1700\text{-}1800\text{ cm}^{-1}$ (carbonyl groups), $1000\text{-}1300\text{ cm}^{-1}$ (ether groups), and $900\text{-}1000\text{ cm}^{-1}$ (vinyl groups). The major increase is at carbonyl regions. The changes in carbonyl index have noted that the thermal treatment show the least rate of degradation as shown in Figure 4.70. It is significantly different with two other treatments: accelerated weathering and natural weathering.

The measurement of elongation at break has also obviously shown the similar trend as depicted in Figure 4.71. Pure HDPE have lost 16.12 % of elongation at break after 1000 hours of thermal treatment, 42.53 % after 1000 hours of accelerated weathering, and 40 % after 24 weeks of natural weathering. On the other hand, MS10 sample experienced loss of elongation at break for 69.49 %; 90.49% and 85.82 % after thermal treatment, accelerated weathering and natural weathering, respectively.

It is also supported by the measurement of average molecular weight (MW) which is presented in Figure 4.72. Accelerated weathering has resulted in greatest reduction of MW. Generally, the differences between accelerated weathering and natural weathering effects are small.

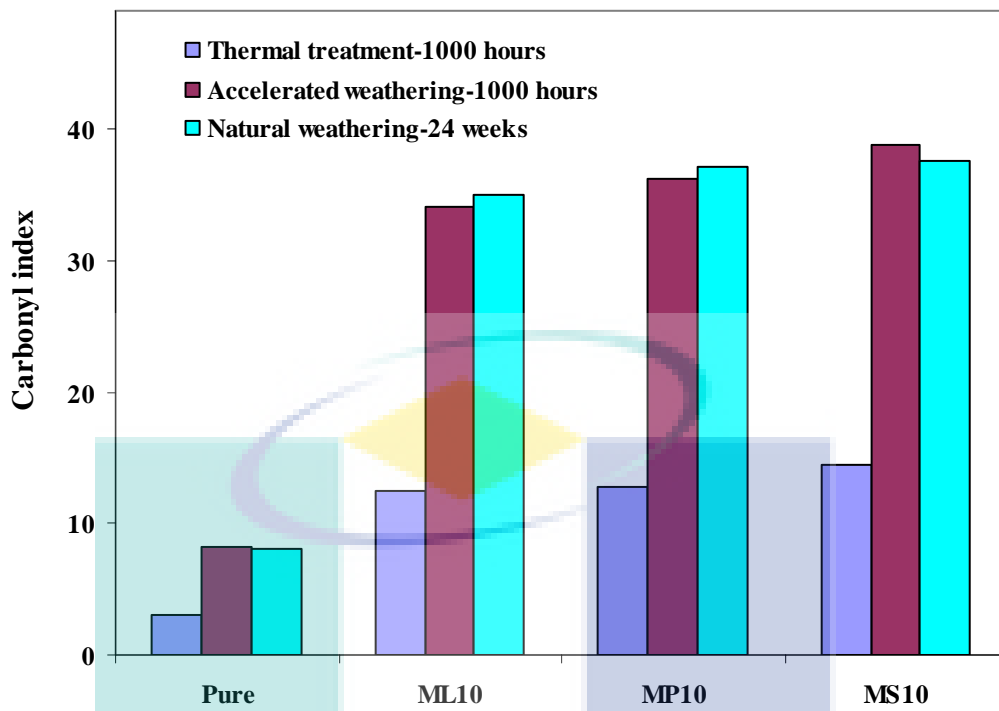


Figure 4.70 Comparison of CI after three different treatments

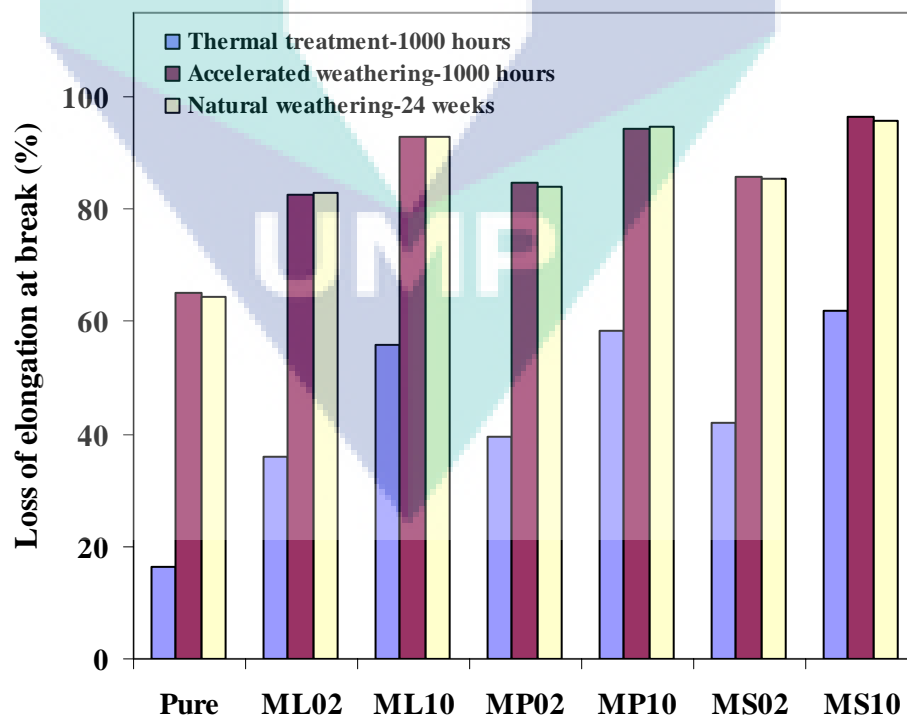


Figure 4.71 Comparison of losses of elongations at break after three different treatments

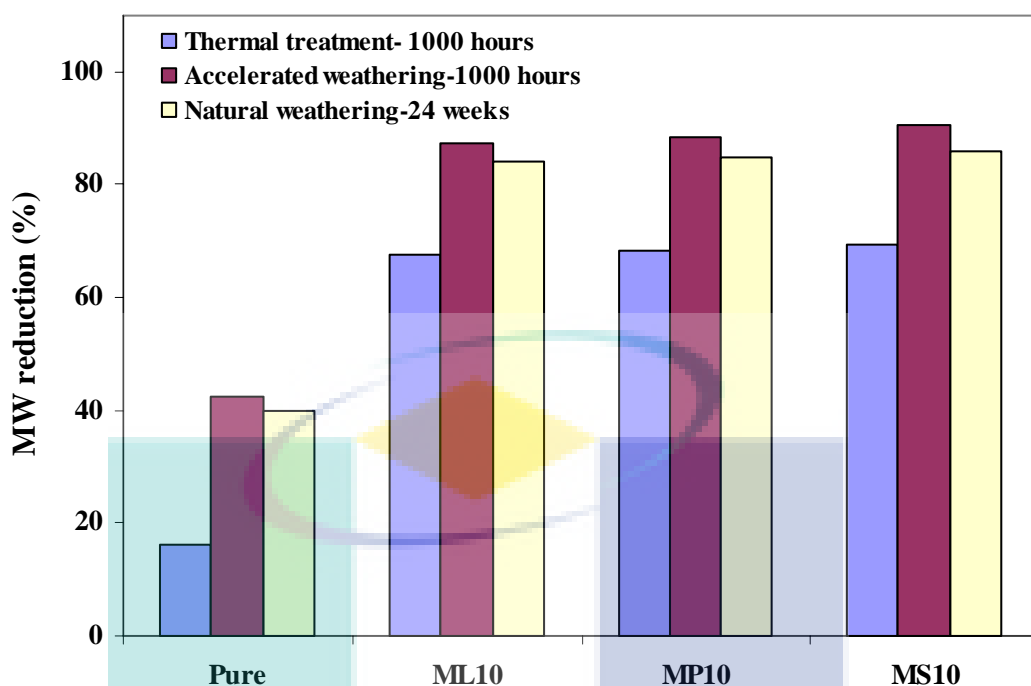


Figure 4.72 MW reductions after three different treatments

Thermal properties of exposed samples have also evidenced the higher impact of accelerated weathering and natural weathering on degradation than thermal treatment. The comparison of thermal stability of pure HDPE and HDPE containing manganese after several different treatments are presented in Table 4.14. The reductions of thermal stabilities as indicated by reduction of degradation temperature and activation energies have occurred most significantly during accelerated weathering. Figure 4.73 represents the TGA traces of MS 10 samples after different treatments. It shows that MS10 sample after accelerated weathering has the lowest degradation temperature.

Table 4.14 Degradation temperatures and activation energies of selected samples before and after three different treatments

Sample	Initial		Thermal treatment		Accelerated weathering		Natural weathering	
	T _{maximum} (°C)	Ea (kJ/mol)	T _{maximum} (°C)	Ea (kJ/mol)	T _{maximum} (°C)	Ea (kJ/mol)	T _{maximum} (°C)	Ea (kJ/mol)
Pure	496.03	332.72	495.16	295.97	493.80	253.37	494.83	283.86
ML10	495.82	317.80	493.26	276.00	490.39	250.08	491.01	270.33
MP10	495.16	328.49	493.10	278.18	488.54	234.89	490.37	231.76
MS10	495.33	311.04	491.87	282.01	486.90	233.42	488.88	248.14

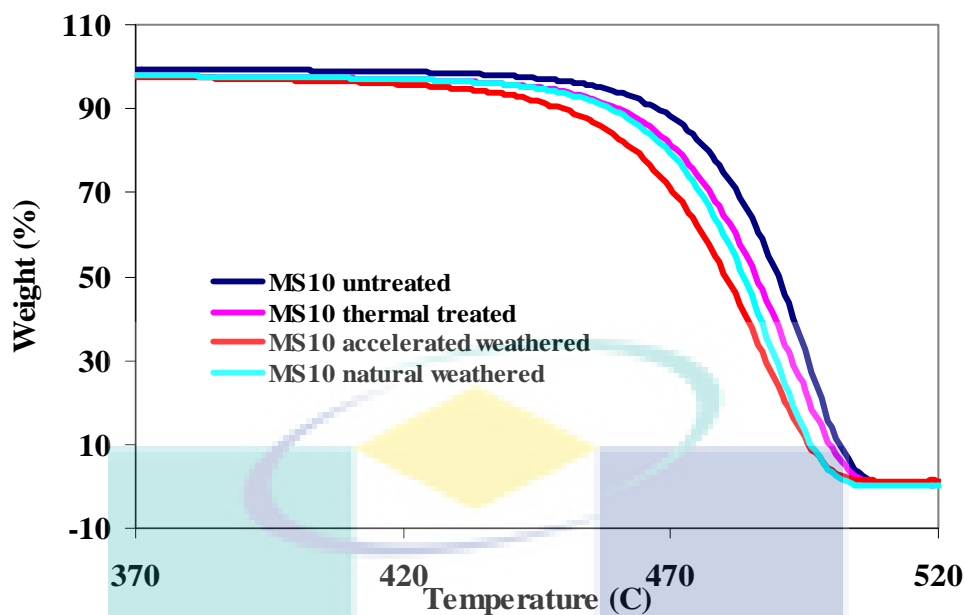


Figure 4.73 TG traces of MS10 samples before and after three different treatments

Melting properties of HDPE samples after several different treatments have demonstrated the similar behaviors with thermal stabilities of samples. Table 4.15 represents melting properties of pure HDPE and HDPE with manganese carboxylates after different treatments. Accelerated weathering has led to the most significant decreases of melting temperatures, in opposite the crystallinities increased most significantly. The DSC scans have obviously described the effect of different treatments on melting behaviors of HDPE, as depicted in Figure 4.74. Thermal treatment has demonstrated lower effect on melting temperature of MS10 sample than accelerated weathering and natural weathering.

Table 4.15 Melting properties of selected samples before and after three different treatments

Sample	Initial		Thermal treatment		Accelerated weathering		Natural weathering	
	T_m (°C)	X_{DSC} (%)	T_m (°C)	X_{DSC} (%)	T_m (°C)	X_{DSC} (%)	T_m (°C)	X_{DSC} (%)
Pure	131.35	48.04	130.65	49.03	130.19	51.45	130.47	51.83
ML10	130.95	48.86	130.29	51.86	127.94	56.19	129.27	53.87
MP10	130.70	49.03	130.03	53.36	127.91	58.10	128.39	55.65
MS10	130.72	48.28	129.96	53.84	127.69	57.45	128.44	56.29

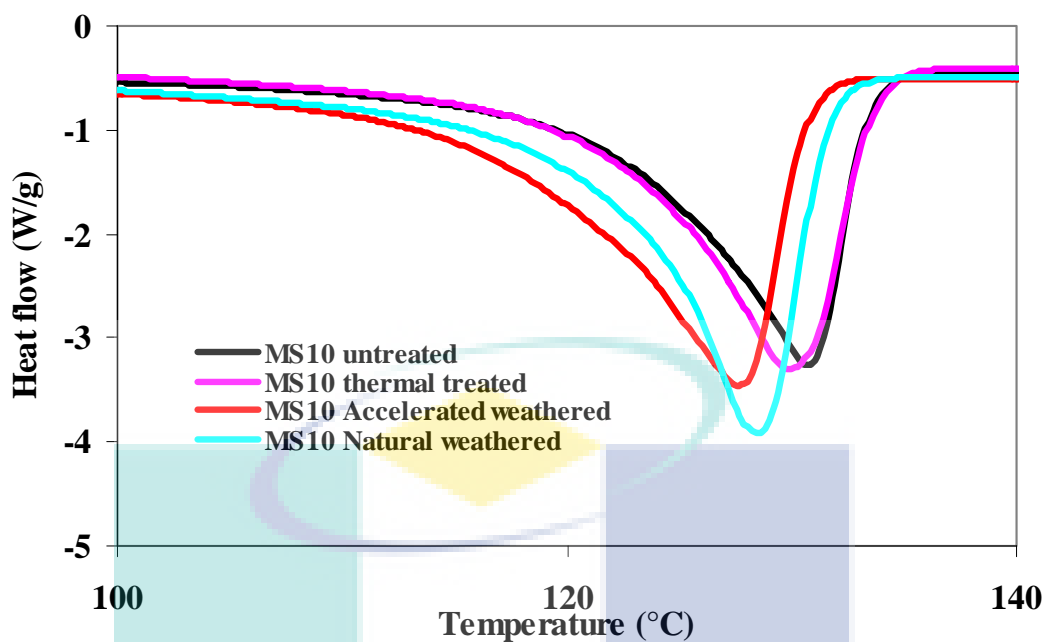


Figure 4.74 DSC scans of MS10 samples before and after three different treatments

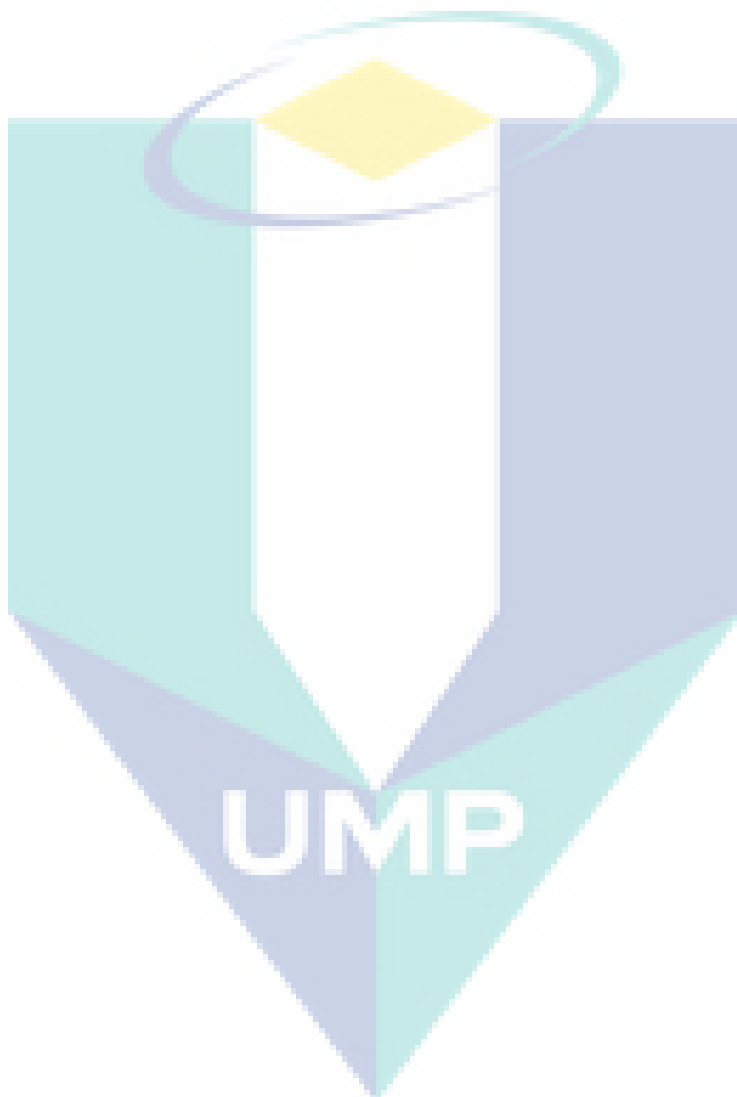
All above results have shown that accelerated weathering demonstrate the most influential effect on degradation. Natural weathering has had almost the same effect with accelerated weathering, whereas thermal treatment has demonstrated the least influential effect. Thermal treatment only involves thermal effect at 70°C, whereas accelerated weathering involves complex factors: UV radiation and thermal at 60°C, also humidity and thermal during condensation, and spray water. Thermal treatment in air-circulated oven involves thermo-oxidative degradation only. Accelerated weathering involves photo-degradation induced by UV radiation and thermo-oxidative degradation. The results have shown obvious differences between thermal treatment and accelerated weathering. Accelerated weathering with UV exposure as the major treatment has demonstrated the greater effects on properties of HDPE than thermal treatment. It suggests that UV exposure (photo-degradation) contributes the major effect on overall degradation while the high temperature enhances it. The presence of spray water and condensation has also supported the degradation process. Natural weathering has had the similar effect on degradation with accelerated weathering. However, natural weathering involves more complex factors than accelerated weathering.

During 1000 hours of accelerated weathering, the UV radiation releases about 0.45 kWh/m² of energy. Whereas during 24 weeks of natural weathering, solar radiation has released approximately 1.94 kWh/m² of energy based on average value of solar radiation in Peninsular Malaysia (4.21 kWh/m²). Despite the different total energy released, the degradation extents of both accelerated weathering and natural weathering are quite similar. It is due to the fact that UV solar radiation fraction is only 5% of total solar radiation (Zeus, 2010) or equal to 0.097 kWh/m². The rest (1.85kWh/m²) comprises energies of visible and IR radiations. The IR solar radiation is mostly converted to heat when absorbed. The visible solar radiation can lead to photochemical reactions in addition to heat up the material. This fact also obviously shows that degradation is mostly affected by UV radiation. UV light has higher energy level than those of IR and visible light. The results have shown that the conditions of site of natural weathering have strongly influenced the degradation process of HDPE.

In general MS has shown the better performance than ML and MP in enhancing degradation during all modes of treatments. All the results have validated that the degradation of HDPE containing manganese carboxylates slightly increases following the order: ML < MP < MS. At the same amount of ML, MP and MS incorporated to HDPE, MS has commonly given the greatest effect, even sometime only gives small difference with ML and MP.

It is well known that the presence of trans-metal in polyethylene has enhanced the decomposition of hydroperoxides produced in the initial stage of degradation. However, the results indicate that the metal content is not the only factor that affects the role of additives in accelerating the degradation. But there is another factor i.e. the type of compound in which the metal is attached. As description, at the same weight of ML, MP and MS, ML has the highest metal content, followed by MP and MS. If degradation was only affected by the metal content, the ML should be the most influential additive. Nevertheless, MS has generally demonstrated the better performance than ML. On the other hand, when the single type of compound such as MS is incorporated into the HDPE, it is found that the degradation increases by increasing amount of MS. Furthermore, MS has a longer chain than the ML and MP.

As discussed previously, Roy et al. (2006b) have reported that as the chain length of additive increases; it is capable of blending easily with the base polymer resulting in its increased capability to act as pro-oxidant. MS also has better thermal properties of a higher melting point and better thermal stability than ML and MP. Thermal stability is very important property of polymer additive. The additive with higher thermal stability is preferable since it ensure to not decompose during processing.



CHAPTER 5

CONCLUSIONS AND RECOMENDATIONS

5.1 CONCLUSIONS

The study on utilization of manganese carboxylates as pro-degradant additive for HDPE was started by synthesizing manganese carboxylates. The synthesis has been conducted successfully through two step reactions: sodium carboxylates synthesis by reacting carboxylic acids with sodium hydroxide and manganese carboxylates production by reacting sodium carboxylates with manganese chloride. The characterization has revealed that all manganese carboxylates are powder with low bulk densities, high melting point (108-117 °C). Manganese carboxylates generally have good thermal stability that meet the requirement of polymer additive, particularly HDPE. However, manganese stearate has the best thermal stability and highest melting temperature. The incorporation of manganese carboxylates into HDPE up to 1% (w/w) has not significantly affected the properties of HDPE.

During thermal treatment, carbonyl groups as the result of oxidation grew faster in the sample with manganese carboxylate than pure sample. Tensile properties were also found to decrease with increasing amount of manganese carboxylate. HDPE with 1% of manganese stearate experienced greater loss of elongation at break (62.11%) than pure HDPE (16.21%). The molecular weights of samples with manganese carboxylate were also found to decrease significantly and consequently MFI increased. Thermal stability and melting temperature were also found to decrease more significantly for HDPE samples with manganese carboxylates than those of pure HDPE. The results indicate that manganese carboxylate accelerates the thermo-oxidative degradation of HDPE.

Accelerated weathering that combined UV radiation and thermal treatment has allowed photo-degradation and thermo-oxidative degradation to take place simultaneously and resulted in much more significant deterioration than thermal treatment only. The results have shown the dramatic increase of carbonyl index during weathering. Tensile properties of HDPE with manganese carboxylate decreased more significantly than those of pure HDPE. The average molecular weights have also shown the dramatic decreases about 42.53 and 90.48 % for pure HDPE and HDPE with 1% of manganese stearate respectively. Degradation temperatures and melting temperatures of various compositions of HDPE were also found to decrease significantly. The crystallinities of HDPE have notably increased. The presence of manganese carboxylates has generally enhanced the degradation process during accelerated weathering.

Natural weathering has been carried out for maximum duration of 24 weeks under weather conditions of Gampang, Malaysia. The tropical condition with high solar radiation and high day-temperature has led to rapid degradation of HDPE. Rapid oxidation has occurred as indicated by rapid increases of carbonyl indexes especially HDPE samples containing manganese carboxylates. The losses of tensile properties of HDPE have been observed after 24 weeks of natural weathering. The average molecular weights have reduced dramatically about 40.00 and 85.82% for pure HDPE and HDPE containing 1% of manganese stearate respectively. The degradation temperatures and melting temperatures have shifted to lower temperatures for all samples. Nevertheless, the crystallinities of HDPE samples generally increased. Manganese carboxylates have demonstrated capability on improving degradation of HDPE under the weather conditions of Gampang, Malaysia.

Generally the incorporation of manganese carboxylates has led to enhancing degradation during either thermal treatment or accelerated weathering or natural weathering. However, manganese stearate has performed the most influential effect among manganese carboxylates on enhancing degradation during all treatments. Manganese stearate is also preferable due to higher thermal stability and melting point. The effects of manganese carboxylates on enhancing degradation have increased by increasing amount of manganese carboxylates incorporated. Moreover, the combination of UV radiation and thermal has resulted in the faster degradation of HDPE. It has been

also confirmed by the degradation of HDPE under weather conditions of Gombang, Malaysia.

5.2 RECOMENDATIONS

In this study, manganese carboxylates are applied as pro-degradant additives for HDPE. They have shown an effective role on enhancing degradation during thermal treatment, accelerated weathering and natural weathering under weather conditions of Gombang, Malaysia. HDPE is used widely in various applications and eventually ends up as waste in the various environments; therefore various conditions of treatments need to be applied to test capability of manganese carboxylates as pro-degradant additive. The other treatments that should be conducted are outdoor exposure or natural weathering at sites of different latitudes where different weathers existed, soil burial or composting environment treatments at some different sites, treatments at different aquatic environments such as river, lake, and sea.

Based on this study, the amount of 0.2% (w/w) of manganese carboxylates is recommended by considering economic aspect. However, the study on optimum composition should be carried out. Optimization of amount of additives loaded in HDPE is required to obtain suitable composition for certain applications by considering cost aspect. The lower amount of manganese carboxylates (<0.2%) may be considered. Furthermore, modeling of degradation is a challenge. If more data are available i.e. data at varying temperature, varying UV light energy, it is possible to generate a general model to predict lifetime of HDPE in natural environment. In addition, it is also important to test the capability of manganese carboxylates on enhancing degradation for other types of polyethylene such as LDPE, LLDPE.

REFERENCES

- Al-Madfa, H., Mohamed, Z. and Kassem, M.E. 1998. Weather ageing characterization of the mechanical properties of the low density polyethylene. *Polymer Degradation and Stability*. **62**(1): 105-109.
- Albertsson, A.-C., Andersson, S.O. and Karlsson, S. 1987. The mechanism of biodegradation of polyethylene. *Polymer Degradation and Stability*. **18**(1): 73-87.
- Albertsson, A.-C., Barenstedt, C. and Karlsson, S. 1992. Susceptibility of enhanced environmentally degradable polyethylene to thermal and photo-oxidation. *Polymer Degradation and Stability*. **37**(2): 163-171.
- Albertsson, A.-C., Barenstedt, C. and Karlsson, S. 1994. Degradation of enhanced environmentally degradable polyethylene in biological aqueous media: Mechanisms during the first stages. *Journal of Applied Polymer Science*. **51**(6): 1097-1105.
- Albertsson, A.-C. and Karlsson, S. 1990. Polyethylene Degradation and Degradation Products. in: J.E. Glass and G. Swift (Eds.), *Agricultural and Synthetic Polymers. Biodegradability and Utilization*. Washington DC: ACS Symposium Series, pp. 60.
- Andrady, A.L., Hamid, H.S. and Torikai, A. 2003. Effect of climate change and UV-B on materials. *Photochemistry and Photobiology Sciences*. **2**: 68-72.
- Andrady, A.L., Hamid, H.S. and Torikai, A. 2006. Effects of stratospheric ozone depletion and climate change on materials damage (Chapter 7), Report of the 2006 Assessment of the Scientific Assessment Panel. United Nations Environment Programme, Ozone Secretariat
- Andrady, A.L., Hamid, S.H., Hu, X. and Torikai, A. 1998. Effects of increased solar ultraviolet radiation on materials. *Journal of Photochemistry and Photobiology B: Biology*. **46**(1-3): 96-103.
- Andrady, A.L., Pegram, J.E. and Nakatsuka, S. 1993a. Studies on enhanced degradable plastics: 1. The geographic variability in outdoor lifetimes of enhanced photodegradable polyethylenes. *Journal of Polymers and the Environment*. **1**(1): 31-43.

- Andrady, A.L., Pegram, J.E. and Tropsha, Y. 1993b. Changes in carbonyl index and average molecular weight on embrittlement of enhanced-photodegradable polyethylenes. *Journal of Polymers and the Environment*. **1**(3): 171-179.
- ASM International. 1988. *Engineering Plastics*. Engineered Materials Handbook. **2**. USA: ASM International: The Materials Information Society.
- ASM International. 2003. *Characterization and failure analysis of plastics*. USA: ASM International: The Materials Information Society.
- Attwood, J., Philip, M., Hulme, A., Williams, G. and Shipton, P. 2006. The effects of ageing by ultraviolet degradation of recycled polyolefin blends. *Polymer Degradation and Stability*. **91**(12): 3407-3415.
- Azapagic, A., Emsley, A. and Hamerton, I. 2003. *Polymers: The environment and sustainable development*. Chichester: John Wiley and Sons Ltd.
- Azhari, A.W., Sopian, K., Zaharim, A. and Al.Ghoul, M. 2008. A New Approach For Predicting Solar Radiation In Tropical Environment Using Satellite Images – Case Study Of Malaysia *WSEAS Transactions on environment and Development*. **4**(4): 373-378.
- Bajer, K., Kaczmarek, H., Dzwonkowski, J., Stasiak, A. and Oldak, D. 2007. Photochemical and thermal stability of degradable PE/paper waste composites obtained by extrusion. *Journal of Applied Polymer Science*. **103**(4): 2197-2206.
- Barr-Kumarakulasinghe, S.A. 1994. Modelling the thermal oxidative degradation kinetics of polyethylene film containing metal pro-oxidants. *Polymer*. **35**(5): 995-1003.
- Basfar, A.A. and Idriss Ali, K.M. 2006. Natural weathering test for films of various formulations of low density polyethylene (LDPE) and linear low density polyethylene (LLDPE). *Polymer Degradation and Stability*. **91**(3): 437-443.
- Bashford, D. 1997. *Termoplastics directory and databook*. London: Chapman and Hall.
- Beg, M.D.H. 2008. *Wood Plastic Composites: Interface, Weathering and Recycling*. Ph.D Thesis. The University of Waikato, New Zealand.
- Beg, M.D.H. and Pickering, K.L. 2008. Accelerated weathering of unbleached and bleached Kraft wood fibre reinforced polypropylene composites. *Polymer Degradation and Stability*. **93**(10): 1939-1946.
- Bicerano, J. 1996. *Prediction of polymer properties*. 2nd ed. New York: Marcel Dekker, Inc.

- Bikiaris, D., Prinos, J. and Panayiotou, C. 1997. Effect of methyl methacrylate-butadiene-styrene copolymer on the thermooxidation and biodegradation of LDPE/plasticized starch blends. *Polymer Degradation and Stability*. **58**(1-2): 215-228.
- Boon, L.K. 2010. Development of the Malaysian plastic industry and its contribution to the economy. *PRIM Golden Jubilee International Polymer Conference, March 16-17, 2010*. Kuala Lumpur: The Plastic and Rubber Institute Malaysia
- Brandt, A.A. 2009. *Cement-based composites: materials, mechanical properties and performance*. 2nd ed. New York: Taylor & Francis.
- Broido, A. 1969. A simple, sensitive graphical method of treating thermogravimetric analysis data. *Journal of Polymer Science Part A-2: Polymer Physics*. **7**(10): 1761-1773.
- Callister, W.D. and Rethwisch, D.G. 2011. *Materials Science and Engineering*. 8th ed. Hoboken, NJ.: John Wiley & Sons, Inc.
- Carraher Jr., C.E. 2003. *Giant Molecules*. 2nd ed. New Jersey: John Wiley & Sons.
- Colom, X., Cañavate, J., Suñol, J.J., Pagès, P., Saurina, J. and Carrasco, F. 2003. Natural and artificial aging of polypropylene-polyethylene copolymers. *Journal of Applied Polymer Science*. **87**(10): 1685-1692.
- Erlandsson, B., Karlsson, S. and Albertsson, A.-C. 1997. The mode of action of corn starch and a pro-oxidant system in LDPE: influence of thermo-oxidation and UV-irradiation on the molecular weight changes. *Polymer Degradation and Stability*. **55**(2): 237-245.
- Espí, E., Salmerón, A., Fontecha, A., García, Y. and Real, A.I. 2007. The effect of different variables on the accelerated and natural weathering of agricultural films. *Polymer Degradation and Stability*. **92**(12): 2150-2154.
- Excelplas. 2003. The impacts of degradable plastic bags in Australia. Final report to Department of the Environment and Heritage. Excelplas Australia, Nolan-ITU, Center for Design at RMIT. Melbourne
- Fried, J.R. 1995. *Polymer Science and Technology*. New Jersey: Prentice Hall PTR.
- Grant, M.H. 1993. *Encyclopedia of chemical technology*. 4th ed. **6**. New York: John Wiley & Sons.
- Griffin, G.J.L. 1993. *Degradable plastics*. U.S. Patent. 5,212,219. United States.

- Gulmine, J.V., Janissek, P.R., Heise, H.M. and Akcelrud, L. 2002. Polyethylene characterization by FTIR. *Polymer Testing*. **21**(5): 557-563.
- Gulmine, J.V., Janissek, P.R., Heise, H.M. and Akcelrud, L. 2003. Degradation profile of polyethylene after artificial accelerated weathering. *Polymer Degradation and Stability*. **79**(3): 385-397.
- Hamid, S.H., Amin, M.B. and Maadhah, A.G. (Eds.), 1992. *Handbook of Polymer Degradation*. New York: Marcel Dekker, pp.246-248.
- Hartman, H.L. (Ed.), 1992. *SME Mining Engineering Handbook*. Colorado: Society for Mining, Metallurgy, and Exploration, Inc.
- Higiro, J., Herald, T.J. and Alavi, S. 2006. Rheological study of xanthan and locust bean gum interaction in dilute solution. *Food Research International*. **39**(2): 165-175.
- Hind, A.R., Bhargava, S.K. and McKinnon, A. 2001. At the solid/liquid interface: FTIR/ATR -- the tool of choice. *Advances in Colloid and Interface Science*. **93**(1-3): 91-114.
- Huggins, M.L. 1942. The Viscosity of Dilute Solutions of Long-Chain Molecules. IV. Dependence on Concentration. *Journal of the American Chemical Society*. **64**(11): 2716-2718.
- Iring, M., Földes, E., Barabás, K., Kelen, T., Tüdös, F. and Ódor, L. 1986. Thermal oxidation of Linear Low Density Polyethylene. *Polymer Degradation and Stability*. **14**(4): 319-332.
- Johnston, R.T. and Morrison, E.J. 1996. Thermal Scission and Cross-Linking during Polyethylene Melt Processing, *Polymer Durability*. Advances in Chemistry: American Chemical Society, pp. 651-682.
- Khabbaz, F., Albertsson, A.-C. and Karlsson, S. 1999. Chemical and morphological changes of environmentally degradable polyethylene films exposed to thermo-oxidation. *Polymer Degradation and Stability*. **63**(1): 127-138.
- Kurata, M. and Tsunashima, Y. 1999. Viscosity-Molecular Weight Relationships and Perturbed Dimensions of Linear Chain Molecules. in: J. Bandrup, E.H. Immergut and G.A. Grulke (Eds.), *Polymer Handbook* Toronto: John Wiley & Sons.Inc.
- Lei, Y., Wu, Q., Yao, F. and Xu, Y. 2007. Preparation and properties of recycled HDPE/natural fiber composites. *Composites Part A: Applied Science and Manufacturing*. **38**(7): 1664-1674.

- Leng, Y. 2008. *Materials Characterization: Introduction to Microscopic and Spectroscopic Methods*. Singapore: John Wiley & Sons (Asia).
- Li, K.-T. and Weng, W.-T. 2009. Ethylene polymerization over Cr/MCM-41 and Cr/MCM-48 catalysts prepared by chemical vapor deposition. *Journal of the Taiwan Institute of Chemical Engineers*. **40**(1): 48-54.
- Liang, G., Xu, J., Bao, S. and Xu, W. 2004. Polyethylene/maleic anhydride grafted polyethylene/organic-montmorillonite nanocomposites. I. Preparation, microstructure, and mechanical properties. *Journal of Applied Polymer Science*. **91**(6): 3974-3980.
- Liang, S., Yang, H., Wang, K., Zhang, Q., Du, R. and Fu, Q. 2008. Unique crystal morphology and tensile properties of injection-molded bar of LLDPE by adding HDPE with different molecular weights. *Acta Materialia*. **56**(1): 50-59.
- Lokensgard, E. 2004. *Industrial plastics: theory and applications*. 4th New York: Thomson Delmar Learning.
- Michler, G.H. 2008. Amorphous Polymers, *Electron Microscopy of Polymers*. Springer Laboratory: Springer Berlin Heidelberg, pp. 277-293.
- MMD. 2010. General Climate of Malaysia. Malaysian Meteorological Department (MMD), Ministry of Science Technology and Innovation (online) http://www.met.gov.my/index.php?option=com_content&task=view&id=75&Itemid=1089 (accessed on 3 August 2010).
- MPMA. 2005. Performance of the Malaysian Plastics Industry Report. Malaysian Plastics Manufacturers Association (MPMA).Kuala Lumpur
- Murata, K., Hirano, Y., Sakata, Y. and Uddin, M.A. 2002. Basic study on a continuous flow reactor for thermal degradation of polymers. *Journal of Analytical and Applied Pyrolysis*. **65**(1): 71-90.
- Murthy, N.S. and Minor, H. 1990. General procedure for evaluating amorphous scattering and crystallinity from X-ray diffraction scans of semicrystalline polymers. *Polymer*. **31**(6): 996-1002.
- Muthana, M.S. and Mark, H. 1949. Solubility of polyethylene in xylene. *Journal of Polymer Science*. **4**(4): 527-529.
- Novak, S. 2006. Accelerated weatherability testing-The right choice, CRRC Membership Meeting. Q-Lab.

- Ojeda, T., Freitas, A., Birck, K.t., Dalmolin, E., Jacques, R., Bento, F.t. and Camargo, F.v. 2011. Degradability of linear polyolefins under natural weathering. *Polymer Degradation and Stability*. **96**(4): 703-707.
- Osawa, Z., Kurisu, N., Nagashima, K. and Nakano, K. 1979. The effect of transition metal stearates on the photodegradation of polyethylene. *Journal of Applied Polymer Science*. **23**(12): 3583-3590.
- Osswald, T.A., Baur, E., Brinkmann, S., Oberbach, K. and Schmachtenberg, E. 2006. *International Plastics Handbook*. Munich: Carl Hanser Verlag.
- Osswald, T.A. and Menges, G. 2003. *Materials Science of Polymers for Engineers*. 2nd ed. Cincinnati: Hanser Gardner Publications Inc.
- Pablos, J.L., Abrusci, C., Marín, I., López-Marín, J., Catalina, F., Espí, E. and Corrales, T. 2010. Photodegradation of polyethylenes: Comparative effect of Fe and Ca-stearates as pro-oxidant additives. *Polymer Degradation and Stability*. **95**(10): 2057-2064.
- Painter, P.C. and Coleman, M.M. 1997. *Fundamentals of Polymer Science*. 2nd ed. Florida: CRC Press,.
- Peacock, A.J. 2000. *Handbook of Polyethylene: Structures, Properties, and Applications*. New York: Marcel Dekker, Inc.
- PlasticsEurope. 2011. Plastics-the Facts 2011: An analysis of European plastics production, demand and recovery for 2010. PlasticsEurope: Association of Plastics Manufacturers.Brussels
- Poyner, W.R. and Cakraborty, K.B. 1993. *Photodegradable compositions*.U.S. Patent. 5,274,019. United States.
- Rimez, B., Rahier, H., Van Assche, G., Artoos, T., Biesemans, M. and Van Mele, B. 2008. The thermal degradation of poly(vinyl acetate) and poly(ethylene-co-vinyl acetate), Part I: Experimental study of the degradation mechanism. *Polymer Degradation and Stability*. **93**(4): 800-810.
- Roy, P.K., Surekha, P., Rajagopal, C., Chatterjee, S.N. and Choudhary, V. 2006a. Accelerated aging of LDPE films containing cobalt complexes as prooxidants. *Polymer Degradation and Stability*. **91**(8): 1791-1799.
- Roy, P.K., Surekha, P., Rajagopal, C., Chatterjee, S.N. and Choudhary, V. 2007a. Studies on the photo-oxidative degradation of LDPE films in the presence of oxidised polyethylene. *Polymer Degradation and Stability*. **92**(6): 1151-1160.

- Roy, P.K., Surekha, P., Rajagopal, C. and Choudhary, V. 2006b. Effect of cobalt carboxylates on the photo-oxidative degradation of low-density polyethylene. Part-I. *Polymer Degradation and Stability*. **91**(9): 1980-1988.
- Roy, P.K., Surekha, P., Rajagopal, C. and Choudhary, V. 2007b. Comparative effects of cobalt carboxylates on the thermo-oxidative degradation of LDPE films. *Journal of Applied Polymer Science*. **103**(6): 3758-3765.
- Roy, P.K., Surekha, P., Rajagopal, C. and Choudhary, V. 2007c. Thermal degradation studies of LDPE containing cobalt stearate as pro-oxidant. *Express Polymer Letters*. **1**(4): 208-216.
- Saccani, A., Toselli, M. and Pilati, F. 2011. Improvement of the thermo-oxidative stability of low-density polyethylene films by organic-inorganic hybrid coatings. *Polymer Degradation and Stability*. **96**(2): 212-219.
- Schoolenberg, G.E. and Meijer, H.D.F. 1991. Ultra-violet degradation of polypropylene: 2. Residual strength and failure mode in relation to the degraded surface layer. *Polymer*. **32**(3): 438-444.
- Sebaa, M., Servens, C. and Pouyet, J. 1992. Natural and artificial weathering of low-density polyethylene (LDPE): Calorimetric analysis. *Journal of Applied Polymer Science*. **45**(6): 1049-1053.
- Seymour, R.B. 1971. *Introduction to Polymer Chemistry*. New York: McGraw-Hill Inc.
- Sharma, N., Chang, L.P., Chu, Y.L., Ismail, H., Ishiaku, U.S. and Mohd Ishak, Z.A. 2001. A study on the effect of pro-oxidant on the thermo-oxidative degradation behaviour of sago starch filled polyethylene. *Polymer Degradation and Stability*. **71**(3): 381-393.
- Sheikh, N., Akhavan, A., Naimian, F., Khoylou, F., Hassanpour, S. and Sohrabpour, M. 2006. Formulation of a photosensitized polyethylene film; Its structure and property variation under the weathering conditions of Tehran. *Journal of Polymers and the Environment*. **14**(1): 103-109.
- Singh, B. and Sharma, N. 2008. Mechanistic implications of plastic degradation. *Polymer Degradation and Stability*. **93**(3): 561-584.
- Stuart, B.H. 2005. *Infrared Spectroscopy: Fundamentals and Application*. Chicester, UK.: John Wiley & Sons, Ltd.

- Sung, W. and Nikolov, Z.L. 1992. Accelerated degradation studies of starch-filled polyethylene films. *Industrial & Engineering Chemistry Research*. **31**(10): 2332-2339.
- Todd, D.B. 2000. Improving incorporation of fillers in plastics. A special report. *Advances in Polymer Technology*. **19**(1): 54-64.
- Vasile, C. and Pascu, M. 2005. *Practical Guide to Polyethylene*. Shawbury: Rapra Technology Limited.
- Wiles, D.M. 2005a. Oxo-biodegradable polyolefins. in: R. Smith (Ed.), *Biodegradable Polymers for Industrial Applications*. Cambridge: Woodhead Publishing, pp. 54-75.
- Wiles, D.M. 2005b. Oxo-biodegradable polyolefins in packaging. in: R. Smith (Ed.), *Biodegradable Polymers for Industrial Applications*. Cambridge: Woodhead Publishing, pp. 437-450.
- Winslow, F.H. 1977. Photooxidation of High Polymers. *Pure and Applied Chemistry*. **49**(4): 495-502.
- Yao, N. 1992. General procedure for evaluating apparent crystallinity and substantial crystallinity from WAXS patterns of binary and ternary copolymers. *Polymer*. **33**(9): 1802-1808.
- Yuan, Q., Yang, Y., Chen, J., Ramuni, V., Misra, R.D.K. and Bertrand, K.J. 2010. The effect of crystallization pressure on macromolecular structure, phase evolution, and fracture resistance of nano-calcium carbonate-reinforced high density polyethylene. *Materials Science and Engineering: A*. **527**(24-25): 6699-6713.
- Zeus. 2010. Weathering of Plastics. *Zeus Technical Newsletter*: 1-7.
- http://www.jobwerx.com/resources/injection_molding.html (accessed on January 3, 2011).
- <http://www.meoweather.com/history/Malaysia/na/3.7166667/103.1/Gambang.html> (accessed on August 3, 2011).

Appendix A

Average Molecular Weight Determination

Average molecular weight of HDPE was determined by using correlation of intrinsic viscosity and molecular weight (Mark-Howink-Sakurada's equation).

The intrinsic viscosity was obtained experimentally by measuring efflux time of solvent and polymer solution in Ostwald glass capillary viscometer. The following procedure was applied:

1. Measure efflux time of solvent.
2. Measure efflux time of polymer dilute solution, with concentration (C) around 0.01-0.05 g/dL or g/100mL.
3. Determine relative viscosity

$$\eta_{rel} = \frac{\eta_{solution}}{\eta_{solvent}} = \frac{t \rho}{t_s \rho_s}$$

Since $\rho \approx \rho_s$ due to very dilute solution or very low concentration of solute in the solution, equation becomes:

$$\eta_{rel} = \frac{t}{t_s}$$

η_{rel} = relative viscosity

t = efflux time of polymer solution

t_s = efflux time of solvent

4. Determine specific viscosity

$$\eta_{sp} = \eta_{rel} - 1$$

η_{sp} = specific viscosity

5. Huggins' Equation (Higiro et al., 2006; Huggins, 1942) is used for determining intrinsic viscosity

$$\frac{\eta_{sp}}{C} = [\eta] + k'[\eta]^2 C$$

$[\eta]$ = intrinsic viscosity

6. Plot a graphic y vs x

$$y = \frac{\eta_{sp}}{C}$$

$$x = C$$

For example:

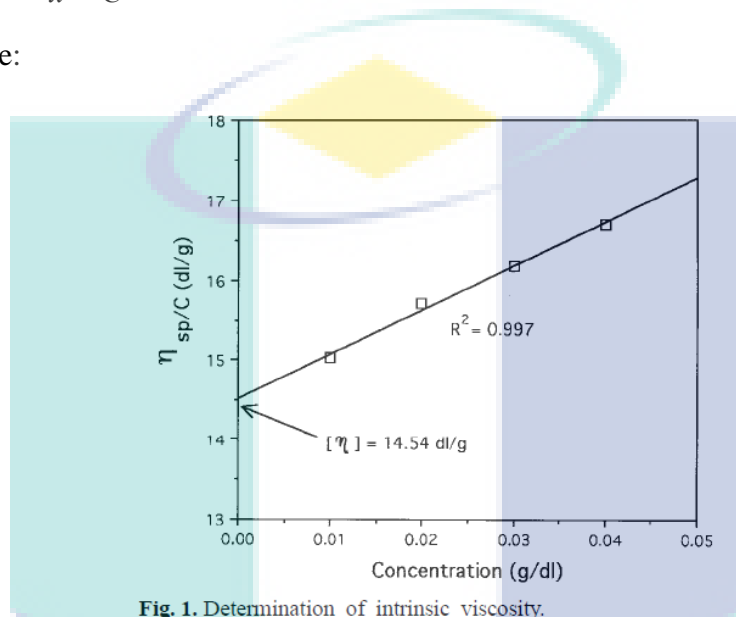


Fig. 1. Determination of intrinsic viscosity.

7. Make a linear regression of a series of data.
8. Intrinsic viscosity is intercept of the trend line with y axis.
9. Intrinsic viscosity and molecular weight are related by Mark-Houwink-Sakurada's equation(Fried, 1995):

$$[\eta] = K \cdot \overline{M}_v^a$$

For polyethylene with xylene solvent at temperature of 105°C (Kurata and Tsunashima, 1999; Roy et al., 2006)

$$K = 16.5 \times 10^{-3} \text{ ml/g.}$$

$$a = 0.83$$

$$\overline{M}_v = \left(\frac{[\eta]}{K} \right)^{1/a}$$

10. Since the unit of $[\eta]$ is dl/g , the equation could be written :

$$M = \left(\frac{[\eta] dl / g \times 100 ml / dl}{K ml / g} \right)^{1/a}$$

$$M = \left(\frac{[\eta] \times 100}{16.5 \times 10^{-3}} \right)^{1/0.83}$$

$$M = \left(\frac{[\eta]}{16.5 \times 10^{-5}} \right)^{1/0.83}$$

References:

- Fried, J.R. 1995. *Polymer Science and Technology*. New Jersey: Prentice Hall PTR.
- Higiro, J., Herald, T.J. and Alavi, S. 2006. Rheological study of xanthan and locust bean gum interaction in dilute solution. *Food Research International*. **39**(2): 165-175.
- Huggins, M.L. 1942. The Viscosity of Dilute Solutions of Long-Chain Molecules. IV. Dependence on Concentration. *Journal of the American Chemical Society*. **64**(11): 2716-2718.
- Kurata, M. and Tsunashima, Y. 1999. Viscosity-Molecular Weight Relationships and Perturbed Dimensions of Linear Chain Molecules. in: J. Bandrup, E.H. Immergut and G.A. Grulke (Editors), *Polymer Handbook* John Wiley & Sons, Inc, Toronto.
- Roy, P.K., Surekha, P., Rajagopal, C. and Choudhary, V. 2006. Effect of cobalt carboxylates on the photo-oxidative degradation of low-density polyethylene. Part-I. *Polymer Degradation and Stability*. **91**(9): 1980-1988.



UMP

Appendix B

Determination of free fatty acid (FFA)

1. Weigh 28.2 ± 0.2 g of sample and pour in Erlenmeyer flask. Add 50 ml of hot neutral-alcohol and 2 ml of phenolphthalein (indicator). Materials should be mixed well in liquid phase during sampling.
2. Titrate with 0.1 N of NaOH solution until the color changes to pink and the color remains in 30 seconds
3. Free fatty acid content is stated in percent (%) following the formula:

$$\% FFA = \frac{\text{volume of NaOH (ml)} \times N \times \text{molecular weight of fatty acid}}{\text{weight of sample (g)} \times 1000} \times 100$$

Reference:

Mehlenbacher, V.C., 1960. *The Analysis of Fats and Oils*. 1st ed., The Garrard Press, Champaign (Illinois)

UMP

Appendix C

List of Papers

International Conference

1. Synthesis and Characterization of Cobalt Carboxylates, International Graduate Conference on Engineering and Science, Universiti Teknologi Malaysia, 23-24 Dec 2008
2. Synthesis and Characterization of Manganese Carboxylates, International Conference On Chemical And Bioprocess Engineering (ICCBPE-2009), Universiti Malaysia Sabah, 12-14 August 2009
3. Degradation of high density polyethylene containing manganese stearate under accelerated weathering, International Conference on Green World in Business and Technology, 23-25 March 2012, Universitas Ahmad Dahlan, Yogyakarta, Indonesia

National Conference

1. Comparison of Thermal Stability of Manganese Carboxylates and Cobalt Carboxylates, Malaysian Technical Universities Conference on Engineering and Technology, June 20-22, 2009, MS Garden, Kuantan, Pahang, Malaysia

Journal

1. Maryudi, R.M. Yunus, A.H. Nour, and M.H. Abidin. Synthesis and Characterization of Manganese Carboxylates, *Journal of Applied Sciences* 9(17):3156-3160, 2009.
2. Maryudi, R.M. Yunus, M.D.H. Beg, A.H. Nour, and M.H. Abidin. Thermo-oxidative degradation of HDPE containing manganese laurate as pro-degradant additives. *Iranian Polymer Journal* (*submitted*)
3. Maryudi, R.M. Yunus, and M.D.H. Beg. Comparison of roles of manganese laurate, manganese palmitate and manganese stearate on the degradation of high density polyethylene during natural weathering in Gambang, Malaysia. *Journal of Polymers and the Environment* (*submitted*)